Consiglio Nazionale delle Ricerche

The Fourth Edition of the

YOUNG APPLIED MATHEMATICIANS CONFERENCE

Rome, 16th–20th September 2024

editors

Elia Onofri
Gennaro Auricchio

BOOK OF ABSTRACTS

The Fourth Edition of the

YOUNG APPLIED MATHEMATICIANS CONFERENCE

Rome, 16th–20th September 2024

editors

Elia Onofri
Gennaro Auricchio

CNR | Istituto per le Applicazioni del Calcolo "M. Picone" (IAC)

Istituto per le Applicazioni
del Calcolo "Mauro Picone"

in collaboration with
Sapienza, University of Rome | Department of Mathematics "G. Castelnuovo"

The conference was financially supported by

The conference was promoted thanks to

Young Applied Mathematicians Conference
16 September 2024 – 20 September 2024
Rome, Italy

Programme

Legend

Plenary talk (60')
[L] Long presentation (40')
Short presentation (20')
[MC] Mini-course (60')
[MS] Mini-symposium (120')
[S] Sponsor presentation (40')
Social event
Coffee break, Launch time, and breaks
Travel time

Monday 16 September 2024

9:00–10:30	**Plenary Session** (room IV, *Chair* G. A. D'inverno) Gabriella Puppo — Conference Opening Stefano Berrone — Variational Physics Informed Neural Networks: quadrature rules, test functions and "a posteriori" error estimates
10:30–11:00	**Coffee Break**
11:00–13:00	**Morning Sessions** (room IV, *Chair* E. Onofri)
	Daniele De Sensi — [MC] Writing, Benchmarking, and Reproducibility in Research Papers
	Federico Nudo — [L] Histopolation via mock-Chebyshev points
	Grazia Gargano — A multi-factor approach to identify differentially expressed genes in transcriptome data
11:00–13:00	**Morning Sessions** (room V, *Chair* C. Graziani)
	G. Alessio D'Inverno — [MC] PINA: A Python Software for Scientific Machine Learning
	Federico Pichi — [L] Graph-based machine learning approaches for model order reduction
	Veronica Tora — Mathematical models on graphs in Alzheimer's brain
13:00–15:00	**Lunch Time**
15:00–18:00	**Afternoon Sessions** (room IV, *Chair* A. Kushova)
	Piero Deidda — The Joint Spectral Radius of Neural Networks
	Eleonora Maggiorelli — An high order AT1 phase-field model for brittle fracture
	Lorenzo Zambon — [MS] Hierarchical Forecasting (part I)
	Break
	Lorenzo Zambon — [MS] Hierarchical Forecasting (part II)
15:00–18:00	**Afternoon Sessions** (room V, *Chair* G. Auricchio)
	Laura Girometti — A non-convex optimization strategy applied to signal decomposition
	Andrea Perchiazzo — Pricing European Options using the Gauss-Laguerre quadrature: Application to a Compound CARMA(p,q)-Hawkes model
	Federico Nudo, Salah Eddargani — [MS] Recent advances in enriched finite element and isogeometric analysis (part I)
	Break
	Federico Nudo, Salah Eddargani — [MS] Recent advances in enriched finite element and isogeometric analysis (part II)

Tuesday 17 September 2024

9:00–10:30	**Plenary Session** (room IV, *Chair* G. Alessio D'Inverno)
	Org. Committee Day opening
	Carla Manni Smooth Splines on Triangulations
10:30–11:00	Coffee Break
11:00–13:00	**Morning Sessions** (room IV, *Chair* C. Graziani)
	Chiara Lucifora [L] The VERSE platform: eXtended Reality in Education
	Alessandro Scagliotti [L] Optimal control of ODEs with dynamics uncertainty
	Paolo Zuzolo Spectral features for 3D shape analysis
	Anna Sanfilippo Approximate Deconvolution Leray Reduced Order Model
11:00–13:00	**Morning Sessions** (room V, *Chair* M. Menci)
	Silvia Preda [L] High order semi-Lagrangian schemes and applications
	Giulia Tatafiore An efficient semi-Lagrangian scheme for Fokker-Planck equations on unstructured grids
	Davide Torlo Divergence–free preserving schemes: how to fix stabilization terms in continuous Galerkin for hyperbolic PDEs
	Elishan C. Braun Numerical study on parameter effects of a new model for water penetration in porous media
	Ibrahim Almuslimani Explicit stabilized implementation of implicit Runge-Kutta methods
13:00–15:00	Lunch Time
15:00–18:00	**Afternoon Plenary Sessions** (room IV, *Chair* E. Onofri)
	Fabrizio M. De Sciscio-olo [S] VERSE, *by Dotslot*: Education and Training in the Metaverse; Italian Innovation for Digital Learning
	Filippo Biancone [S] VERSE, *by Dotslot*: bringing schools to the digital world
	Roberta Bianchini (In-)stability in nonhomogeneous density fluids
	Break
	Org. Committee Organization, General Information, YAMC2025 et al.

Wednesday 18 September 2024

9:00–10:30	**Plenary Session** (room IV, *Chair* A. Marchetti)
	Org. Committee — Day Opening
	Maurizio Parton — A Systematization of the Wagner Framework: Graph Theory Conjectures and Reinforcement Learning
10:30–11:00	Coffee Break
11:00–13:00	**Morning Sessions** (room IV, *Chair* S. Marziali)
	Anastasia Istratuca — [MC] Multilevel Monte Carlo Methods
	Stephan Gerster — [L] Feedback control for hyperbolic balance laws
	David Mavrodiev — Computational Model for Text Optimization: Substantive Reduction to Improve the Semantic Perception of Information
11:00–13:00	**Morning Sessions** (room V, *Chair* G. Auricchio)
	Federico Nudo — [MC] Cubic and quadratic polynomial enrichments of the Crouzeix–Raviart finite element
	Bruno Degli Espositi — [L] Point cloud generation algorithm for 3D domains in B-Rep format
	Simone Milanesi — A funnel plot approach for monitoring Antibiotic Resistance in EU countries based on the WHO GLASS dashboard
13:00–15:00	Lunch Time
15:00–18:00	**Afternoon Sessions** (room IV, *Chair* S. Marziali)
	G. Alessio D'Inverno — [S] The iNEST project
	Nella Rotundo — [MS] Mathematical Frameworks and Numerical Methods for Complex Physical Systems (part I)
	Break
	Nella Rotundo — [MS] Mathematical Frameworks and Numerical Methods for Complex Physical Systems (part II)
15:00–18:00	**Afternoon Sessions** (room V, *Chair* C. Carrara)
	Elisa Calzola, Federica Ferrarese — [MS] Exploring efficient advanced numerical methods for Partial Differential Equations (part I)
	Break
	Elisa Calzola, Federica Ferrarese — [MS] Exploring efficient advanced numerical methods for Partial Differential Equations (part II)
19:30–23:30	**Social Dinner** *at La Limonaia, Villa Torlonia*
	Via Lazzaro Spallanzani, 1/A, 00161 Roma

Thursday 19 September 2024

9:00–10:30	**Plenary Session** (room IV, *Chair* E. Onofri)
	Org. Committee — Day Opening
	Roberto Natalini — Vector BGK approximations to compressible and incompressible fluids
10:30–11:00	Coffee Break
11:00–13:00	**Morning Sessions** (room IV, *Chair* E. Onofri)
	Francesca Ignoto — Numerical Computation of Generalized Wasserstein Distances with Applications to Traffic Model Analysis
	Ilaria Ciaramaglia — Non-local traffic flow models with time delay: well-posedness and numerical approximation
	Davide Moretti — About clustering of time series: A case study using real traffic data
	Matteo Piu — Mathematical models for multilane traffic flow
	Luca Simi — Improving Mapper with Metric Trees
	Alessandro Ravoni — Studying long-lasting diseases using an agent-based model of the immune response
11:00–13:00	**Morning Sessions** (room V, *Chair* G. A. D'Inverno)
	Kateryna Morozovska — [L] Optimal Sensor Placement in Power Transformers Using Physics-Informed Neural Networks
	Daniel Fakhouri — On the expressivity of the ExSpliNet model
	Josephine Westermann — Neural Networks vs Sparse Polynomials for Spectral Operator Surrogates
	Dimitrios G. Patsatzis — Learning Slow Invariant Manifolds with Physics-Informed Neural Networks
	Asli Larbi — Automatic Character Recognitions Tamahaqt in Amazigh Language
13:00–15:00	Lunch Time
15:00–18:00	Free Time

Friday 20 September 2024

9:00–10:30	**Plenary Session** (room IV, *Chair* M. Menci)	
	Org. Committee	Day Opening
	Giuseppe Visconti	A general framework of implicit high-order schemes for hyperbolic systems
10:30–11:00	Coffee Break	
11:00–14:00	**Morning Sessions** (room IV, *Chair* M. Menci)	
	Vincenzo S. Di Cola, Fabio V. Difonzo, Giovanni Pagano	[MS] Computational Techniques in Agriculture, Epidemiology, and Plant Pathology
11:00–12:40	**Morning Sessions** (room V, *Chair* C. Carrara)	
	Domenico Caparello	A hierarchical hybrid numerical method for multi-scale Boltzmann equation with geometry
	Tommaso Tenna	Projective and Telescopic Projective Integration for the Multi-species Boltzmann Equation
	Eya Zougar	Stochastic heat equation in heterogeneous medium
	Robin Theriault	The Loss Landscape of Dense Associative Memory
	Federico M. Quetti	A Bayesian Approach to Clustering via the Proper Bayesian Bootstrap
13:00–15:00	Lunch Time	
15:00–18:00	Travel Time	

Timetable

Time	Mon 16 Aula IV	Mon 16 Aula V	Tue 17 Aula IV	Tue 17 Aula V	Wed 18 Aula IV	Wed 18 Aula V	Thu 19 Aula IV	Thu 19 Aula V	Fri 20 Aula IV	Fri 20 Aula V
08:30 - 09:00	Badge Pickup		Badge Pickup		Badge Pickup		Badge Pickup		Badge Pickup	
09:00 - 09:30	Opening		Opening		Opening		Opening		Opening	
09:30 - 10:30	Berrone		Manni		Parton		Natalini		Visconti	
10:30 - 11:00	Coffee break		Coffee break		Coffee break		Coffee break		Coffee break	
11:00 - 11:20	[MC] De Sensi	[MC] D'Inverno	Lucifora	Preda	[MC] Istratuca	[MC] Nudo	Ignoto	Morozovska		Caparello
11:20 - 11:40							Ciaramaglia		[MS] Schiano Di Cola / Difonzo / Pagano	Tenna
11:40 - 12:00			Scagliotti	Tataflore			Moretti	Fakhouri		Zougar
12:00 - 12:20	Nudo	Pichi		Torlo	Gerster	Degli Esposti	Piu	Westermann		Theriault
12:20 - 12:40			Zuzolo	Braun	Mavrodiev	Milanesi	Simi	Patsatzis		Quetti
12:40 - 13:00	Gargano	Tora	Sanfilippo	Almuslimani			Ravoni	Larbi		
13:00 - 13:20	Lunch break		Lunch break		Lunch break		Lunch break		Lunch break	
13:20 - 13:40										
13:40 - 14:00										
14:00 - 14:20									Travel Time	
14:20 - 14:40										
14:40 - 15:00							Free Time			
15:00 - 15:20	Deidda	Girometti	DOTSLOT (Marra/Biancone)	Bianchini	iNEST (D'Inverno)					
15:20 - 15:40	Maggiorelli	Perchiazzo								
15:40 - 16:00	[MS] Zambon	[MS] Nudo / Eddargani			[MS] Nella Rotundo	[MS] Cazola / Ferrarese				
16:00 - 16:20										
16:20 - 16:40										
16:40 - 17:00	Break		Break		Break					
17:00 - 17:20	[MS] Zambon	[MS] Nudo / Eddargani	Organization, General Information, YAMC2025 et al.		[MS] Nella Rotundo	[MS] Cazola / Ferrarese				
17:20 - 17:40										
17:40 - 18:00										

The Fourth Edition of the

YOUNG APPLIED MATHEMATICIANS CONFERENCE

Index

Long Presentations

Short Presentations

Mini-Courses

Mini-Symposium
Computational Techniques in Agriculture, Epidemiology, and Plant Pathology

Mini-Symposium
Exploring efficient advanced numerical methods for Partial Differential Equations

Mini-Symposium
Hierarchical Forecasting

Mini-Symposium
Mathematical Frameworks and Numerical Methods for Complex Physical Systems

Mini-Symposium
Recent advances in enriched finite element and isogeometric analysis

Preface

The present book collects the long abstracts of 43 out of 46 talks (6 plenary, 3 sponsor, 8 long, and 29 short presentations), 3 out of 4 mini-courses, and 27 out of 29 contributions in 5 mini-symposia presented and organised during the fourth edition of the "Young Applied Mathematicians Conference" (YAMC). The conference, held from September 16th to 20th, 2024, in the historic city of Rome, Italy, was generously hosted by the Department of Mathematics "Guido Castelnuovo" at Sapienza, University of Rome.

We are pleased that the conference successfully built upon and replicated the substantial achievements of its previous editions, continuing to provide a vibrant and inspiring platform for young researchers –primarily PhD students and postdoctoral fellows. This year's conference promoted novel collaboration, innovation, and the exchange of ideas across a wide array of topics. Over the course of five days, we gathered together 78 speakers from 37 universities and research centres across 8 countries (24 from Italy, 5 from France, 3 from Germany, and 1 from Algeria, England, Scotland, Sweden, and Switzerland respectively), who presented innovative solutions applied to cutting-edge challenges in applied mathematics.

We were honored to host six esteemed plenary speakers, whose contributions significantly enhanced the success of the conference. In particular, we extend our sincere gratitude to:

Prof. **Giuseppe Visconti** (Sapienza, University of Rome) for his invaluable assistance in arranging the conference venue and his determination in overcoming the numerous obstacles we faced.

Prof. **Stefano Berrone** (Politecnico di Torino), Prof.sa **Carla Manni** (University of Rome Tor Vergata), and once again, Prof. **Giuseppe Visconti** for their commitment to proposing, alongside this book, a special issue in the esteemed Journal of Computational and Applied Mathematics (JCAM), which will offer a platform for the extension of the works presented at YAMC.

Director **Roberto Natalini** (Institute for Applied Mathematics "M. Picone", IAC–CNR) for his support in both the venue arrangement and the publication of the present volume.

Regarding this last point, one of the most exciting developments this year was the publication of all accepted contributions in this collection of long abstracts, curated by CNR Edizioni. We hope this initiative will become a *de facto* standard for future editions, making the research presented at YAMC widely accessible to the global scientific community. This open-access effort reflects our commitment to disseminating cutting-edge knowledge and supporting the professional growth of emerging scholars, which has always been the inspirational driving force behind this event: *a conference for young mathematicians, organised by young mathematicians*.

We extend our heartfelt thanks to all participants, speakers, and organisers whose dedication and passion made this event possible and laid the foundation for the success of YAMC. We are also deeply grateful to our sponsors and partners for their invaluable

support. In particular, we thank Dotslot s.r.l., who not only provided financial assistance but also helped disseminate the event and showcased their innovative learning technology, Verse, which powered the AI assistant for the conference itself.

We hope that YAMC provided a memorable and enriching experience for all attendees, inspiring new ideas, collaborations, and friendships that will continue to flourish long after the event.

Rome, Italy
September 24th, 2024
Elia Onofri, *editor*

Sponsors

VERSE, *by Dotslot*: Education and Training in the Metaverse Italian Innovation for Digital Learning

Fabrizio Marra De Scisciolo* **and Filippo Biancone**
Dotslot s.r.l. Impresa Sociale, Roma Viale dei Promontori 440, Italia

In this talk we present VERSE [2], an innovative educational software platform developed by Dotslot s.r.l.. Entirely designed in Italy, VERSE was born to address the evolving demands of teaching and learning in the digital era. Leveraging on cutting-edge technologies and gamification strategies, VERSE aims to revolutionize the educational experience by providing an engaging, immersive, and personalized learning environment. In particular, we explore the key components, the technological underpinnings, and the pedagogical implications of VERSE, as well as its potential to transform traditional educational paradigms.

Interactive Learning Environment VERSE offers a comprehensive and interactive learning environment that integrates advanced multimedia and multisensory experiences. Students engage in missions aligned with the school's curricula, which not only reinforce subject matter but also foster critical thinking and problem-solving skills. Furthermore, the platform's adaptive scoring system provides real-time feedback, enabling a personalized learning curve that adapts to the individual needs of each individual student. Such a dynamic approach is designed to increase student motivation and retention of knowledge by making learning an active and engaging process.

Comprehensive Teacher Support To enhance the effectiveness of the teaching process, VERSE provides educators with a robust and innovative set of tools, including detailed lesson plans, instructional video tutorials, and practical tips tailored to the platform's features. These resources, realized under multiple collaborations with the Italian universities, are intended to ease the integration of digital tools into traditional teaching methodologies, allowing educators to seamlessly blend physical and virtual classroom experiences. Finally, the platform includes analytics features that enable teachers to monitor student progress and tailor instruction accordingly, allowing a more data-driven approach to education.

Technological Integration and Accessibility VERSE is designed since its birth with a focus on accessibility and technological integration, supporting a wide range of devices and platforms, including PCs, tablets, and VR headsets. This cross-platform compatibility ensures that the educational content is accessible to a diverse range of learners, regardless

of their technological resources. By bridging the gap between physical classrooms and virtual environments, VERSE facilitates the creation of hybrid learning models that can be adapted to various educational contexts, from primary schools to higher education and beyond, and can help filling the physical distances that might arise due to critical situations, like *e.g.* the sadly well-known lockdown.

Customizable Virtual Labs (VERSE Labs)   One of the distinctive features of VERSE is its customizable virtual laboratories, known as VERSE Labs. These labs are specifically designed to support experiential learning in various disciplines, including languages, natural sciences, robotics, food science, and the arts. VERSE Labs enable students to engage in hands-on, practical learning experiences that complement theoretical knowledge that can be driven in safe environments, like, *e.g.*, a chemistry laboratory. The labs are designed to be flexible and scalable, allowing educators to modify content and experiments to suit different educational levels and objectives.

Cooperative and Peer-to-Peer Learning   VERSE promotes cooperative learning by facilitating the formation of peer-to-peer study groups within its virtual environment. These groups can engage in collaborative projects, discussions, and problem-solving activities, mirroring the dynamics of real-world teamwork. The platform's flexibility allows it to be tailored to the unique needs of different learning communities, making it an ideal tool for fostering a collaborative learning culture that prepares students for the demands of modern work environments.

Facilitating the School-to-Work Transition   In addition to its educational applications, VERSE is designed to support the transition from school to the workforce by equipping students with practical, job-ready skills. The platform emphasizes the development of soft skills such as logical reasoning and the ability to contextualize information—qualities that are increasingly valued in the modern labor market. By providing students with a simulated work environment, VERSE helps bridge the gap between academic learning and professional application, thereby enhancing employability and career readiness.

Strategic Technological Partnerships   In order to further enrich its educational ecosystem, VERSE has established strategic partnerships with leading technology providers, including Promethean (Digital Board, [4]), Convai (Conversational AI, [1]), and Labster (3D simulations, [3]). These collaborations allow VERSE to integrate state-of-the-art technologies into its platform, offering users an enhanced educational experience that is both cutting-edge and deeply immersive. These partnerships are crucial in ensuring that VERSE remains at the forefront of educational innovation, continually adapting to emerging technological trends and educational needs.

Conclusion   VERSE represents a significant leap forward in the field of educational technology, combining advanced digital tools with innovative pedagogical strategies to cre-

ate a transformative learning experience. By merging the physical and virtual worlds, VERSE not only enhances the traditional classroom setting but also prepares students for the challenges of a rapidly changing digital landscape. As educational institutions world-wide seek to modernize and adapt to the digital age, VERSE stands out as a pioneering solution that is poised to shape the future of education.

References

[1] Convai Tech. *Embodied AI Characters For Virtual Worlds*. URL: `https://convai.com`.

[2] Dotslot s.r.l. *VERSE: Istruzione e Formazione nel Metaverso*. URL: `http://dotslot.it`.

[3] Labster A.p.s. *Virtual Labs for Universities and High Schools*. URL: `https://labster.com`.

[4] Mind Ai. *Promethean: The all-new ActivPanel*. URL: `https://prometheanworld.com/en/`.

VERSE, *by Dotslot*: bringing schools to the digital world

Fabrizio Marra De Scisciolo and Filippo Biancone[*]
Dotslot s.r.l. Impresa Sociale, Roma Viale dei Promontori 440, Italia

We present VERSE [2], an innovative education software platform developed by Dotslot s.r.l.. Dotslot is a social enterprise committed to revolutionizing the education sector through software development, training for individuals and organizations, research and AI. The company is currently cooperating with the National Research Council and the Universities of Bari, Florence, la Sapienza, and Roma Tre by funding doctorates and research positions. Dotslot's mission is to provide innovative software solutions and training opportunities with the aim of

- Support professional development

- Provide people with easy access to knowledge.

- Ease the transition of Italian schools towards a digitally driven world.

About VERSE

Verse is a multi-platform software committed to offering an engaging learning experience for students of all ages that is also intuitive for teachers to use. It contains a 3D digital school through which students and teachers can freely explore 3D spaces in a creative way, easily accessible digital labs and activities, and interact with conversational AI avatars.

The primary goal

VERSE's primary goal is to create a more accessible, efficient, and future-ready educational environment that adapts to the constant technological advancements, ensuring both students and educators can thrive in a digitally driven world. In order to reach this goal, our work focusses on two main aspects:

Accessibility: to be accessible to all students, VERSE offers an expanding catalogue of digital labs with many options for customization. This allows teachers to adapt the experience to their students' needs. They can also create their own custom conversational AI avatars that can be interacted with through both text and speech in up to 24 languages.

Efficiency: VERSE allows students to integrate their knowledge using digital exercises and labs while also balancing education with entertainment, creating an optimal

learning environment. Teachers will also be able to easily switch between and, in future, keep track of their classes' activities and progress to better organize their lessons.

The main industrial partners

In the following, we describe two of our principal industrial partners which allow us reaching the previously described goals:

Labster [3] is a company specialized in the development of advanced interactive simulations of scientific labs, each of which is designed for educational and research purposes. As of now, the simulations that are available on our software cover biology, chemistry and physics and allow users to interact with a 3D digital lab while also submitting them to multiple choice quizzes that keep track of their progress.

Convai [1] lends its conversational AI, allowing users to create their own custom avatars that can provide highly adaptable and engaging experiences, for entertainment and/or for educational purposes. It's also possible to "train" these avatars on one or more desired subjects by simply loading a text file onto their knowledge bank.

The principal contents

In what follows, we describe the wide range of possible activities VERSE offers for teachers and students.

Educational digital labs: VERSE offers a growing collection of educational labs, each of which is designed to entertain and challenge students across all subjects in the Italian school curriculum. The lab content can be either generated by AI or created/verified by subject matter experts.

Arenas: Users can explore an expanding selection of 3D environments called "Arena"s, where they can instantiate conversational AI avatars, 3D models, and digital blackboards that can be filled out with either text or images to allow (i) students to fully express their creativity and (ii) teachers to design fun and interactive lessons. In future, it will also be possible to engage with themed 3D activities within each Arena.

AI quizzes: Users can generate multiple-choice quizzes on a topic of their choice with varying difficulty using AI. Each quiz consists of 10 questions and allows the user to review their answers, giving the teacher the ability to review results, identify areas for improvement, and adjust the lesson according to the students' needs.

Future work

VERSE is a living organism that keeps evolving and expanding its features day-by-day. In particular, the ongoing collaboration with the University structures allows us bringing new digital activities that can be useful to the Italian school portfolio, while also creating new Arenas and instantiable 3D models for users to use in the 3D spaces. Furthermore, as previously mentioned, we will soon develop 3D themed activities that can be engaged

within the Arenas themselves. Finally, we also plan on integrating within the VERSE platforms an AI chatbot (ZunoAI) that students and teachers can interact with whenever they feel the need to.

Conclusions

VERSE aims to significantly impact the education sector by providing a versatile, innovative, and interactive platform that supports both students and educators. By focusing on accessibility and efficiency, VERSE enhances the learning experience through its 3D digital environments, AI-driven features, and customizable educational labs. Its collaboration with esteemed institutions and industrial partners like Labster and Convai further strengthens its ability to offer novel engaging educational tools.

Looking forward, VERSE will continue evolving to meet the needs of the digital learning landscape. With plans to expand its 3D environments, add themed activities, and integrate advanced AI capabilities, VERSE remains committed to supporting the professional development of educators and improving the accessibility of knowledge for students. This dynamic and forward-thinking platform is well-positioned to play a key role in the digital transformation of Italian schools and beyond, ensuring that education is both engaging and future-ready.

References

[1] Convai Tech. *Embodied AI Characters For Virtual Worlds*. URL: `https://convai.com`.

[2] Dotslot s.r.l. *VERSE: Istruzione e Formazione nel Metaverso*. URL: `http://dotslot.it`.

[3] Labster A.p.s. *Virtual Labs for Universities and High Schools*. URL: `https://labster.com`.

The iNEST project

Giuseppe Alessio D'Inverno
SISSA, International School for Advanced Studies, Trieste

iNEST: an Ecosystem for Innovation

Innovation Ecosystems are networks of Universities, Public Research Institutions, Territorial Institutions and Companies. Such Ecosystems are active in technology specialization areas which are coherent with territorial industrial & research missions, and promote and strengthen cooperation among Research, Economic players and Institutions. Ecosystems add value to research outcomes, make easier technology transfer and digital transformation of companies and related processes, taking care of economic and environmental sustainability and of social impacts.

The iNEST Project aims to define a new Innovation Ecosystem paradigm, based on:

- multi-vocationality;

- ability to generate added value through an integrated and interconnected approach, overcoming

- the risks of fragmentation;

- networking, with a partnership-based approach.

The key tools for the development of this new paradigm are:

- information and communication technologies (ICT) and digitisation;

- innovative technologies for the well-being of people, the diffusion of culture and growth economic and entrepreneurial.

The iNEST project is located in the north-east of Italy, in a region characterized by:

- Strong territorial background (Historical, social, cultural), as driving force for cooperation;

- Key-area for Italian economy: 12% of people, 14% of GNP, 20% of Italian export;

- Variety of vocations, from industry to tourism and cultural heritage;

- Hign number of interconnections, well represented by Smart Specialization Strategies;

Digital Twins: from mathematics, a catalyst for innovation

A dramatic shift is on the horizon in modern economics, and at its core lies the transformative force of digitalization. This revolutionary process allows for the constant optimization of processes and substantial cost savings, hence marking the beginning of a new era of efficiency across industries. Digitalization is a pillar of the iNEST Consortium: it is the key for industries in North-Eastern Italy to establish themselves as efficiency models and innovation drivers.

At the forefront of this digital revolution stands the visionary concept of the **Digital Twin (DT),** the virtual replica of a real-world product or process. iNEST Spoke 9 dedicates all its research efforts to the development of Digital Twins and their application across diverse fields. Yet, to truly harness their potential, a deep understanding of the underlying behaviors and functions of their real-world counterparts is essential. In the quest to create accurate Digital Twins, scientists wield sophisticated tools of mathematical and numerical modeling. Real-time data flows between physical objects and virtual replicas facilitate constant communication and refinement. To ensure ever-closer alignment between DTs and their real counterparts, invaluable support is provided by mathematical and numerical tools such as **Reduced Order Models** and Uncertainty Quantification techniques.

References

[1] *Consorzio iNEST*. URL: https://www.consorzioinest.it/en/#content-1-en.

[2] *Spoke 9 – Consorzio iNEST*. URL: https://inest.spoke9.sissa.it.

Plenary Presentations

Variational Physics Informed Neural Networks: quadrature rules, test functions and "a posteriori" error estimates.

Stefano Berrone[a,∗], Claudio Canuto[a], and Moreno Pintore[b]

[a] Politecnico di Torino, Italy
[b] Inria, Sorbonne University, France

Recent advances in artificial intelligence, particularly in deep learning, have driven the development of several innovative numerical techniques for solving partial differential equations (PDEs). These methods approximate solutions by training neural networks that leverage the knowledge of the underlying differential equations. One of the earliest models employing a neural network was described in [9], which introduced the concept of Physics-Informed Neural Networks (PINNs). This work inspired subsequent studies, such as [10] and [11], culminating in the recent paper [8], which presents a comprehensive framework for solving operator equations using deep neural networks. Approximation properties of PINN solutions can be evaluated [4, 7]. The PINN paradigm was further refined in [5] to develop Variational Physics-Informed Neural Networks (VPINNs). Key differences from PINNs include the use of the weak formulation of the PDE, replacing collocation points with test functions, and employing quadrature points to compute the integrals involved in the variational residuals. In this method, the solution is still approximated by a neural network, but the test functions are represented by either a finite set of known functions or a secondary neural network (see [6]), making the technique a variant of the Petrov-Galerkin method.

In [3], we examine the impact of varying the precision of quadrature rules and the degrees of piecewise polynomial test functions on the convergence rate of VPINNs when addressing elliptic boundary-value problems through mesh refinement. Utilizing a Petrov-Galerkin framework, we derive an "a priori" error estimate in the energy norm. The proposed interpolation operator is crucial for obtaining an inf-sup stable method and eliminating spurious modes from the neural network's output. Counterintuitively, our results suggest that for smooth solutions, the optimal approach for achieving rapid error decay is to use test functions with the lowest polynomial degree while employing highly precise quadrature formulas. Specifically, for sufficiently smooth solutions, the error decay rate is determined by $q + 2 - k_{test}$, where q is the polynomial degree of the quadrature formula and k_{test} is the local polynomial degree of the test functions. Numerical experiments validate our theoretical predictions. The error between the exact solution and the approximated solution represented by the computed neural network decays asymptotically at the same rate as predicted by our theory for the network's interpolant. However, this behavior cannot be rigorously guaranteed in general without the use of the interpolation operator, as the minimization problem defining the computed neural network is

generally underdetermined, potentially leading to spurious components. Indeed, for a problem with zero boundary conditions and right hand side, minimizing the loss function may result in non-vanishing neural networks. The method proposed in [3] combines the efficiency of the VPINN approach with a rigorous convergence analysis.

In [2], we define a computable residual-type "a posteriori" error estimator and prove its reliability and efficiency in controlling the energy error between the exact solution and the VPINN solution. In our estimates, the global error is upper-bounded by a constant multiple of the estimator (reliability), moreover the estimator does not overestimate the energy error, as the latter is lower-bounded by a constant multiple of the former (efficiency), up to data oscillation terms. Reliability is connected to the possibility of refining the test space by adding test functions whose support is located where the estimator is large (refining the mesh of the test functions) to improve the solution, whereas efficiency could be used to coarsen the test space by removing functions with support in regions where the estimator is small (coarsening the mesh).

The proposed estimator is the sum of several terms: a classical residual-type estimator similar to that used in finite elements, which measures the residual of the strong form of the differential equation when the solution is replaced by the VPINN and the inter-element gradient jumps; a term accounting for the magnitude of the loss function after minimization; and additional terms measuring data oscillations, i.e., the errors resulting from locally projecting the equation's coefficients and right-hand side onto suitable polynomial spaces. The estimator can be expressed as a sum of elemental contributions (local in space), enabling its use within an adaptive discretization strategy that refines the elements contributing the most to the estimator.

Dirichlet boundary conditions can significantly influence the behavior of VPINNs, particularly in the presence of highly complex geometries. In [1] a comprehensive exploration of distinct approaches for enforcing Dirichlet boundary conditions in PINNs and VPINNs is performed.

References

[1] S. Berrone, C. Canuto, M. Pintore, and N. Sukumar. "Enforcing Dirichlet boundary conditions in physics-informed neural networks and variational physics-informed neural networks". In: *Heliyon* 9.8 (2023), e18820. ISSN: 2405-8440. DOI: 10.1016/j.heliyon.2023.e18820.

[2] S. Berrone, C. Canuto, and M. Pintore. "Solving PDEs by variational physics-informed neural networks: an a posteriori error analysis". In: *Annali dell'Università di Ferrara* 68 (2022), pp. 575–595. DOI: 10.1007/s11565-022-00441-6.

[3] S. Berrone, C. Canuto, and M. Pintore. "Variational Physics Informed Neural Networks: the role of quadratures and test functions". In: *Journal of Scientific Computing* 92.3 (2022), pp. 1–27. DOI: 10.1007/s10915-022-01950-4.

[4] D. Elbrächter, D. Perekrestenko, P. Grohs, and H. Bölcskei. "Deep neural network approximation theory". In: *IEEE Trans. Inform. Theory* 67.5 (2021), pp. 2581–2623. DOI: https://doi.org/10.1109/TIT.2021.3062161.

[5] E. Kharazmi, Z. Zhang, and G. Karniadakis. "VPINNs: Variational physics-informed neural networks for solving partial differential equations". In: (2019). ᴀʀxɪᴠ: 1912.00873.

[6] R. Khodayi-Mehr and M. Zavlanos. "VarNet: Variational neural networks for the solution of partial differential equations". In: *Learning for Dynamics and Control*. PMLR. 2020, pp. 298–307. ᴜʀʟ: https://proceedings.mlr.press/v120/khoda yi-mehr20a.html.

[7] G. Kutyniok, P. Petersen, M. Raslan, and R. Schneider. "A theoretical analysis of deep neural networks and parametric PDEs". In: *Constructive Approximation* (2021), pp. 1–53. ᴅᴏɪ: 10.1007/s00365-021-09551-4.

[8] S. Lanthaler, S. Mishra, and G. E. Karniadakis. "Error estimates for DeepONets: a deep learning framework in infinite dimensions". In: *Transactions of Mathematics and Its Applications* 6.1 (Mar. 2022). ɪssɴ: 2398-4945. ᴅᴏɪ: 10.1093/imatrm/tnac0 01.

[9] M. Raissi, P. Perdikaris, and G. Karniadakis. "Physics-informed neural networks: A deep learning framework for solving forward and inverse problems involving nonlinear partial differential equations". In: *Journal of Computational Physics* 378 (2019), pp. 686–707. ɪssɴ: 0021-9991. ᴅᴏɪ: 10.1016/j.jcp.2018.10.045.

[10] A. Tartakovsky, C. Marrero, P. Perdikaris, G. Tartakovsky, and D. Barajas-Solano. "Learning parameters and constitutive relationships with physics informed deep neural networks". ᴀʀxɪᴠ: 1808.03398. 2018.

[11] Y. Yang and P. Perdikaris. "Adversarial uncertainty quantification in physics-informed neural networks". In: *Journal of Computational Physics* 394 (2019), pp. 136–152. ᴅᴏɪ: 10.1016/j.jcp.2019.05.027.

(In-)stability in nonhomogeneous density fluids

Roberta Bianchini

Istituto per la Applicazioni del Calcolo "M. Picone" (IAC), CNR, Rome, Italy

The following system describes the evolution of non-homogeneous incompressible flows under the influence of gravity:

$$
\begin{aligned}
&\partial_t \rho + \mathbf{u} \cdot \nabla_{\mathbf{x}} \rho + w \partial_z \rho = 0, \\
&\rho\big(\partial_t \mathbf{u} + \mathbf{u} \cdot \nabla_{\mathbf{x}} \mathbf{u} + w \partial_z \mathbf{u}\big) = -\nabla_{\mathbf{x}} P, \\
&\rho\big(\partial_t w + \mathbf{u} \cdot \nabla_{\mathbf{x}} w + w \partial_z w\big) = -\partial_z P - g\rho, \\
&\nabla_{\mathbf{x}} \cdot \mathbf{u} + \partial_z w = 0, \\
&P|_{z=\zeta} = P_{\text{atm}}, \quad w|_{z=-H} = 0.
\end{aligned}
\tag{6.1}
$$

Here, t denotes time, and $(\mathbf{x}, z)$ are horizontal and vertical spatial coordinates. The operators $\nabla_{\mathbf{x}}, \nabla_{\mathbf{x}}\cdot$, and $\Delta_{\mathbf{x}}$ represent the gradient, divergence, and Laplacian with respect to $\mathbf{x}$, respectively. The unknowns are the velocity field $(\mathbf{u}, w) \in \mathbb{R}^2 \times \mathbb{R}$ (horizontal and vertical components), the density $\rho > 0$, and the pressure $P \in \mathbb{R}$, all depending on $(t, \mathbf{x}, z)$. In general, the spatial domain Ω_t is bounded by a free surface:

$$
\Omega_t = \{(\mathbf{x}, z) : \mathbf{x} \in \mathbb{R}^2, -H < z < \zeta(t, \mathbf{x})\},
$$

where H is the resting depth, and the free surface $\zeta(t, \mathbf{x})$ evolves according to the kinematic boundary condition

$$
\partial_t \zeta + \mathbf{u}|_{z=\zeta} \cdot \nabla_{\mathbf{x}} \zeta - w|_{z=\zeta} = 0,
$$

which ensures that fluid particles remain on the surface. The gravitational field is assumed constant and vertical, with $g > 0$ denoting the acceleration due to gravity. The atmospheric pressure at the surface is given by $P|_{z=\zeta} = P_{\text{atm}}$. In shallow water flows, particularly in coastal oceanography (see [5]), where the depth is much smaller than the horizontal scale, inertial terms in the vertical momentum equation can be neglected. In this regime, the pressure P approximately satisfies the hydrostatic balance law:

$$
\partial_z P + g\rho = 0.
\tag{6.2}
$$

Replacing the vertical momentum equation with the hydrostatic balance law (6.2) yields

the *hydrostatic equations*:

$$\partial_t \rho + \mathbf{u} \cdot \nabla_{\mathbf{x}} \rho + w \partial_z \rho = 0,$$

$$\rho\big(\partial_t \mathbf{u} + \mathbf{u} \cdot \nabla_{\mathbf{x}} \mathbf{u} + w \partial_z \mathbf{u}\big) = -\nabla_{\mathbf{x}} P,$$

$$\partial_t \zeta + \mathbf{u}|_{z=\zeta} \cdot \nabla_{\mathbf{x}} \zeta - w|_{z=\zeta} = 0,$$

$$\nabla_{\mathbf{x}} \cdot \mathbf{u} + \partial_z w = 0,$$

$$P = P_{\text{atm}} + g \int_z^\zeta \rho(z', \cdot)\, dz', \quad w = -\int_{-H}^z \nabla_{\mathbf{x}} \cdot \mathbf{u}(z', \cdot)\, dz'.$$

$$(6.3)$$

In this hydrostatic regime, there is no explicit evolution equation for the vertical velocity, which must instead be derived from the incompressibility condition. This aspect is central to the mathematical challenges encountered in the hydrostatic limit. Additionally, there is a strong connection to the inviscid primitive equations, as discussed in [4]. The *hydrostatic approximation* can be further clarified by introducing the non-dimensional *shallowness parameter* $\varepsilon^2 := \frac{H^2}{L^2}$, which represents the ratio of the depth H to the typical horizontal scale L, with $L \gg H$ or $0 < \varepsilon \ll 1$, and the dimensionless quantities:

$$\tilde{x} := \frac{x}{L}, \; \tilde{z} := \frac{z}{H}, \; \tilde{t} := \frac{\sqrt{gH}}{L} t, \; \tilde{\mathbf{u}} := \frac{\mathbf{u}}{\sqrt{gH}}, \; \tilde{w} := \frac{L}{H} \frac{w}{\sqrt{gH}}, \; \tilde{P} := \frac{P}{gH}, \; \tilde{\zeta} := \frac{\zeta}{H},$$

so that, dropping the tildes, Eqs. (6.1) become

$$\partial_t \rho + \mathbf{u} \cdot \nabla_{\mathbf{x}} \rho + w \partial_z \rho = 0,$$

$$\rho\big(\partial_t \mathbf{u} + \mathbf{u} \cdot \nabla_{\mathbf{x}} \mathbf{u} + w \partial_z \mathbf{u}\big) = -\nabla_{\mathbf{x}} P,$$

$$\varepsilon^2 \rho\big(\partial_t w + \mathbf{u} \cdot \nabla_{\mathbf{x}} w + w \partial_z w\big) = -\partial_z P - \rho,$$

$$\partial_t \zeta + \mathbf{u}|_{z=\zeta} \cdot \nabla_{\mathbf{x}} \zeta - w|_{z=\zeta} = 0,$$

$$\nabla_{\mathbf{x}} \cdot \mathbf{u} + \partial_z w = 0,$$

with the boundary conditions

$$P|_{z=\zeta} = P_{\text{atm}}, \quad w|_{z=-1} = 0.$$

Heuristically, taking the limit $\varepsilon \to 0$ leads to Eq. (6.2) and thus to the *hydrostatic equations* (6.3). This limit can be understood as a long-wave asymptotic and is also related to the long-time dynamics of the original system (6.1).

Mathematically, the main challenges are the study of the well-posedness of the limiting system (6.3) and its rigorous derivation as $\varepsilon \to 0$. Recently, a proof of well-posedness with isopycnal diffusivity or Gent-McWilliams correctors [3], establishing the validity of the hydrostatic (or shallow water) approximation, has been provided in [2]. On the other hand, in the fully inviscid and non-diffusive regime, an explicit steady state has been identified that is unstable according to the Miles-Howard criterion, allowing the breakdown of the hydrostatic limit to be proven. This leads to the generic ill-posedness of the limiting hydrostatic equations in finite regularity spaces, as shown in [1].

References

[1]   R. Bianchini, M. Coti Zelati, and L. Ertzbischoff. "Ill-posedness of the hydrostatic Euler-Boussinesq equations and failure of hydrostatic limit". ARXIV: 2403 . 17857. 2024.

[2]   R. Bianchini and V. Duchêne. "On the hydrostatic limit of stably stratified fluids with isopycnal diffusivity". In: *Comm. Partial Differential Equations* in press (2024). ARXIV: 2206 . 01058.

[3]   P. R. Gent and J.-C. McWilliams. "Isopycnal mixing in ocean circulation models". In: *J. Phys. Oceanogr.* 1 (1990), pp. 591–609.

[4]   S. M. Griffies. *Fundamentals of ocean climate models*. With a foreword by Trevor J. McDougall. Princeton University Press, Princeton, NJ, 2004, pp. xxxiv+518. ISBN: 0-691-11892-2.

[5]   D. Lannes. "Modeling shallow water waves". In: *Nonlinearity* 33.5 (2020), R1–R57. ISSN: 0951-7715. DOI: 10 . 1088/1361–6544/ab6c7c.

Smooth Splines on Triangulations

Carla Manni

Department of Mathematics, University of Rome Tor Vergata, Italy

Splines are ubiquitous in a wide range of contexts such as geometric modeling, signal processing, data analysis, visualization, and solution of partial differential equations by the finite-element method, including the isogeometric analysis paradigm. In the classical sense of the term, splines are piecewise functions consisting of polynomial pieces glued together smoothly by imposing equality of derivatives up to a given order. For many applications, a high smooth join between the different pieces is beneficial or even required.

In the univariate case, splines of maximal smoothness, i.e., piecewise polynomials of degree d with C^{d-1} joins, are probably the best known and most used splines [7]. Tensor-product splines are the simplest and most well-known multivariate spline functions. Their tensor structure, however, is a severe weakness as it hinders adequate local refinement. Splines on triangulations emerge as the natural and most powerful bivariate extension of univariate splines.

The space of splines of degree d and smoothness r over a triangulation $\mathcal{T}$ of a domain Ω is

$$\mathbb{S}_d^r(\mathcal{T}) := \{ s \in C^r(\Omega) : s\big|_\Delta \in \mathbb{P}_d, \ \forall \Delta \in \mathcal{T} \}, \quad 0 \le r < d,$$

where Δ denotes any triangle of $\mathcal{T}$ and $\mathbb{P}_d$ stands for the space of bivariate polynomials of degree up to d. Dealing with highly smooth splines on triangulations is an arduous task. Splines with too low degree compared to the smoothness are exposed to several shortcomings: they may lack a stable dimension, optimal approximation power, and stable locally supported bases. In addition, the practical wish of constructing any function of the spline space locally on each of the elements of the partition may require a significant gap between the degree and the smoothness. For instance, on a general triangulation a degree $d \ge 4r + 1$ is necessary to admit such a local construction [1, 6, 14].

The above drawbacks can be mitigated by considering a so-called *macro-structure*, where each triangle Δ of $\mathcal{T}$ is further refined in a specific manner (often referred to as *split*). The most famous examples are the Clough–Tocher split [1, 2, 6, 12] and the Powell–Sabin 6 and 12 splits [6, 11, 12]. They subdivide each triangle of $\mathcal{T}$ into 3, 6, and 12 subtriangles, respectively. Nevertheless, no spline spaces of maximal smoothness $r = d - 1$ can be constructed over general triangulations with the above mentioned splits for degree $d > 2$; see, e.g., [6].

In [13], Wang and Shi introduced a family of degree-dependent splitting schemes to refine any triangle Δ of a given triangulation. The split of degree d is obtained by uniformly distributing $d + 1$ points on each edge of Δ and by taking the complete graph connecting these boundary points. For $d = 1$ we have no split and for $d = 2$ the Wang–Shi (WS)
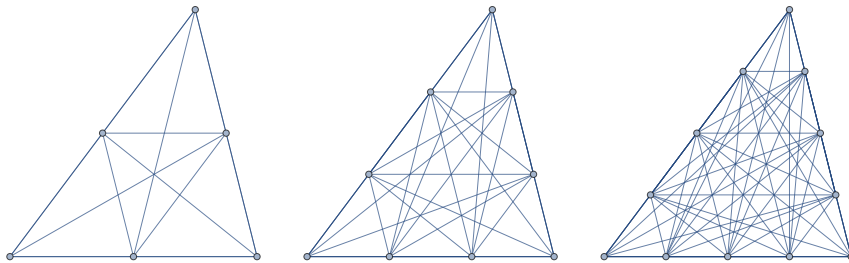
Figure 7.1: WS splits of degree d for $d = 2, 3, 4$.

split reduces to the Powell–Sabin 12 split; see Figure 7.1. Contrarily to the well-known splits mentioned above, when d increases, the family of WS splits generates a very large number of polygonal pieces in each triangle of $\mathcal{T}$. For cubics we get a set of 75 polygons which includes triangles, quadrilaterals, and pentagons while for quartics the split consists of 250 polygonal regions; see Figure 7.1.

Thanks the very articulated geometry of the split, the cubic/quartic WS splits allow us to locally construct C^2 cubic / C^3 quartic spline spaces on general triangulations. On the other hand, this complex geometry hampers a piecewise treatment – in terms of a local polynomial basis – of spline functions on WS splits and makes imperative to produce a basis for the local spline space over each refined triangle Δ of $\mathcal{T}$ that intrinsically avoids the need of dealing with separate polynomial representations on each of the numerous polygonal subelements of Δ. Due to the complete graph structure of the WS split, a basis formed by simplex splines emerges as the natural solution to the problem [10].

Simplex spline bases for the local spaces of C^2 cubics and of C^3 quartics on the corresponding WS splits of any triangle in $\mathcal{T}$ have been presented in [8, 9]. Such bases behave like a B-spline basis within each triangle of $\mathcal{T}$ and like a Bernstein basis for imposing smoothness across the edges of $\mathcal{T}$. More precisely, the basis functions form a nonnegative partition of unity, inherit recurrence relations and differentiation formulas from the simplex spline structure, and enjoy a Marsden-like identity for the representation of cubic and quartic polynomials respectively. Moreover, they admit simple conditions for C^r joins $r = 2, 3$ to neighboring triangles in $\mathcal{T}$ and a control net can be set up that mimics the shape of the spline function. A simplex spline basis for C^1 quadratic splines on the Powell–Sabin 12 split has been considered in [3]. The local representation in terms of such simplex spline bases makes that the complex geometry of the WS split is transparent to the user, offering a pathway for effective use of the related spline space.

In this talk, we review the main issues concerning construction, and efficient representations in terms of proper bases, of highly smooth splines on general triangulations where each element is refined according to the WS split [8, 9] and we briefly discuss some applications of these splines spaces [5] in the context of Isogeometric Analysis [4], a successful paradigm for the numerical discretization of differential problems.

References

[1]   P. G. Ciarlet. *The Finite Element Method for Elliptic Problems*. Vol. 40. Classics in Applied Mathematics. Society for Industrial and Applied Mathematics (SIAM), 2002.

[2]   R. W. Clough and J. L. Tocher. "Finite element stiffness matrices for analysis of plates in bending". In: *Proceedings of the Conference on Matrix Methods in Structural Mechanics*. Wright-Patterson Air Force Base, 1965, pp. 515–545.

[3]   E. Cohen, T. Lyche, and R. F. Riesenfeld. "A B-spline-like basis for the Powell–Sabin 12-split based on simplex splines". In: *Math. Comp.* 82 (2013), pp. 1667–1707.

[4]   J. A. Cottrell, T. J. R. Hughes, and Y. Bazilevs. *Isogeometric Analysis: Toward Integration of CAD and FEA*. Wiley Publishing, 2009.

[5]   S. Eddargani, T. Lyche, C. Manni, and H. Speleers. "Quadrature rules for C^1 quadratic spline finite elements on the Powell–Sabin 12-split". In: *Comput. Methods Appl. Mech. Eng.* 430 (2024), p. 117196.

[6]   M.-J. Lai and L. L. Schumaker. *Spline Functions on Triangulations*. Vol. 110. Encyclopedia of Mathematics and its Applications. Cambridge University Press, 2007.

[7]   T. Lyche, C. Manni, and H. Speleers. "Foundations of spline theory: B-splines, spline approximation, and hierarchical refinement". In: *Splines and PDEs: From Approximation Theory to Numerical Linear Algebra*. Ed. by T. Lyche, C. Manni, and H. Speleers. Lecture Notes in Mathematics 2219, Springer Cham, 2018, pp. 1–76.

[8]   T. Lyche, C. Manni, and H. Speleers. "Construction of C^2 cubic splines on arbitrary triangulations". In: *Found. Comput. Math.* 22 (2022), pp. 1309–1350.

[9]   T. Lyche, C. Manni, and H. Speleers. "A local simplex spline basis for C^3 quartic splines on arbitrary triangulations". In: *Appl. Math. Comput.* 462 (2024), p. 128330.

[10] C. A. Micchelli. "On a numerically efficient method for computing multivariate B-splines". In: *Multivariate Approximation Theory*. Ed. by W. Schempp and K. Zeller. Vol. 51. Internat. Ser. Numer. Math. Birkhäuser, 1979, pp. 211–248.

[11] M. J. D. Powell and M. A. Sabin. "Piecewise quadratic approximations on triangles". In: *ACM Trans. Math. Software* 3 (1977), pp. 316–325.

[12] P. Sablonnière. "Composite finite elements of class C^k". In: *J. Comput. Appl. Math.* 12–13 (1985), pp. 541–550.

[13] R.-H. Wang and X.-Q. Shi. "$S_{\mu+1}^{\mu}$ surface interpolations over triangulations". In: *Approximation, Optimization and Computing: Theory and Applications*. Ed. by A. G. Law and C. L. Wang. Elsevier Science Publishers B.V., 1990, pp. 205–208.

[14] A. Ženíšek. "A general theorem on triangular finite $C^{(m)}$-elements". In: *Rev. Française Automat. Informat. Recherche Opérationnelle Sér. Rouge* 8 (1974).

A Systematization of the Wagner Framework: Graph Theory Conjectures and Reinforcement Learning

Flora Angileri, Giulia Lombardi, Andrea Fois, Renato Faraone, Carlo Metta, Michele Salvi, Luigi Amedeo Bianchi, Marco Fantozzi, Silvia Giulia Galfrè, Daniele Pavesi, Maurizio Parton*, Francesco Morandin

CuriosAI research group, University of Chieti-Pescara

In 2021, Adam Zsolt Wagner proposed an approach to disprove conjectures in graph theory using Reinforcement Learning (RL) [2]. Wagner frames a conjecture as $f(G) < 0$ for every graph G, for a certain invariant f; one can then play a single-player graph-building game, where at each turn the player decides whether to add an edge or not. The game ends when all edges have been considered, resulting in a certain graph G_T, and $f(G_T)$ is the final score of the game; RL is then used to maximize this score. This brilliant idea is as simple as innovative, and it lends itself to systematic generalization. Several different single-player graph-building games can be employed, along with various RL algorithms. Moreover, RL maximizes the cumulative reward, allowing for step-by-step rewards instead of a single final score, provided the final cumulative reward represents the quantity of interest $f(G_T)$. In this abstract, we briefly present three distinct single-player "build your graph" games: Linear, Local, Global. Each game employs both a step-by-step reward system and a single final score. The games have been implemented as environments in the Gymnasium framework, and along with the dataset and a simple interface to play with the environments, are available at `https://github.com/CuriosAI/graph_conjectures`.

All games are played on undirected graphs with a fixed number n of nodes, and without multiple edges. The environments are parametric with respect to several aspects: for instance, one can choose the starting graph, or whether to enforce the agent excluding self-loops.

Linear

Linear is a variation of the game used by Wagner. The name comes from the state's vector internal representation. In Linear, edges are ordered, and then at each time t the agent can choose between leaving the edge number t as it is (i.e. passing it), or flipping it. The Edge-flipping operation (as defined in [1]) changes the state of an edge like a boolean *not* operator, as follows: let $e \in \{0, 1\}$ be the single bit representing the edge, then

$$flip(e) = \begin{cases} 1 & \text{if } e = 0 \\ 0 & \text{otherwise} \end{cases}$$

The state is given by the graph and the current time t, and the action space is $\{0, 1\}$, where 0 means that the current edge is left unchanged, and 1 that the edge is flipped.

With its default values, Linear differs from Wagner's game for the ordering of the edges: in Wagner's game, edges are numbered by forming and expanding cliques first, that is, $(1, 2), (1, 3), (2, 3), (1, 4), \ldots$, while in Linear is given by $(1, 2), (1, 3), \ldots, (1, n), (2, 3), \ldots$. Moreover, Wagner starts from the empty graph, while the default setting in our games is to start from the complete graph. Episodes in Linear always end at time $T = \frac{n(n-1)}{2}$, if self-loops are not allowed, and at time $T = \frac{n(n+1)}{2}$, otherwise.

Local

In Local, the agent explores the graph space by moving from one node to another. When moving from node i to node j, the agent has the option either to flip the edge (i, j) or to pass it. This ensures that from node i, the agent's actions are "locally" confined, impacting only the directly connected edge (i, j). Note that this is different from Linear, because the agent can choose any node j to move to. The state is given by the current graph, the current node i where the agent is located, and the current time. An action is given by a target node j to move to from node i, and a binary value $\{0, 1\}$, where 0 means taking no action, and 1 means flipping the edge (i, j). In our implementation, this action logic is represented by a single integer value k within the range $[0, 2n - 1]$ where n is the number of nodes. Assuming to start from node i, if $k \in [0, n - 1]$, we move to node $j = k$ without taking any action on edge (i, j). If $k \in [n, 2n - 1]$, we move to node $j = k$ mod n, and the edge (i, j) is flipped. Episodes in Local end at a termination time T that can be passed as optional input when the game is initialized, and defaults to $T = \frac{n(n-1)}{2}$, if self-loops are not allowed, and to $T = \frac{n(n+1)}{2}$, otherwise.

Global

In Global, the agent explores the graph space by acting on any edge across the entire graph at any time. The agent can choose any edge to act upon, deciding either to flip it or to pass it. This "global" approach ensures that the agent's actions are not confined to its immediate location, allowing interaction with any part of the graph. Episodes end at a termination time T that can be given as input at game's initialization, with same Local defaults. Similar to Local, the possibility to pass on an action without flipping an edge is maintained, because it helps mitigate the risk of choosing a wrong termination time for the game. For instance, if flipping were mandatory, excessively long matches could potentially disrupt an optimal configuration previously achieved. Allowing the passing of actions enables the agent to maintain an optimal configuration indefinitely. The state is given by the current graph, and the current time. An action is given by a target edge, and a binary value $\{0, 1\}$, where 0 means taking no action, and 1 means flipping the edge. In our implementation, the action logic is similar to that seen in Local, but generalized to handle global movements along the graph. Here, the action is represented by a single integer value k within the range $[0, 2m - 1]$, where m is the number of edges. If $k \in [0, m - 1]$, edge (i, j), where $i = \lfloor \frac{k}{n} \rfloor$ and $j = k$ mod m, remains unchanged. If $k \in [m, 2m - 1]$, edge (i, j), where $i = \lfloor \frac{k-m}{n} \rfloor$ and $j = k$ mod m is flipped.

References

[1] A. Mehrabian et al. *Finding Increasingly Large Extremal Graphs with AlphaZero and Tabu Search*. NeurIPS 2023 MATH-AI workshop. ARXIV: 2311.03583. 2023.

[2] A. Z. Wagner. *Constructions in combinatorics via neural networks*. ARXIV: 2104.14516. 2021.

A general framework of implicit high-order schemes for hyperbolic systems

Gabriella Puppo[a], Matteo Semplice[b], and Giuseppe Visconti[a,*]
[a] Department of Mathematics, Sapienza University of Rome
[b] Dipartimento di Scienza e Alta Tecnologia, Università degli Studi dell'Insubria, Italy

In this talk, we consider systems of $m \geq 1$ hyperbolic conservation laws:

$$\frac{\partial}{\partial t}\mathbf{u}(x,t) + \frac{\partial}{\partial x}\mathbf{f}(\mathbf{u}(x,t)) = \mathbf{o}, \tag{9.1}$$

where, $\mathbf{u} : \mathbb{R} \times \mathbb{R}_0^+ \to \mathbb{R}^m$ is the quantity of interest, and $\mathbf{f} : \mathbb{R}^m \to \mathbb{R}^m$ is the vector of the flux functions. System (9.1) is hyperbolic when the eigenvalues $\{\lambda_j(\mathbf{u}(x,t))\}_{j=1}^m$ of the associated Jacobian matrix are real and determine a complete set of eigenvectors. Phenomena governed by hyperbolic conservation laws often exhibit multiple scales, which are associated with the eigenvalues of the Jacobian of the flux function. Specifically, one has $\frac{\max_{j=1,\ldots,m}|\lambda_j(\mathbf{u})|}{\min_{j=1,\ldots,m}|\lambda_j(\mathbf{u})|} \gg 1$. In this case, we say that the system is stiff.

Numerical methods for solving hyperbolic problems are frequently explicit, as these methods are capable of resolving all relevant scales in many applications. For example, in gas-dynamics, explicit methods can accurately capture both convective and acoustic waves. However, integrating a system of hyperbolic equations with an explicit numerical scheme requires choosing the time-step as $\Delta t = \min(\Delta t_{\text{acc}}, \Delta t_{\text{stab}})$, where Δt_{acc} is determined by accuracy constraints, and Δt_{stab} is constrained by the stability condition, which is related to the inverse of the fastest scale in the system. Therefore, the stability requirements of explicit methods can become overly restrictive, i.e. $\Delta t_{\text{stab}} \ll \Delta t_{\text{acc}}$, when fast acoustic waves are present. In such scenarios, implicit methods become appealing, as they are not constrained by stability conditions and thus allow for larger time-steps despite requiring more computational effort per step.

Another cornerstone for the numerical integration of (9.1) is achieving high-order. First-order schemes are entirely linear, with the only non-linearity stemming from the non-linear flux function, which is inherent to the model's physical structure and thus unavoidable. However, these schemes tend to produce significant dissipation errors. To enhance the accuracy of the scheme, it is essential to employ higher-order methods, which involve piecewise polynomial reconstructions in space and a corresponding high-order time integration method. Although high-order schemes can address the low resolution of first-order methods, they typically necessitate the use of spatial limiting to prevent spurious oscillations. This spatial limiting process introduces additional significant non-linearity, which becomes a computational challenge, particularly when using implicit methods due to the large nonlinear systems that must be solved at each time-step.

We are concerned with the challenges of developing efficient high-order implicit sche-

mes for stiff hyperbolic systems. The key idea is to remain as linear as possible while avoiding spurious oscillations, even with large time-steps.

In our proposed approach [5, 6, 8], we initially apply implicit integration using the backward Euler method with a piecewise constant reconstruction. This step generates an initial estimate of the solution at a given time t, which we refer to as the predictor $\mathbf{u}^\star(t)$. It is well established that the backward Euler method, when combined with piecewise constant reconstruction, produces a solution that is unconditionally stable and TVD. As a result, the predictor inherits these properties. However, this approach also leads to a solution that is highly diffusive, as discussed above. In this talk, to enhance the accuracy avoiding spurious oscillations, we propose to pre-compute the non-linearity of the space-limiting procedure of the high-order scheme using the predictor. In this way, the resulting implicit scheme is nonlinear only because of the non-linearity of the flux function.

So far, this approach has been tailored to the third-order implicit finite volume approximation. Specifically, we adopt a third-order Diagonally Implicit Runge-Kutta (DIRK) for the time-integration and the CWENO reconstruction in [7] for the space approximation. CWENO constructs a local polynomial within each cell

$$R_j(x; t) = \sum_{\ell \in \mathcal{S}} \omega_{j+\ell}(\mathbf{u}_{\mathcal{S}}(t)) \mathbf{u}_{j+\ell}(t).$$

Here, j represents a general spatial cell, while $\mathcal{S}$ defines the stencil centered on cell j, which is used for reconstruction. The variable $\mathbf{u}_{\mathcal{S}}$ encompasses all the data within the stencil associated with the j-th cell, and $\mathbf{u}_{j+\ell}(t)$ represents the solution being determined at time t. The nonlinear weights $\omega_{j+\ell}$ are calculated by assessing the local smoothness of the solution based on the data $\mathbf{u}_{\mathcal{S}}$ contained within the stencil of the j-th cell. By using the predictor to estimate the nonlinear weights, the reconstruction becomes

$$R_j(x; t) = \sum_{\ell \in \mathcal{S}} \omega_{j+\ell}(\mathbf{u}_{\mathcal{S}}^\star(t)) \mathbf{u}_{j+\ell}(t).$$

In this approach, the weights are determined using information from the predictor at the correct time level, ensuring that the reconstruction remains linear in relation to the solution being computed. Following this, a high-order implicit time integrator, such as a DIRK method, is applied. The resulting solution is both high-order accurate and free from spatial oscillations, while retaining linearity for linear problems. Any non-linearity in the solution arises solely from the non-linearity inherent in the flux function.

Even with spatial limiting, spurious oscillations can still occur during implicit integration, particularly at high Courant numbers. To mitigate these oscillations in implicit time integration - where large time-steps can cause waves to traverse multiple adjacent cells in a single step - we consider the application of time-limiting techniques. Specifically, flux-based conservative time-limiting methods, inspired by the MOOD approach [1, 2], are utilized. These methods replace the high-order numerical fluxes at the interfaces of problematic cells with low-order fluxes, using the numerical entropy production error [3, 4] as an indicator of non-smooth regions in the solution.

Several numerical results on the nonlinear Euler equations of gas dynamics are presented.

References

[1]   S. Clain, S. Diot, and R. Loubère. "A high-order finite volume method for hyperbolic systems: Multi-dimensional Optimal Order Detection (MOOD)". In: *J. Comput. Phys.* 230.10 (2011), pp. 4028–4050.

[2]   S. Clain, S. Diot, and R. Loubère. "Improved Detection Criteria for the Multi-dimensional Optimal Order Detection MOOD on unstructured meshes with very high-order polynomials". In: *Comp. & Fluids* 64 (2012), pp. 43–63.

[3]   G. Puppo. "Numerical entropy production for central schemes". In: *SIAM J. Sci. Comput.* 25.4 (2004), pp. 1382–1415.

[4]   G. Puppo and M. Semplice. "Numerical entropy and adaptivity for finite volume schemes". In: *Comm. Computat. Phys.* 10.5 (2011), pp. 1132–1160.

[5]   G. Puppo, M. Semplice, and G. Visconti. "Quinpi: Integrating conservation laws with CWENO implicit methods". In: *Comm. Appl. Math. & Comput.* 5 (2023), pp. 343–369.

[6]   G. Puppo, M. Semplice, and G. Visconti. "Quinpi: Integrating stiff hyperbolic systems with implicit high order finite volume schemes". In: *Comm. Computat. Phys.* 36.1 (2024), pp. 30–70.

[7]   M. Semplice, E. Travaglia, and G. Puppo. "One- and Multi-dimensional CWENOZ Reconstructions for Implementing Boundary Conditions Without Ghost Cells". In: *Comm. Appl. Math. & Comput.* 5 (2023), pp. 143–169.

[8]   G. Visconti, S. Tozza, M. Semplice, and G. Puppo. "A conservative a-posteriori time-limiting procedure in Quinpi schemes". In: *Advances in Numerical Methods for Hyperbolic Balance Laws and Related Problems. YR 2021.* Ed. by G. Albi, W. Boscheri, and M. Zanella. Vol. 32. SEMA-SIMAI Springer Series. Springer Cham, 2023, pp. 191–212.

Long Presentations

Point cloud generation algorithm for 3D domains in B-Rep format

Bruno Degli Esposti
University of Florence

Despite great advances in mesh generation algorithms, one of the most challenging and time consuming parts of mesh-based numerical simulation on geometrically complex 3D domains remains to this day the generation and management of meshes [4]. An increasingly popular alternative approach to numerical simulation that avoids the issue of mesh generation entirely is that of *meshless* (or *meshfree*) methods, in which approximations of unknown functions are determined exclusively from pointwise values at a scattered set of nodes. The step of mesh generation is replaced by the generation of a point cloud, and this provides a strong motivation for studying robust and efficient ways of generating scattered nodes with prescribed density over arbitrary domains in $\mathbb{R}^3$ [10].

Although the topic of point cloud generation has been an active area of research for more than 20 years [5], interest has recently grown, as demonstrated by three different algorithms being published by distinct research groups in the last five years, along with corresponding open source implementations [3, 7, 8].

All three algorithms can handle 3D geometries and are based on the advancing front method, which works in two stages. First, a set of nodes is placed on the boundary of the domain, and outward-pointing surface normal vectors are computed at these points. Second, boundary points act as an initial front, and the front is advanced towards the interior of the domain, in the direction opposite to the normal vectors. Newly generated interior points are used as sources to create another set of interior points, until the whole domain is filled. A local node spacing function is used when generating new nodes, and also when rejecting nodes based on their distance to nearest neighbour, so that in the end a node distribution with a prescribed density is obtained.

Traditional Computer-Aided Engineering workflows rely on simulations on meshes generated from CAD geometries, and the standard format in CAD is boundary representation (B-Rep). From a mathematical point of view, a B-Rep is the description of the boundary of a 3D domain as a finite union of parametric surfaces called *patches*, along with connectivity information and trimming curves in the parametric domain of each patch. Trimming curves are closed simple curves that enclose regions in parametric space whose image in 3D space is excluded from the patch, and, hence, from the boundary of the domain. Trimming is treated by all CAD kernels as one of the most fundamental operations that allows the construction of complex geometries, although its use comes at a price, such as the introduction of small gaps and overlaps between patches caused by the inevitable approximation of trimming curves [6].

To this day, only commercial software packages for meshless simulations provide ad-

vancing front methods on B-Rep geometries, and no detailed studies have been published on this subject [10]. On the contrary, the problem of mesh generation from CAD geometries has been studied extensively, and today mature open source software exists for this task, such as `gmsh` [2]. This is the reason why, even today, a large share of meshless literature paradoxically uses the vertices of a mesh as the point cloud for meshless methods, and this can lead to the misconception that point cloud generation is as computationally intensive and algorithmically complex as mesh generation, even though meshless advancing front algorithms are an order of magnitude faster than advancing front mesh generation algorithms [5].

In this talk, we aim to bridge the gap in literature and algorithms by describing a variable density advancing front method specifically designed for domains in $\mathbb{R}^3$ in B-Rep format. Our work overcomes two key issues.

First, nodes must be placed on the boundary of a domain taking trimming into account. Rather than generating nodes over the whole parametric domain of each patch and discarding nodes enclosed by trimming curves, we propose to generate nodes in parametric space with a 2D advancing front algorithm, using equispaced nodes on trimming curves as the boundary nodes for this inner advancing front algorithm. The image of interior nodes produced by the 2D advancing front algorithm will then contribute to the set of boundary nodes for the 3D advancing front algorithm.

Second, generation of interior nodes for an advancing front algorithm requires a containment query to check whether newly generated points belong to the domain or not. Although containment queries can be answered exactly (up to machine precision) using ray casting or generalised winding number algorithms, such methods are impractical in this setting because of their high computational cost (although it could be reduced, see [9] for the case of 2D domains). Instead, a cheaper containment check based on normal vectors orientation and nearest-neighbour boundary node search is usually employed, although this technique is only accurate to first order and can sometimes lead to points being generated outside of the domain.

We propose a more robust first-order containment query that prevents artefacts in the generation of points near sharp features of the domain's boundary caused by incorrect advancement of the point cloud front. We remark that point clouds generated by advancing front methods using approximate containment queries do not limit the order of convergence of meshless numerical methods.

Our implementation consists of a C++ library, along with a MATLAB interface, and builds upon the advancing front algorithm described in [1]. The necessary tools to work with domains in B-Rep format are provided by the Open CASCADE CAD kernel. The effectiveness of our node generation algorithm is demonstrated by numerical experiments such as the solution of partial differential equations on 3D geometries in B-Rep format using a meshless method.

References

[1] U. Duh, G. Kosec, and J. Slak. "Fast variable density node generation on parametric surfaces with application to mesh-free methods". In: *SIAM Journal on Scientific Computing* 43.2 (2021), A980–A1000.

[2] C. Geuzaine and J.-F. Remacle. "Gmsh: A 3-D finite element mesh generator with built-in pre-and post-processing facilities". In: *International journal for numerical methods in engineering* 79.11 (2009), pp. 1309–1331.

[3] Jožef Stefan Institute. *Medusa*. 2021. URL: https://gitlab.com/e62Lab/medusa.

[4] G.-R. Liu and Y.-T. Gu. *An introduction to meshfree methods and their programming*. Springer Science & Business Media, 2005.

[5] R. Löhner and E. Onate. "An advancing front point generation technique". In: *Communications in numerical methods in engineering* 14.12 (1998), pp. 1097–1108.

[6] B. Marussig and T. J. Hughes. "A review of trimming in isogeometric analysis: challenges, data exchange and simulation aspects". In: *Archives of computational methods in engineering* 25 (2018), pp. 1059–1127.

[7] P. Negi and P. Ramachandran. *SPHGeom*. 2019. URL: https://gitlab.com/pypr/sph_geom.

[8] K. van der Sande. *Node generation*. 2019. URL: https://github.com/kierav/node_generation.

[9] A. Sommariva and M. Vianello. "inRS: implementing the indicator function of NURBS-shaped planar domains". In: *Applied Mathematics Letters* 130 (2022), p. 108026.

[10] P. Suchde, T. Jacquemin, and O. Davydov. "Point cloud generation for meshfree methods: An overview". In: *Archives of Computational Methods in Engineering* 30.2 (2023), pp. 889–915.

The VERSE platform: eXtended Reality in Education

Chiara Lucifora[a,b]
[a] Department of Philosophy, University of Bologna, Italy
[b] Institute of Cognitive Sciences and Technologies (ICST), CNR, Rome, Italy

Extended Reality (XR) is a broad term that refers to technologies capable of extending the boundaries of the real world. Amongst the most used XR technologies we find [8] (i) Virtual Reality (VR), which comprises a fully artificial environment where users can interact with 3D objects, and (ii) Augmented Reality (AR), which is a partially artificial environment that overlays virtual objects onto the real world. Such technologies promise important advantages capable of revolutionizing many scientific fields [3].

Concerning education, VR and AR technologies have been increasingly adopted to enhance student learning [5]. For instance, the study of mathematics has received important benefits from VR technologies, as it enables the transformation of abstract concept into tangible and interactive elements [11]. In this context, Su *et al.* [12] conducted a study with 40 students using immersive technologies to learn basic geometry concepts; results showed that virtual reality technologies improve students' learning motivation and learning performance. Similarly, Hwang and Hu [6] found that collaborative learning in VR improved the learning of geometric concepts compared to traditional learning. In the field of medical education, XR allows students "to do" activities rather than "to observe" activities [11]. For example, Schwaab *et al.* [10] used VR to study emergency medicine; the authors designed a virtual examination room in which students could treat virtual patients (avatars) while being monitored by teachers remotely in real time: The results showed that students defined the VR system as easy to use, pleasant, realistic, and efficient. In the field of industrial education, XR enhance learning by enabling experiences that are not feasible in the real world [11]. As an example, Abichandani *et al.* [2] designed a virtual wind farm to facilitate education on wind energy where students can modify the parameters of the wind turbines to study the corresponding effect on the environment.

Today, numerous AR/VR commercial applications are available to support students in the learning process [12]: ClassVR and GeoGebra mixed reality are some example, to cite a few. In this context, the VERSE project [4] stands out as an innovative educational software platform, designed for on-life teaching using XR technologies. Using a multi-platform system, VERSE promotes collaborative learning creating joint environments that support students and teachers in their educational process. Leveraging on cutting-edge technologies and gamification strategies, VERSE aims to revolutionise the educational experience by providing an engaging, immersive, and personalised learning environment.

The Verse Platform

VERSE is at the forefront of educational innovation, being the first software to seamlessly integrate 2D mathematics labs that use gaming mechanics to present students with engaging, game-like challenges. These labs are designed to make mathematical problem-solving not only more accessible but also enjoyable, transforming traditional exercises into dynamic experiences that captivate students' attention. In addition to the 2D labs, VERSE offers a 3D ARENA mode, which elevates the learning experience by creating immersive mathematics activities. These activities are enhanced by conversational avatars, powered by advanced CONVAI technology, which interact with students in real-time, providing personalised guidance and feedback. VERSE encourages active learning by placing students in the centre of the educational process. Through the use of interactive avatars and immersive environments, students are not merely recipients of information but active participants in their learning journey. Moreover, the collaboration with LABSTER, a leader in STEM education, brings a wealth of expertise in creating virtual laboratories that bridge the gap between theory and practice. The activities offered in VERSE, particularly in the fields of mathematics and physics, are designed to be highly interactive and relevant to real-world applications, making complex scientific concepts more tangible and easier to grasp. One of the most compelling advantages of a software platform like VERSE is its ability to transform the learning of abstract disciplines, such as mathematics and physics, into an interactive and accessible experience. Traditionally, students often struggle with the abstract nature of mathematical formulas, which can be challenging to visualise and comprehend when taught in isolation. However, VERSE addresses this challenge by embedding these concepts within gamified, immersive experiences that make learning both engaging and intuitive.

An example of VERSE gamification Let us consider the study of vectors and scalars, a fundamental concept in physics that is often difficult for students to fully grasp. In a traditional classroom, students would be introduced to the subject through a series of well-known formulas:

$$\|\vec{v}\| = \sqrt{v_x^2 + v_y^2 + v_z^2} \tag{11.1}$$

$$\vec{a} \cdot \vec{b} = a_x b_x + a_y b_y + a_z b_z \tag{11.2}$$

$$\vec{a} \times \vec{b} = (a_y b_z - a_z b_y, a_z b_x - a_x b_z, a_x b_y - a_y b_x) \tag{11.3}$$

While understanding this abstract formula is crucial, the concept can be far more easily figured out when applied in a practical, gamified context. As an example, consider a simulation within VERSE where students are tasked with a space mission to Mars: as part of the mission, they need to navigate the spacecraft by applying their knowledge of vectors. Through this interactive experience, students can directly engage with (11.1) by calculating the magnitude and direction of vectors to determine the correct trajectory for the spacecraft, or they can revise (11.2) and (11.3) to solve a problem related to the spacecraft's rotation.

Conclusion   XR technologies promise significant changes in the educational field, allowing students to learn in a more engaging and enjoyable way [12]. As we highlight in this presentation, there are several advantages to using XR technologies in the educational field, including: (i) enhance the transition from knowledge to competence [1], (ii) access unlimited resources (*e.g.* scientific equipment) that could not be available in the real-world [11], (iii) recreate environments that do not exist or are too dangerous in the real world [1], and (iv) promote high emotional involvement in online learning [9]. Based on these advantages, XR technology can be considered a valid support for education. Immersivity and presence seem to positively influence human emotions [7] which could also improve students' self-esteem, self-efficacy, awareness, and resilience.

References

[1]   E. Abdul Rahim et al. "A desktop virtual reality application for chemical and process engineering education". In: *Proceedings of the 24th Australian computer-human interaction conference*. 2012, pp. 1–8.

[2]   P. Abichandani, W. Fligor, and E. Fromm. "A cloud enabled virtual reality based pedagogical ecosystem for wind energy education". In: *2014 IEEE–FIE*. 2014, pp. 1–7.

[3]   M. Cevikbas, N. Bulut, and G. Kaiser. "Exploring the benefits and drawbacks of AR and VR technologies for learners of mathematics: Recent developments". In: *Systems* 11.5 (2023), p. 244.

[4]   Dotslot s.r.l. *VERSE: Istruzione e Formazione nel Metaverso*. url: verse-edu.com.

[5]   J. H. Graafland. "New technologies and 21st century children: Recent trends and outcomes". In: *OECD Education Working Papers* (2018).

[6]   W.-Y. Hwang and S.-S. Hu. "Analysis of peer learning behaviors using multiple representations in virtual reality and their impacts on geometry problem solving". In: *Computers & Education* 62 (2013), pp. 308–319.

[7]   C. Lucifora, M. Schembri, F. Poggi, G. M. Grasso, and A. Gangemi. "Virtual reality supports perspective taking in cultural heritage interpretation". In: *Computers in Human Behavior* 148 (2023), p. 107911.

[8]   N. B. Milman. "Defining and conceptualizing mixed reality, augmented reality, and virtual reality". In: *Distance Learning* 15.2 (2018), pp. 55–58.

[9]   A. Peña-Ríos, V. Callaghan, M. Gardner, and M. J. Alhaddad. "Remote mixed reality collaborative laboratory activities: Learning activities within the InterReality Portal". In: *2012 IEEE/WIC/ACM WI-IAT*. Vol. 3. IEEE. 2012, pp. 362–366.

[10] J. Schwaab et al. "Using second life virtual simulation environment for mock oral emergency medicine examination". In: *Academic Emergency Medicine* 18.5 (2011).

[11] M. Slater and M. V. Sanchez-Vives. "Enhancing our lives with immersive virtual reality". In: *Frontiers in Robotics and AI* 3 (2016), p. 74.

[12] Y.-S. Su, H.-W. Cheng, and C.-F. Lai. "Study of virtual reality immersive technology enhanced mathematics geometry learning". In: *Frontiers in Psychology* 13 (2022).

Optimal Sensor Placement in Power Transformers Using Physics-Informed Neural Networks

Sirui Li, Federica Bragone, Matthieu Barreau, and Kateryna Morozovska*
KTH Royal Institute of Technology

Our work aims at simulating and predicting the temperature conditions inside a power transformer using Physics-Informed Neural Networks (PINNs). The predictions obtained are then used to determine the optimal placement for temperature sensors inside the transformer, under the constraint of a limited number of sensors, enabling efficient performance monitoring. The method consists of combining PINNs with Mixed Integer Optimization Programming to obtain the optimal temperature reconstruction inside the transformer. First, we introduce a novel approach for the regularization of the PINN model through physical unit scaling. Then, we extend our PINN model for thermal modelling of power transformers to solve the heat diffusion equation from 1D to 2D space. Finally, we construct an optimal sensor placement model inside the transformer that can be applied to problems in 1D and 2D.

According to the working principle of the transformer, its change in temperature can be described as the heat equation of an object with an internal heat source $\mathbf{x}, t \mapsto P_0 + P_k(\mathbf{x}, t)$ where $\mathbf{x} \in \Omega$ is the spatial position and $t \geq 0$ is the time, that is,

$$\frac{1}{\alpha} \frac{\partial T}{\partial t} = \Delta T + \frac{1}{k}[P_0 + P_K(\mathbf{x}, t) - h(T(\mathbf{x}, t) - T_a)],$$

where $\alpha = \frac{k}{c_p \rho}$, T is the temperature of the power transformer, Δ is the Laplacian, P_0 is the load loss. In this work, we assume variable separation for the source term, that is

$$P_K(\mathbf{x}, t) = P_K^t(t) P_K^x(\mathbf{x}), \quad \text{for } \mathbf{x} \in \Omega, t \geq 0$$

In the monitoring and maintenance of power transformer performance, temperature is a key factor. The common method is to use a general model, such as the mineral-oil-immersed transformer model [2, 3] and the thermal circuit model [5, 6, 7], to measure the critical temperature and then to use numerical methods to simulate and analyze the internal temperature of the transformer. However, the computational complexity of numerical methods increases exponentially with the complexity of the model and its accuracy depends on the suitability of the model grid discretization. To reduce such limitations authors in [1] and [4] propose Physics-Informed Neural Networks (PINNs) to simulate and predict the internal temperature of the transformer. On this basis, we extended and applied this method to find the most suitable internal temperature monitoring positions inside of the transformer under the restriction of a limited number of temperature sensors to achieve efficient performance monitoring.

Assuming n_{max} is the maximum number of temperature sensors that can be placed inside the transformer, and n_{min} is a minimum required number of sensors, we use a mixed-integer optimization model to find the temperature-stable points inside the transformer. These points would result in the optimal placement of sensors that can effectively reconstruct the temperature under given limitations. A stable temperature point refers to the point where the absolute value of the time-averaged temperature change $\frac{\partial T}{\partial x}$ is minimum. The basic optimization model for this case follows.

$$\min_{\mathbf{s}} \quad \frac{1}{N_t} \sum_{i=1}^{N_t} |\nabla_{\mathbf{x}} \cdot T(\mathbf{x}, t_i)|_{\mathbf{x}=\bar{\mathbf{x}}}| \cdot \mathbf{s}$$
$$\text{s.t.} \quad \mathbf{s} = [s_1, s_2, \dots, s_{N_x}]$$
$$s_i \in \{0, 1\}$$
$$n_{\min} \leq \sum_i s_i \leq n_{\max},$$

where N_t is the number of training points, T is the temperature, $\nabla\cdot$ is the divergence operator, $\bar{\mathbf{x}}$ is a grid of N_x points over Ω, $t \geq 0$ is the time, s_i is a binary directional variable, indicating whether there is a sensor at the corresponding position x_i.

Results

Figure 12.1 shows a snapshot of the 2D solution with the results for sensor placement. The plot on the left shows the time-averaged temperature results, while the plot on the right displays the time-averaged first-order spatial derivatives of the temperature ($\frac{\partial T}{\partial x} + \frac{\partial T}{\partial y}$)$_{mean}$ with $n_{min} = 5$, $n_{max} = 10$, $d = 0.05$ and $d_1 = 0.1$.
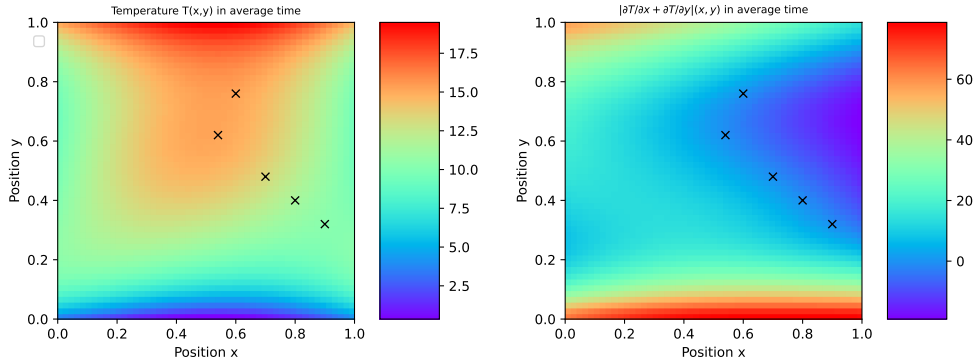
Figure 12.1: The optimal placement of sensors for 2D spacial problem, with $n_{min} = 5$, $n_{max} = 10$, $d = 0.05$ and $d_1 = 0.1$.

References

[1] F. Bragone, K. Morozovska, P. Hilber, T. Laneryd, and M. Luvisotto. "Physics-informed neural networks for modelling power transformer's dynamic thermal behaviour". In: *Electric power systems research* 211 (2022), p. 108447.

[2] IEC. "Power transformers – Part 7: Loading guide for oil-Immersed power transformers". In: *IEC 60076-7:2018* (2018).

[3] "IEEE Guide for Loading Mineral-Oil-Immersed Transformers and Step-Voltage Regulators". In: *IEEE Std C57.91-2011 (Revision of IEEE Std C57.91-1995)* (2012), pp. 1–123. DOI: 10.1109/IEEESTD.2012.6166928.

[4] T. Laneryd, F. Bragone, K. Morozovska, and M. Luvisotto. "Physics informed neural networks for power transformer dynamic thermal modelling". In: *IFAC-PapersOnLine* 55.20 (2022), pp. 49–54.

[5] D. Susa and M. Lehtonen. "Dynamic thermal modeling of power transformers: further Development-part I". In: *IEEE transactions on power delivery* 21.4 (2006), pp. 1961–1970.

[6] D. Susa and M. Lehtonen. "Dynamic thermal modeling of power transformers: further Development-part II". In: *IEEE transactions on power delivery* 21.4 (2006), pp. 1971–1980.

[7] D. Susa, M. Lehtonen, and H. Nordman. "Dynamic thermal modelling of power transformers". In: *IEEE transactions on Power Delivery* 20.1 (2005), pp. 197–204.

Histopolation via mock-Chebyshev points

Federico Nudo
University of Padua, Italy
email: federico.nudo@unipd.it

In many numerical applications, we often encounter phenomena for which we only have measurements at a set of equally spaced points. When using standard polynomial interpolation to approximate such phenomena, the results can be highly inaccurate due to the Runge phenomenon. Several techniques have been introduced to mitigate this issue, for example, the mock-Chebyshev subset interpolation and the constrained mock-Chebyshev least squares approximation [1, 5, 6, 7]. The excellent accuracy achieved by these approximations has led to their widespread use in various applications. Motivated by the success of these techniques in the classical polynomial interpolation, we aim to extend the mock-Chebyshev subset interpolation and the constrained mock-Chebyshev least squares approximation to the case of interpolation on segments. Specifically, we present three detailed generalizations of these methods in this context:

- Concatenated segmental mock-Chebyshev method;

- Quasi-nodal mock-Chebyshev method;

- Constrained segmental mock-Chebyshev method.

The interpolation on segments is a mathematical technique used to approximate a function f over a specific interval $I = [a, b]$. It offers a distinct approach compared to classical polynomial interpolation. While the classical polynomial interpolation relies solely on function evaluations at specific points, the interpolation on segments leverages information about the integral of the function f over a set of subintervals of the interval I. This difference is crucial because the interpolation on segments only requires the function to be essentially bounded, a less restrictive condition than the continuity required for classical polynomial interpolation. We demonstrate that two of these three new methods achieve optimal growth rates for the Lebesgue constant of the corresponding Vandermonde matrix. Specifically, one method boasts logarithmic growth, while another exhibits growth between logarithmic and square-root. Finally, we compare the performance of these new approximation techniques through various numerical experiments. Other informations can be find in [3].

References

[1] J. P. Boyd and F. Xu. "Divergence (Runge phenomenon) for least-squares polynomial approximation on an equispaced grid and Mock–Chebyshev subset interpolation". In: *Applied Mathematics and Computation* 210.1 (2009), pp. 158–168.

[2] L. Bruni Bruno and W. Erb. "Polynomial Interpolation of Function Averages on Interval Segments". In: *SIAM Journal on Numerical Analysis* 62.4 (2024), pp. 1759–1781.

[3] L. B. Bruno, F. Dell'Accio, W. Erb, and F. Nudo. "Polynomial histopolation on mock-Chebyshev segments". ARXIV: 2407.16825. 2024.

[4] L. B. Bruno and W. Erb. "The Fekete problem in segmental polynomial interpolation". ARXIV: 2403.09378. 2024.

[5] S. De Marchi, F. Dell'Accio, and M. Mazza. "On the constrained mock-Chebyshev least-squares". In: *Journal of Computational and Applied Mathematics* 280 (2015), pp. 94–109.

[6] F. Dell'Accio, F. Di Tommaso, and F. Nudo. "Generalizations of the constrained mock-Chebyshev least squares in two variables: Tensor product vs total degree polynomial interpolation". In: *Applied Mathematics Letters* 125 (2022), p. 107732.

[7] F. Dell'Accio, F. Marcellán, and F. Nudo. "An extension of a mixed interpolation–regression method using zeros of orthogonal polynomials". In: *Journal of Computational and Applied Mathematics* 450 (2024), p. 116010.

Graph-based machine learning approaches for model order reduction

Federico Pichi

SISSA - International School for Advanced Studies

Introduction

The solution of parametrized partial differential equations (PDEs) using high-fidelity techniques is computationally expensive, especially in real-time simulations and many-query context. Reduced Order Methods (ROMs) aim to build surrogate models to simplify complex parametric systems, generating efficient and reliable approximations [3, 8].

Non-intrusive and data-driven approaches based on Deep Learning recently gained a lot of interests in the development of efficient models overcoming some of the limitations of traditional approaches via linear and non-linear strategies [1, 2, 4, 6].

Autoencoder architectures can be considered as the non-linear generalization of the Proper Orthogonal Decomposition (POD), and are usually exploited for unsupervised learning tasks in combination with Convolutional Neural Networks. When dealing with complex domains defined on unstructured meshes, such approaches lack of geometrical consistency, decoupling the geometric bias from the learning procedure.

Here, we presents two frameworks for nonlinear model order reduction based on Graph Convolutional Autoencoders (GCA) [7] and Graph Feedforward Network (GFN) [5] to discover unseen patterns and perform efficient approximations in different physical contexts, including bifurcating behavior, high-dimensional parameter space, multifidelity applications, slow Kolmogorov-decay, and varying domains.

Graph convolutional autoencoder architecture (GCA-ROM) [7]

With GCA-ROM[1], we introduce a data-driven nonlinear surrogate ROM for PDEs defined on complex unstructured grids, capturing their physical and geometric features through a combination of Graph Neural Networks (GNNs) and Convolutional Autoencoders.

The architecture (see Figure 14.1) is designed to cope with parametrized scalar/vector and linear/nonlinear PDEs, possibly exploiting pooling/unpooling operations to up/down-sample large meshes. Our approach is characterized by spatial convolutions, defined on neighbourhoods of nodes through message passing and aggregation procedures.

By exploiting geometric priors in the learning phase, our methodology learns the latent space's evolution for an efficient reconstruction with consistent speedup, and shows great performance in generalizing to new configurations, especially in the low-data regime.

---

[1]www.github.com/https://github.com/fpichi/gca-rom
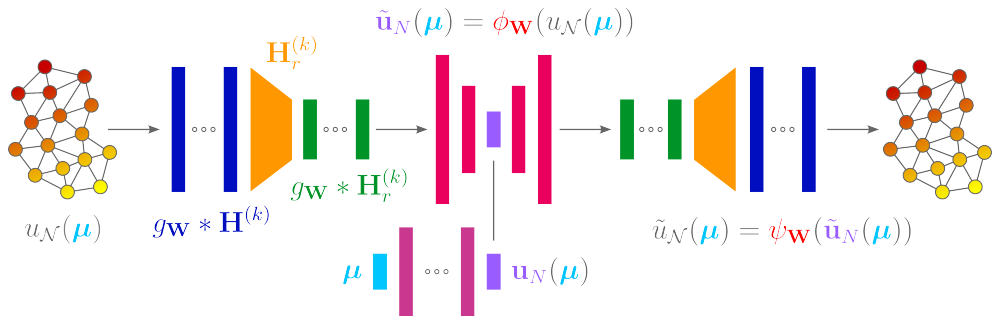
Figure 14.1: GCA-ROM architecture for the learning phase.
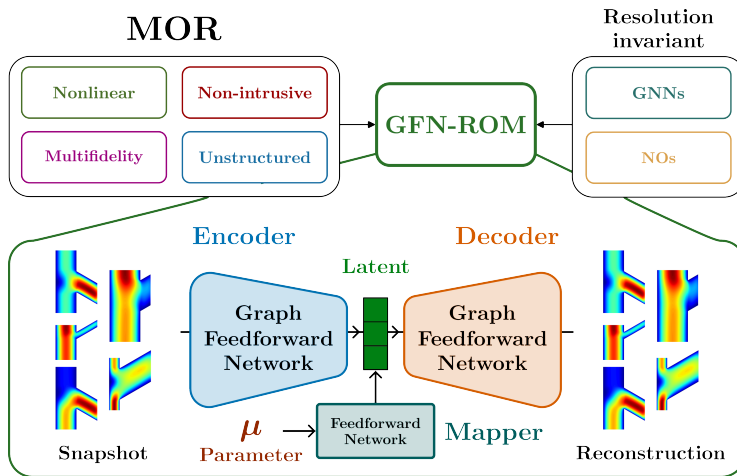
Figure 14.2: GFN-ROM is a nonlinear non-intrusive multifidelity surrogate model.

Graph Feedforward Network architecture (GFN) [5]

To overcome the limitations of the up/down-sampling procedures, we introduce GFN[2], a novel neural network layer extending the concept of feedforward networks to graph-structured data. By exploiting the connection between the weights of a neural network and the nodes of a mesh, we build a resolution-invariant GFN-ROM strategy (see Figure 14.2) for multifidelity applications, capable of training and testing on different mesh sizes.

The approach results in a more lightweight and flexible strategy when compared to state-of-the-art models, showing impressive generalisation performance in both single fidelity and multifidelity scenarios. Moreover, we provide provable guarantees on the performance under suitable assumptions, identifying the different sources for the error.

---

[2]www.github.com/https://github.com/Oisin-M/GFN

Conclusions

We developed two novel non-intrusive reduced-order architecture based on GNNs and GFN. Both strategies are interpretable and efficient, taking advantage of the geometrical information and extracting a compressed representation of the dynamics into the latent variables. We tested our methodologies on several challenging physical and geometrical multi-parametrized models, such as Poisson, Graetz, Stokes and Navier-Stokes, comparing their performance for bifurcating and advection-dominated phenomena, for which classical ROMs are not suited. The main advantage of both architectures is their remarkable accuracy and high speedup while working with small training set even for complex problems defined on varying geometries.

References

[1] S. Fresca, L. Dede', and A. Manzoni. "A Comprehensive Deep Learning-Based Approach to Reduced Order Modeling of Nonlinear Time-Dependent Parametrized PDEs". In: *Journal of Scientific Computing* 87.2 (2021), p. 61. DOI: 10.1007/s10915–021–01462–7.

[2] J. S. Hesthaven and S. Ubbiali. "Non-Intrusive Reduced Order Modeling of Nonlinear Problems Using Neural Networks". In: *Journal of Computational Physics* 363 (2018), pp. 55–78. DOI: 10.1016/j.jcp.2018.02.037.

[3] J. S. Hesthaven, G. Rozza, and B. Stamm. *Certified Reduced Basis Methods for Parametrized Partial Differential Equations.* 1st ed. 2016. SpringerBriefs in Mathematics. Cham: Springer International Publishing AG, 2015. ISBN: 978-3-319-22469-5. DOI: 10.1007/978–3–319–22470–1.

[4] K. Lee and K. T. Carlberg. "Model Reduction of Dynamical Systems on Nonlinear Manifolds Using Deep Convolutional Autoencoders". In: *Journal of Computational Physics* 404 (2020), p. 108973. DOI: 10.1016/j.jcp.2019.108973.

[5] O. M. Morrison, F. Pichi, and J. S. Hesthaven. *GFN: A Graph Feedforward Network for Resolution-Invariant Reduced Operator Learning in Multifidelity Applications.* 2024. arXiv: 2406.03569 [cs, math].

[6] F. Pichi, F. Ballarin, G. Rozza, and J. S. Hesthaven. "An Artificial Neural Network Approach to Bifurcating Phenomena in Computational Fluid Dynamics". In: *Computers & Fluids* 254 (2023), p. 105813. DOI: 10.1016/j.compfluid.2023.105813.

[7] F. Pichi, B. Moya, and J. S. Hesthaven. "A Graph Convolutional Autoencoder Approach to Model Order Reduction for Parametrized PDEs". In: *Journal of Computational Physics* 501 (2024), p. 112762. DOI: 10.1016/j.jcp.2024.112762.

[8] G. Rozza, F. Ballarin, L. Scandurra, and F. Pichi. *Real Time Reduced Order Computational Mechanics: Parametric PDEs Worked Out Problems.* Vol. 5. SISSA Springer Series. Cham: Springer Nature Switzerland, 2024. ISBN: 978-3-031-49891-6. DOI: 10.1007/978–3–031–49892–3.

High order semi-Lagrangian schemes and applications

Silvia Preda[a,∗]**, Elisabetta Carlini**[b]**, Roberto Ferretti**[c]**, and Matteo Semplice**[a]

[a] Dipartimento di Scienza e Alta Tecnologia, Università degli Studi dell'Insubria, Como, Italy

[b] Dipartimento di Matematica, Università La Sapienza, Roma, Italy

[c] Dipartimento di Matematica e Fisica, Università degli Studi Roma Tre, Roma, Italy

We examine a high-order numerical scheme for time-dependent first-order Hamilton–Jacobi–Bellman equations. In particular, we propose to couple a semi-Lagrangian scheme with a Central Weighted Non-Oscillatory (CWENO) reconstruction. Convergency is studied in the case of state- and time-independent Hamiltonians and numerical simulations are presented in one and two space dimensions. Our experiments show the superior performance in terms of CPU time gain by the Central version of the scheme with respect to the one combined with traditional WENO reconstructions. This type of numerical scheme is then generalized to the case of second-order evolutive Hamilton–Jacobi equation which arises in the level set formulation of mean curvature motion [3, 4] and, in particular, in the case of a curvature-related level set model first proposed by Zhao et al. [5], to reconstruct unknown surfaces from an unorganized set of points [2]. The variational problem it is associated with a partial differential equation (PDE) formulation with a curvature constraint that minimizes the surface area weighted by its distance from the point cloud. Level-set methods are used in this framework to track the evolution of an initial surface and to find an implicit representation of the final shape. Among all the possible representations, we compute the signed distance function at least in proximity to the reconstructed surface. Regarding the numerical approximation of the solution, the use of the semi-Lagrangian scheme coupled with a local interpolator allows us to save computational costs, compared to global ones [1], while also enhancing the parallel implementation of the algorithm. Numerical tests in two and three dimensions are presented to evaluate the accuracy of the approximated solution and the efficiency of the algorithm in terms of CPU times.

References

[1]   E. Carlini and R. Ferretti. "A Semi-Lagrangian Scheme with Radial Basis Approximation for Surface Reconstruction". In: *Comput. Vis. Sci.* 18.2-3 (2017), pp. 103–112. DOI: 10.1007/s00791-016-0274-2.

[2]   A. Coco, S. Preda, and M. Semplice. "From Point Clouds to 3D Simulations of Marble Sulfation". In: *Proceeding MACH21*. Vol. 55. 2023, pp. 153–174. DOI: `10.1007/978-9 81-99-3679-3_10`.

[3]   M. Falcone and R. Ferretti. "Consistency of a large time-step scheme for mean curvature motion". In: *Numerical Mathematics and Advanced Applications*. Ed. by F. Brezzi, A. Buffa, S. Corsaro, and A. Murli. Springer Milan, 2003, pp. 495–502. DOI: `10.1007/978-88-470-2089-4_46`.

[4]   S. Osher and J. A. Sethian. "Fronts propagating with curvature-dependent speed: Algorithms based on Hamilton-Jacobi formulations". In: *J. Computat. Phys.* 79.1 (1988), pp. 12–49. DOI: `10.1016/0021-9991(88)90002-2`.

[5]   H.-K. Zhao, S. Osher, B. Merriman, and M. Kang. "Implicit and Nonparametric Shape Reconstruction from Unorganized Data Using a Variational Level Set Method". In: *Computer Vision and Image Understanding* 80.3 (2000), pp. 295–314. DOI: `10.1006 /cviu.2000.0875`.

Optimal control of ODEs with dynamics uncertainty

Alessandro Scagliotti

Technical University of Munich & Munich Center for Machine Learning (MCML).

General setting

In this presentation, we consider an ensemble of affine-control systems in $\mathbb{R}^n$ of the form

$$\dot{x} = A^\theta(x)u + b^\theta(x), \quad x(0) = x_0^\theta,$$

parametrised by $\theta \in \Theta$ (a compact subset of an Euclidean space). We insist on the fact that all the ODEs of the ensemble are *simultaneously* driven on the time horizon $[0, T]$ by the same control $u \in \mathcal{U} := L^2([0, T], \mathbb{R}^m)$. If we understand θ as a random vector, we can consider its law, associated with the probability measure $\mu \in \mathcal{P}(\Theta)$. Hence, we consider the weighted functional $J_\mu : \mathcal{U} \to \mathbb{R}$ defined as

$$J_\mu(u) := \int_\Theta a\big(x_u^\theta(T), \theta\big) \, d\mu(\theta) + \lambda\|u\|_{L^2}^2, \tag{16.1}$$

where $\lambda > 0$ tunes the regularisation, and $a : \mathbb{R}^n \times \Theta \to \mathbb{R}$ is a C^1-regular function that designs the end-point cost for the elements of the ensemble. We observe that in (16.1) the dependence on the uncertain parameter is saturated by considering the *expected end-point cost*, that we are interested in minimizing. Another important approach for eliminating the dependence on θ involves considering the *least favorable conjuncture* and minimizing the worst-case cost. More precisely, this traduces into defining the following functional:

$$G(u) := \sup_{\theta \in \Theta} a\big(x_u^\theta(T), \theta\big) + \lambda\|u\|_{L^2}^2. \tag{16.2}$$

We report that the main difference between (16.1) and (16.2) is that the first functional depends smoothly on the control u, while the second is in general non-differentiable. We also mention that our analysis embraces also more general running costs than the L^2-norm squared on the control, *e.g.* we can consider an integral term $u \mapsto \int_0^T f(u(t)) \, dt$ that makes the functionals (16.1) and (16.2) coercive and lower semi-continuous in the L^p-weak topology (for $1 < p < \infty$).

From infinite to finite ensembles

If Θ or the support of μ consist of infinitely many points, dealing with the functionals J_μ (16.1) or G (16.2) requires (just for a *single evaluation*) to handle simultaneously infinitely many ODEs. To overcome this issue, we establish a Γ-convergence result. Namely, let us

consider a sequence of probability measures $(\mu_n)_n \subset \mathcal{P}(\Theta)$ such that $\mu_n \rightharpoonup \mu$ as $n \to \infty$ and such that $\#\operatorname{supp}(\mu_n) < \infty$ for every $n \geq 1$. Then, for every $n \geq 1$, we define the functional J_{μ_n} as in (16.1), with the measure μ_n in place of μ in the first integral. Similarly, given a sequence of subsets $(\Theta_n)_n$ with $\Theta_n \subset \Theta$, $\#\Theta_n < \infty$ such that $d_H(\Theta_n, \Theta) \to 0$ (Hausdorff distance) as $n \to \infty$, we define G_n as in (16.2), but taking the sup on the finite subset Θ_n instead of Θ. In this framework, it is possible to prove that $J_{\mu_n} \to_\Gamma J_\mu$ and $G_n \to_\Gamma G$ as $n \to \infty$ (Γ-convergence of the functionals). This implies the strong convergence of the minimisers $\hat{u}_n$ of J_{μ_n} and $\bar{u}_n$ of G_n to the minimisers of J_μ and of G, respectively. From a numerical perspective, such a result allows us to address the minimization of J_{μ_n} and G_n (which involve enembles with a *finite number* of elements) in place of J_μ and G, respectively. It is worth mentioning that our Γ-convergence result is useful also for theoretical purposes, since we have been able to use the convergence of the minimisers to establish necessary optimality conditions for J_μ and G by passing to the limit in the Pontryagin Maximum Principle. In this way, we extended to affine-control systems the necessary conditions previously obtained [1, 6]. We studied the *averaged* problem (16.1) in [2], and in [4] we applied those techniques to a setting concerning Normalizing Flows and the approximation of optimal trnasport maps. Moreover, the *minimax* problem (16.2) has been recently addressed in [3].

Applications: models for chemotherapy

Let us consider the following model for chemotherapy in metastatic cancer with innate (primary) resistance to a drug:

$$\begin{cases} \dot{x}_1 = \xi_1 x_1 \left(1 - \frac{x_1 + x_2}{M}\right) - \mu x_1 u, & \text{(sensitive population)} \\ \dot{x}_2 = \xi_2 x_2 \left(1 - \frac{x_1 + x_2}{M}\right). & \text{(resistant population)} \end{cases} \tag{16.3}$$

The first row of the system represents the evolution of the *sensitive* population, i.e., the cells of cancer that the drug can kill. In contrast, the second row describes the evolution of the population with primary resistance to the medicament. We observe that the two populations interact since *they compete for the same (limited) resources*. In (16.3), we have that $u = u(t) \in [0, u_{\max}]$ is the control, which is related to the dosage of medicament prescribed to the patient, while ξ_1, ξ_2, M, μ are the (patient-specific) parameters of the system. For further details and more sophisticated models, we refer to [5]. The baseline therapy consists of giving the patient the maximal dose of the drug, corresponding to the strategy $\bar{u} \equiv u_{\max}$, and changing medicament when a progression of the disease is observed. This approach has the advantage of being parameter-independent, i.e., it can be applied to every patient without the need for a precise estimate of the values of the model's parameters. On the one hand, as we can see in Figure 16.1, it is possible to develop strategies that achieve improved behavior in the long-term treatment. On the other hand, such dosage policies may need to be carefully calibrated according to the patient-specific parameters in order to be effective. In this scenario, it seems natural to design and analyze pharmacological treatments with an *ensemble optimal control standpoint*.
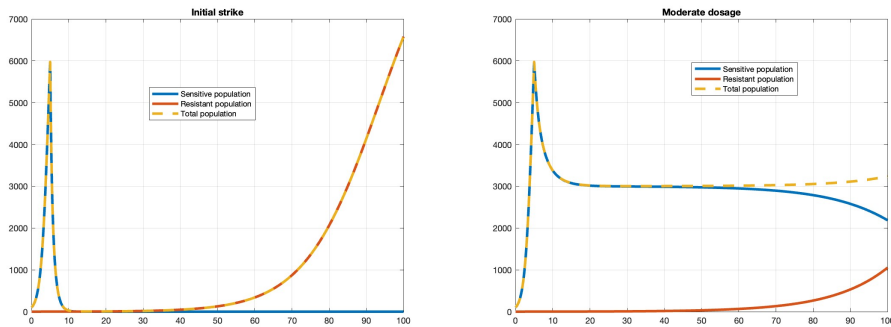
Figure 16.1: In the graphs, we simulated the evolution of the sensitive population (blue), the resistant (red), and the cancer's total population (yellow dashed). The pharmacological treatment starts at the instant $t = 5$ in both the simulations, with the same conditions in terms of population size and patient-specific parameters. On the left, we reported the typical evolution related to the baseline strategy $\bar{u} \equiv u_{\mathsf{max}}$. The sensitive population is rapidly extincted, and –after a quiescence period– we observe that the resistant population takes over, so that at the final evolution time we have a large cancer population made of resistant cells. On the right, we performed the same long-term simulation using the following dosage policy: $\bar{u} \equiv 60\% \, u_{\mathsf{max}}$. In this way, we avoid killing completely the sensitive population at the beginning of the therapy, and the total cancer's population is kept under control for a longer time. This is due to the fact that the two populations compete for the available resources, and the presence of a stable sensitive population delays the progress of the resistant one. We stress that the strategy related to the picture on the right depends on the patient-specific model's parameters.

References

[1]   P. Bettiol and N. Khalil. "Necessary optimality conditions for average cost minimization problems". In: *Discete Contin. Dyn. Syst. - B* 24.5 (2019).

[2]   A. Scagliotti. "Optimal control of ensembles of dynamical systems". In: *ESAIM: Control Optim. Calc. Var.* 29 (2023).

[3]   A. Scagliotti. "Minimax problems for ensembles of control-affine systems". ᴀʀᴄʜɪᴠ: 2405.05782. 2024.

[4]   A. Scagliotti and S. Farinelli. "Normalizing flows as approximations of optimal transport maps via linear-control neural ODEs". ᴀʀᴄʜɪᴠ: 2311.01404. 2023.

[5]   H. Schättler and U. Ledzewicz. *Optimal control for mathematical models of cancer therapies*. Springer, 2015.

[6]   R. Vinter. "Minimax Optimal Control". In: *SIAM J. Control Optim.* 44.3 (2005).

Short Presentations

Explicit stabilized implementation of implicit Runge-Kutta methods

Ibrahim Almuslimani[a,*], Gilles Vilmart[b], and Konstantinos C. Zygalakis[c]
[a] École Polytechnique Fédérale de Lausanne
[b] University of Geneva, Switzerland
[c] University of Edinburgh, Scotland

The explicit stabilized Runge-Kutta-Chebyshev (RKC) methods offer a valuable middle ground between standard explicit and implicit Runge-Kutta methods for handling stiff, high-dimensional, diffusion-dominated equations. Their extended stability region, which increases *quadratically* with the number of internal stages, allows for larger time steps without needing to solve complex systems. Due to their two-term recurrence relations, these methods are also memory-efficient and simple to implement [1].

Consider the ordinary differential equation (ODE)

$$\dot{y} = g(y), \qquad y(0) = y_0, \tag{17.1}$$

where $y(t) \in \mathbb{R}^d$ and the vector field $g : \mathbb{R}^d \mapsto \mathbb{R}^d$ is assumed smooth. The first-order s-stage RKC method with step size Δt to integrate (17.1) reads for all $n \geq 0$,

$$y_n^0 = y_n, \quad y_n^1 = y_n^0 + \mu_1 \Delta t g(y_n^0),$$
$$y_n^j = \mu_j \Delta t g(y_n^{j-1}) + \nu_j y_n^{j-1} + (1 - \nu_j) y_n^{j-2}, \quad j = 2, \ldots, s, \tag{17.2}$$
$$y_{n+1} = y_n^s,$$

To keep the discussion on track, we refer the reader to [1] for the definition of the equation coefficients. The stability function of the RKC method oscillates between $-\alpha_s(\eta)$ and $\alpha_s(\eta)$ where $0 < \alpha_s(\eta) < 1$ and $\eta > 0$ are the damping parameters (see [3] for details).

Application to optimization

In [3], and based on RKC, a new algorithm called RKCD, is introduced to solve stiff optimization problems efficiently. Stiff optimization problems, in this context, refer to cases where the second derivative of the objective function has large eigenvalues concentrated near the positive real axis. Let $d \in \mathbb{N}\setminus\{0\}$ and a ℓ-strongly convex differentiable function $f : \mathbb{R}^d \to \mathbb{R}$, with L-Lipschitz derivative. We then consider the following optimization problem

$$\min_{x \in \mathbb{R}^d} f(x). \tag{17.3}$$

To solve (17.3), the authors of [3] consider the gradient flow

$$\dot{x} = -\nabla f(x), \qquad x(0) = x_0 \in \mathbb{R}^d, \tag{17.4}$$

where x_0 is an initialization value. For stiff gradients ($L \gg l$), an explicit Euler method needs to severely restrict the step size to ensure stability. The RKCD method uses instead the first order RKC (17.2) to iterate on (17.4) (see [3, Algorithm 1]). In particular, if the function f is quadratic, i.e.

$$f(x) = \frac{1}{2}x^T A x + b^T x,$$

where $A \in \mathbb{R}^{d \times d}$ is a positive definite and symmetric matrix with condition number $\kappa = L/\ell$, and $b \in \mathbb{R}^d$, we have the following.

Proposition 1 (Proposition [3])**.** *Consider the minimization problem (17.3) where f is quadratic. Now let x_k be the iterate of the RKC method (17.2) applied to (17.4), i.e, $g = -\nabla f$. If the number of stages s and the time-step h are chosen according to [3, Condition (3.6)], then we have*

$$\|x_k - x_\star\| \le \alpha_s(\eta)^k \|x_0 - x_\star\|,$$

where $x_\star$ is the unique minimizer of f.

New explicit implementation of implicit methods

We now revisit equation (17.1) under the additional assumption that the eigenvalues of the Jacobian matrix of g have strictly negative real parts. The internal stages of an implicit Runge-Kutta method of coefficient matrix $\mathcal{A}$ applied to (17.1) with step size Δt are the steady state solution of

$$\dot{\mathcal{Y}} = \Delta t \mathcal{A} \otimes I_d g[\mathcal{Y}] - \mathcal{Y} + \mathcal{Y}^0, \qquad \mathcal{Y}(0) = \mathcal{Y}_0, \qquad (17.5)$$

where $\mathcal{Y} = \begin{pmatrix} Y_1 \\ Y_2 \\ \vdots \\ Y_m \end{pmatrix}$, $\mathcal{Y}^0 = \begin{pmatrix} y_0 \\ y_0 \\ \vdots \\ y_0 \end{pmatrix}$, $g[\mathcal{Y}] = \begin{pmatrix} g(Y_1) \\ g(Y_2) \\ \vdots \\ g(Y_m) \end{pmatrix}$, m is the number of stages of the implicit method, $\otimes$ is for the Kronecker product, and $\mathcal{Y}_0$ is an initialization that needs not to be equal to $\mathcal{Y}^0$. Notice that, if the vector field $\mathcal{A} \otimes I_d g[\mathcal{Y}]$ can be written as $-\nabla F(\mathcal{Y})$, then (17.5) corresponds to the gradient flow (17.4) for $f(\mathcal{Y}) = \Delta t F(\mathcal{Y}) + \frac{1}{2}\|\mathcal{Y} - \mathcal{Y}^0\|_2^2$.

The idea is now to apply RKC method (17.2) to (17.5) until the solution of the implicit Runge-Kutta method is found.

The problem of non-symmetric coefficients matrix. When the matrix $\mathcal{A}$ is not symmetric, Proposition 1 does not hold. To illustrate this, we apply our approach to a one-dimensional linear diffusion partial differential equation (PDE) using the backward Euler method with $\mathcal{A}_E = 1$ and a five-stage, fourth-order, singly diagonally implicit Runge-Kutta method (SDIRK4) [4, Chap. IV.6]. In the SDIRK4 method, the lower triangular matrix $\mathcal{A}_S \in \mathbb{R}^{5 \times 5}$ has all diagonal entries equal to $1/4$. We conduct a single time step and examine the increments produced by each method. The results indicate that the increments converge to machine precision when using the backward Euler method, whereas

Method	tol	Diffusion evals	Reaction evals	Steps acc(rej)	error in v
expSDIRK4	10^{-3}	1509	118	7(0)	8.2×10^{-5}
PIROCK	10^{-3}	292	67	13(0)	1.2×10^{-2}
expSDIRK4	10^{-5}	3072	842	54(8)	8.7×10^{-7}
PIROCK	10^{-5}	1594	1384	267(7)	2.1×10^{-4}
expSDIRK4	10^{-6}	4659	1630	105(7)	6.5×10^{-8}
PIROCK	10^{-6}	6383	7391	1470(7)	2.1×10^{-5}
expSDIRK4	10^{-7}	7233	3267	216(7)	3.6×10^{-9}
PIROCK	10^{-7}	16362	22515	4495(185)	3×10^{-7}

Table 17.1: comparison between expSDIRK4 and PIROCK.

the same level of convergence is not observed with SDIRK4. Indeed, a Jordan decomposition of $\mathcal{A}_S$ in this case shows that, when the stability function of RKC is applied to $\mathcal{A}_S \otimes I_d g[\mathcal{Y}]$, unbounded terms appear. To deal with this issue, we consider the following modification of the equation

$$\dot{\mathcal{Y}} = \Delta t \gamma I_m \otimes I_d g[\mathcal{Y}] + \mathcal{Y}^0 - \mathcal{Y} + \Delta t (\mathcal{A} - \gamma I_m) \otimes I_d g[\mathcal{Y}],$$

where in the case of SDIRK4 $\gamma = 1/4$ and $m = 5$ we apply a modified RKC in a partitioning framework. This allows the stability function to act on the diagonal part $\Delta t \gamma I_m \otimes I_d g[\mathcal{Y}] + \mathcal{Y}^0 - \mathcal{Y}$ as its argument, while only multiplying the other (nilpotent) term.

Advection-diffusion-reaction equations. For problems with stiff diffusion, advection, and highly stiff reaction terms, we propose a more elaborated partitioning that treats the reaction terms implicitly using a backward Euler scheme to iterate in the gradient flow. This idea is similar to the one used in the PIROCK integrator [2]. In Table 17.1, we compare the solution obtained by SDIRK4 implemented using our approach with the PIROCK stabilized integrator from [2], both applied to a stiff diffusion-reaction Brusselator problem. We use the error estimator described in [4] for SDIRK4. We can clearly see, especially for higher accuracy, that our method is much less costly in terms of vector fields evaluation.

References

[1] A. Abdulle. "Explicit Stabilized Runge–Kutta Methods". In: *EACM*. Springer, 2015, pp. 460–468. DOI: 10.1007/978-3-540-70529-1_100.

[2] A. Abdulle and G. Vilmart. "PIROCK: a swiss-knife partitioned implicit-explicit orthogonal Runge-Kutta Chebyshev integrator for stiff diffusion-advection-reaction problems with or without noise". In: *J. Comput. Phys.* 242 (2013), pp. 869–888. ISSN: 0021-9991. DOI: 10.1016/j.jcp.2013.02.009.

[3] A. Eftekhari, B. Vandereycken, G. Vilmart, and K. C. Zygalakis. "Explicit stabilised gradient descent for faster strongly convex optimisation". In: BIT Numerical Mathematics, 61(1):119–139. 2021.

[4] E. Hairer and G. Wanner. *Solving ordinary differential equations II. Stiff and differential-algebraic problems*. Berlin and Heidelberg: Springer-Verlag, 1996.

Numerical study on parameter effects of a new model for water penetration in porous media

Elishan C. Braun*, **Gabriella Bretti**
Istituto per la Applicazioni del Calcolo "M. Picone" (IAC), CNR, Rome, Italy

KEYWORDS: mathematical modelling · porous media · water flow · numerical simulations

MSC2020: 65M06 · 76S05 · 35Q35

Natural stones used in historical buildings are open porous systems that are subject to different damaging processes because of their exposure to the environment. Most weathering processes affecting porous materials, such as salt-crystallization, freezing-thawing cycles, dissolution of soluble fractions, etc., are associated to liquid water penetration, either in the form of meteoric precipitation or groundwater moisture infiltration. In addition, the microstructural modifications induced by the above-mentioned processes may lead to an increase in water penetration, thus contributing to an ongoing decay process. Hence capillary absorption measurements may provide fundamental indications for monitoring the progress of materials degradation. In this framework, the present work describes a mathematical model using Darcy's law (see later (18.1)) to simulate the water uptake into a porous medium, where the physical properties of the material are described by some crucial parameters representing the diffusion rate of water in the medium, the residual value of saturation that ensures the hydraulic continuity, and the absorption properties of the material. We start from the mathematical model describing capillary rise and water flow in porous media introduced in [4] and applied with promising results to different materials, also in presence of protective treatments, see [3].

The mass balance equation for the liquid (water) having density ρ_l is $\partial_t \theta = \partial_z q$, where q is the *volumetric flux* given by the well known Darcy's law [1]:

$$q = -\frac{k\left(\frac{\theta_l}{n_0}\right)}{\mu_l}\left(\partial_z P_c\left(\frac{\theta_l}{n_0}\right) - \rho_l g\right). \qquad (18.1)$$

Note that P_c is the capillary pressure, *i.e.* the pressure drop on the interface between liquid and gas, k is the (intrinsic) *permeability* of the porous matrix to vapour density, μ_l the *viscosity* of the fluid, with g the acceleration due to gravity, n_0 is the open *porosity* of the material, *i.e.* the fraction of volume occupied by voids, while θ_l is the *fraction of volume occupied by the fluid*. As usual in the literature [1], we assume the capillary pressure as a function of the fluid saturation $s = \theta_l/n_0$ only. Note that the term $\rho_l g$ in (18.1) takes into account the effect of the gravity in the vertical flow and it can be disregarded for small specimens of a given material. Formula (18.1) can thus be written as $q = \partial_z B(s) + \frac{k(s)}{\mu_l}\rho_l g$, with B a function such that:

$$\partial_z B(s) = -\frac{k(s)}{\mu_l}\partial_z P_c(s). \qquad (18.2)$$

In [4], $B(s)$ and $B'(s)$ have a mathematical formulation of a polynomial of third and second degree, respectively, see the dotted line curves in the right panel of Figure 18.2, and they depend on three crucial parameters: the residual saturation s_R that ensures the hydraulic continuity, and the maximum value of saturation s_S, the diffusion rate of water in the medium B'_{max}. Following the idea in [4], a new formulation of function B and the related mathematical model based on Darcy's law is introduced [2] in order to express separately the permeability function $k(s)$ and the capillary pressure $P_c(s)$, see the solid line curves depicted in the right panel of Figure 18.2.

Here we deal with five model parameters to be calibrated against data: the two saturation parameters defined above (s_R, s_S), two characteristic coefficients for the given material for the capillary rise in the material (α, c), and a parameter related to permeability properties (γ). The one-dimensional mathematical model for the experiment of imbibition, with B the function satisfying relation (18.2), is given by the equation:

$$\partial_t \theta_l = \partial_z \left(\partial_z B(s) + \frac{g\rho_l}{\mu_l} k(s) \right). \tag{18.3}$$

It is coupled with suitable initial and boundary conditions in order to have that the bottom side of the sample is always saturated, while at the top side an exchange of the specimen with the humidity within the bucket occurs, thus it is assumed as the value of humidity on the facelet on the top.

We solve the problem (18.3) numerically by computing $\theta(z, t_k)$ in $s_j^k = \theta_j^k / n_0$ with the forward-central approximation scheme including gravity effect:

$$\theta_j^{k+1} = \theta_j^k + \frac{\Delta t}{\Delta z^2} (B(s_{j+1}^k) - 2B(s_j^k) + B(s_{j-1}^k)) + g \frac{\Delta t}{2\Delta x \mu} (k(s_{j+1}^k) - k(s_{j-1}^k)),$$

and suitable discretized boundary conditions. We assume the CFL condition

$$\frac{\Delta t}{\Delta z^2} \leq \frac{n_0}{2 \max_{[s_R, s_S]} B'(s)},$$

with $\theta_j^k = \theta(z_j, t_k)$, $z_j = j\Delta z, j = 0, ..., N = \left[\frac{h_1}{\Delta z}\right], \{t_k\}_{k=1,...,N_{meas}}$. With numerical integration we compute the quantity of water within the specimen obtained by the model at time t_k and we then solve nonlinear minimization problem by computing the forward problem for each step in a suitable optimization method to calibrate parameters for $B(s)$ against experimental data. The calibrated model is then used for predicting the chemical damage on building heritage due to the interplay with damaging substances penetrating in the material, such as CO2 pollutant in the environment.
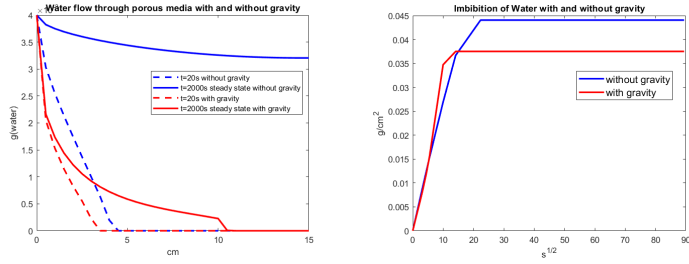
Figure 18.1: Effect on gravity on water flow through porous media.
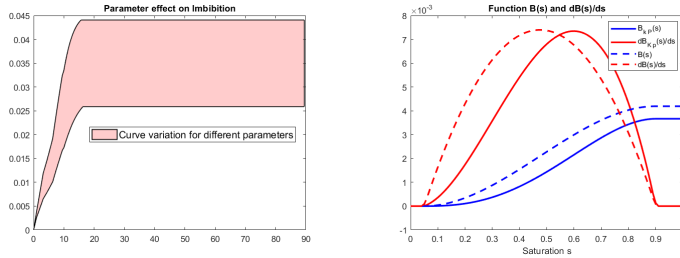
Figure 18.2: Left Panel: Effect of parameters $s_R, s_R, c, \alpha, \gamma$ on $B_{kP}(s)$, changes the imbibition curve, shown in the red marked area. Right Panel: Plots of symmetrical $B(s)$, $\frac{dB(s)}{ds}$ and asymmetrical $B_{kP}(s)$, $\frac{dB_{kP}}{ds}$.

References

[1] J. Bear. *Dynamics of flow in porous media*. Dynamics of flow in porous media, 1972.

[2] G. Bretti and C. M. Belfiore. "Mathematical modelling of degradation for historical lime-based mortars from Catania". In: *Preprint* (2024).

[3] G. Bretti, B. De Filippo, R. Natalini, S. Goidanich, M. Roveri, and L. Toniolo. "Modelling the effects of protective treatments in porous materials, Mathematical Modeling in Cultural Heritage." In: *Applied and Industrial Mathematics in Italy III: SIMAI Conference, Rome* (2008).

[4] F. Clarelli, R. Natalini, C. Nitsch, and M. L. Santarelli. "A mathematical model for consolidation of building stones". In: *Applied and Industrial Mathematics in Italy III: Selected Contributions from the 9th SIMAI Conference, Rome, Italy* (2008).

A hierarchical hybrid numerical method for multi-scale Boltzmann equation with geometry

Domenico Caparello[a,*], Thomas Rey[a], and Lorenzo Pareschi[b,c]

[a] Université Côte d'Azur, Nice, France
[b] Heriot-Watt University, Edinburgh, Scotland
[c] University of Ferrara, Italy

Several physical and engineering problems involve fluids in transitional regimes, in which the fluid description breaks down due to the presence of boundary layers or shocks. In this context, the use of a kinetic model is necessary to describe the system. Unfortunately, kinetic models are computationally more expensive than the fluid description itself, making it preferable to use it only locally in space.

In this work, we present a hierarchy of hybrid numerical methods for the multi-scale Boltzmann equation. We use a criterion to split the two-dimensional spatial integration domain into three regimes each one governed by a different equation: Euler equations, BGK equation, and full Boltzmann equation. The main advantage of this approach is using Euler equations in spatial regions in which the fluid is in the hydrodynamic regime, and the Boltzmann or BGK equation elsewhere. This ensures high precision in regions where the hydrodynamic description breaks down, and an overall faster computation of the solution thanks to the low numerical cost of the approximation of the Euler equations.

The novelty of this work is the spatial 2D - velocity 3D hybrid kinetic/fluid numerical method implementing the three regimes. To speed up the code execution, we take advantage of the CPU multi-thread capability and we use the fast spectral method for the computation of the Boltzmann operator.

It is important to identify a good regime indicator to automatically switch between the three different regimes. In literature, most of the works concerning hybrid methods rely on the domain technique introduced by Boyd, Chan and Chandler in [1]. It consists of a macroscopic criterion to pass from the hydrodynamic description (fast to compute numerically, but not accurate near boundary layers or shocks) to the kinetic one (computationally expansive, but accurate in most cases). To decide which equation to use, they evaluate the local Knudsen number, and if this quantity is below a certain threshold, the kinetic description is used.

Other criteria used in literature are based on the macroscopic description of the model,

which are inaccurate when the fluid is far from the thermal equilibrium [2].

In our work, we introduce a criterion to switch from the hydrodynamic regime to the kinetic regimes (BGK equation or full Boltzmann equation) based on the works of Levermore, Morokoff and Nadiga in [4], Filbet and Rey in [2], and Filbet and Xiong in [3]. All these works leverage the Chapman-Enskog expansion of the distribution, they only depend on macroscopic quantities given by a closure of the kinetic model and do not require the evaluation of the distribution function. The criterion we use to pass from the kinetic descriptions to the corresponding hydrodynamical limit is based on comparing the truncation of the Chapman-Enskog expansion with its hydrodynamical equilibrium.

To validate the algorithm, we carry out several simulations to test its accuracy in the transitional regimes. In particular, we simulate the movement of an object inside a fluid at rest; a 2D Riemann problem with initial datum in four quadrants (similar to the one reported in [3]), and a fluid moving around a fixed obstacle. From our results, we observe a great improvement in the execution speed with respect to algorithms that only perform numerical integration using kinetic models.

References

[1]   I. D. Boyd, G. Chen, and G. V. Candler. "Predicting failure of the continuum fluid equations in transitional hypersonic flows". In: *Physics of Fluids* 7.1 (Jan. 1995), pp. 210–219. DOI: 10.1063/1.868720.

[2]   F. Filbet and T. Rey. "A Hierarchy of Hybrid Numerical Methods for Multiscale Kinetic Equations". In: *SIAM Journal on Scientific Computing* 37 (2014). DOI: 10.1137/140958773.

[3]   F. Filbet and T. Xiong. "A hybrid discontinuous Galerkin scheme for multi-scale kinetic equations". In: *Journal of Computational Physics* 372 (2018), pp. 841–863. ISSN: 0021-9991. DOI: 10.1016/j.jcp.2018.06.064.

[4]   C. D. Levermore, W. J. Morokoff, and B. T. Nadiga. "MOMENT REALIZABILITY AND THE VALIDITY OF THE NAVIER-STOKES EQUATIONS FOR RAREFIED GAS DYNAMICS". In: *Physics of Fluids* 10 (1998), pp. 3214–3226. DOI: 10.1063/1.869849.

Non-local traffic flow models with time delay: well-posedness and numerical approximation

Ilaria Ciaramaglia[a,*], Paola Goatin[a], Gabriella Puppo[b]
[a] Inria Sophia Antipolis
[b] Sapienza, Università di Roma

Traffic flow is a complex phenomenon that deeply impacts our daily lives, the economy and the environment. Studying and understanding traffic behaviour is crucial to develop solutions that can alleviate congestion and improve road safety.

We aim to investigate heterogeneity in traffic by introducing a mathematical model which is able to study the interactions between human drivers and autonomous vehicles (AVs). One of the potential benefits of an intelligent transportation system (ITS) regards safety: AVs can dramatically reduce accidents caused by human error, with an estimated fatal crash-rate reduction of at least 40% [6]. In addition, AV technology has the potential to improve traffic flow and reduce congestion and fuel consumption. This is due to the fact that AVs could enable quicker reaction times and closer spacing between vehicles to counteract increasing demand, thus leading to smoother traffic patterns [9].

We propose a scalar macroscopic model which can capture some specific features of human behaviour on the road, including nonzero reaction time and short/long-range interactions among vehicles [4]. The model considers a constant reaction time $\tau > 0$ and is formulated as:

$$\partial_t \rho(t,x) + \partial_x \big(\rho(t,x) f(\rho(t,x)) v((\rho * \omega)(t - \tau, x)) \big) = 0, \tag{20.1}$$

where $\rho : \mathbb{R}^+ \times \mathbb{R} \to [0, R]$ is the vehicle density, $v : [0, R] \to [0, V]$ is the mean traffic speed, and $\omega : [0, L] \to \mathbb{R}^+$ is a convolution kernel. The positive constants R, V and L are respectively the maximal traffic density, the maximal speed, and the look-ahead distance of drivers. The model is a non-local extension of the Lighthill-Whitham [12] and Richards [13] (LWR) model. Such non-local extensions have been recently introduced in the literature [2, 7] to overcome some drawbacks of local dynamic descriptions and they are based on the assumption that drivers adapt their speed to a weighted mean of the downstream traffic density or velocity. The model also incorporates a delay, thus taking into account humans' reaction time. The function $f : [0, R] \to [0, 1]$ is chosen to play the role of a saturation function and it represents the main difference with the delayed non-local model introduced in [11]. Such a function guarantees that the density does not exceed R, modelling that the density can never exceed the maximum capacity of the road. This is an improvement with respect to both the local [8] and the non-local [11] existing models with time delay, as they fail to ensure such a bound also for small times.

We provide well-posedness of entropy weak solutions. To prove existence, we construct finite-volume approximate solutions using a Hilliges-Weidlich (HW) scheme [10] and we provide uniform $\mathbb{L}^\infty$ and **BV** estimates, thus ensuring convergence. Then, we prove that the limit function is an entropy weak solution of the model. We also achieve an $\mathbb{L}^1$ stability result by adapting Kružkov's doubling of variables technique, from which both uniqueness and convergence to the associated non-delayed model follow. This is also an improvement of the result obtained in [11] as in the current scenario we prove the convergence for any chosen time horizon. We propose some numerical tests, with a particular focus on the capability of the saturation function f in guaranteeing the maximum principle, and on the influence of the delay on the increase of the total variation of the solution.

Equation (20.1) constitutes a good basis for building a multi-class model. Through this extension, we intend to further investigate the interactions among several classes of vehicles with different behaviours in terms of look-ahead distance and reaction time. Indeed, we can assume that smart cars can collect information on the surrounding traffic within a large perimeter and are able to instantaneously respond to external events, whereas human drivers react to downstream traffic in a shorter range and with a non-zero time delay. In line with this idea, we propose the following system of non-local delayed conservation laws [5]:

$$\partial_t \rho_i(t,x) + \partial_x(\rho_i(t,x)f_i(\rho_i(t,x))v_i((r * \omega_i)(t - \tau_i, x))) = 0, \qquad \forall i = 1, \ldots, M,$$

where $\rho_i : \mathbb{R}^+ \times \mathbb{R} \to [0, R_i]$ is the vehicle density, $v_i : [0, +\infty) \to [0, V_i]$ is the mean traffic speed, $\omega_i : [0, L_i] \to \mathbb{R}^+$ a convolution kernel, $f_i : [0, R_i] \to [0, 1]$ the saturation function, and $\tau_i \geq 0$ is the reaction time associated to the i-th class. The positive constants R_i, V_i, L_i are respectively the maximal density, the maximal speed, and the look-ahead distance of drivers and they can be different among the classes. Multi-class traffic models were first proposed in [1, 14] to account for the diversity in vehicle types, characteristics, and behaviours, also in non-local patterns [3].
We extend to the multi-class scenario the theoretical analysis conducted for the scalar model, thus obtaining well-posedness and $\mathbb{L}^1$ stability estimates, improving also the results in [3] where the absence of saturation functions did not allow to obtain global $\mathbb{L}^\infty$ estimates. Finally, we conduct a numerical investigation analyzing the impact of saturation terms and delays and particularly focusing on the stabilizing effect induced by the presence of AVs in a mixed autonomous/human-driven environment.

References

[1]   S. Benzoni-Gavage and R. M. Colombo. "An n-populations model for traffic flow". In: *European J. Appl. Math.* 14.5 (2003). https://www.cambridge.org/core/journals/european-journal-of-applied-mathematics/article/an-npopulations-model-for-traffic-flow/A1765AE6E035F8FB8D3157B60D2781EF, pp. 587–612. ISSN: 0956-7925.

[2] F. A. Chiarello and P. Goatin. "Global entropy weak solutions for general non-local traffic flow models with anisotropic kernel". In: *ESAIM Math. Model. Numer. Anal.* 52.1 (2018), pp. 163–180. ISSN: 2822-7840,2804-7214. DOI: 10.1051/m2an/2017066.

[3] F. A. Chiarello and P. Goatin. "Non-local multi-class traffic flow models". In: *Netw. Heterog. Media* 14.2 (2019), pp. 371–387. ISSN: 1556-1801,1556-181X. DOI: 10.3934/nhm.2019015.

[4] I. Ciaramaglia, P. Goatin, and G. Puppo. "Non-local traffic flow models with time delay: well-posedness and numerical approximation". 2024. DOI: 10.3934/dcdsb.2024113.

[5] I. Ciaramaglia, P. Goatin, and G. Puppo. "A multi-class non-local macroscopic model with time delay for mixed autonomous / human-driven traffic". In: (). In preparation.

[6] D. J. Fagnant and K. Kockelman. "Preparing a nation for autonomous vehicles: opportunities, barriers and policy recommendations". In: *Transportation Research Part A: Policy and Practice* 77 (2015), pp. 167–181. ISSN: 0965-8564. DOI: 10.1016/j.tra.2015.04.003.

[7] J. Friedrich, O. Kolb, and S. Göttlich. "A Godunov type scheme for a class of LWR traffic flow models with non-local flux". In: *Networks and Heterogeneous Media* 13.4 (2018), pp. 531–547. ISSN: 1556-1801. DOI: 10.3934/nhm.2018024.

[8] S. Göttlich, E. Iacomini, and T. Jung. "Properties of the LWR model with time delay". In: *Networks and Heterogeneous Media* 16.1 (2021), pp. 31–47. ISSN: 1556-1801. DOI: 10.3934/nhm.2020032.

[9] M. Herty, G. Puppo, and G. Visconti. "Model of vehicle interactions with autonomous cars and its properties". In: *Discrete and Continuous Dynamical Systems - B* 28.2 (2023), pp. 833–853. ISSN: 1531-3492. DOI: 10.3934/dcdsb.2022100.

[10] M. Hilliges and W. Weidlich. "A phenomenological model for dynamic traffic flow in networks". In: *Transportation Research Part B: Methodological* 29.6 (1995), pp. 407–431. ISSN: 0191-2615. DOI: 10.1016/0191-2615(95)00018-9.

[11] A. Keimer and L. Pflug. "Nonlocal conservation laws with time delay". In: *NoDEA Nonlinear Differential Equations Appl.* 26.6 (2019), Paper No. 54, 34. ISSN: 1021-9722,1420-9004. DOI: 10.1007/s00030-019-0597-z.

[12] M. J. Lighthill and G. B. Whitham. "On kinematic waves. II. A theory of traffic flow on long crowded roads". In: *Proc. Roy. Soc. London. Ser. A.* 229 (1955), pp. 317–345. DOI: 10.1098/rspa.1955.0089.

[13] P. I. Richards. "Shock waves on the highway". In: *Operations Res.* 4 (1956), pp. 42–51. DOI: 10.1287/opre.4.1.42.

[14] G. Wong and S. Wong. "A multi-class traffic flow model – an extension of LWR model with heterogeneous drivers". In: *Transportation Research Part A: Policy and Practice* 36.9 (2002), pp. 827–841. ISSN: 0965-8564. DOI: 10.1016/S0965-8564(01)00042-8.

The Joint Spectral Radius of Neural Networks

Piero Deidda[a,b,*], Nicola Guglielmi[b], and Francesco Tudisco[c]
[a] Scuola Normale Superiore, Pisa, Italiy
[b] Gran Sasso Science Institute, L'Aquila, Italy
[c] University of Edinburgh, Scotland

A feed-forward neural network can be interpreted as a discrete switched system

$$x_{k+1} = f_{\sigma(k)}(x_k) \qquad k = 1, \dots$$

where the function $f_{\sigma(k)}$ at the k-th layer is chosen from an infinite family of functions $\mathcal{F} := \{f_i\}_{i \in I}$, according to a switching rule σ that is determined by the training process to minimize a loss function. In particular, different issues related to the training or reliability of Neural Networks can be intrepreted in terms of properties of the system, *e.g.* "oversmoothing in graph neural networks" [6] can be studied in terms of existence and convergence to fixed points of the system, while "exploding gradients" [8] and "vulnerability to adversarial attacks" [2] can be seen as a stability problem of the system.

When the switching rule is unknown the stability of a switched system is established by considering the worst possible case. This topic has been extensively investigated in the linear case, where the stability or instability of the system can be established in terms of the joint spectral radius of the underlying family of matrices [4]. However, neural networks used in modern deep learning make use of nonlinear activation functions and thus require a different theoretical investigation.

In this talk we present our investigation of switched systems that alternate maps from a (possibly infinite) class $\mathcal{F} := \{f_i\}_{i \in I}$ of nonlinear functions, following an unknown switching rule σ. In particular, we focus on families of sub-homogeneous nonlinear functions having an invariant cone, where they preserve the natural ordering induced by the cone. Such functions are naturally non-expansive with respect to proper metrics, and their spectral properties have been studied in the nonlinear Perron-Frobenius theory [5]. We point out that the subhomogeneous hypothesis is not restrictive in deep learning applications since activation functions used by neural networks are typically subhomogeneous [10]. Similarly, the order-preserving hypothesis has deserved attention in different recent applications, like deep equilibrium models [9] and investigation of the cut-off phenomenon [1].

For such a family of function, say $\mathcal{F}$, we introduce the notion of nonlinear joint spectral radius (JSR)

$$\rho(\mathcal{F}) = \limsup_k \sup_{f \in \Sigma_k(\mathcal{F})} \|f\|^{\frac{1}{k}}$$

where $\Sigma_k(\mathcal{F})$ is the set of functions that are composition of k functions in $\mathcal{F}$. Then, we prove that the JSR establishes the stability or instability of the system. In particular

Theorem 1.

- *If $\rho(\mathcal{F}) < 1$, then all the possible orbits of the system are asymptotically stable.*

- *If $\rho(\mathcal{F}) > 1$, there exists some divergent orbit.*

After that, we investigate properties of the nonlinear JSR. In particular, first we prove a dual formulation of the JSR in terms of monotone prenorms [7] of the functions in $\mathcal{F}$

$$\rho(\mathcal{F}) = \inf_{\substack{\Theta \text{ Monotone} \\ \text{Prenorm}}} \sup_{f \in \mathcal{F}} \Theta(f),$$

where a monotone prenorm is an absolutely homogeneous, positive definite functional that preserve the ordering induced by the cone.

Second, we recall that the nonlinear Perron-Frobenius theory [5] introduces a notion of joint spectral radius $\rho(f)$ of any function $f \in \Sigma(\mathcal{F})$, where $\Sigma(\mathcal{F})$ denotes the semi-group generated by $\mathcal{F}$. We use this information, to investigate a third formulation of the JSR of $\mathcal{F}$

$$\rho(\mathcal{F}) = \limsup_{n} \sup_{f \in \Sigma_k(\mathcal{F})} \rho(f)^{\frac{1}{k}},$$

where we prove that the equality holds under generic hypotheses.

Finally, we present an algorithm devoted to the computation of the nonlinear JSR. Our algorithm is inspired by the polytope algorithm used in the linear case [3] and iteratively builds a monotone extremal prenorm for the system in terms of the Minkowski functional of a finitely generated subset of the cone. To conclude, we use the different formulations of the JSR to provide sufficient conditions for the convergence of the algorithm.

References

[1] B. Avelin and A. Karlsson. "Deep Limits and a Cut-Off Phenomenon for Neural Networks". In: *Journal of Machine Learning Research* 23.191 (2022), pp. 1–29. URL: http://jmlr.org/papers/v23/21-0431.html.

[2] I. Goodfellow, J. Shlens, and C. Szegedy. "Explaining and Harnessing Adversarial Examples". In: *International Conference on Learning Representations*. 2015. URL: http://arxiv.org/abs/1412.6572.

[3] N. Guglielmi and V. Protasov. "Exact computation of joint spectral characteristics of linear operators". In: *Foundations of Computational Mathematics* 13 (2013), pp. 37–97. DOI: 10.1007/s10208-012-9121-0.

[4] R. Jungers. *The joint spectral radius: theory and applications*. Vol. 385. Springer Science & Business Media, 2009. DOI: 10.1007/978-3-540-95980-9.

[5]   B. Lemmens and R. Nussbaum. *Nonlinear Perron-Frobenius Theory*. Vol. 189. Cambridge University Press, 2012. DOI: 10.1017/CBO9781139026079.

[6]   Q. Li, Z. Han, and X.-m. Wu. "Deeper Insights Into Graph Convolutional Networks for Semi-Supervised Learning". In: *Proceedings of the AAAI Conference on Artificial Intelligence* 32.1 (Apr. 2018). DOI: 10.1609/aaai.v32i1.11604.

[7]   J. K. Merikoski. "On c-norms and c-antinorms on cones". In: *Linear Algebra and its Applications* 150 (1991), pp. 315–329. ISSN: 0024-3795. DOI: 10.1016/0024-3795(91)90177-X.

[8]   R. Pascanu, T. Mikolov, and Y. Bengio. "On the difficulty of training recurrent neural networks". In: *Proceedings of the 30th International Conference on Machine Learning*. Vol. 28. 3. 2013, pp. 1310–1318. URL: https://proceedings.mlr.press/v28/pascanu13.html.

[9]   T. J. Piotrowski, R. L. G. Cavalcante, and M. Gabor. "Fixed points of nonnegative neural networks". In: *Journal of Machine Learning Research* 25.139 (2024), pp. 1–40. URL: http://jmlr.org/papers/v25/23-0167.html.

[10] P. Sittoni and F. Tudisco. "Subhomogeneous Deep Equilibrium Models". In: *Proceedings of the 41st International Conference on Machine Learning*. Vol. 235. 2024, pp. 45794–45812. URL: https://proceedings.mlr.press/v235/sittoni24a.html.

On the expressivity of the ExSpliNet model

Daniele Fakhoury and **Hendrik Speleers**
Department of Mathematics, University of Rome Tor Vergata, Rome, Italy

The approximation of high-dimensional functions is an extremely challenging task. Classical methods, based on a mesh, suffer in general from the so-called *curse of dimensionality* — their complexity has an exponential growth $\mathcal{O}(\epsilon^{-D})$ as the accuracy ϵ tends to zero in D dimensions — and thus in practice they are only suited for addressing lower-dimensional problems. On the other hand, machine learning techniques that are mesh-free, and in particular (deep) neural networks, seem to be able to overcome this issue for different kinds of high-dimensional problems, especially in the context of image analysis and pattern recognition.

Kolmogorov [3] proved that any multivariate continuous function can be written in terms of univariate continuous functions. More formally, the Kolmogorov superposition theorem (KST) states that any continuous function $f : [0,1]^D \to \mathbb{R}$ can be decomposed as

$$f(x_1, \ldots, x_D) = \sum_{i=1}^{2D+1} \Phi_i \left(\sum_{d=1}^{D} \Psi_{i,d}(x_d) \right),$$

with $\Psi_{i,d}$ and Φ_i univariate continuous functions on $[0,1]$, called *inner* and *outer functions*, respectively. Theoretical connections of the KST with neural networks started with the work of Hecht-Nielsen [2], where the inner and outer functions of the KST were interpreted as activation functions of a neural network. Later, Kůrková discussed the relevance of the KST [4] and provided a direct proof of the universal approximation theorem of multilayer neural networks based on the KST [5]. Recently, in [7], Montanelli and Yang applied the KST in the context of ReLU neural networks in order to get round the curse of dimensionality.

In this talk, we focus on a specific neural network model, called ExSpliNet, and discuss its expressivity. The ExSpliNet model, introduced in [1], is a model that combines ideas of Kolmogorov neural networks, ensembles of probabilistic trees, and multivariate B-spline representations. Inspired by the KST, an ExSpliNet function has the form

$$\sum_{t=1}^{T} \Phi_{\mathbf{w}^t}^{\mathbf{M},\mathbf{q}} \left(\left[\sum_{d=1}^{D} \Psi_{\mathbf{v}^{t,\ell,d}}^{N_\ell, p_\ell}(x_d) \right]_{\ell=1,\ldots,L} \right),$$

where univariate splines $\Psi_{\mathbf{v}^{t,\ell,d}}^{N_\ell, p_\ell}$ are used as inner functions that feed L-variate tensor-product splines $\Phi_{\mathbf{w}^t}^{\mathbf{M},\mathbf{q}}$ as outer functions, all of them represented in terms of B-splines.

The ExSpliNet model can be efficiently evaluated thanks to the computational properties of B-splines. Moreover, it is explicitly differentiable when taking B-splines of degrees at least two. In [1], a preliminary theoretical study of the universal approximation properties of ExSpliNet was carried out. Specifically, for the two cases $L = 1$ and $L = D$, it was shown that ExSpliNet has the ability of a universal approximator. Both approximation results are not completely satisfactory yet. Indeed, the proof of the former case is not constructive, while the ExSpliNet approximation considered in the latter case is affected by the curse of dimensionality.

We continue the analysis of the expressivity of the ExSpliNet model and provide two constructive approximation theorems that mitigate the curse of dimensionality, so improving upon the limitations encountered by the approximation results in [1].

Firstly, following ideas from [7] and using the explicit spline error bound in [6], we are able to have a fully constructive proof for a particular subset of multivariate continuous functions. Specifically, we show that such a function can be approximated up to an error ϵ by an ExSpliNet function with weight complexity $\mathcal{O}(\epsilon^{-\log_2(2D+2)})$ in D dimensions, so the curse of dimensionality is lessened.

Secondly, inspired by the neural network construction in [8] and using the explicit spline error bound in [9], we show a result on the approximation capabilities of the ExSpliNet model for multivariate generalised bandlimited functions. This time, the ExSpliNet model completely overcomes the curse of dimensionality. Specifically, a D-variate generalised bandlimited function can be approximated up to an error ϵ by an ExSpliNet function with weight complexity $\mathcal{O}(\epsilon^{\frac{-2}{q+1}-2})$, where q can be chosen independently of D.

References

[1] D. Fakhoury, E. Fakhoury, and H. Speleers. "ExSpliNet: An interpretable and expressive spline-based neural network". In: *Neural Networks* 152 (2022), pp. 332–346.

[2] R. Hecht-Nielsen. "Kolmogorov's mapping neural network existence theorem". In: *Proceedings of the IEEE First International Conference on Neural Networks*. Vol. 3. IEEE Press, 1987, pp. 11–13.

[3] A. N. Kolmogorov. "On the representation of continuous functions of several variables by superposition of continuous functions of one variable and addition". In: *Doklady Akademii Nauk SSSR* 114 (1957), pp. 953–956.

[4] V. Krurková. "Kolmogorov's theorem is relevant". In: *Neural Computation* 3 (1991), pp. 617–622.

[5] V. Kůrková. "Kolmogorov's theorem and multilayer neural networks". In: *Neural Networks* 5 (1992), pp. 501–506.

[6] M. Marsden. "On uniform spline approximation". In: *Journal of Approximation Theory* 6 (1972), pp. 249–253.

[7] H. Montanelli and H. Yang. "Error bounds for deep ReLU networks using the Kolmogorov–Arnold superposition theorem". In: *Neural Networks* 129 (2020), pp. 1–6.

[8]   H. Montanelli, H. Yang, and Q. Du. "Deep ReLU networks overcome the curse of di-
      mensionality for generalized bandlimited functions". In: *Journal of Computational
      Mathematics* 39 (2021), pp. 801–815.

[9]   G. Vainikko. "Error estimates for the cardinal spline interpolation". In: *Zeitschrift
      für Analysis und ihre Anwendungen* 28 (2009), pp. 205–222.

A multi-factor approach to identify differentially expressed genes in transcriptome data

Grazia Gargano[*]**, Flavia Esposito, and Nicoletta Del Buono**
Department of Mathematics, University of Bari Aldo Moro

Microarray and RNA-sequencing technologies are powerful tools for the analysis of gene expression across the genome and transcriptome, allowing the comprehensive study of transcriptional changes associated with different biological conditions. A critical application of these high-throughput gene expression technologies is the identification of differentially expressed genes (DEGs) between different biological states (disease versus normal, treatment versus control), different cell populations, or across different time points. Typically, a gene is considered to be differentially expressed if the observed difference or change in expression levels or read counts between different experimental conditions is statistically significant. The identification of DEGs helps to uncover the underlying molecular mechanisms that differentiate these conditions. While DEGs are crucial in transcriptomic research, there is still a need to determine the most effective methods for identifying genes that are significantly differentially expressed between two or more groups of samples, tissues, or cell populations. Numerous statistical methods and data analysis pipelines have been developed to identify DEGs using various predefined statistical or filtering thresholds for gene selection [3, 7]. These analyses often focus on pairwise group comparisons, providing limited insight into the underlying biology by excluding potential differences in other conditions. Such a restrictive analytical framework inherently limits the discovery of biological variation that may be present in more complex experimental designs. In addition, many analytical pipelines are heavily tailored to the platform used for transcriptomic analysis and may not be easily adaptable to other types of data. The current methodological landscape also lacks the capability to perform unsupervised DEGs analysis, which is essential for exploratory data-driven discovery.

We propose a mathematical framework based on multi-factor nonnegative matrix factorization (NMF) [5] to identify genes that exhibit differential expression across two or more distinct experimental conditions. Our data analysis pipeline is designed to apply this differential expression framework consistently across different experimental designs and high-throughput technologies. We consider a gene expression matrix $\mathbf{X} \in \mathbb{R}_+^{n \times m}$, where n is the number of samples (which may represent different patient groups, tissues, experiments, or time points) and m is the number of genes. To compare specific experimental conditions, we propose a semi-supervised framework based on three-factor NMF, which can be formulated as a constrained penalized optimization task:

$$\min_{\mathbf{U} \geq 0, \mathbf{S} \geq 0, \mathbf{V} \geq 0} D(\mathbf{X} | \mathbf{USV}^\top) + \lambda_\mathbf{U} \mathcal{P}_1(\mathbf{U}) + \lambda_\mathbf{S} \mathcal{P}_2(\mathbf{S}) + \lambda_\mathbf{V} \mathcal{P}_3(\mathbf{V})$$

where $D(\cdot, \cdot) : \mathbb{R}_+^{n \times m} \times \mathbb{R}_+^{n \times m} \to \mathbb{R}_+$ denotes some divergence function, which evaluates the goodness of fitting; $\mathbf{U} \in \mathbb{R}_+^{n \times k}$, $\mathbf{S} \in \mathbb{R}_+^{k \times r}$ and $\mathbf{V} \in \mathbb{R}_+^{m \times r}$ are the factors of data low-rank representation, $\mathcal{P}_1 : \mathbb{R}^{n \times k} \to \mathbb{R}$, $\mathcal{P}_2 : \mathbb{R}^{k \times r} \to \mathbb{R}$, $\mathcal{P}_3 : \mathbb{R}^{m \times r} \to \mathbb{R}$ codify regularization constraints to enforce specific properties on the factor matrices, while $\lambda_{\mathbf{U}}$, $\lambda_{\mathbf{S}}$ and $\lambda_{\mathbf{V}}$ are some positive regularization parameters. For the DEGs task, we consider the generalized Kullback-Leibler divergence as the cost function and set $k = r$ ($k, r < min(n, m)$) equal to the number of different conditions we want to compare. The sample label information is encoded in the structure of the factor $\mathbf{U}$. We impose $\mathbf{U}$ to be a binary matrix representing sample clusters, where $\mathbf{U}_{ij} \in \{0, 1\}$ and $\sum_{j=1}^{k} \mathbf{U}_{ij} = 1$. This ensures that each sample is assigned to exactly one cluster. Imposing sparsity and orthogonality constraints on the columns of $\mathbf{V}$ ensures that the extracted list of DEGs has minimal or no overlap of genes. Reconstruction error is minimized by using an alternating scheme with an appropriate choice of the multiplicative update rules [6]. We extract DEGs by considering genes that have relatively large coefficients in each biological process via the nonnegative factor $\mathbf{V}$ obtained from the decomposition. For discovery purposes, when sample label information is not available, the proposed three-factor NMF framework reduces to the standard unsupervised two-factor NMF [2] through the transformation $\mathbf{U} \leftarrow \mathbf{US}$. Two-factor NMF is a robust method for class discovery, which, in turn, allows for the identification of DEGs. This technique enables the detection of underlying patterns and structures within gene expression data that may not be apparent using traditional approaches. To gain functional insights, DEG lists are further analyzed by examining gene interaction networks. This approach aims to elucidate their role in biological processes, identify core pathways, reveal functional relationships, and improve the interpretability of results.

We applied the proposed DEGs identification framework to two oncology case studies. In the first case, we used the framework to develop a DEGs signature for transcriptomic stratification of mediastinal gray zone lymphoma (MGZL), a rare and diagnostically challenging lymphoma with features overlapping with primary mediastinal B-cell lymphoma (PMBL) and classical Hodgkin lymphoma (CHL) [4]. The framework, used in an unsupervised manner, generated a robust gene expression-based signature that helps categorize MGZL based on its transcriptomic similarity to either CHL or PMBL, potentially leading to improved diagnostic accuracy and therapeutic strategies. In the second case study, we apply the pipeline to extract two DEGs signatures from profiles representative of wild-type and resistance MCF-7 cells [1]. Subsequent pathway analysis revealed key genes, such as MAOA, IL4I1, RRM2, DUT, NME4, and SUMO3, as novel elements in resistance pathways. This analysis enhances our understanding of resistance mechanisms in MCF-7 cells and may guide the development of more effective treatments.

References

[1] A. Boccarelli, N. Del Buono, and F. Esposito. "Cluster of resistance-inducing genes in MCF-7 cells by estrogen, insulin, methotrexate and tamoxifen extracted via NMF". In: *Pathology - Research and Practice* 242 (2023), p. 154347. ISSN: 0344-0338. DOI: 10.1016/j.prp.2023.154347.

[2] J.-P. Brunet, P. Tamayo, T. R. Golub, and J. P. Mesirov. "Metagenes and molecular pattern discovery using matrix factorization". In: *Proceedings of the National Academy of Sciences* 101.12 (Mar. 2004), pp. 4164–4169. ISSN: 1091-6490. DOI: 10.1073/pnas.0308531101.

[3] Z. Fang, J. Martin, and Z. Wang. "Statistical methods for identifying differentially expressed genes in RNA-Seq experiments". In: *Cell & Bioscience* 2.1 (Jan. 2012). ISSN: 2045-3701. DOI: 10.1186/2045-3701-2-26.

[4] G. Gargano et al. "A targeted gene signature stratifying mediastinal gray zone lymphoma into classical HL-like or PMBL-like subtypes". In: *Haematologica* (2024). DOI: 10.3324/haematol.2024.285266.

[5] N. Gillis. *Nonnegative Matrix Factorization*. Philadelphia: SIAM, 2020.

[6] D. Lee and H. Seung. "Algorithms for Non-negative Matrix Factorization". In: *Adv. Neural Inform. Process. Syst.* 13 (Feb. 2001).

[7] D. Rosati et al. "Differential gene expression analysis pipelines and bioinformatic tools for the identification of specific biomarkers: A review". In: *Comput. Struct. Biotechnol. J.* 23 (Mar. 2024), pp. 1154–1168. DOI: 10.1016/j.csbj.2024.02.018.

A non-convex optimization strategy applied to signal decomposition

Laura Girometti

University of Bologna

Many applications in signal and image processing, wireless communications and machine learning, can be formulated as non-convex and non-smooth optimization problems. From the perspective of the mathematical model, they are computationally challenging to solve due to the presence of multiple local stationary points that are not necessarily global optima, while from the algorithmic point of view, the difficulties reside in the sensitivity to initialization, low efficiency, and critical convergence.

In this work, we address the following generic non-convex parametric optimization problem

$$x^* \in \arg \min_{x \in \mathbb{R}^N} \left\{ \mathcal{J}(x; a, \gamma_1, \gamma_2, \ldots) := \gamma_1 \mathcal{J}_1(x; a) + \gamma_2 \mathcal{J}_2(x) + \gamma_3 \mathcal{J}_3(x) + \cdots + \mathcal{J}_M(x) \right\},$$

where the cost function $\mathcal{J}$ is parameterized by a set of parameters $\gamma_1, \gamma_2, ..$ which balance the action of M different energy terms. The function $\mathcal{J}$ is defined by the sum of a non-convex parametric term $\mathcal{J}_1(x; a)$, which makes $\mathcal{J}(x; a, \gamma_1, \gamma_2, \ldots)$ eventually non-convex, and other convex smooth energy terms $\mathcal{J}_2(x), \mathcal{J}_3(x), \ldots, \mathcal{J}_M(x)$.
The parameter a tunes the degree of non-convexity of the functional $\mathcal{J}_1(x; a)$ and in the following, we will assume that setting $a = 0$ ensures $\mathcal{J}_1(x; a)$ to be convex and non-convex for $a > 0$. In [4], there are popular examples of (sparsity-promoting) parameterized non-convex penalty functions.
Different strategies have been proposed to tackle these non-convex and eventually non-smooth optimization problems: the underlying idea is to convexify the objective function by using the convex envelope or by applying, if possible, a ConvexNonConvex strategy [4] such that, although the functional contains a non-convex term, the overall functional is convex. An other approach, the "Graduated NonConvexity" (GNC), term coined by Blake and Zisserman in [1], solves a well-constructed sequence of non-convex problems of increasing complexity to gradually approach the target solution reducing the problem of local minimizers by estimating a good initial guess[6].
Combining the idea of GNC with an automatic setting of the parameters, we propose our Predictor-Corrector Algorithmic Framework, also inspired by the Predictor– Corrector (PC) method [2], designed to integrate ordinary differential equations, which uses a suitable combination of an explicit and an implicit technique to improve the approximation accuracy while obtaining better convergence characteristics.
Given a non-convex optimization problem in the above form, the proposed general PC

algorithmic framework consists in estimating a good starting point $\widehat{y}$ as the global minimizer of the convex functional $\mathcal{J}(x; a = 0, \widehat{\gamma}_1, \widehat{\gamma}_2, ..)$, where $\widehat{\gamma}_1, \widehat{\gamma}_2, ..$ are the optimal values for the multi-parameters that characterize the cost function $\mathcal{J}$ obtained by minimizing a context-aware function $\mathcal{E}(\gamma_1, \gamma_2, \dots) : \mathbb{R}^{M-1} \to \mathbb{R}$ which represents properties of the specific application context. The global minimizer $\widehat{y}$ is the output of the `Predictor()` step and it's used as inizialization for the iterative procedure used for solving the non-convex `Corrector()` minimization of $\mathcal{J}(\widehat{y}; a > 0, \widehat{\widehat{\gamma}}_1, \widehat{\widehat{\gamma}}_2, ..)$, where the parameter a is estimated imposing an optimal non-convexity degree and $\widehat{\widehat{\gamma}}_1, \widehat{\widehat{\gamma}}_2, ..$ are computed by applying the same strategy proposed for $\widehat{\gamma}_1, \widehat{\gamma}_2, \dots$ The convergence to a local (and, possibly, global) minimizer of the original optimization problem with the parameters $a, \gamma_1, \gamma_2, \dots$ selected is therefore favored and accelerated by having a good initialization.

An example of application is the additive decomposition of a 1D signal into semantically distinct components, that is usually addressed as a non-convex optimization problem where each energy term is suitable to capture a specific component. In particular, we estimate the signal components cartoon c, smooth s, and oscillatory o of a given sampled signal $f \in \mathbb{R}^N$ by solving the following optimization problem

$$\{\widehat{c}, \widehat{s}, \widehat{o}\} \quad \in \quad \underset{c,s,o \in \mathbb{R}^N}{\arg \min} \left\{ \gamma_1 \sum_{i=1}^{N} \phi\left(|(\mathsf{D}c)_i|_2; a\right) + \frac{\gamma_2}{2} \|\mathsf{H}s\|_2^2 + \|o\|_G \right\}, \quad (24.1)$$

$$\text{subject to}: \ c + s + o = f, \ \sum_{i=1}^{N} c_i = 0, \quad (24.2)$$

where the penalty function ϕ is the minimax concave (MC) penalty function $\phi : \mathbb{R} \to \mathbb{R}_+$ with parameter $a \in \mathbb{R}_+$ and $\phi(t; 0) = \lim_{a \to 0} \phi(t; a) = |t|$, $\mathsf{D}, \mathsf{H} \in \mathbb{R}^{N \times N}$ are finite difference matrices discretizing the first- and second- order derivatives and the G-norm $\|o\|_G$ [5] is defined as

$$\|o\|_\mathsf{G} := \inf \left\{ \|g\|_\infty \ \big| \ o = -\mathsf{D}^\mathsf{T} g, \ g \in \mathbb{R}^N \right\},$$

with $\|g\|_\infty := \max_i |g_i|$. The PC framework is successfully applied to the signal decomposition problem, where a convergent ADMM-based algorithm is proposed to solve the general minimization problem in (24.1)-(24.2) and a cross-correlation function which measures the separability among the different components, properly captures the optimal parameters γ_1, γ_2 of the cost function [3].

References

[1] A. Blake and A. Zisserman. *Visual Reconstruction*. Cambridge, MA, USA: MIT Press, 1987. ISBN: 0262022710.

[2] J. C. Butcher. *Numerical Methods for Ordinary Differential Equations*. John Wiley & Sons, Ltd, 2016. ISBN: 9781119121534. DOI: 10.1002/9781119121534.fmatter.

[3] L. Girometti, M. Huska, A. Lanza, and S. Morigi. "Convex Predictor–Nonconvex Corrector Optimization Strategy with Application to Signal Decomposition". In: *Journal of Optimization Theory and Applications* (2024). DOI: 10.1007/s10957-024-02479-2.

[4] A. Lanza, S. Morigi, I. W. Selesnick, and F. Sgallari. "Convex Non-convex Variational Models". In: *Handbook of Mathematical Models and Algorithms in Computer Vision and Imaging: Mathematical Imaging and Vision*. Ed. by K. Chen, C.-B. Schönlieb, X.-C. Tai, and L. Younces. Cham: Springer International Publishing, 2021, pp. 1–57. ISBN: 978-3-030-03009-4. DOI: 10.1007/978-3-030-03009-4_61-1.

[5] Y. Meyer and D. Lewis. *Oscillating Patterns in Image Processing and Nonlinear Evolution Equations: The Fifteenth Dean Jacqueline B. Lewis Memorial Lectures*. Memoirs of the American Mathematical Society. American Mathematical Society, 2001.

[6] M. Nikolova, M. K. Ng, and C.-P. Tam. "Fast Nonconvex Nonsmooth Minimization Methods for Image Restoration and Reconstruction". In: *IEEE Transactions on Image Processing* 19.12 (2010), pp. 3073–3088. DOI: 10.1109/TIP.2010.2052275.

Numerical Computation of Generalized Wasserstein Distances with Applications to Traffic Model Analysis

Maya Briani[a], Emiliano Cristiani[a], Giovanni Franzina[a], Francesca L. Ignoto[a,b,∗]
[a] Istituto per la Applicazioni del Calcolo "M. Picone" (IAC), CNR, Rome, Italy
[b] Dipartimento di Scienze di Base e Applicate per l'Ingegneria (SBAI), Sapienza Università di Roma, Italy

Introduction. In this work we are concerned with the numerical computation of Wasserstein distance (WD) and Generalized Wasserstein distance (GWD) in the context of traffic flow models. As for all dynamical systems, the study of the sensitivity of the models can be realized measuring the 'distance' between two solutions obtained with different inputs (like, e.g., any of the model parameters, initial conditions, boundary conditions, etc.). This allows one to understand their impact on the final solution, and ultimately quantify the degree of chaoticity of the system. The question arises which distance is more suitable to this kind of investigation. It is by now well understood that L^p distances do not catch the natural concept of distance among traffic (vehicle) densities, see, e.g., the discussion in [3, Sec. 7.1], while the WD appears more natural in the context of traffic flow, see, e.g., [1, 3]. The drawback is that WD is limited to balanced mass distribution (equal masses), while real traffic problems often need to consider scenarios with a different amount of vehicles, especially because of different inflow/outflow at boundaries. This suggests to move towards GWDs, which allows to deal with unbalanced mass distributions. We consider the three GWDs introduced by Figalli & Gigli (FG) [4], Piccoli & Rossi (PR) [5], Savaré & Sodini (SS) [6], and we propose three numerical approaches for the approximation of these distances: the first two approaches are based on the reformulation of the original problems in terms of linear programming problems, while the third one is based on a gradient-free descent method.

Numerical comparison. In the following test we compare the three GWDs in order to understand which one is the most suitable in the context of traffic flow modeling. Denoting by χ the indicator function, we consider the case of two time-dependent distributions with parameters $\alpha, \beta, \eta > 0$,

$$\rho^{\mathsf{s}}(x,t) = \alpha\chi_{[-t-\eta,-t+\eta]}(x), \qquad \rho^{\mathsf{D}}(x,t) = \beta\chi_{[t-\eta,t+\eta]}(x), \qquad 0 \leq t \leq T \qquad (25.1)$$

in the domain $X = [-T - \eta, T + \eta]$ (T being the final time). The two step functions start with perfectly overlapping support, then supply mass moves leftward while demand mass moves rightward, until they both reach the boundary of the domain.

Fig. 25.1 shows the behavior of the three GWDs between ρ^{s} and ρ^{D} as defined in (25.1), as a function of time, with $\alpha \in \{1,2\}$, $\beta = 2$, $\eta = 1$, $T = 4$. This comparison test
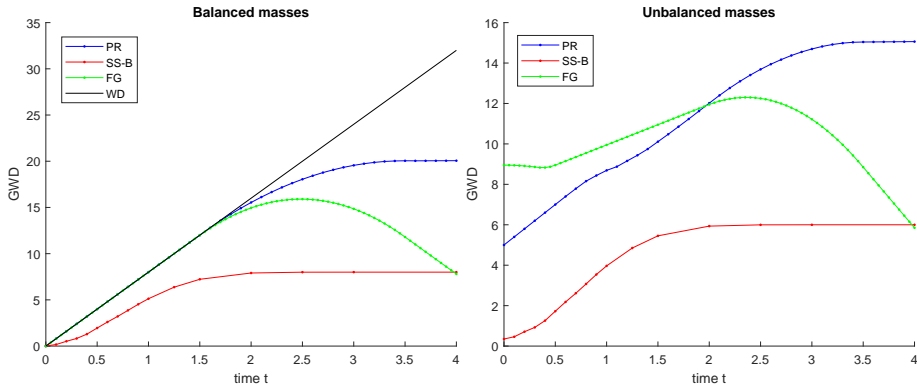
Figure 25.1: Test on numerical comparison.

allows us to sketch some preliminary conclusions. First of all, the SS approach seems to be computationally unfeasible. In fact, it is impossible to deal with a reasonably fine discretization grid. Second, SS and PR approaches share with L^p an important drawback: they saturate when distributions do not overlap and they are far enough to each other. This can be a problem in some scenarios. Lastly, FG approach has an important feature: it tends to diminish if distributions are close to the boundaries, even if they are very far from each other. On first glance, this seems to be an issue, but it can be also be seen as a good point. Basically it implies that what happens near the boundaries is less important than what happens on the rest of the road. Considering the fact that boundary conditions are typically unknown in traffic flow modeling, it could make sense to give priority to that part of the road which is less or not at all influenced by boundary conditions.

Sensitivity to boundary conditions. In this test we investigate the sensitivity to boundary conditions. In the same spirit of [2], we assume that the time interval is divided in two subintervals: $[t_0, 0]$ and $(0, T)$, where $t = 0$ corresponds to the time the simulation is actually performed. We compare two vehicle distributions which evolves through the LWR model: the "exact" solution ρ^s and the "predicted" solution ρ^p. The first is obtained by using the exact boundary fluxes $F_{IN}(t)$, $F_{OUT}(t)$, randomly generated, in the whole interval $[t_0, T]$. Instead the second is obtained by using flux boundary data until time $t = 0$ and then by using the constant predicted average values

$$\hat{F}_{IN} = \frac{1}{T} \int_0^T F_{IN}(t)dt, \qquad \hat{F}_{OUT} = \frac{1}{T} \int_0^T F_{OUT}(t)dt,$$

until time T. At any time t, the vehicle distributions $\rho^s(\cdot, t)$ and $\rho^p(\cdot, t)$ are numerically approximated by means of the Godunov scheme and they are compared computing the GWDs introduced by FG and PR.

Fig. 25.2 shows a snapshot of the simulations at times $t = 12$ (left) and the GWDs between $\rho^s(\cdot, t)$ and $\rho^D(\cdot, t)$ at any time (right).
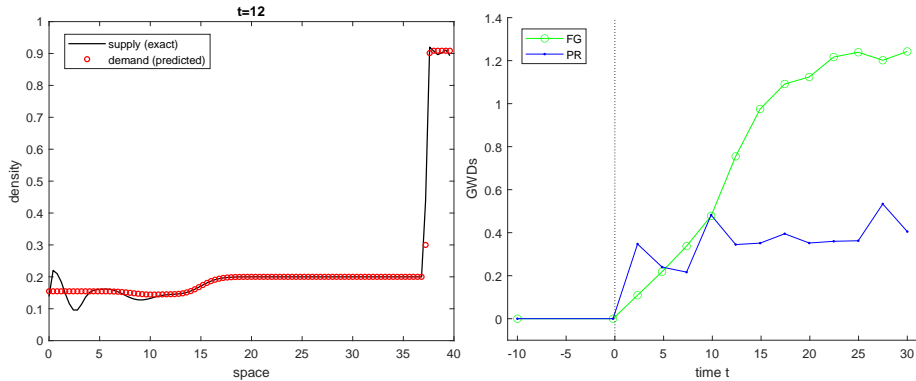
Figure 25.2: Test on sensitivity to boundary conditions.

We can conclude that the FG approach seems to be more suitable for the context of vehicular traffic because it better catches the growth of the error when the difference between the two vehicle distributions spreads towards the inside of the road.

References

[1] M. Briani, E. Cristiani, and E. Iacomini. "Sensitivity analysis of the LWR model for traffic forecast on large networks using Wasserstein distance". In: *Commun. Math. Sci.* 16.1 (2018), pp. 123–144. DOI: 10.1016/j.matpur.2009.11.005.

[2] M. Briani, E. Cristiani, and E. Onofri. "Inverting the fundamental diagram and forecasting boundary conditions: How Machine Learning can improve macroscopic models for traffic flow". ARXIV: 2303.12740.

[3] E. Cristiani, B. Piccoli, and A. Tosin. *Multiscale modeling of pedestrian dynamics*. Vol. 12. Series Modeling, Simulation & Applications. Springer, 2014.

[4] A. Figalli and N. Gigli. "A new transportation distance between non-negative measures, with applications to gradients flows with Dirichlet boundary conditions". In: *Journal de Mathématiques Pures et Appliquées* 94.2 (2010), pp. 107–130. DOI: 10.1016/j.matpur.2009.11.005.

[5] B. Piccoli and F. Rossi. "Generalized Wasserstein distance and its application to transport equations with source". In: *Archive for Rational Mechanics and Analysis* 211 (2014), pp. 335–358. DOI: 10.1007/s00205-013-0669-x.

[6] G. Savaré and G. E. Sodini. "A relaxation viewpoint to Unbalanced Optimal Transport: Duality, optimality and Monge formulation". In: *Journal de Mathématiques Pures et Appliquées* 188 (2024), pp. 114–178. DOI: 10.1016/j.matpur.2024.05.009.

Automatic Character Recognitions Tamahaqt in Amazigh Language

Larbi Asli[a,*], Nada Djouhira[a], Chahinaz Ben Haddadi[a], and Ali Zaidi[b]

[a] LaMOS Laboratory UAMB University, Algeria

[b] Center of Research in Amazigh Culture and Language(CRLCA), Bejaia, Algeria

Introduction

In recent years, with the evolution of computer systems and sophisticated software, advanced technology has been integrated into many fields related to industry, ranging from construction, transportation and manufacturing to business intelligence, education and healthcare.

In the continuous pursuit of technological advancements, character recognition is emerging as a new testing ground for various advanced solutions. The ultimate goal, shared by all developers of this technology, is to leverage innovation in all its forms to enhance the tools of tomorrow. This emerging technology is set to become a key component in the future development of recognition systems.

Automatic character recognition is a broad field of research. When applied to a specific language, such as Tamahaqt within the Amazigh language family, it requires a deep understanding and cognitive expansion of the language, which is spoken by a minority of the population in North Africa.

Tamahaqt, the language of the Tuaregs, faces significant challenges in terms of preservation and education. Learning this language for knowledge purposes is hindered by a lack of available tools and information.

ⵏⵛⴻⵜ ⵜⵏ ⵜⵏⵛⴻⵏ ⵙⵜⴻⵏⵥⴻ ⵔ ⵏⵯⵓⵜⴻ ⵔ
ⵏⵓⵛⴻⵏ ⵉ ⵙⵙ ⴻⵏⵏⴻⵏ ⵛⴻ ⴻⵏⵉ ⵉⵗⵍ ⵜⵙⵓⵜⵏⵏⵙⵉ
ⵐ ⵙⴻⵏ ⴻⵏⵓⴻⵏⵉ ⴻⵛⵙⵓ ⵐ ⵉⴻⵏ ⵉⵏⵏⵗⵛ ⵛⵔ
ⵏⵛⵯⵉⵔⵛ

In this project, we aim to develop advanced tools for processing the Tamahaqt dialect of the Amazigh language, addressing significant challenges in computational linguistics. The Tamahaqt dialect, with its rich morphology, lacks sufficient tools for automatic processing. Creating effective tools through extensive research is essential for preserving and promoting the Tamahaqt dialect and Amazigh culture.

Materiel requirements and results

This work aims to address the lack of documentation and data on the Tamahaqt language by using automatic character recognition through CNN. By exploring various aspects of

this issue, we seek to provide a deep understanding and propose perspectives for the future development of this technology. We focus on the use of CNNs, which are particularly effective for image recognition, including Tamahaqt characters. To overcome the lack of resources, we have adopted a structured methodology, collecting data from books [2] and final year theses from the University of Tamanrasset [4, 6].

Summary of OCR Functionality

Optical Character Recognition (OCR) systems use advanced technologies to extract information from scanned documents and convert it into text files. They identify characters by comparing black and white colours, then convert them into ASCII text. Typical steps in ORC processing are as follows:

Image Preprocessing. Enhancing image quality for better recognition, including resizing, binarization, noise removal, and normalization.

Segmentation. Identifying and separating characters by extracting local features.

Character Recognition. Comparing normalized characters with a library of shapes to find the most likely match, using techniques like feature classification, metric methods, and static methods.

Post-processing. Using linguistic and contextual approaches to minimise errors, with systems based on rules or statistical methods.

Using CNNs for Character Recognition

CNNs are particularly effective for character recognition due to their ability to automatically extract complex features from images.

Preprocessing. The images of characters in our dataset were preprocessed to standardise size and improve image quality (binarization, resizing, etc.).

Training. A large labelled dataset of characters was used to train the CNN. The network learns to recognise the distinctive patterns of each character through thousands of examples.

Prediction. Once trained, the CNN model can take an image of a character as input and predict, with a certain probability, which character it corresponds to.

Implementation Methodology

For the implementation methodology, we will present the various stages of our source code, which are: (i) importing the necessary libraries, (ii) importing the dataset, (iii) pre-processing the images in the dataset, (iv) initializing hyperparameters, constructing the CNN architecture, (v) compiling and tuning the model, and (vi) evaluating the model.

The loss and accuracy values for both training and validation are plotted in Figure 26.1, with red representing training and green representing validation. The loss curve shows a decrease in training loss from 17.9457 to 15.9152, while the validation loss decreases from 15.9019 to 15.8160. For what concerns accuracy, training remains stable at approximately 0.0103, and validation accuracy increases slightly from 0.0116 to 0.0124.

These results suggest that the model is gradually improving its performance on the validation set, albeit marginally.
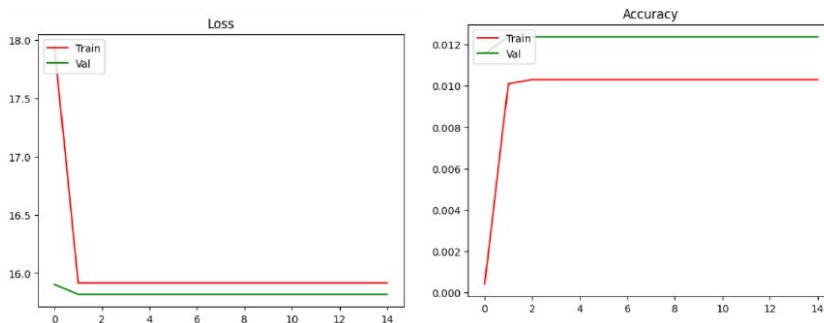
Figure 26.1: Results visualisation

Conclusion and future works

Our study investigated automatic character recognition for the Tamahaqt language using Python and Convolutional Neural Networks (CNNs). After detailing the tools and development environment, we conducted experiments by importing packages and data, performing preprocessing, and applying the CNN model.

The results indicate limited performance, primarily due to insufficient data and hardware constraints. To address these challenges, we recommend utilising cloud computing services such as Google Cloud Platform, which can provide the necessary computational power and enhance prediction accuracy, provided there is an adequate database for deep learning methods.

References

[1]   F. Ataallah and S. Boulaknadel. "La promotion de l'amazighe à travers les technologies de l'information et de la communication". In: *Asinag* 9 (2014), pp. 33–48.

[2]   G. Karl. *A Grammatical Sketch of the Tamaheq or Towarek Language*. Ed. by R. Crescent. Vol. 4. Dec. 1861.

[3]   C. Iarsonneur. "Intelligence artificielle et/ou diversité linguistique : les paradoxes du traitement automatique des langues". In: *Hybrid journal* 7.avril (2021).

[4]   I. Lkan and X. Mlenad. "imodrn oin t asi li t an ah gar d ta saq tat lt girisn doadmn." MA thesis. Université de Tamanghasset, 2022.

[5]   D. Prasad, M. Sanhita, and J. Smrutisikha. "Image classification using machine learning". In: *Indonesian Journal of Electrical Engineering and Computer Science* 31.3 (2023).

[6]   T. Zinab and T. Saghida. "Initn dghtmnghstu." MA thesis. Université de Tamanghasset, 2022.

An high order AT1 phase-field model for brittle fracture

Eleonora Maggiorelli
University of Pavia

Fracture represents one of the most severe failure modes for solid materials or structures. Accurately predicting fracture nucleation and propagation is crucial in engineering, especially from the standpoint of safety. This requirement has led to the development of several theoretical models and numerical methods.

Phase-field modeling is based on the variational formulation of brittle fracture [3], and the evolution of cracks is posed in terms of the equilibrium configurations of the total energy, i.e. the sum of elastic and fracture energy. The description of the cracks depends on a damage parameter $d \in [0, 1]$, assessing the integrity of the material, together with an internal length parameter ϵ, controlling the width of the transition layer between $d = 0$ and $d = 1$. These two values of the phase field parameter correspond respectively to sound material and fracture. The phase-field approach relies on the solid base of Γ-*convergence* [1, 2] and specifically on the convergence of the phase-field energy to the sharp crack energy, as the internal length ϵ vanishes. There are many choices for both the elastic and fracture energy functionals. In [4], we focus on the fracture energy $\mathcal{K}$ and propose a novel model. In literature it is customary to call:

1. $\mathcal{K}(d) = \int_{\Omega} \epsilon^{-1}\phi(d) + \epsilon|\nabla d|^2 \, dx,$
2. $\mathcal{K}(d) = \int_{\Omega} \epsilon^{-1}\phi(d) + \epsilon|\nabla d|^2 + \epsilon^3|\Delta d|^2 \, dx,$

second- and fourth-order energies respectively, making reference to the associated Euler-Lagrange equations. Simulations based on **high-order functionals** are generally more accurate in approximating dissipated energy [5], and they allow the use of larger mesh sizes, offsetting the computational costs associated with second-order derivatives.

The most common choices for ϕ are $\phi(d) = d$ and $\phi(d) = d^2$, corresponding to the AT1 and AT2 functionals, respectively. From a mechanical standpoint, **AT1 functionals** typically exhibit better properties than AT2, as they result in a clear linear elastic regime before the onset of fracture [7]. On the contrary, AT2 generates damage at arbitrarily small values of stress. Moreover, for given values of internal length and mesh size the damage profile around the crack is usually narrower with AT1.

Our goal in [4] was to combine both these advantages and propose a novel AT1 fourth-order phase-field model for brittle fracture, within an isogeometric framework, which provides a straightforward discretization of the high-order term in the fracture energy functional.

For the introduced AT1 functional, we first proved a Γ-**convergence result** (in both the continuum and discretized isogeometric setting) based on a careful study of the optimal

transition profile. To do so, we defined the crack surface energy as follows

$$\mathcal{K}_\rho(d) = \frac{1}{c_\rho} \int_\Omega \epsilon^{-1}d + \epsilon|\nabla d|^2 + \rho\,\epsilon^3|\Delta d|^2\,dx,$$

where $\rho > 0$ is a parameter weighting the effects of the high-order term. Technically, previous results in the literature, see e.g. [1, 6] do not apply here due to the combination of the high order term and the constraint $d \in [0,1]$. Hence, we developed a novel line of proof.

The value c_ρ is generically characterized as a function of the optimal profile d_*, that needs to be explicitly computed. Nevertheless, the constraint $d \in [0,1]$ does not allow to directly employ the linear ODE resulting from the Euler-Lagrange equation. Therefore, we proceed in the following way:

- we introduce an auxiliary localized unconstrained problem, whose solution d_R is characterized by the ODE with suitable boundary conditions on $\{0, R\}$ and can be explicitly computed;

- since the solution does not satisfy the constraint $d_R \in [0,1]$, not all of these profiles are admissible (see Figure 27.1 left) and we prove that the optimal profile is the admissible solution with the largest support;

- we provide an explicit formula for the width of the support of the optimal profile from which we finally get the optimal profile d_* and the value of c_ρ.

This approach is quite general and indeed it applies also to the other AT1 functionals in the literature.

We carried out a detailed study of the **numerical** performance of the model. For AT1, we linked the mesh size to the finite support of the optimal profile, and just adopted the same choice for AT2 (since it has infinite support). As can be seen in Figure 27.1, the optimal profile in our model has wider support than that in the second-order model (obtainable for $\rho \to 0$) so a coarser mesh size can be employed to solve them. We considered different benchmarks and we report as an example in Figure 27.2 the results for the DCB test. In terms of effective toughness, the proposed fourth-order AT1 model is more accurate than the other AT models examined (red box in Figure 27.2). Moreover, as anticipated, once the accuracy is fixed, the model allows to employ larger mesh sizes entailing a lower computational cost (blue box in Figure 27.2).

References

[1] A. Braides. *Approximation of Free-Discontinuity Problems*. Springer-Verlag, Berlin, 1998.

[2] G. Dal Maso. *An introduction to Γ-convergence*. Boston: Birkhäuser, 1993, pp. xiv+340. ISBN: 0-8176-3679-X.
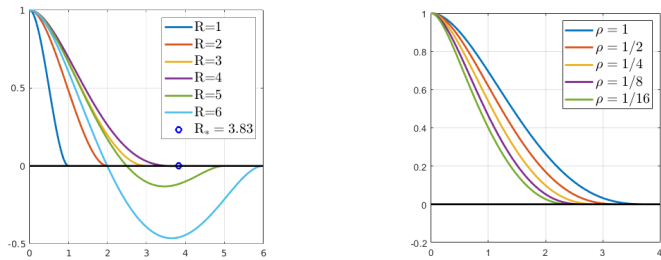
Figure 27.1: Left: The solution of the unconstraind auxilairy problems as a function of R for $\rho = 1$. Right: The optimal profiles d_* as a function of ρ.
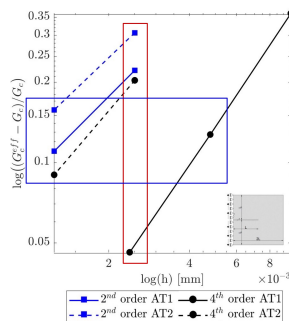
Figure 27.2: Numerical results for the DCB test. The red box compares the accuracy at a fixed mesh size while the blue box compares the mesh size at a fixed accuracy.

[3] G. A. Francfort and J.-J. Marigo. "Revisiting brittle fracture as an energy minimization problem". In: *Journal of the Mechanics and Physics of Solids* 46.8 (1998), pp. 1319–1342.

[4] L. Greco, E. Maggiorelli, M. Negri, A. Patton, and A. Reali. "AT1 fourth-order isogeometric phase-field model for brittle fracture".

[5] L. Greco, A. Patton, M. Negri, A. Marengo, U. Perego, and A. Reali. "Higher order phase-field modeling of brittle fracture via isogeometric analysis". In: *Engineering with Computers* (2024), pp. 1–20.

[6] M. Negri. "Γ-convergence for high order phase field fracture: Continuum and isogeometric formulations". In: *Computer Methods in Applied Mechanics and Engineering* 362 (2020), p. 112858.

[7] K. Pham, H. Amor, J.-J. Marigo, and C. Maurini. "Gradient damage models and their use to approximate brittle fracture". In: *International Journal of Damage Mechanics* 20.4 (2011), pp. 618–652.

Computational Model for Text Optimization: Substantive Reduction to Improve the Semantic Perception of Information

David Mavrodiev

University College London (UCL)

This study explores the development of a computational model designed for the optimization of textual content through systematic content reduction. The core objective is to enhance the comprehension of information presented in texts by reducing content while retaining essential meaning. Two key hypotheses guide this research. The first hypothesis posits that it is possible to construct a computational model capable of optimizing text via content reduction, improving the reader's ability to grasp the semantic depth of the material. The second hypothesis asserts that this model is not merely a theoretical construct but can also be practically applied across various real-world scenarios, enhancing text accessibility and clarity in diverse contexts.

In analyzing textual information, the model treats text as a composition of fundamental elements such as paragraphs, sentences, words, and even individual characters or bits. The model decomposes the text into these basic units, facilitating a granular analysis of the informational content carried by each element. Information within a text is defined as a set of elements, where each element contributes to the total information. The sum of these contributions always equals one, indicating that the overall information within the text is distributed among its individual components. Although this distribution might be assumed to be uniform, this assumption often does not hold true in practice. Depending on the reader's objectives and the context, some text elements carry more informational weight than others.

A key feature of the model is its assumption of linear relationships between the text elements, allowing for efficient computation of information distribution. However, the model also recognizes that in certain cases, these relationships might be non-linear, necessitating more complex computational strategies than simple summation.

The comprehension of textual information is evaluated through a metric designed to measure the reader's ability to answer questions based on the text. Textual comprehension is represented by a score, that accounts for the correct answers derived from the text's information. The score is computed by analyzing the proportion of questions that can be answered using the available information weighted by the significance of each text element.

The quality of text reduction, represented by a metric, is another critical aspect of the model. This metric evaluates the balance between the length of the reduced text and the information loss incurred during the reduction process, also allowing for the comparison

of the quality of different versions of text reductions.

The model also outlines fundamental properties that guide its operation. For instance, optimization by removing redundant information is based on identifying and eliminating semantically repetitive elements that do not contribute additional information. Similarly, enhancing comprehension by removing contradictions involves detecting and eliminating elements that introduce semantic inconsistencies within the text. The goal of the model is to reduce the given text to its optimal version based on the context by removing all repetitive and contradictory elements. The described definitions and properties, which lead to the definition of the optimal text, provide evidence in support of the first hypothesis, demonstrating that a computational model can effectively optimize textual content through systematic reduction and also improve comprehension.

Practical applications of the model are diverse, ranging from summarization of text based on context (e.g., answering specific questions) to transforming large, unspecialized textual datasets into more specialized ones. This transformation facilitates the training of domain-specific language models by breaking down large datasets into smaller, more focused datasets. Additionally, the model can be used to explore differences in text perception between language models and human readers, offering insights into how different audiences interpret the same text.

These applications demonstrate that the computational model has practical utility, thus validating the second hypothesis, which posits that the model is applicable to real-world scenarios.

References

[1] J. Devlin, M.-W. Chang, K. Lee, and K. Toutanova. "BERT: Pre-training of Deep Bidirectional Transformers for Language Understanding". ARXIV: 1810.04805. 2018.

[2] A. Radford, J. Wu, R. Child, D. Luan, D. Amodei, and I. Sutskever. *Language Models are Unsupervised Multitask Learners*. Tech. rep. OpenAI, 2019.

[3] C. Shannon. "A Mathematical Theory of Communication". In: *Bell System Technical Journal* 27 (1948), pp. 379–423, 623–656.

A funnel plot approach for monitoring Antibiotic Resistance in EU countries based on the WHO GLASS dashboard

Simone Milanesi

Department of Mathematics, University of Pavia

Antimicrobial Resistance (AMR) poses a significant global health challenge [5], necessitating robust surveillance methods to monitor its prevalence and trends across different hospitals, regions or countries. According to [3], "Setting up country-level surveillance of resistance and consumption is vital for understanding the impact of AMR and to reduce the spread of resistant pathogens".

This work introduces *funnel plots* [7] as a statistical process control method [4] which, unlike tools designed to identify increases in the AMR percentage, detects when a region's AMR percentage deviates significantly from the global average, thus indicating an anomaly. Control limits with a prescribed false alarm rate are derived under the assumption that the distribution of regional AMR percentages is well approximated by a Gaussian with variance inversely proportional to the number of tested isolates.

The main objectives of this work are

(a) to define a model of natural variability of AMR that considers the number of performed tests and provides alarm limits;

(b) to develop a diagnostic tool for statistically monitoring AMR at country level, as reported in the GLASS (Global Antimicrobial Resistance and Use Surveillance System) dashboard [6];

(c) to study how the distribution of antimicrobial resistance between countries depends on the Gross Domestic Product (GDP).

In order to achieve these objectives, we propose the following mathematical modeling. Let $\{1, \ldots, i, \ldots, n\}$ be the countries that belong to WHO Europe region, and let (x_i, y_i, g_i) the observations of the i-th country, where x_i denotes the number of tested isolates (AST), y_i the percentage of AMR on the isolates and g_i the GDP (Gross Domestic Product).

AMR resistance data for year 2020, pertaining to the WHO European region, were acquired from the GLASS dashboard, which presents global antibiotic consumption and resistance data for countries, territories, and areas, enrolled in GLASS. For each pathogen-antibiotic pair, the GLASS dashboard provides the number of performed Antibiotic Susceptibility Tests (AST) and the corresponding resistance percentage for each country. GDP data in US dollars (\$) for year 2021 have been acquired from the World Bank DataBank [1].

First, for each pathogen-antibiotic pair, we studied the relationship between the GDP and the AMR percentage of the WHO European countries. Based on the visual inspection of the scatter plot $\{(g_i, y_i)\}_{i=1,\ldots,n}$, we modelled the relationship using the following monotonic function.

$$y = f(g) = \frac{e^\beta g^\alpha}{1 + e^\beta g^\alpha}$$

where $\alpha < 0$ and $\beta > 0$.

Second, we aimed to construct a surface whose g-sections are funnel plots, hence defined by

$$y_g(x) = \theta_g \pm z_p \sqrt{\phi \frac{\sigma_g^2}{x}} = \theta_g \pm z_p \sqrt{\phi \frac{\theta_g(1 - \theta_g)}{x}} \quad \forall g$$

where z_p is such that $\mathbb{P}(Z \leq z_p) = 1-p$ for a standard normal variable Z. For each value of the GDP g, the parameter θ_g is a reference value that specifies the expectation $E[y|g]$, i.e. the centerline of the associated funnel. The multiplicative parameter ϕ is included in the model to account for overdispersion with respect to the variance $\theta_g(1 - \theta_g)/x$ predicted by a simple binomial model [8]. Parameters α and β were estimated by weighted linear squares, with the weights corresponding to the number of AST, whereas θ and ϕ were derived using f. In particular, $\theta_g = f(g)$ and $\phi = \frac{1}{n} \sum_i \frac{(y_i - f^\beta(g_i))^2}{f^\beta(g_i)(1 - f^\beta(g_i))/x_i}$.

Specific results are shown in Fig 29.1. The picture refers to Escherichia Coli pathogens that are resistant to Ceftriaxone. The left panel shows a standard 2D funnel plot that does not account for GDP, whereas the right panel shows a 3D funnel plot derived according to the proposed model. In the left panel, the red curves represent the $99,8\%$ alarm limits that, in the right panel, become surfaces, whose shape changes with GDP.

The charts are used as follows: when a point lies within the alarm limits, it is regarded consistent with natural variability. Conversely, when it falls outside the funnel, it highlights the possible presence of a special cause that warrants further investigation (with the probability of false alarm rate specified by z_p).

In the left panel, it appears that a single funnel is not adequate, as seen also from the large overdispersion parameter, equal to 81.11. The new model overcomes the shortcomings of the standard formulation and also identifies a critical situation. The GDP-dependent centerline, ranging between 0.1 and 0.4, explains better the data, as witnessed by the decrease of the overdispersion. In the right panel, moreover, there is a point outside the alarm limits, namely Italy, a finding consistent with the literature [2]. Possible explanations include a higher number of persistent infections (beacuse of poor practices, or environmental factors) or inconsistencies in the definition of indicators.

Finally, the proposed approach offers a very effective visual tool that can highlight situations that deserve further investigation and that other methods may overlook. For example, the WHO GLASS website uses boxplots that neglect the AST size parameter. Consequently, an anomalous AMR such as the Italian one could be mistaken as consistent with the general distribution.
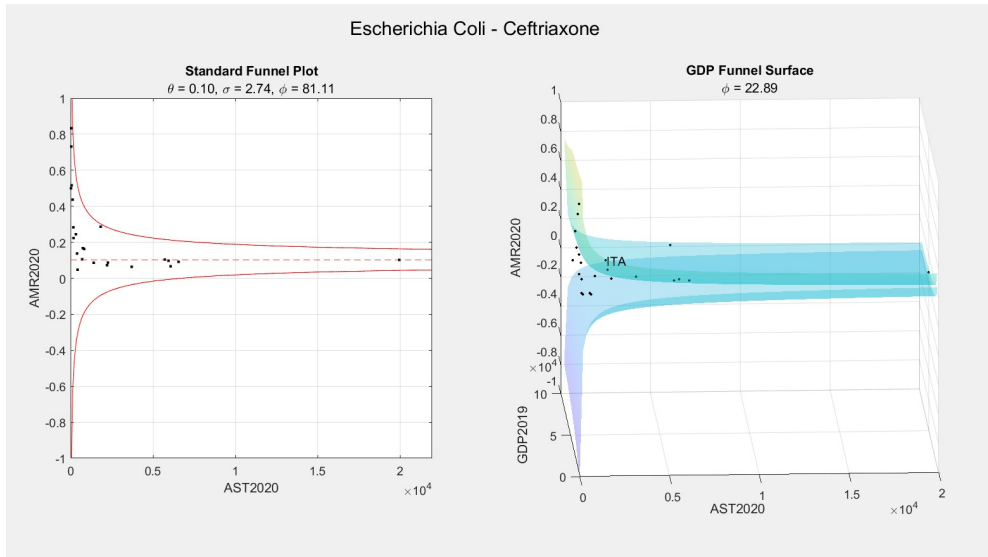
Figure 29.1: Specific results for Ceftriaxone-resistant Escherichia coli pathogens are shown. The left panel shows a standard funnel plot, while the right panel illustrates the proposed model. Left: a single 2D funnel appears insufficient to model the phenomenon, as indicated by the large overdispersion parameter. Right: the new 3D model better describes the distribution of the data and highlights Italy as being outside the alarm limits.

References

[1] T. W. Bank. *GDP per capita (current US$)*. data retrieved from World Development Indicators, `https://data.worldbank.org/indicator/NY.GDP.PCAP.CD`. 2023.

[2] A. Cassini et al. "Attributable deaths and disability-adjusted life-years caused by infections with antibiotic-resistant bacteria in the EU and the European Economic Area in 2015: a population-level modelling analysis". In: *The Lancet infectious diseases* 19.1 (2019), pp. 56–66.

[3] S. Kumar. "Antimicrobial resistance: A top ten global public health threat". In: *EClinicalMedicine* 41 (2021), p. 101221.

[4] M. A. Mohammed, K. Cheng, A. Rouse, and T. Marshall. "Bristol, Shipman, and clinical governance: Shewhart's forgotten lessons". In: *The Lancet* 357.9254 (2001), pp. 463–467.

[5] W. H. Organization et al. "Antimicrobial resistance surveillance in Europe 2022–2020 data". In: (2022).

[6] W. H. Organization. *Global antimicrobial resistance and use surveillance system (GLASS) report 2022*. World Health Organization, 2022.

[7] D. J. Spiegelhalter. "Funnel plots for comparing institutional performance". In: *Statistics in medicine* 24.8 (2005), pp. 1185–1202.

[8] D. J. Spiegelhalter. "Handling over-dispersion of performance indicators". In: *BMJ Quality & Safety* 14.5 (2005), pp. 347–351.

About clustering of time series: A case study using real traffic data

Davide Moretti

Istituto per la Applicazioni del Calcolo "M. Picone" (IAC), CNR, Rome, Italy

Advancements in technology have enabled extensive collection and storage of data from real-world applications, forming the basis for time series, which are data that are recorded in an orderly fashion and correlated to a temporal variable. Due to the intricate nature of temporal information, valuable patterns and structures are often concealed by a superficial analysis, making the exploration of time series an essential pursuit. Such a large amount of information provides an opportunity for researchers to perform data mining in an attempt to extract all possible meaningful pieces of knowledge.

Our work focuses on real-world vehicular traffic data provided by Autostrade Alto Adriatico S.p.A. Here, the time series represents flux data obtained from fixed sensors deployed on four highways in the northeastern part of Italy, which shape are displayed in Figure 30.1. Such yet-to-be-published data is part of a bigger dataset (detailed in [3]) provided to IAC-CNR as part of the collaboration with Autostrade Alto Adriatico. Our ultimate goal is to perform clustering on this data to obtain meaningful clusters, enhancing our general understanding of the common traffic patterns, and also to help the creation of a standard dataset for future and existing projects like [3]. Clustering is a well-known data mining technique where unlabeled data are partitioned into homogeneous groups, without a priori knowledge of said groups' definitions, following a notion of similarity. Further progress can be made by using these newly discovered traffic patterns as a baseline for anomaly detection.

The first step in time-series clustering [1] is choosing an adequate representation of time series, as it affects the accuracy of the final results. Most raw time-series data is highly dimensional and noisy, and performing clustering directly can lead to counterintuitive results. Representation can help highlight different dataset characteristics and speed up the distance measure calculation, moving series to low-dimensional spaces while maintaining a similarity between them [4]. We chose to focus on shape-based approaches (rather than feature-based) that keep the overall shape of the series for an easier results evaluation. The three representations we implemented are the Piecewise Aggregate Approximation (PAA) [6], the Symbolic Aggregate approXimation (SAX) [7] and the Extended SAX (ESAX) [8].

Then, a measure of similarity between series has to be defined. Other than the simple L^2 norm, which can be surprisingly competitive [1], on SAX and ESAX series we employed the symbolic distance MINDIST, which is proposed in the same seminal paper as the SAX, while on numeric series we also implemented the Dynamic Time Warping [10, 12], a type of elastic distance.
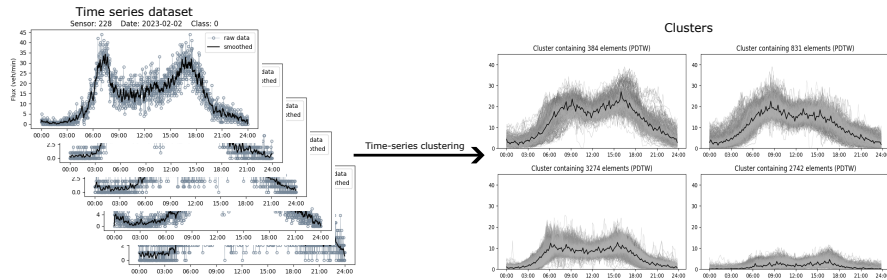
Figure 30.1: On the left is an extract from the time series dataset used in our work; the vehicular flux data is collected at one-minute intervals, forming series of 1440 points in time. On the right, clusters are created based on the similarity in shape of the series.

As for clustering methods, time-series clustering is usually performed using either partitioning or hierarchical methods [1]. From the former group, we tried both k-means [9] and the fuzzy c-means [2], and from the latter, an agglomerative hierarchical approach [5].

While several combinations between representation, similarity measure, and clustering methods are possible, only the most promising were carried out based on the literature and initial results. Since the approach is unsupervised, we also implemented clustering evaluation methods to extract the most significant number of clusters for each approach; namely, the Silhouette index [11] for partitions and the Partition Coefficient And Exponential Separation (PCAES) index [13] for fuzzy clustering. For hierarchical clustering, the number was selected via a heuristic based on the growth of significant clusters.

In our conclusion, all clustering results were presented, showing the shapes of the clusters if a satisfying result was obtained, and the reasoning behind any exclusion if the method has been proven not suitable for the type of data.

The same results were also employed to perform anomaly detection based on the similarity between individual time series and cluster centroids. As part of the collaboration with Autostrade Alto Adriatico, we developed a closed-source online procedure to generate daily reports that showcase the most anomalous data from the previous day using their distance from the closest centroid as an anomaly score.

References

[1] S. Aghabozorgi, A. S. Shirkhorshidi, and T. Wah. "Time-series clustering - A decade review". In: *Information Systems* 53 (May 2015). DOI: 10.1016/j.is.2015.04.007.

[2] J. Bezdek. "Cluster Validity with Fuzzy Sets". In: *Journal of Cybernetics* Volume 3 (July 1973). DOI: 10.1080/01969727308546047.

[3] M. Briani, E. Cristiani, and E. Onofri. "Inverting the fundamental diagram and fore-casting boundary conditions: How machine learning can improve macroscopic models for traffic flow". ARXIV: 2303.12740. 2023.

[4] P. Esling and C. Agon. "Time-series data mining". In: *ACM Computing Surveys (CSUR)* 45.1 (2012), pp. 1–34.

[5] J. Han, J. Pei, and H. Tong. "Data mining: concepts and techniques". In: Morgan Kaufmann, 2022, pp. 383–416.

[6] E. Keogh, K. Chakrabarti, M. Pazzani, and S. Mehrotra. "Dimensionality reduction for fast similarity search in large time series databases". In: *Knowledge and information Systems* 3 (2001), pp. 263–286.

[7] J. Lin, E. Keogh, L. Wei, and S. Lonardi. "Experiencing SAX: a novel symbolic representation of time series". In: *Data Mining and knowledge discovery* 15 (2007), pp. 107–144.

[8] B. Lkhagva, Y. Suzuki, and K. Kawagoe. "Extended SAX: extension of symbolic aggregate approximation for financial time series data representation". In: *Proceeding of IEICE the 17th Data Engineering Workshop* (Jan. 2006).

[9] J. MacQueen et al. "Some methods for classification and analysis of multivariate observations". In: *Proceedings of the fifth Berkeley symposium on mathematical statistics and probability*. Vol. 1. 14. Oakland, CA, USA. 1967, pp. 281–297.

[10] F. Petitjean, A. Ketterlin, and P. Gançarski. "A global averaging method for dynamic time warping, with applications to clustering". In: *Pattern recognition* 44.3 (2011), pp. 678–693.

[11] P. J. Rousseeuw. "Silhouettes: a graphical aid to the interpretation and validation of cluster analysis". In: *Journal of computational and applied mathematics* 20 (1987), pp. 53–65.

[12] H. Sakoe and S. Chiba. "Dynamic programming algorithm optimization for spoken word recognition". In: *IEEE transactions on acoustics, speech, and signal processing* 26.1 (1978), pp. 43–49.

[13] K.-L. Wu and M.-S. Yang. "A cluster validity index for fuzzy clustering". In: *Pattern Recognition Letters* 26.9 (2005), pp. 1275–1291.

Learning Slow Invariant Manifolds with Physics-Informed Neural Networks

Dimitrios G. Patsatzis

Modelling Engineering Risk and Complexity, Scuola Superiore Meridionale, Naples, Italy

The dynamics of complex systems often deploy on multiple scales in time and space. To enable their understanding and systematic numerical analysis, it is therefore useful to introduce simplification processes, generally performed with Reduced Order Models (ROMs), which reduce the computational complexity of mathematical models in numerical simulation. The construction of ROMs is based on the assumption that the effective dynamics evolves on low-dimensional spaces, the manifolds. In the case of systems of ODEs with multiple timescales, these spaces are referred to as Slow Invariant Manifolds (SIMs) due to the slow timescales that govern the long-term evolution of the system when attracted towards them [3]. The introduction of SIMs has been crucial for constructing ROMs free of fast time scales and for providing useful insights regarding the physical understanding of the system [4, 7].

The approximation of SIMs fits into in the context of Geometric Singular Perturbation Theory (GSPT) [3], originally developed to tackle stiff dynamical systems with an explicitly known separation between fast/slow timescales. In the case under consideration, we consider the more general class of stiff dynamical systems, in which the fast/slow timescale decomposition exists, but is not explicitly known as well as the decomposition of fast/slow variables and their number. For this class of systems, there is a variety of methods for constructing SIM approximations, either analytical or numerical, in the context of GSPT [8, 10]. The advantage gained by these methods lies in the fact that they discover the SIM as a function of the state variables themselves, which is crucial for revealing the physical processes that lead the dynamical system to the emergent SIM. However, this often results in SIM approximations (analytical or numerical) of implicit form [5, 7], introducing a significant computational cost when SIM expressions are used for high-dimensional environmental space reconstruction (e.g., after the time integration of the ROM).

Within the framework of data-driven methods, a plethora of Machine Learning (ML) methodologies have been developed for constructing black or gray-box ROM surrogates of complex systems, bypassing the explicit computation of SIMs. These procedures usually involve first detecting the low-dimensional space with manifold learning algorithms [1, 11] and then using, for example, Artificial Neural Networks (ANNs) [2, 9] to construct the ROM. An alternative for performing systems-level tasks is provided by the Equation-Free framework [6], recently coupled with manifold learning techniques [13], which however overcomes the explicit computation of the underlying SIMs.

To combine the advantages of ML techniques and avoid the drawbacks of GSPT methods, we presented a physics-informed ML approach based on the GSPT framework for the analytical SIM derivation of singularly perturbed systems in an explicit closed form [12]. In particular, we used single-layer ANNs and random projection ANNs via symbolic differentiation to solve the *invariance equation* (IE) PDE, that constraints the system dynamics to lie on the SIM. We demonstrated that the proposed physics-informed ML approach outperforms other classical GSPT-based methods, especially for relatively large values of the perturbation parameter.

Here, we take a step forward by relaxing the assumption of explicit timescale splitting. We introduce a physics-informed neural network (PINN) approach [14] for learning explicit functionals of SIMs for the most general class of stiff dynamical systems, for which the fast/slow timescale splitting and the dimension of the SIM are not explicitly known a-priori. Furthermore, unlike the other ML methods proposed so far which create surrogate models via regression, our approach offers a functional expression of the SIM. Since the fast and slow variables are not known *a priori*, this is achieved by the proposed PINN approach by simultaneously (i) finding the transformations that decompose the state variables into fast and slow components, and (ii) solving the IE for computing the SIM functional in an explicit closed form.

The performance of the proposed PINN scheme is assessed via three benchmark problems, namely, the Michaelis-Menten (MM), the Target Mediated Drug Disposition (TMDD), and a fully competitive substrate-inhibitor (fCSI) mechanisms. For a straightforward comparison with the GPST methods, we also derived analytic or numeric SIM approximations provided on the basis of well-known GPST mehtods, such as the *Quasi Steady-State Approximation*, the *Computational Singular Perturbation* (CSP) method, etc.

We demonstrate that the proposed PINN scheme provides SIM approximations of equivalent or even higher accuracy than those computed by GSPT methods, especially close to the boundaries of the underlying SIMs. Finally, we note that for the TMDD and fCSI problems, the CSP method (which is the most accurate among the GSPT-based ones) does not provide the SIM approximations in an explicit closed form. In these cases, the computational time required for training the proposed PINN is comparable to the one required by CSP to numerically approximate the SIM with Newton-iterations.

References

[1] M. Balasubramanian, E. L. Schwartz, J. B. Tenenbaum, V. de Silva, and J. C. Langford. "The Isomap algorithm and topological stability". In: *Science* 295.5552 (2002), pp. 7–7.

[2] W. Chen, Q. Wang, J. S. Hesthaven, and C. Zhang. "Physics-informed machine learning for reduced-order modeling of nonlinear problems". In: *Journal of computational physics* 446 (2021), p. 110666.

[3] N. Fenichel. "Geometric singular perturbation theory for ordinary differential equations". In: *Journal of differential equations* 31.1 (1979), pp. 53–98.

[4] D. A. Goussis. "Quasi steady state and partial equilibrium approximations: their relation and their validity". In: *Combustion Theory and Modelling* 16.5 (2012), pp. 869–926.

[5] D. A. Goussis and M. Valorani. "An efficient iterative algorithm for the approximation of the fast and slow dynamics of stiff systems". In: *Journal of Computational Physics* 214.1 (2006), pp. 316–346.

[6] I. G. Kevrekidis, C. W. Gear, J. M. Hyman, P. G. Kevrekidis, O. Runborg, and C. Theodoropoulos. "Equation-Free, Coarse-Grained Multiscale Computation: Enabling Microscopic Simulators to Perform System-Level Analysis". In: *Communications in Mathematical Sciences* 1.4 (2003), pp. 715–762. DOI: 10.4310/cms.2003.v1.n4.a5.

[7] C. Kuehn. *Multiple time scale dynamics*. Vol. 191. Springer, 2015.

[8] S.-H. Lam and D. A. Goussis. "Understanding complex chemical kinetics with computational singular perturbation". In: *Symposium (International) on Combustion*. Vol. 22. Elsevier. 1989, pp. 931–941.

[9] S. Lee, M. Kooshkbaghi, K. Spiliotis, C. I. Siettos, and I. G. Kevrekidis. "Coarse-scale PDEs from fine-scale observations via machine learning". In: *Chaos: An Interdisciplinary Journal of Nonlinear Science* 30.1 (2020), p. 013141. DOI: 10.1063/1.5126869.

[10] U. Maas and S. B. Pope. "Simplifying chemical kinetics: intrinsic low-dimensional manifolds in composition space". In: *Combustion and flame* 88.3-4 (1992), pp. 239–264.

[11] B. Nadler, S. Lafon, R. R. Coifman, and I. G. Kevrekidis. "Diffusion maps, spectral clustering and reaction coordinates of dynamical systems". In: *Applied and Computational Harmonic Analysis* 21.1 (2006), pp. 113–127.

[12] D. G. Patsatzis, G. Fabiani, L. Russo, and C. Siettos. "Slow Invariant Manifolds of Singularly Perturbed Systems via Physics-Informed Machine Learning". In: *SIAM Journal on Scientific Computing, in press* (2024).

[13] D. G. Patsatzis, L. Russo, I. G. Kevrekidis, and C. Siettos. "Data-driven control of agent-based models: An equation/variable-free machine learning approach". In: *Journal of Computational Physics* 478 (2023), p. 111953.

[14] D. G. Patsatzis, L. Russo, and C. Siettos. "A physics-informed neural network method for the approximation of slow invariant manifolds for the general class of stiff systems of ODEs". ARXIV: 2403.11591. 2024.

Pricing European Options using the Gauss-Laguerre quadrature: Application to a Compound CARMA(p,q)-Hawkes model

Andrea Perchiazzo

Università degli Studi di Milano

In this work, we propose a novel method for pricing European options numerically in an efficient manner using the Gauss-Laguerre quadrature. The approach is initially tested on the Black-Scholes model to confirm its efficiency and then applied to a compound CARMA(p, q)-Hawkes model, which is our subject of interest and provides a rationale for introducing the new methodology.

A self-exciting point process featuring a continuous-time autoregressive moving average (CARMA) intensity process has recently been introduced in the literature. This model, named CARMA(p, q)-Hawkes [5], extends the traditional Hawkes process [3, 4] by integrating a CARMA(p, q) intensity in place of an Ornstein-Uhlenbeck. The proposed model maintains the same level of mathematical tractability as the Hawkes process with exponential kernel (e.g., infinitesimal generator, high-order moments, autocorrelation function, and joint characteristic function), but it shows enhanced capability in reproducing complex time-dependent structures evident in several market data.

Based on this framework, we propose the aforementioned compound CARMA(p, q)-Hawkes model incorporating a random jump size independent of both the counting and intensity processes. Subsequently, we proceed to price European options using the characteristic function. Instead of employing the Carr-Madan formula [1], which requires an appropriate choice for the damping factor, or the COS method of Fang and Oosterlee [2] in which three approximation errors are introduced (e.g. truncation of the integration range in the risk-neutral valuation formula) as discussed in [6, Chapter 6.2.3], the pricing of European options using the characteristic function is based on the Gauss-Laguerre quadrature. Our approach does not necessitate the truncation of the integration range in the risk-neutral valuation formula and the approximation error term is controlled by the order of the Laguerre polynomials. The computation of European option prices based on the Gauss-Laguerre quadrature appears to be a stable and less time-consuming approach, particularly within the context of calibration exercises.

In addition, a comparison between the novel approach based on the Gauss-Laguerre quadrature and the COS method is performed.

References

[1] P. Carr and D. Madan. "Option valuation using the fast Fourier transform". In: *Journal of computational finance* 2.4 (1999), pp. 61–73.

[2] F. Fang and C. W. Oosterlee. "A Novel Pricing Method for European Options Based on Fourier-Cosine Series Expansions". In: *SIAM Journal on Scientific Computing* 31.2 (2009), pp. 826–848. DOI: 10.1137/080718061.

[3] A. G. Hawkes. "Point spectra of some mutually exciting point processes". In: *Journal of the Royal Statistical Society Series B: Statistical Methodology* 33.3 (1971), pp. 438–443.

[4] A. G. Hawkes. "Spectra of some self-exciting and mutually exciting point processes". In: *Biometrika* 58.1 (1971), pp. 83–90.

[5] L. Mercuri, A. Perchiazzo, and E. Rroji. "A Hawkes model with CARMA(p,q) intensity". In: *Insurance: Mathematics and Economics* 116 (2024), pp. 1–26. DOI: https://doi.org/10.1016/j.insmatheco.2024.01.007.

[6] C. W. Oosterlee and L. A. Grzelak. *Mathematical modeling and computation in finance: with exercises and Python and MATLAB computer codes*. World Scientific, 2019.

Mathematical models for multilane traffic flow

Matteo Piu
Università degli Studi di Verona, Italy

Introduction

We focus on modeling and analyzing the stability of vehicular multilane traffic flow using the microscopic and macroscopic scales. Traffic flow analysis is essential for understanding and improving transportation systems, as congestion and efficiency remain major concerns. By studying lane changing (LC) dynamics and developing multilane models, this work aims to provide a comprehensive approach that connects individual vehicle behaviours at the microscopic level with traffic flow patterns at the macroscopic level, thereby offering valuable insights for enhancing overall traffic management and road safety.

Hybrid microscopic models with lane changing

The microscopic approach is based on the dynamics of individual vehicles, considering the behaviour of each driver. Consequently, such models consist of systems of ODEs, where the variables represent properties like the position x_n and velocity v_n of single vehicles. Here, we extend some one-lane microscopic models to multilane roads. In particular, we obtain systems where both continuous (dynamical evolution of the vehicles) and discrete dynamics terms (lane change events) are present, leading to hybrid models [5].

Consider a road with J lanes and a fixed number of vehicles N. Let $I_j(t)$ denote the set of vehicles in lane j at time t. For a vehicle with index n, we name the adjacent vehicles as shown in Fig. 33.1. We present the multilane version of the "Bando–FtL" model [2, 3, 6, 10], a one-lane microscopic model that combines an optimal velocity term involving an optimal (desired) velocity function $V_j(\cdot)$ dependent only on the headway between vehicles, and a classical Follow-the-Leader (FtL) term. The multilane model [8] consists

Figure 33.1: Schematic representation of a multi-lane road. Here, the reference vehicle is n, travelling in lane j. Whereas, p_n^k and s_n^k represent the vehicles just behind and in front of vehicle n in lane $k = j - 1, j, j + 1$, respectively.
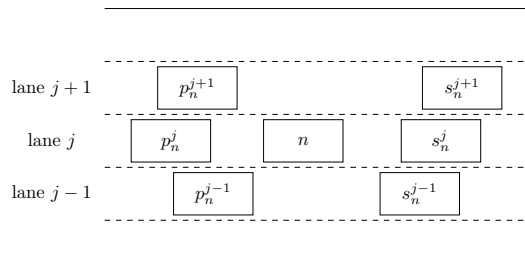
of the following system, for $n \in I_j$ and $j = 1, \ldots, J$.

$$
\begin{cases}
\dot{x}_n = v_n \\
\dot{v}_n = \alpha(V_j(\Delta x_n^j) - v_n) + \beta \dfrac{\Delta v_n^j}{(\Delta x_n^j)^{\gamma+1}} \\
\text{LC conditions:} \quad \alpha(V_j(\Delta x_n^{j'}) - v_n) + \beta \dfrac{\Delta v_n^{j'}}{(\Delta x_n^{j'})^{\gamma+1}} > (1+\eta)\dot{v}_n \quad \text{(incentive criterion)} \\
\qquad\qquad\qquad \Delta x_n^{j'} > l + d_s \quad \text{and} \quad x_n - x_{p_n^{j'}} > l + d_s \quad \text{(safety criterion)}
\end{cases}
$$

where l is the vehicles length, and $\Delta x_n^h = x_{s_n^h} - x_n$, $\Delta v_n^h = v_{s_n^h} - v_n$ with $h \in \{j, j \pm 1\}$.

The lane changing rules are based on two criteria. An incentive criterion, that allows a vehicle to change lanes if it would travel faster in a new lane, and a safety criterion, which requires the lane change to be safe, ensuring adequate distance d_s from the follower and leader in the new lane to avoid collisions. Experimental studies show that lane changing is infrequent, and to incorporate this behaviour into our model, we introduce a stochastic component for such occurrences. We use two stochastic processes to model the lane change dynamics: one for selecting candidate vehicles and another for determining the expected times of lane changes. For further details, see [8], where an analysis of the equilibria of this model is also discussed.

Macroscopic multilane models

Macroscopic models aim to describe traffic flow in terms of aggregate quantities such as density ρ_j, flux f_j, and average speed v_j, using systems of hyperbolic PDEs, particularly conservation or balance laws. Although these models originate from fluid dynamics, they can be viewed also as a macroscopic limit of appropriate microscopic traffic models. Following this approach, we derived macroscopic multilane models from the hybrid microscopic models presented in the previous section. The resulting models consist of systems of balance laws, where the derived source terms, describing lane change dynamics, are strongly motivated by microscopic dynamics. Unlike other macroscopic multilane models in the literature, these source terms are not directly modeled at the macroscopic level.

The first model we present is a first-order model [7], constructed as the macroscopic limit of a first-order microscopic hybrid model with lane changing. The model consists of the following system of balance laws, obtained as the expected value of a stochastic density due to lane changes.

$$
\partial_t \rho_j + \partial_x(\rho_j v(\rho_j)) = \nu S \qquad j = 1, \ldots, J
$$

where the source term $S = \displaystyle\sum_{j' \in T_j} \pi^{j' \to j}(\rho_j, \rho_{j'}) A(\rho_{j'}, \rho_j)\rho_j - \pi^{j \to j'}(\rho_{j'}, \rho_j) A(\rho_j, \rho_{j'})\rho_{j'}$

models the gain and loss of mass due to lane changes. Here, $\pi^{h \to k}$ is the probability of a lane change from lane h to lane k, $A(\cdot, \cdot)$ is a density amplification function and ν is a frequency of LC. This model can also be seen as a multilane extension of the one-lane LWR model [4, 11]. For a deeper analysis, see [7], where a study of the equilibria is detailed.

In first-order models, the mean velocity is assumed to be a function of the density. By relaxing this assumption and treating velocity as an independent variable, we obtain second-order models. Here, we propose a second-order macroscopic multilane model derived as the macroscopic limit of the hybrid "Bando–FtL" model with lane changing. The model [9] consists of a 2×2 system of balance laws given by

$$\begin{cases} \partial_t \rho_j + \partial_x(\rho_j v_j) = \nu S, \\ \partial_t y_j + \partial_x(y_j v_j) = \alpha \rho_j(V(\rho_j) - v_j) + Q \end{cases} \qquad j = 1, \dots, J$$

with $y_j = \rho_j(v_j + P(\rho_j))$, where the source terms describe the mass exchange due to lane changing (S) and the momentum variation (Q) due to these occurrences:

$$Q = \sum_{j' \in T_j} \pi^{j' \to j} \left(\rho_j^G \left(v_j + P(\rho_j^G) \right) - y_j \right) + \pi^{j \to j'} \left(\rho_j^L \left(v_j + P(\rho_j^L) \right) - y_j \right).$$ Here, $P(\cdot)$

is called pressure function, and ρ_j^G, ρ_j^L describe the density in the gain (G) and loss (L) scenarios. This model can be seen as a multilane extension of the one-lane ARZ model [1].

References

[1] A. Aw and M. Rascle. "Resurrection of "second order" models of traffic flow". In: *SIAM J. Appl. Math.* 60.3 (2000), pp. 916–938.

[2] M. Bando, K. Hasebe, A. Nakayama, A. Shibata, and Y. Sugiyama. "Dynamical model of traffic congestion and numerical simulation". In: *Phys. Rev. E* 51.2 (1995), p. 1035.

[3] D. C. Gazis, R. Herman, and R. W. Rothery. "Nonlinear follow-the-leader models of traffic flow". In: *Oper. Res.* 9.4 (1961), pp. 545–567.

[4] M. J. Lighthill and G. B. Whitham. "On kinematic waves II. A theory of traffic flow on long crowded roads". In: *Proc. Roy. Soc. London. A* 229.1178 (1955), pp. 317–345.

[5] B. Piccoli. "Hybrid systems and optimal control". In: *Proceedings of the 37th IEEE Conference on Decision and Control*. Vol. 1. IEEE. 1998, pp. 13–18.

[6] L. A. Pipes. "An operational analysis of traffic dynamics". In: *J. Appl. Phys.* 24.3 (1953), pp. 274–281.

[7] M. Piu, M. Herty, and G. Puppo. "Derivation and Stability Analysis of a Macroscopic Multilane Model for Traffic Flow". In: *SIAM J. Appl. Math.* 83.5 (2023).

[8] M. Piu and G. Puppo. "Stability analysis of microscopic models for traffic flow with lane changing". In: *Networks and Heterogeneous Media* 17.4 (2022), pp. 495–518.

[9] M. Piu, G. Puppo, and G. Visconti. "Investigating new second order models for traffic flow with lane changing". In preparation.

[10] A. Reuschel. "Vehicle movements in a platoon with uniform acceleration or deceleration of the lead vehicle, Zeit. D". In: *Oster. Ing. U. Architekt Vereines Ed* (1950).

[11] P. I. Richards. "Shock waves on the highway". In: *Oper. Res.* 4.1 (1956), pp. 42–51.

A Bayesian Approach to Clustering via the Proper Bayesian Bootstrap

Federico Maria Quetti[a,*], Elena Ballante[b], and Silvia Figini[b]
[a] Department of Mathematics, Università degli studi di Pavia, Italy
[b] Department of Political and Social Sciences, Università degli studi di Pavia

A large body of literature exists in the field regarding methods of clustering [5, 6]; yet, since the problem is unsupervised, the research on improvements to existing methods is still an open point. In particular, the integration of Machine Learning with techniques from Bayesian statistical learning has been shown to provide significant improvements in the supervised framework by [4] and [1]. In an unsupervised setting, it has been shown in the literature that the application of bagging techniques to standard clustering methods improves results and brings new information of fuzzy clustering type. The proposed approach stems from the work of [2], where the authors linked bootstrap with clustering in the definition of the BagClust1 algorithm. The aim is to extend the current state of the art in clustering, adopting Bayesian Bootstrap techniques in unsupervised learning resorting to a prior knowledge integration scheme.

Bootstrap is a statistical resampling technique used to estimate the distribution of a statistic, by providing an approximation of the empirical distribution function of data. Formally, given $\{X_1, \ldots, X_n\}$ i.i.d. realization of a random variable X, we are interested in estimating the distribution of a functional $\Phi(F, X)$, depending on the cumulative distribution function F of the variable X. In order to generate the distribution of the estimator $\hat{\Phi}$ for the functional, an approximation for the cumulative distribution of X is needed. The Bayesian approach to the evaluation of the conditional distribution requires to elicit a prior distribution for F on the space of distribution functions, with the aim of using the posterior of F to estimate the distribution of the functional Φ given the sample values. In the work [3], Ferguson defined a prior for the random distribution referred to as Dirichlet process. Given a proper distribution function F_0 interpreted as the prior guess at F, and a positive real number k interpreted as a confidence parameter in this guess, kF_0 is the parameter of the process denoted as $\mathcal{DP}(kF_0)$. The conjugacy property holds: given a random sample from $F \sim \mathcal{DP}(kF_0)$, the posterior is again a Dirichlet process, with updated parameter as convex combination of the prior guess F_0 and the empirical cdf F_n: $F|X \sim \mathcal{DP}((k+n)G_n), G_n = \frac{k}{k+n}F_0 + \frac{n}{k+n}F_n$. Posterior estimations of different functionals $\Phi(F, X)$ are then easily computable.
The first approach to prior knowledge integration to the process of resampling data was proposed by Muliere and Secchi in [7]. B iterations are performed to obtain B bootstrap samples, with the following procedure:

1. m new observations $x_1^*, \ldots, x_m^*$ are generated from the mixture:
   $x_i^* \sim \frac{k}{k+n} F_0 + \frac{n}{k+n} F_n$.

2. weights $w_1^b, \ldots, w_m^b$ for each observation are drawn from a Dirichlet distribution:
   $(w_1^b, \ldots, w_m^b) \sim \mathsf{Dir}\left(\frac{k+n}{m}, \ldots, \frac{k+n}{m}\right)$.

We apply the proposed bootstrap method focusing on K-means algorithm, as representative of partition-based clustering methods. In the following, memberships u_k are assigned to data points and indicate the degree to which they belong to each cluster: $u_k \in [0,1], \ \sum_{k=1}^{K} u_k = 1$, not by an optimization procedure, instead being the result of the aggregation of labels obtained applying clustering on the bootstrap replicas.

The first proposal is the Bayesian Bagged Clustering algorithm, aimed at bettering the chosen partitioning algorithm in stability as well as gaining additional information about the uncertainty in the assignments for the dataset: the procedure is as follows. In the initial step, we apply the partitioning P with a chosen number of clusters K on data. This information is used to define a suitable baseline prior for the generating process underlying bootstrap resampling. F_0 is imposed as the cumulative of a suitable Gaussian mixture probability density $f_{\boldsymbol{\theta}} = \sum_{j=1}^{K} p_j f_{\boldsymbol{\mu_j}, \boldsymbol{\Sigma_j}}$, where $\boldsymbol{\theta} = (p_j, \boldsymbol{\mu_j}, \boldsymbol{\Sigma_j})$, $j = 1, \ldots, K$ are the mixture parameters, and $f_{\boldsymbol{\mu_j}, \boldsymbol{\Sigma_j}} \sim \mathcal{N}(\boldsymbol{\mu_j}, \boldsymbol{\Sigma_j})$ is the multivariate Gaussian distribution with mean $\boldsymbol{\mu_j}$ and covariance matrix $\boldsymbol{\Sigma_j}$.

The mixture parameters associated to each component j are the weights p_j, $0 \leq p_j \leq 1, \ \sum_{j=1}^{K} p_j = 1$, evaluated as the proportion of data assigned to cluster j in the dataset initial cluster labeling. The mean $\boldsymbol{\mu_j}$, representing the cluster centroid, taken as centroid j from the partitioning P. The variance matrix $\boldsymbol{\Sigma_j}$, defined as the empirical covariance matrix of the data points in cluster j, $\boldsymbol{\Sigma_j^*}$, multiplied for a constant value s as to consider different concentrations. The second step of the procedure is based on proper Bayesian bootstrap: $m = n$ observations are generated from the convex combination of the defined prior and empirical cdf: $G_n = (k + n)^{-1}(kF_0 + nF_n)$, where k is the assigned confidence parameter. The proper Bayesian bootstrap resamples present newly sampled values as well as original dataset values, which are the focus of the cluster labels assignment. K-means is applied to the B resampled learning sets, obtaining a cluster partitioning for each. Each of the original data points will be assigned to a given cluster a certain total number of times: cluster memberships are evaluated as the fraction between this total and the number of times the point has been selected overall. The procedure finally gives an aggregated value of the cluster label for the original data points from the memberships, as $\mathrm{argmax}_{1 \leq k \leq K} u_k(\boldsymbol{x_i})$.

Directly from the above proposal, a second part of the work focuses on its exploitation by discussing an optimal choice scheme for the number of clusters K. The K-dimensional vectors of cluster memberships of data points $\boldsymbol{x_i}$, denoted as $\boldsymbol{u}(\boldsymbol{x_i})$, $i = 1, \ldots, n$, will depend on the parameters of the proper Bayesian bootstrap, on the chosen clustering algorithm P and in particular on the number of clusters K. This fact motivates the analysis of their behaviour under clustering algorithm P, with fixed parameters, for varying K,

in order to recover the underlying cluster structure of the dataset, as the algorithm is effectively enforcing a K-cluster structure of data by implementing the prior as prescribed. The fundamental idea of our proposal is that better choices of K lead to easily assignable labels for the dataset, because the algorithm is more able to disambiguate between clusters. To quantify the uncertainty about the membership assignments, we seek to determine how the weight of the components is distributed over the normalized membership vector $\boldsymbol{u}(\boldsymbol{x_i})$. To do so, we employ the following two measures:

- $S(\boldsymbol{u}(\boldsymbol{x_i})) = -\sum_{i=1}^{k} u_k(\boldsymbol{x_i}) \log_2 u_k(\boldsymbol{x_i})$, Shannon entropy of the vector, quantifies how the decision is dispersed between every vector component

- $S_{l,m}(\boldsymbol{u}(\boldsymbol{x_i})) = -(\frac{u_l}{u_l+u_m} \log_2 \frac{u_l}{u_l+u_m} + \frac{u_m}{u_l+u_m} \log_2 \frac{u_l}{u_m+u_m})$, Shannon entropy of the normalized two component vector (u_l, u_m), quantifies the pairwise indecision between clusters l, m in labeling the data point.

If the number is optimal, one expects the results of the algorithm to give the most crisp assignments of data points to the clusters: from an information theory viewpoint, the smallest mean value of S as function of K corresponds to the best choice of number of clusters. Moreover, for each K, the arguments l, m of the maximum assumed by the dataset average of $S_{l,m}$ indicate which two clusters are most ill defined as separated instead of joint; the corresponding value of the measure quantifies the worst case of pairwise indecision stemming from the choice of K.

Finally, the joint usage of the two parameters leads to a taxonomy of clustering results for the original dataset based on information theory, aimed at enriching the understanding about the behaviour for different choices of K.

References

[1] E. Ballante. "An extension of generalized bayesian ensemble tree models to survival analysis". In: *Far East Journal of Theoretical Statistics* 67.2 (2023), pp. 137–146.

[2] S. Dudoit and J. Fridlyand. "Bagging to improve the accuracy of a clustering procedure". In: *Bioinformatics* 19.9 (2003), pp. 1090–1099.

[3] T. S. Ferguson. "A Bayesian analysis of some nonparametric problems". In: *The annals of statistics* (1973), pp. 209–230.

[4] M. Galvani, C. Bardelli, S. Figini, and P. Muliere. "A Bayesian nonparametric learning approach to ensemble models using the proper Bayesian bootstrap". In: *Algorithms* 14.1 (2021), p. 11.

[5] T. Hastie, R. Tibshirani, J. H. Friedman, and J. H. Friedman. *The elements of statistical learning: data mining, inference, and prediction*. Vol. 2. Springer, 2009.

[6] A. K. Jain, M. N. Murty, and P. J. Flynn. "Data clustering: a review". In: *ACM computing surveys (CSUR)* 31.3 (1999), pp. 264–323.

[7] P. Muliere and P. Secchi. "Bayesian nonparametric predictive inference and bootstrap techniques". In: *Annals of the institute of statistical mathematics* 48 (1996), pp. 663–673.

Studying long-lasting diseases using an agent-based model of the immune response

Alessandro Ravoni[a,*], Filippo Castiglione[a,b], Enrico Mastrostefano[a], Christine Nardini[a], Elia Onofri[a], Maria Concetta Palumbo[a], and Paolo Tieri[a]

[a] Istituto per la Applicazioni del Calcolo "M. Picone" (IAC), CNR, Rome, Italy
[b] Biotechnology Research Center, Technology Innovation Institute, Abu Dhabi, UAE

Personalized medicine strategies are gaining momentum nowadays, enabling the introduction of targeted treatments based on individual differences that can lead to greater therapeutic efficacy by reducing adverse effects. Despite its crucial role, studying the contribution of the immune system (IS) in this context is difficult because of the intricate interplay between host, pathogen, therapy, and other external stimuli. To address this problem, a multidisciplinary approach involving in silico models can be of great help. In this perspective, we will discuss the use of a well-established agent-based model of the immune response, C-ImmSim [1, 3], to study the relationship between long-lasting diseases and the combined effects of IS, drug therapies and exogenous factors such as physical activity and dietary habits.

C-ImmSim simulates the dynamics of various computational entities involved in the immune response. Cellular entities, such as adipocytes, lymphocytes, antigen-presenting cells, antigens, antibodies, immune complexes and intercellular signaling molecules are included in the model. In addition, simple pharmacokinetic (PK) and pharmacodynamic (PD) models based on experimental data are implemented to simulate the effect drugs against specific targets. A key element of the model is its stochastic nature: fixed values of parameters produce realizations of the dynamics that can differ from each other in the immunological initial state (immune repertoire, basal concentrations of metabolites, systemic inflammatory cytokines, and blood leukocyte counts), and in the occurrence of probabilistic events. This allows us to associate each simulation run with a virtual patient, thus mimicking the evolution of disease within a virtual cohort of individuals by simulating multiple virtual patients. Over the years, C-ImmSim was used to simulate several diseases. Here we discuss three main applications.

Metabolic homeostasis, inflammation and diabetes

We developed an integrated, multilevel patient-specific model for the simulation and prediction of metabolic and inflammatory processes in the onset and progress of the type 2 diabetes (T2D), as part of the two projects "*Multiscale Immune System SImulator for the Onset of Type 2 Diabetes integrating genetic, metabolic and nutritional data*" (MISSION-T2D) and "*Physics informed machine learning-based prediction and reversion of impaired fasting glucose management*" (PRAESIIDIUM).

To reproduce the metabolic and inflammatory processes that determine the transition

to T2D pathophenotypes, C-ImmSim has been equipped with a model based on differential equations to take into account the contribution of physical activity and food intake to the inflammatory state of an individual [6, 7], and that considers both the glucose regulation due to the balance between glucagon and insulin. The kinetics of oxygen consumption, the dynamics of epinephrine and the production of the cytokine IL-6 as a function of physical exercise are also included [5, 7] and the model is personalized on the individual functional capacity and based on age, sex, anthropometric characteristics, and current fitness status. Absorption of glucose, alanine and triglycerides are computed starting from the ingestion of carbohydrates, proteins, and fats. Periods of excessive caloric intake determine the volume growth of adipocytes that, over a certain volume threshold, secrete cytokines in a process that can eventually result in a continuous inflammatory state [8].

Mycobacterium tubercolosis infection

We used an in silico approach for the management of tubercolosis due to Mycobacterium tuberculosis (Mtb) infection, as part of the project "European Accelerator of Tuberculosis Regime" (ERA4TB).

In order to simulate the Mtb infection occurring in the lung, we model the bacterium as an agent able to move and interact with macrophages and lymphocytes. These interactions are described by a set of specific rules that allow to reproduce the phenotypes and associated behaviours of Mtb, such as the small replication rate of non-phagocytosed bacteria, the switch between fast- and slow-replicating Mtb engulfed by macrophages, the transition to a latent state invisible to the IS to mimic the presence of granulomas, and the spread of bacteria following both the burst of infected macrophages and the reactivation of granulomas [4]. As a result, a variety of long term behaviours is explored by the simulated dynamics, that can be classified into clinical states. We are able, in particular, to both reproduce the key characteristics of the disease (e.g., bacterial load dynamics) as well as the epidemiological curves in presence of treatment.

Cancer therapy and hepatoblastoma

Finally, we used C-ImmSim to model and predict standard and experimental therapies for each child with hepatoblastoma (HB), the most common pediatric liver cancer, as part of the project "Individualized Paediatric Cure" (iPC).

HB is a liver cancer with high heterogeneity that can be classified into two main subtypes: C1, characterized by a high percentage of fetal cells and high survival rates, and C2, with a high percentage of proliferative embryonal cells and corresponding to a significant reduction in the survival probability [2]. We introduce a population of cancer cells constituted by 2 subtypes, non-aggressive (NC) and aggressive (AC) cancer cells, that differ in their duplication time. We use these cell types to discriminate between C1 and C2 cancer subtypes [9]. Both cell types can interact with the IS. The interaction is very weak in the absence of treatment and is enhanced by cell death induced by drug therapy. The model was validated both by reproducing survival curves and clinical percentages and by using statistical methods such as factor analysis and linear discriminant analysis.

References

[1] M. Bernaschi and F. Castiglione. "Design and implementation of an immune system simulator". In: *Computers in Biology and Medicine* 31.5 (2001), pp. 303–331. ISSN: 0010-4825. DOI: 10.1016/S0010-4825(01)00011-7.

[2] S. Cairo et al. "A combined clinical and biological risk classification improves prediction of outcome in hepatoblastoma patients". In: *European Journal of Cancer* 141 (Dec. 2020), pp. 30–39. DOI: 10.1016/j.ejca.2020.09.026.

[3] F. Castiglione and F. Celada. *Immune System Modelling and Simulation*. Taylor & Francis Group, 2020. ISBN: 9780367738389.

[4] E. Mastrostefano, A. Ravoni, E. Onofri, P. Tieri, and F. Castiglione. "Harnessing computational models to uncover the role of the immune system in tuberculosis treatment". In: *2023 IEEE International Conference on Bioinformatics and Biomedicine (BIBM)* 2 (Dec. 2023), pp. 3725–3732. DOI: 10.1109/BIBM58861.2023.10385440.

[5] M. Morettini, M. C. Palumbo, M. Sacchetti, F. Castiglione, and C. Mazzá. "A system model of the effects of exercise on plasma Interleukin-6 dynamics in healthy individuals: Role of skeletal muscle and adipose tissue." In: *PLoS One* 12.7 (2017), e0181224. DOI: 10.1371/journal.pone.0181224.

[6] M. C. Palumbo, A. A. de Graaf, M. Morettini, P. Tieri, S. Krishnan, and F. Castiglione. "A computational model of the effects of macronutrients absorption and physical exercise on hormonal regulation and metabolic homeostasis". In: *Computers in Biology and Medicine* 163 (Sept. 2023). DOI: 10.1016/j.compbiomed.2023.107158.

[7] M. C. Palumbo, M. Morettini, P. Tieri, F. Diele, M. Sacchetti, and F. Castiglione. "Personalizing physical exercise in a computational model of fuel homeostasis." In: *PLoS computational biology* 14.4 (2018). DOI: 10.1371/journal.pcbi.1006073.

[8] V. Prana, P. Tieri, M. C. Palumbo, E. Mancini, and F. Castiglione. "Modeling the Effect of High Calorie Diet on the Interplay between Adipose Tissue, Inflammation, and Diabetes". In: *Computational and Mathematical Methods in Medicine* 2019 (Feb. 2019), pp. 1–8. ISSN: 1748-6718. DOI: 10.1155/2019/7525834.

[9] A. Ravoni, C. Nardini, M. R. Kappler, C. Armengol, and F. Castiglione. *Mimicking cancer therapy in an agent-based model: the case of Hepatoblastoma*. In preparation.

Approximate Deconvolution Leray Reduced Order Model

Anna Sanfilippo

Department of Mathematics, Università di Trento, via Sommarive 14, Povo, 38123, Italy

Galerkin reduced order models (G-ROMs) are advanced computational methods designed to utilize data to significantly lower the dimensionality of full order models (FOMs). These FOMs are derived from traditional numerical discretizations, such as the finite element method (FEM). By reducing the dimensionality, G-ROMs have been successfully employed to decrease computational costs incurred to simulate laminar fluid flows governed by the Navier-Stokes equations (NSE). However, in scenarios where the number of ROM degrees of freedom is insufficient to accurately represent the complex dynamics of the flow, G-ROMs yield inaccurate results. These inaccuracies usually manifest as numerical oscillations, which can severely impact the reliability of the simulations. Various ROM stabilization techniques have been developed to address and mitigate these inaccuracies.

One prominent method for stabilizing ROMs in fluid flow simulations is the regularized ROM (Reg-ROM), which employs ROM filters to smooth certain terms in the NSE. There are two primary types of ROM filters currently in use: the ROM projection filter, which operates exclusively in the ROM space, and the ROM differential filter, which operates in the physical space. Among the various Reg-ROMs, the Leray ROM (L-ROM) has gained particular popularity for its effectiveness in stabilizing under-resolved, convection-dominated flows. The L-ROM is inspired by Jean Leray's work on the NSE and involves replacing the nonlinear term in the NSE with a filtered velocity term, which enhances both computational stability and accuracy.

Despite its advantages, the L-ROM has flaws. One major issue is that the L-ROM can become over-diffusive, particularly when the ROM filter radius is excessively large, leading to the introduction of too much dissipation. Another significant drawback is the sensitivity of the L-ROM's accuracy to small perturbations in the filter radius. These issues necessitate further refinement and improvement of the model.

To address these limitations, we propose a new type of Reg-ROM, the approximate deconvolution Leray ROM (ADL-ROM)[2]. This new approach incorporates the technique of approximate deconvolution, a strategy widely used in image processing and inverse problems, to enhance the accuracy and reduce the sensitivity of the L-ROM. Specifically, in the ADL-ROM, the filtered velocity in the L-ROM is replaced with an approximately deconvoluted velocity in the nonlinear term, thereby improving the model's performance.

This talk aims to present and analyze this novel Reg-ROM, the ADL-ROM. In the first part of the talk, we will introduce the well-known L-ROM and elaborate on the development and mechanics of our new ADL-ROM. This includes a detailed discussion of how

the approximate deconvolution technique is applied to the L-ROM framework and the theoretical foundations that support its use.

The second part of the talk will provide a detailed commentary and comparison of these Reg-ROMs with each other and with the standard G-ROM. This will include presenting numerical results obtained from the ADL-ROM, highlighting its superior performance in various test cases. We will compare the outcomes of the ADL-ROM with those of the L-ROM and standard G-ROM, focusing on metrics such as accuracy, stability, and computational efficiency. Additionally, we will conduct a thorough analysis of the associated errors, examining how the ADL-ROM mitigates issues like over-diffusivity and sensitivity to filter radius perturbations.

In conclusion, we showcase our ongoing work [1], in which we provide rigorous numerical analysis results, such as stability and convergence, for the ADL-ROM. More importantly, we develop rigorous parameter scalings to ensure that the ROM parameters can automatically adapt to any changes in the corresponding FOM parameters. This approach stands in stark contrast to currently available data-driven ROMs, which often require fine-tuning of model parameters when the computational setting changes. We illustrate these numerical analysis results through the numerical simulation of convection-dominated flows, showcasing the practical applicability and robustness of our proposed ADL-ROM. Finally, we discuss future research directions, including potential extensions of the ADL-ROM framework to other types of fluid dynamics problems and the integration of additional stabilization techniques to further enhance its performance.

References

[1]   I. R. Moore, A. Sanfilippo, F. Ballarin, and T. Iliescu. "Numerical Analysis of the Approximate Deconvolution Leray Reduced Order Model". In: *in preparation* (2024).

[2]   A. Sanfilippo, I. R. Moore, F. Ballarin, and T. Iliescu. "Approximate deconvolution Leray reduced order model". In: *Finite Elem. Anal. Des.* 226 (2023), p. 104021.

Improving Mapper with Metric Trees

Luca Simi

In recent years, Topological Data Analysis (TDA) has gained significant traction in the field of data science due to its ability to extract valuable insights from complex datasets. TDA uses topological methods that are resilient to noise and dimensionality, making it a robust mathematical framework for data analysis. A well-known technique in TDA is the *Mapper algorithm*. Mapper provides a visual representation of data in the form of a graph, called *Mapper graph*, enabling easy exploration and interpretation. Unlike conventional algorithms, such as *clustering algorithms* or *Principal Component Analysis (PCA)*, Mapper excels at visualizing data by preserving their connected components, making it very effective for shape analysis and pattern discovery. The effectiveness of Mapper was initially demonstrated in the analysis of medical data, as showcased in the pioneering work by Singh et al. [10]. Since then, Mapper has proven to be a versatile and powerful tool for data exploration, capable of uncovering hidden patterns even in high-dimensional datasets.

Data exploration is an interactive process that requires constant fine-tuning and adjustments to obtain relevant information. Therefore, the running time performance of software for Mapper is essential for its widespread adoption. The original description of Mapper [10] includes what has now become a standard approach, involving the construction of an *open cover* made of overlapping hyperrectangles, also known as *cubical cover*. Currently, researchers and developers have access to several established open-source libraries for Mapper. However, these libraries often implement an inefficient construction of the cubical cover. This crucial step has been consistently overlooked and neglected, reinforcing the misconception that Mapper is inefficient with high-dimensional data. Motivated by these limitations, recent advancements in the field have led to the development of a wide family of *Mapper-type* algorithms, each proposing a distinct adaptation of the original concept. For instance, *Ball Mapper* [4] and *Mapper on Ball Mapper* [5] construct the open cover by creating an ϵ-net [7], using open balls in $\mathbb{R}^n$ instead of hyperrectangles. Additionally, specialized variations like *NeuMapper* [6], designed specifically for neuroscience data, adopt a more complex approach. This method, partially inspired by Ball Mapper, employs an intrinsic metric derived from *reciprocal kNN*. These adaptations all shift towards using balls instead of hyperrectangles for constructing open covers, which improves performance but also introduces some randomness and implicit choices due to the ϵ-net construction [7]. While this is often acceptable, there are cases where using a cubical cover is more convenient, especially given its foundational role in many Mapper-

related results. For instance, one key benefit of the cubical cover is being able to estimate optimal parameters [2], minimizing the need for time-consuming manual fine-tuning.

In our work, we present a novel and more efficient approach for computing Mapper-type algorithms, using ideas from computational geometry. Our method allows to construct open covers more efficiently, preserving the open sets of the *cubical cover* as defined in the original implementation of Mapper. We obtain the cubical cover by applying the ϵ-net construction [7] to a pseudo-metric that we define, and improve the running time performance by adopting *metric trees* [1, 3, 12, 14]. By employing the ϵ-net construction we also derive a theoretical upper bound for the time complexity of building the open cover. This upper bound improves upon the estimation given in [4], highlighting the explicit dependency on the *doubling dimension* [8] of the dataset. We present theoretical insights into our method and validate its effectiveness through experimental evaluations on well-known datasets, demonstrating significant improvements in running time compared to existing approaches. These experiments include direct comparisons with existing libraries, namely *Kepler Mapper* [13] and *giotto-tda* [11], against our new library, *tda-mapper* [9]. Our library, available on GitHub [1] and Zenodo [2] is, to the best of our knowledge, the only open-source library implementing our approach.

References

[1]   S. Brin. "Near Neighbor Search in Large Metric Spaces". In: *Proceedings of the 21th International Conference on Very Large Data Bases*. VLDB '95. San Francisco, CA, USA: Morgan Kaufmann Publishers Inc., 1995, pp. 574–584. ISBN: 1558603794.

[2]   M. Carrière, B. Michel, and S. Oudot. "Statistical Analysis and Parameter Selection for Mapper". In: *Journal of Machine Learning Research* 19.12 (2018), pp. 1–39. URL: http://jmlr.org/papers/v19/17-291.html.

[3]   K. L. Clarkson. "Nearest-Neighbor Searching and Metric Space Dimensions". In: *Nearest-Neighbor Methods in Learning and Vision: Theory and Practice*. The MIT Press, Mar. 2006. ISBN: 9780262256957. DOI: 10.7551/mitpress/4908.003.0005.

[4]   P. Dłotko. *Ball mapper: a shape summary for topological data analysis*. ARXIV: 1901 .07410. 2019.

[5]   P. Dłotko, D. Gurnari, and R. Sazdanovic. *Mapper-type algorithms for complex data and relations*. ARXIV: 2109.00831. 2023.

[6]   C. Geniesse, S. Chowdhury, and M. Saggar. "NeuMapper: A scalable computational framework for multiscale exploration of the brain's dynamical organization". In: *Network Neuroscience* 6.2 (June 2022), pp. 467–498. ISSN: 2472-1751. DOI: 10.1162 /netn_a_00229.

[7]   T. F. Gonzalez. "Clustering to minimize the maximum intercluster distance". In: *Theoretical Computer Science* 38 (1985), pp. 293–306. ISSN: 0304-3975. DOI: 10.1 016/0304-3975(85)90224-5.

---

[1]https://github.com/lucasimi/tda-mapper-python
[2]https://zenodo.org/doi/10.5281/zenodo.10642381

[8] R. Krauthgamer and J. R. Lee. "Navigating nets: simple algorithms for proximity search". In: *Proceedings of the Fifteenth Annual ACM-SIAM Symposium on Discrete Algorithms*. SODA '04. New Orleans, Louisiana: Society for Industrial and Applied Mathematics, 2004, pp. 798–807. ISBN: 089871558X.

[9] L. Simi. *lucasimi/tda-mapper-python: v0.3.0*. Version v0.3.0. Feb. 2024. DOI: `10.5281/zenodo.10642382`.

[10] G. Singh, F. Memoli, and G. Carlsson. "Topological Methods for the Analysis of High Dimensional Data Sets and 3D Object Recognition". In: *Eurographics Symposium on Point-Based Graphics*. Ed. by M. Botsch, R. Pajarola, B. Chen, and M. Zwicker. The Eurographics Association, 2007. ISBN: 978-3-905673-51-7. DOI: `10.2312/SPBG/SPBG07/091-100`.

[11] G. Tauzin et al. "giotto-tda: A Topological Data Analysis Toolkit for Machine Learning and Data Exploration". In: *Journal of Machine Learning Research* 22.39 (2021), pp. 1–6. URL: `http://jmlr.org/papers/v22/20-325.html`.

[12] J. K. Uhlmann. "Satisfying general proximity / similarity queries with metric trees". In: *Information Processing Letters* 40.4 (1991), pp. 175–179. ISSN: 0020-0190. DOI: `10.1016/0020-0190(91)90074-R`.

[13] e. a. Van Veen. "Kepler Mapper: A flexible Python implementation of the Mapper algorithm". In: *Journal of Open Source Software* 4.42 (2019), p. 1315. DOI: `10.21105/joss.01315`.

[14] P. N. Yianilos. "Data Structures and Algorithms for Nearest Neighbor Search in General Metric Spaces". In: *Proceedings of the Fourth Annual ACM/SIGACT-SIAM Symposium on Discrete Algorithms, 25-27 January 1993, Austin, Texas, USA*. Ed. by V. Ramachandran. ACM/SIAM, 1993, pp. 311–321. URL: `http://dl.acm.org/citation.cfm?id=313559.313789`.

An efficient semi-Lagrangian scheme for Fokker-Planck equations on unstructured grids

Simone Cacace[a], Roberto Ferretti[b], and Giulia Tatafiore[a],*
[a] Dipartimento di Matematica, La Sapienza, Università di Roma, Italy
[b] Dipartimento di Matematica e Fisica, Università degli Studi Roma Tre, Italy

In this work, we propose an efficient application of the barycentric walk algorithm and Sutherland-Hodgman algorithm to address the problems that arise when implementing semi-Lagrangian schemes on unstructured grids. Additionally, we propose a new semi-Lagrangian scheme for Fokker-Planck equations.

We consider the linear, constant diffusion, Fokker-Planck equation in $\mathbb{R}^2$,

$$
\begin{cases}
\partial_t m + \text{div}(b(x,t)m) - \frac{1}{2}\sigma^2 \Delta m = 0, & (x,t) \in \mathbb{R}^2 \times [0,T] \\
m(x,0) = m_0(x), & x \in \mathbb{R}^2
\end{cases}
\tag{38.1}
$$

where $b : \mathbb{R}^2 \times [0,T] \to \mathbb{R}^2$ is assumed to be Lipschitz, $\sigma > 0$ and $m_0 \in \mathcal{P}^2(\mathbb{R}^2)$, the space of probability measures with second bounded moments. Then, the Fokker-Planck equation in (38.1) can be interpreted as the equation that describes the evolution of the law of a diffusion process with drift term given by b, volatility given by σ and initial law given by m_0. This allows us to derive a representation formula for the solution of equation (38.1), which can then be discretized to obtain a semi-Lagrangian scheme, as in [3, 4]. The scheme proposed in this work has been specifically studied for the implementation on unstructured Delaunay triangulations [7] and conducts a $\mathbb{P}_0$ solution approximation. The combination of unstructured grid with semi-Lagrangian schemes allows for stable and high-customizable realistic applications. However, the need to locate the feet of characteristics and the challenge of dealing with flux-deformed grid elements may cause a significant drop in efficiency when using unstructured space grids. Additionally, when working on unstructured grids, since each cell is placed and oriented differently from the others as well as they present a different surface area, we observed that the numerical solution can be subject to a rapid loss of smoothness and mass dispersion. Therefore, we implemented the following strategies to address these issues. The first one consists in solving the equation in terms of the density of the solution, the second in locating the feet of the characteristics corresponding to all three vertices of each cell element [1, 6]. This allows us to compute the area of intersection of each grid cell with the flux deformed element, and therefore compute its contribution to the solution [5]. Then, given a time approximation step $\Delta t > 0$ and a Delaunay triangulation of the domain, the approximate

solution m_i^n in the i-th cell at time $t_n = n\Delta t$, is computed as follows

$$\begin{cases} m_i^0 = m_0(\mathcal{I}_i), & i = 0, \dots, M \\ m_i^{n+1} = \frac{1}{4} \sum_{k=1}^{4} \sum_{j=0}^{N} \left(|\beta_j(\tilde{\mathcal{I}}_i^k)| \, / \, |\mathcal{I}_i| \right) m_j^n & n = 0, \dots, N_T, \end{cases} \quad (38.2)$$

where $\mathcal{I}_i$ represents the grid cell of index i, $\tilde{\mathcal{I}}_i^k$ represents one of the four flux deformed elements that result from the discretization of the diffusion term using a two-dimensional random walk, $|\cdot|$ represents the area operator, and $\beta_j, j \in \{0, \dots, M\}$ represent the $\mathbb{P}_0$ finite element basis associated with the triangulation.

Regarding the implementation of the scheme, we use the efficiently initialized version of the barycentric walk algorithm [2] for dealing with point location problems. Moreover, we propose an efficient application of the Sutherland-Hodgman algorithm [8] to compute the intersection $\beta_j(\tilde{\mathcal{I}}_i^k)$ between $\mathcal{I}_j$ and $\tilde{\mathcal{I}}_i^k$, in (38.2).

Finally, we present some experimental results.

References

[1]   E. K. A. Vyatkin and V. Shaydurov. "The conservative semi-Lagrangian approximation for three-dimensional convection-diffusion problem". In: *AIP Conference Proceedings* (2022).

[2]   S. Cacace and R. Ferretti. "Efficient implementation of characteristic-based schemes on unstructured triangular grids". In: *Computational and Applied Mathematics* (2022).

[3]   E. Carlini and F. Silva. "A Semi-Lagrangian scheme for the Fokker-Planck equation". In: *2nd IFAC Workshop on Control of Systems Governed by Partial Differential Equations CPDE*. 2016.

[4]   E. Carlini and F. Silva. "On the discretization of some nonlinear Fokker-Planck-Kolmogorov equations and applications". In: *SIAM Journal on Numerical Analysis* (2018).

[5]   A. Iske and M. Käser. "Conservative Semi-Lagrangian Advection on Adaptive Unstructured Meshes". In: *Numerical Methods for Partial Differential Equations* (2004).

[6]   J. Scroggs and F. H. M. Semazzi. "A conservative Semi-Lagrangian method for multidimensional fluid dynamics applications". In: *Numerical Methods for Partial Differential Equations* (1995).

[7]   J. R. Shewchuk. "Triangle: Engineering a 2D Quality Mesh Generator and Delaunay Triangulator". In: *Applied Computational Geometry Towards Geometric Engineering*. 1996.

[8]   I. E. Sutherland and G. W. Hodgman. "Reentrant Polygon Clipping". In: *Communications of the ACM* (1974).

Projective and Telescopic Projective Integration for the Multispecies Boltzmann Equation

Tommaso Tenna
Université Côte D'Azur

The seminal Boltzmann Equation represents the cornerstone to describe the dynamics of a rarefied gas which is not in thermodynamical equilibrium, under the assumption of a very large number of monoatomic identical particles interacting via microscopic binary collisions. The necessity of studying more complex systems have lead to models involving mixtures of gases, whose particles are not identical.

Let us consider a mixture of M species with $\mathbf{f} = (f_1, \ldots, f_M)$ being the distribution function. Given $\mathbf{x} \in \Omega \in \mathbb{R}^{D_x}$, $\mathbf{v} \in \mathbb{R}^{D_v}$, then the distribution $\mathbf{f}(t, \mathbf{x}, \mathbf{v})$ evolves according to the so called multispecies Boltzmann equation [3], which, in absence of external forces, takes the following form:

$$\partial_t f_i + \mathbf{v} \cdot \nabla_{\mathbf{x}} f_i = \frac{1}{\varepsilon} \mathcal{Q}_i(\mathbf{f}) = \frac{1}{\varepsilon} \sum_{j=1}^{M} Q^{ij}(f_i, f_j), \qquad \forall\, i = 1, \ldots, M.$$

The parameter $\varepsilon > 0$ is the *Knudsen number* and the Q^{ij} are the collision operators describing interactions between species i and species j.

The mass of each species is preserved, whereas only the total momentum and the total kinetic energy of the gas are conserved. In the limit of small Knudsen number, that is $\varepsilon \to 0$, the frequency of collisions increases to infinity and the solution could be completely described by its local hydrodynamic fields, formally obtaining the so called multispecies Euler limit [2].

The main goal of this talk is to describe an *asymptotic preserving* numerical method which is able to capture the asymptotic limit of the original system at the discrete level. In this perspective, we introduce projective integration schemes.

Projective integration combines a few small time steps with an *inner* timestepping method with a much larger (*projective* or *outer*) time step, obtaining a computational complexity essentially independent of the stiffness of the problem [4, 6]. We consider the semidiscrete version of the original system obtained through the phase space discretization of the form:

$$\partial_t f_i = -D_{x,v}(f_i) + \varepsilon^{-1} \hat{\mathcal{Q}}_i(\mathbf{f}) =: D_i^{\varepsilon,t}(\mathbf{f}),$$

where $D_{x,v}(\cdot)$ and $\hat{\mathcal{Q}}_i(\cdot)$ represent a suitable discretization of the convective derivative $\mathbf{v} \cdot \nabla_x$ and the collision operator $\mathcal{Q}_i$.

Introducing δt and Δt, which represent the inner and the outer time steps respectively, we can define as $\mathbf{f}^{n,k}$ the approximation of the solution $\mathbf{f}$ at $t^{n,k} = n\Delta t + k\delta t$. As inner integrator we choose an explicit time integration scheme (here the *forward Euler method*), obtaining

$$\mathbf{f}^{n,k+1} = \mathbf{f}^{n,k} + \delta t D^\varepsilon(\mathbf{f}^{n,k}) \qquad k = 0, 1, \ldots.$$

Starting from a computed numerical solution $\mathbf{f}^n$ at time $t^n = n\Delta t$, one first takes $K + 1$ inner steps of size δt using the inner integrator and then approximate the time derivative of $\mathbf{f}$, computing $\mathbf{f}^{n+1}$ via extrapolation in time as

$$\mathbf{f}^{n+1} = \mathbf{f}^{n,K+1} + (\Delta t - (K+1)\delta t)\frac{\mathbf{f}^{n,K+1} - \mathbf{f}^{n,K}}{\delta t}.$$

The projective integration method is suited for problems in which the spectrum consists exactly of two eigenvalue clusters with a spectral gap between them. The main problem is that many multi-scale problems, like the multispecies Boltzmann equation, have more relaxation time scales, with spectrum containing more than two eigenvalue clusters.

For this purpose, telescopic projective integration (TPI) methods were introduced in [5] and then extended in [1, 7] to the kinetic framework. Indeed, the procedure of the projective method can be recursively repeated on a hierarchy of nested projective levels to construct a telescopic projective method.

In this work, we propose to use TPI for the multispecies Boltzmann equation. The choice of integration parameters relies on accurate spectral information which is difficult to establish. Therefore, the spectrum is approximated numerically and parameters are chosen to ensure the stability of the method. Finally, the scheme is validated against different test cases, providing solutions in the hyperbolic scaling with very small Knudsen numbers.

References

[1] R. Bailo and T. Rey. "Projective and telescopic projective integration for non-linear kinetic mixtures". English. In: *J. Comput. Phys.* 458 (2022), p. 24. ISSN: 0021-9991. DOI: 10.1016/j.jcp.2022.111082.

[2] M. Bisi, M. Groppi, and G. Martalò. "Macroscopic equations for inert gas mixtures in different hydrodynamic regimes". English. In: *J. Phys. A, Math. Theor.* 54.8 (2021), p. 23. ISSN: 1751-8113. DOI: 10.1088/1751-8121/abbd1b.

[3] M. Briant and E. S. Daus. "The Boltzmann equation for a multi-species mixture close to global equilibrium". English. In: *Arch. Ration. Mech. Anal.* 222.3 (2016), pp. 1367–1443. ISSN: 0003-9527. DOI: 10.1007/s00205-016-1023-x.

[4] C. W. Gear and I. G. Kevrekidis. "Projective methods for stiff differential equations: Problems with gaps in their eigenvalue spectrum". English. In: *SIAM J. Sci. Comput.* 24.4 (2003), pp. 1091–1106. ISSN: 1064-8275. DOI: 10.1137/S1064827501388157.

[5] C. W. Gear and I. G. Kevrekidis. "Telescopic projective methods for parabolic differential equations". English. In: *J. Comput. Phys.* 187.1 (2003), pp. 95–109. ISSN: 0021-9991. DOI: 10.1016/S0021-9991(03)00082-2.

[6] P. Lafitte, A. Lejon, and G. Samaey. "A high-order asymptotic-preserving scheme for kinetic equations using projective integration". English. In: *SIAM J. Numer. Anal.* 54.1 (2016), pp. 1–33. ISSN: 0036-1429. DOI: 10.1137/140966708.

[7] W. Melis, T. Rey, and G. Samaey. "Projective and telescopic projective integration for the nonlinear BGK and Boltzmann equations". English. In: *SMAI J. Comput. Math.* 5 (2019), pp. 53–88. ISSN: 2426-8399. DOI: 10.5802/smai-jcm.43.

The Loss Landscape of Dense Associative Memory

Robin Thériault[*] **and Daniele Tantari**
Scuola Normale Superiore di Pisa

Studying the loss landscape of artificial neural networks is crucial for our understanding of machine learning. For example, [5] demonstrated that the shape of the loss landscape of neural networks makes them generalize well even when they converge to a local minimum of the loss. Morever, [6] showed that saddle-points are much more numerous than local minima in large neural networks. Identifying and classifying individual critical points of the loss can help us understand how neural networks learn [17]. However, despite recent progress by [17], it is still largely an open problem. An interesting way forward is through dense associative memory (DAM) models based upon the Hopfield network [9, 11]. In fact, the interpretability of DAMs and their learning dynamics hints that they may have a relatively simple loss landscape [3].

The Hopfield network was originally introduced as a simple model of biological associative memory [9]. The DAM are a generalized Hopfield networks [4, 13] that were developed to improve upon the limited storage capacity of the original model [2, 9].

In recent years, the DAM were made into trainable machine learning models capable of accurate pattern classification [11, 14]. In a nutshell, the DAM introduced in [11] learns prototypes of patterns in a trainable weight matrix. Patterns awaiting classification are then attributed the class of the prototype that resemble them the most. The resulting classification scheme is considerably more adversarially robust and interpretable than that of a typical feedforward neural network with ReLU activation functions [10, 11]. Since then, deep connections were made between modern Hopfield networks and transformers [14] as well as score-based diffusion models [1]. In particular, the modern Hopfield network used to implement the attention mechanism of transformers [14, 15] has been attracting a lot of interest in fundamental [8, 12] and applied research [7, 8, 15]. Recently, it was observed that the trainable weights of DAMs for pattern classification are channeled towards minima by a low-dimensional network of valleys in the loss landscape [3]. Moreover, the critical points where valleys branch out from one another were identified to be saddles in the simple case where the DAM has two patterns to learn. In general, the loss landscape of neural networks can be very complicated, so it is difficult to identify and classify their fixed points [17]. However, the interpretability of DAMs and the results of [3] suggest that DAM fixed points may be easier to study than that of generic neural networks. With this goal in mind, we revisit dense associative memory for pattern classification using the framework of restricted Boltzmann machines (RBM) and statistical mechanics.

First of all, we derive a DAM model for classification from three basic assumptions about the distribution of data to be classified:

1. The data is scale invariant, i.e. any data point $\mathbf{x}$ is equivalent to $c\mathbf{x}$.

2. The data can be partitioned in disjoint clusters.

3. The clusters are subsets of mutually exclusive classes $\mathbf{y}$.

Second of all, we show that our DAM learns similar weights and is just as interpretable as the DAM introduced in [11]. Third of all, we use the replica method of statistical mechanics to study the loss landscape of dense associative memory trained on real data. We show that local minima of DAM models are embedded in larger DAM models, where they become saddle points. We then relate these findings to the learning dynamics guided by valleys and saddles studied in [3]. Finally, we implement a network growing algorithm [16] that leverages saddle points to significantly reduce the cost of training dense associative memory.

References

[1] L. Ambrogioni. "In search of dispersed memories: Generative diffusion models are associative memory networks". ARXIV: 2309.17290. Sept. 2023.

[2] D. J. Amit, H. Gutfreund, and H. Sompolinsky. "Storing Infinite Numbers of Patterns in a Spin-Glass Model of Neural Networks". In: *Phys. Rev. Lett.* 55 (14 Sept. 1985), pp. 1530–1533. DOI: 10.1103/PhysRevLett.55.1530.

[3] N. E. Boukacem, A. Leary, R. Thériault, F. Gottlieb, M. Mani, and P. Fran çois. "Waddington landscape for prototype learning in generalized Hopfield networks". In: *Phys. Rev. Res.* 6 (3 July 2024), p. 033098. DOI: 10.1103/PhysRevResearch.6.033098.

[4] H. H. Chen, Y. C. Lee, G. Z. Sun, H. Y. Lee, T. Maxwell, and C. L. Giles. "High order correlation model for associative memory". In: *AIP Conference Proceedings* 151.1 (Aug. 1986), pp. 86–99. ISSN: 0094-243X. DOI: 10.1063/1.36224.

[5] A. Choromanska, M. Henaff, M. Mathieu, G. Ben Arous, and Y. LeCun. "The Loss Surfaces of Multilayer Networks". In: *Proceedings of the Eighteenth International Conference on Artificial Intelligence and Statistics*. Ed. by G. Lebanon and S. V. N. Vishwanathan. Vol. 38. Proceedings of Machine Learning Research. ARXIV: 1412.0233. San Diego, California, USA: PMLR, May 2015, pp. 192–204.

[6] Y. N. Dauphin, R. Pascanu, C. Gulcehre, K. Cho, S. Ganguli, and Y. Bengio. "Identifying and attacking the saddle point problem in high-dimensional non-convex optimization". In: *Advances in Neural Information Processing Systems*. Ed. by Z. Ghahramani, M. Welling, C. Cortes, N. Lawrence, and K. Weinberger. Vol. 27. ARXIV: 1406.2572. Curran Associates, Inc., 2014.

[7] A. Fürst et al. "CLOOB: Modern Hopfield Networks with InfoLOOB Outperform CLIP". In: *Advances in Neural Information Processing Systems*. Ed. by S. Koyejo, S. Mohamed, A. Agarwal, D. Belgrave, K. Cho, and A. Oh. Vol. 35. ARXIV: 2110.11316. Curran Associates, Inc., 2022, pp. 20450–20468.

[8] B. Hoover et al. "Energy Transformer". In: *arXiv e-prints* (Feb. 2023). ARXIV: 2302.07253.

[9] J. J. Hopfield. "Neural networks and physical systems with emergent collective computational abilities." In: *Proceedings of the National Academy of Sciences* 79.8 (1982), pp. 2554–2558. DOI: 10.1073/pnas.79.8.2554.

[10] D. Krotov and J. Hopfield. "Dense Associative Memory Is Robust to Adversarial Inputs". In: *Neural Computation* 30.12 (Dec. 2018), pp. 3151–3167. ISSN: 0899-7667. DOI: 10.1162/neco_a_01143.

[11] D. Krotov and J. J. Hopfield. "Dense Associative Memory for Pattern Recognition". In: *Advances in Neural Information Processing Systems*. Ed. by D. Lee, M. Sugiyama, U. Luxburg, I. Guyon, and R. Garnett. Vol. 29. ARXIV: 1606.01164. Curran Associates, Inc., 2016.

[12] D. Krotov and J. J. Hopfield. "Large Associative Memory Problem in Neurobiology and Machine Learning". In: *International Conference on Learning Representations*. ARXIV: 2008.06996. 2021.

[13] D. Psaltis and C. H. Park. "Nonlinear discriminant functions and associative memories". In: *AIP Conference Proceedings* 151.1 (Aug. 1986), pp. 370–375. ISSN: 0094-243X. DOI: 10.1063/1.36241.

[14] H. Ramsauer et al. "Hopfield Networks is All You Need". In: *International Conference on Learning Representations*. ARXIV: 2008.02217. 2021.

[15] M. Widrich et al. "Modern Hopfield Networks and Attention for Immune Repertoire Classification". In: *Advances in Neural Information Processing Systems*. Ed. by H. Larochelle, M. Ranzato, R. Hadsell, M. Balcan, and H. Lin. Vol. 33. Curran Associates, Inc., 2020, pp. 18832–18845.

[16] L. Wu, D. Wang, and Q. Liu. "Splitting Steepest Descent for Growing Neural Architectures". In: *Advances in Neural Information Processing Systems*. Ed. by H. Wallach, H. Larochelle, A. Beygelzimer, F. d'Alché-Buc, E. Fox, and R. Garnett. Vol. 32. ARXIV: 1910.02366. Curran Associates, Inc., 2019.

[17] Y. Zhang, Z. Zhang, T. Luo, and Z. J. Xu. "Embedding Principle of Loss Landscape of Deep Neural Networks". In: *Advances in Neural Information Processing Systems*. Ed. by M. Ranzato, A. Beygelzimer, Y. Dauphin, P. Liang, and J. W. Vaughan. Vol. 34. ARXIV: 2105.14573. Curran Associates, Inc., 2021, pp. 14848–14859.

Mathematical models on graphs in Alzheimer's brain

Veronica Tora

Istituto per la Applicazioni del Calcolo "M. Picone" (IAC), CNR, Rome, Italy

Alzheimer's disease (AD) is the most common form of dementia. It is well-known that two proteins, namely beta amyloid and misfolded forms of tau protein, have a key role in neurodegenerative processes. The mechanisms linking the widespread and progressive deposition of these toxic proteins to the development of the disease are only partially understood and are subject of active ongoing investigation. In this talk, we will present two different mathematical approaches to the modeling of toxic proteins' spreading throughout the brain in AD by means of reaction-transport equations on a finite graph, whose vertices represent functionally homogeneous brain regions and whose edges describe the connections between such regions. In the first model, the spreading of toxic tau and beta amyloid protein between regions is described using models of "network diffusion": given an initial distribution of regional pathology in the brain, the diffusion process is governed by the concentration gradients and the weights between all region pairs and it is suitably modeled by means of the graph laplacian matrix.

However, an underexplored aspect of tau spreading is that it is governed not simply by diffusion but also active transport along axonal microtubules. Spread can therefore take on a directional bias, resulting in distinct patterns of deposition. A two neurons mathematical model of the axonal transport of toxic tau protein has been recently developed in [4]. The second model that we will present for tau protein is based on a novel approach to model tau spreading in Alzheimer's brain. Indeed, this model, which we call the Network Transport Model (NTM), combines the dynamics of soluble and insoluble tau in the gray-matter regions and Torok et al. axonal transport model [4] in the white-matter tracts, and enables us to simulate the dynamics of soluble and insoluble tau in terms of the diffusion–advection and aggregation–fragmentation processes at the network level. More precisely, the full network model involves a transport–reaction PDE on each edge, which describes the dynamics of soluble and insoluble tau within the white-matter tracts whereas the tau dynamics in the gray-matter regions is modeled by a system of ordinary differential equations at the nodes of the graph. A straightforward mass transfer mechanism of soluble tau between edges and nodes determines the incoming flux of soluble tau into the nodes.

However, the full NTM is computationally infeasible to simulate on the full network, thus we provide and implement a quasi-static approximation to the NTM that maintains the basic properties of the full NTM and is more tractable numerically. Some of the numerical challenges related to the implementation of the NTM will be discussed.

For both NTM and network diffusion–reaction model, some numerical simulations will be shown and the suitability of each model of delivering insights on specific patterns of AD progression will be discussed. In particular, for network diffusion–reaction model its capability to predict some *in vivo* patterns of tau progression will be shown. As regards the NTM model, its ability to govern directionally biased flows on the connectome will be discussed, an aspect that has received almost no theoretical attention so far and that has been observed in mouse models of tauopathy.

References

[1] M. Bertsch, B. Franchi, M. C. Tesi, and V. Tora. "The role of Abeta and Tau proteins in Alzheimer's disease: a mathematical model on graphs". In: vol. 87. 3. Sept. 2023, p. 49. DOI: 10.1007/s00285-023-01985-7.

[2] A. Raj et al. "Combined Model of Aggregation and Network Diffusion Recapitulates Alzheimer's Regional Tau-Positron Emission Tomography". In: vol. 11. 8. Oct. 2021, pp. 624–638. DOI: 10.1089/brain.2020.0841.

[3] V. Tora, J. Torok, M. Bertsch, and A. Raj. "A network-level transport model of tau progression in the Alzheimer's brain". In: ARXIV: 2401.02407. 2024.

[4] J. Torok et al. "Emergence of directional bias in tau deposition from axonal transport dynamics". In: *This Book of Abstract*. *PLoS Comput Biol 17(7): e1009258*. 2021.

Divergence–free preserving schemes: how to fix stabilization terms in continuous Galerkin for hyperbolic PDEs

Davide Torlo***, Wasilij Barsukow, and Mario Ricchiuto**
Università di Roma, La Sapienza

The emergence of physical structures and equilibrium solutions, such as divergence-free solutions in contexts like shallow water and magneto-hydrodynamics, poses a significant challenge. A simple linear approximation of such systems that already show these behavior is the linear acoustic system of equations (in 2 dimensions)

$$\begin{cases} \partial_t u + \partial_x p = 0, \\ \partial_t v + \partial_y p = 0, \\ \partial_t p + \partial_x u + \partial_y v = 0 \end{cases} \tag{42.1}$$

We focus on Cartesian grid discretizations of such systems in 2 dimensions and in the preservation of stationary solutions that arise due to a truly multidimensional balance of terms, which corresponds to the divergence-free solutions for acoustic systems. Conventional methods, like the continuous Finite Element SUPG that reads

$$\begin{cases} \int \varphi_i \left(\partial_t u + \partial_x p \right) + \Delta x \alpha \partial_x \varphi_i (\partial_t p + \partial_x u + \partial_y v) = 0 & \forall i, \\ \int \varphi_i \left(\partial_t v + \partial_y p \right) + \Delta y \alpha \partial_y \varphi_i (\partial_t p + \partial_x u + \partial_y v) = 0 & \forall i, \\ \int \varphi_i \left(\partial_t p + \partial_x u + \partial_y v \right) + \Delta x \alpha \partial_x \varphi_i (\partial_t u + \partial_x p) + \Delta y \alpha \partial_y \varphi_i (\partial_t u + \partial_y p) = 0 & \forall i, \end{cases}$$

face limitations in maintaining these structures due to the employed stabilization techniques that do not effectively vanish when the discrete divergence is zero. One might believe that having a residual formulation, as SUPG, should preserve a discrete divergence-free solution ($\partial_x u + \partial_y v = 0, p = c \in \mathbb{R}$). The problem is that we cannot describe discrete divergence-free solutions that vanish for both the divergence operator $\int \varphi_i \left(\partial_x u + \partial_y v \right)$ and for the diffusion operator $\int \nabla \varphi_i \left(\partial_x u + \partial_y v \right)$. Indeed, the kernel of the combination of the two operator is very complicated and allows for unphysical equilibria, see center of Figure 42.1.

We propose to use the Global Flux procedure, which has proven to be successful in preserving 1-dimensional equilibria [2, 3], to define some auxiliary variables U, V in the same Finite Element space defined as

$$\begin{cases} U(x, y) := \int_{y_0}^{y} u(x, s) ds, \\ V(x, y) := \int_{x_0}^{x} v(s, y) ds, \end{cases}$$
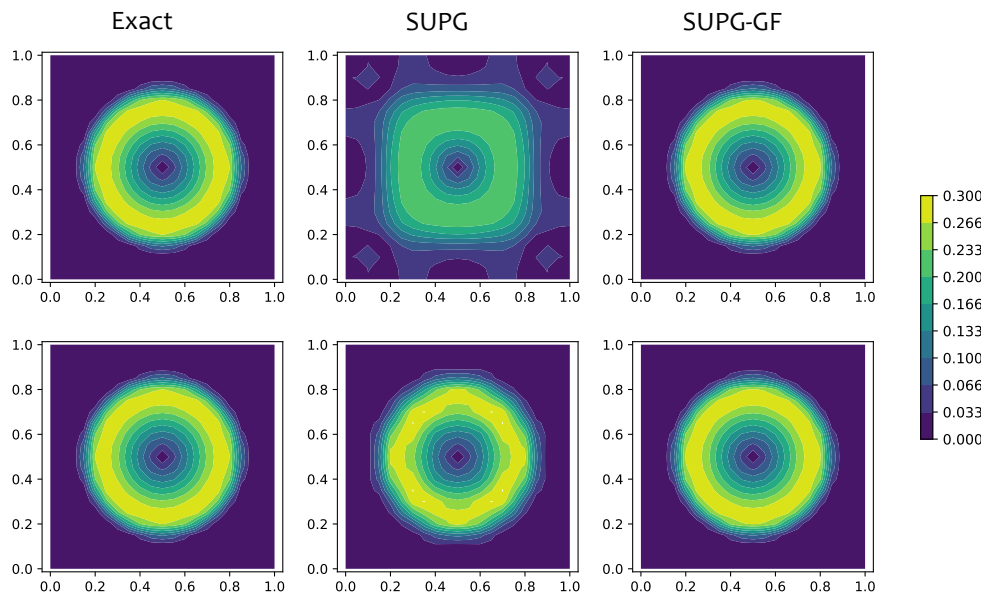
Figure 42.1: Simulation of norm of u at time $T = 100$ of a vortex with 20×20 cells and $\mathbb{P}^1$ elements (top) and 10×10 cells with $\mathbb{P}^2$ elements (bottom). Comparison of exact (left), SUPG (center) and SUPG-GF (right)

so that $\partial_x u + \partial_y v = \partial_{xy}(U + V)$ and we can use these variables to define a new SUPG method where the divergence term and the stabilization terms are

$$\begin{cases} \int \varphi_i(\partial_x u + \partial_y v) \approx \int \varphi_i \partial_x \partial_y (U + V), \\ \int \partial_x \varphi_i(\partial_x u + \partial_y v) \approx \int \partial_x \varphi_i \partial_x \partial_y (U + V), \\ \int \partial_y \varphi_i(\partial_x u + \partial_y v) \approx \int \partial_y \varphi_i \partial_x \partial_y (U + V). \end{cases}$$

This results in a suitable discretization of both the divergence and stabilization operators [1]. This approach naturally preserves divergence-free solutions, characterized by the discrete steady state solutions of type $\partial_x \partial_y (U + V) = 0$, and more intricate equilibria involving various sources. Most of the other spurious kernel elements of the divergence discrete operator are proven to be dissipated by the stabilization operator.

We use the Deferred Correction time discretization, obtaining explicit arbitrarily high order methods. Numerous numerical tests validate the accuracy of our proposed scheme compared to classical approaches. Our method not only (discretely) preserves divergence-free solutions and their perturbations but it also maintains the original order of accuracy.

We plot the SUPG-GF solutions at the right of Figure 42.1 and they nicely catch the divergence-free equilibria.

References

[1] W. Barsukow, M. Ricchiuto, and D. Torlo. "Structure preserving nodal continuous Finite Elements via Global Flux quadrature". ARXIV: 2407.10579. 2024.

[2] Y. Cheng, A. Chertock, M. Herty, A. Kurganov, and T. Wu. "A new approach for designing moving-water equilibria preserving schemes for the shallow water equations". In: *Journal of Scientific Computing* 80 (2019), pp. 538–554.

[3] M. Ciallella, D. Torlo, and M. Ricchiuto. "Arbitrary High Order WENO Finite Volume Scheme with Flux Globalization for Moving Equilibria Preservation". In: *Journal of Scientific Computing* 96 (2023), p. 53. DOI: 10.1007/s10915-023-02280-9.

Neural Networks vs Sparse Polynomials for Spectral Operator Surrogates

Josephine Westermann[a,*], Thomas O'Leary-Roseberry[b], and Jakob Zech[a]
[a]University of Heidelberg, Germany
[b]University of Texas at Austin, USA

Motivation. Let $\mathcal{P}$ and $\mathcal{Q}$ be two separable Hilbert spaces and consider an operator $F : \mathcal{P} \to \mathcal{Q}$. Here, $q := F(p) \in \mathcal{Q}$ can be interpreted as the response of some physical system depending on a parameter p. Analyzing such a system when p and/or q are uncertain typically requires numerous evaluations of F. This is challenging when evaluation is costly, such as when $F(p)$ is the solution to a partial differential equation (PDE). Therefore, constructing operator surrogates that are cheaper to evaluate while maintaining acceptable approximation error is a focus of current research. Both neural networks [1, 7, 8, 9] and polynomial methods [3, 4, 5] have been successful. Convergence results for both surrogate types exist [6, 10, 12]. However, for neural networks, they indicate existence without practical guarantees, whereas polynomial surrogates yield constructive and deterministic algorithms. This work presents an extensive comparison of the empirical performance of polynomial and network-based surrogates for various applications driven by PDEs.

Operator Surrogate Architecture. In typical applications, $\mathcal{P}$ and/or $\mathcal{Q}$ are infinite-dimensional function spaces. To use approximation methods like interpolation or neural networks, the operator's input and output must be mapped to coefficient representations in suitable bases and truncated to finite dimensions. Here, we express the parameter p as a Karhunen-Loève expansion $\sum_{j \in \mathbb{N}} a_j \Phi_j$ with $\Phi_j \in \mathcal{P}$, $a_j \in \mathbb{R}$ for all $j \in \mathbb{N}$, and construct an encoder $E : \mathcal{P} \to \mathbb{R}^{d_E}$ mapping p to its first d_E coefficients $(a_j)_{j=1}^{d_E}$. We express $q = F(p)$ as a linear combination of principal components $\sum_{j \in \mathbb{N}} b_j \Psi_j$ with $\Psi_j \in \mathcal{Q}$, $b_j \in \mathbb{R}$ for all $j \in \mathbb{N}$, and construct a decoder $D : \mathcal{Q} \to \mathbb{R}^{d_D}$ mapping q to its first d_D coefficients $(b_j)_{j=1}^{d_D}$. We then approximate the coefficient map $D^{-1} \circ F \circ E^{-1} : \mathbb{R}^{d_E} \to \mathbb{R}^{d_D}$ with a polynomial interpolant S_{IP} or a neural network S_{NN}. The final operator surrogate is $\hat{F} := D \circ S \circ E$ with $S \in \{S_{\text{IP}}, S_{\text{NN}}\}$. For our study, we construct S_{NN} as a feed-forward network with about 10^3 parameters and a smooth activation function, training it with the Adam optimizer. The polynomial approximation S_{IP} is a sparse grid interpolant tailored to smoothness assumptions on the operator as derived in [6].

Test applications. We test both surrogate types on the parameter-to-solution map of two PDEs on the unit square $[0, 1]^2$. The first is the parametric second order elliptic PDE $-\nabla \cdot (e^{p(\mathbf{x})} \nabla q(\mathbf{x})) = 0$ with parameter $p \in L_\infty([0, 1]^2)$. The second describes the deformation of a hyperelastic material under stress in dependence on an anisotropic stiffness modulus adapted from [2]. For both test problems, we obtain qualitatively similar results,

discussed and illustrated below.

Results and discussion. We measure the performance $\varepsilon_{H^1}(S)$ of an operator surrogate S in terms of a Monte-Carlo approximation of the relative error in the H^1-norm, $\varepsilon_{H^1}(S) := \left(\sum_{k=1}^{N} \|q_k - D \circ S \circ E(p_k)\|_{H^1}^2 \right) / \left(\sum_{k=1}^{N} \|q_k\|_{H^1}^2 \right)$, using $N = 250$ parameter-solution pairs $(p_k, q_k)_{k=1}^{N}$. The convergence of both surrogate types in the hyperelasticity problem is shown in Figure 43.1. We observe that in terms of accuracy per number of training data, the polynomial surrogate outperforms the neural surrogate. This observation is qualitatively similar in both of our test problems and across a range of smoothness scales of the parameter p. The key strength of neural surrogates is their evaluation speed, which is independent of the number of training samples used, see Figure 43.2. This can be leveraged to trade accuracy for speed by first approximating the coefficient map with a low-degree polynomial S_{IP}, and then approximating the *difference* between the approximation target and the low-degree interpolant with a neural network, S_{NN}. The coefficient map is then approximated by the combination $S_{\text{LC}} := S_{\text{IP}} + S_{\text{NN}}$, see Figure 43.2.

Note that both methods require careful fine-tuning – of hyperparameters such as the layer architecture, activation functions, and optimizer for networks, and of interpolation points and ansatz spaces for polynomial interpolation. For neural networks, more sophisticated architectures, which may lead to improved performance, have been studied, e.g. [9, 11] and references there.
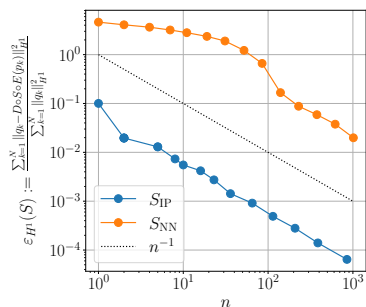
Figure 43.1: Surrogate accuracy ε_{H^1} in the hyperelasticity problem as a function of the number of training data n used for the construction of the surrogate.
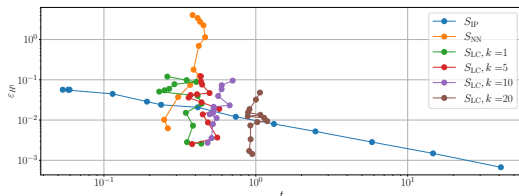
Figure 43.2: Surrogate accuracy in the hyperelasticity problem in dependence of surrogate evaluation time t for 5000 evaluations. The results for S_{LC} are shown for different degrees k of the polynomial interpolant S_{IP}.

References

[1] K. Bhattacharya, B. Hosseini, N. B. Kovachki, and A. M. Stuart. "Model reduction and neural networks for parametric PDEs". In: *The SMAI journal of computational mathematics* 7 (2021), pp. 121–157.

[2] L. Cao, T. O'Leary-Roseberry, P. K. Jha, J. T. Oden, and O. Ghattas. "Residual-based error correction for neural operator accelerated infinite-dimensional Bayesian inverse problems". In: *Journal of Computational Physics* 486 (2023), p. 112104.

[3] A. Chkifa, A. Cohen, R. DeVore, and C. Schwab. "Sparse adaptive Taylor approximation algorithms for parametric and stochastic elliptic PDEs". In: *ESAIM: Mathematical Modelling and Numerical Analysis* 47.1 (2013), pp. 253–280.

[4] A. Chkifa, A. Cohen, and C. Schwab. "High-dimensional adaptive sparse polynomial interpolation and applications to parametric PDEs". In: *Foundations of Computational Mathematics* 14 (2014), pp. 601–633.

[5] A. Chkifa, A. Cohen, and C. Schwab. "Breaking the curse of dimensionality in sparse polynomial approximation of parametric PDEs". In: *Journal de Mathématiques Pures et Appliquées* 103.2 (2015), pp. 400–428.

[6] L. Herrmann, C. Schwab, and J. Zech. "Neural and spectral operator surrogates: unified construction and expression rate bounds". In: *Advances in Computational Mathematics (accepted)* (2024). arXiv: 2207.04950.

[7] J. S. Hesthaven and S. Ubbiali. "Non-intrusive reduced order modeling of nonlinear problems using neural networks". In: *Journal of Computational Physics* 363 (2018), pp. 55–78.

[8] M. V. de Hoop, D. Z. Huang, E. Qian, and A. M. Stuart. "The cost-accuracy trade-off in operator learning with neural networks". arXiv: 2203.13181. 2022.

[9] N. Kovachki et al. "Neural operator: Learning maps between function spaces with applications to PDEs". In: *Journal of Machine Learning Research* 24.89 (2023), pp. 1–97.

[10] S. Lanthaler. "Operator learning with PCA-Net: upper and lower complexity bounds". In: *Journal of Machine Learning Research* 24.318 (2023), pp. 1–67.

[11] T. O'Leary-Roseberry, P. Chen, U. Villa, and O. Ghattas. "Derivative-informed neural operator: an efficient framework for high-dimensional parametric derivative learning". In: *Journal of Computational Physics* 496 (2024), p. 112555.

[12] C. Schwab and J. Zech. "Deep learning in high dimension: Neural network expression rates for generalized polynomial chaos expansions in UQ". In: *Analysis and Applications* 17.01 (2019), pp. 19–55.

Stochastic heat equation in heterogeneous medium

Eya Zougar

University of Polytechnique Hauts-de-France, CERAMATHS, Campus Mont Houy, 59313,Valenciennes, CEDEX 9-FRANCE

In my presentation, I focused on introducing and investigating various stochastic counterparts of a specific equation, defined in the following general form:

$$\frac{\partial u(t,x)}{\partial t} = \mathcal{L}_g u(t,x), \tag{44.1}$$

where $\mathcal{L}_g$ is the elliptic divergence form operator defined by

$$\mathcal{L}_g = \frac{1}{r(x)} \frac{d}{dx}\left(R(x) \frac{d}{dx} \right),$$

R and r are two measurable and bounded functions defined on $\mathbb{R}$ and satisfying: $\mu_1 \leq R(x)$ and $\mu_2 \leq r(x)$, $\forall x \in \mathbb{R}$; where μ_1 and μ_2 are two strictly positive real constants. While these equations have been studied by various authors, an explicit expression for their fundamental solutions remains elusive. One interesting particular case of PDE (44.1) is the particular one which the operator, $\mathcal{L}_g = \mathcal{L}$, is given as well:

$$\mathcal{L} = \frac{1}{2\rho(x)} \frac{d}{dx}\left(\rho(x) A(x) \frac{d}{dx} \right); \tag{44.2}$$

with

$$A(x) = a_1 \mathbf{1}_{\{x \leq 0\}} + a_2 \mathbf{1}_{\{x > 0\}} \quad \text{and} \quad \rho(x) = \rho_1 \mathbf{1}_{\{x \leq 0\}} + \rho_2 \mathbf{1}_{\{x > 0\}},$$

a_i, ρ_i ($i = 1, 2$) are strictly positive constants and $\dfrac{df}{dx}$ denotes the derivative of f in the distributional sense. Equations (44.1) appears in the mathematical modeling of diffusion phenomena in many fields, for example, in geophysics, ecology, biology and so on. The non-smoothness of the coefficients in Operator (44.2) reflects the heterogeneity of the medium in which the process under study propagates. What makes the study of this equation interesting is that the expression for the fundamental solution has been determined. It can be explicitly expressed as well:

$$
\begin{aligned}
G(t-s, x, z) \;=\; & \frac{\mathbf{1}_{\{t>s\}}}{\sqrt{2\pi(t-s)}} \left(\frac{\mathbf{1}_{\{z \leq 0\}}}{\sqrt{a_1}} + \frac{\mathbf{1}_{\{z>0\}}}{\sqrt{a_2}} \right) \times \left\{ \exp\left(-\frac{(f(x)-f(z))^2}{2(t-s)} \right) \right. \\
& \left. + \; \beta\, \mathrm{sign}(z)\, \exp\left(-\frac{(|f(x)|+|f(z)|)^2}{2(t-s)} \right) \right\}
\end{aligned}
\tag{44.3}
$$

where

$$f(z) = \frac{z}{\sqrt{a_1}}\mathbf{1}_{\{z\leq0\}} + \frac{z}{\sqrt{a_2}}\mathbf{1}_{\{z>0\}}$$

$$\beta = \frac{\sqrt{a_1} + \sqrt{a_2}(\alpha - 1)}{\sqrt{a_1} - \sqrt{a_2}(\alpha - 1)}, \quad \alpha = 1 - \frac{\rho_1 a_1}{\rho_2 a_2}, \quad \text{sign}(z) = \begin{cases} -1 & if\ z \leq 0 \\ 1 & if\ z > 0 \end{cases}$$

My study was based on applying various Gaussian noises on our model given in (44.1). So, the problem under studying will be expressed as well:

$$\frac{\partial u(t,x)}{\partial t} = \mathcal{L}u(t,x) + \dot{W}(t,x) \tag{44.4}$$

for every $t \in (0,T]$, $x \in \mathbb{R}$, with vanishing initial condition $u(0,x) = 0$, $\forall x \in \mathbb{R}$. Here, $\dot{W}$ denotes the formal derivative of a space-time white noise. More precisely, W is a centered Gaussian field $W = \{W(t,C); t \in [0,T], C \in B_b(\mathbb{R}^d)\}$ with covariance

$$\mathbb{E}(W(t,C)W(s,B)) = (t \wedge s)\lambda_d(C \cap B),$$

where λ_d denotes the Lebesgue measure. So W behaves as a Wiener process both in time and in space. My main interest is to focus on studying the existence of the mild solution to the SPDE (44.4), which is a wiener process defined as well:

$$u(t,x) = \int_0^t \int_{\mathbb{R}} G(t-s,x,y)\,W(ds,dy), \tag{44.5}$$

here G is the fundamental solution of the deterministic equation defined in (44.3) and the integral in (44.5) is a Wiener integral with respect to the Gaussian noise W.

My focus was on analyzing various properties of the solution such as sharp Hölder regularity of the sample paths, non-differentiability of the trajectories, or scaling properties. Every time, I try to compare the behavior exhibited by the solution of SPDE defined in (44.4) with the classical case, that is the heat equation in homogeneous domain. Moreover, I expand the quartic variations in time and the quadratic variations in space of the solution to a stochastic partial differential equation with piecewise constant coefficients. Both expansions allow us to deduce an estimation method of the parameters appearing in the equation. The outcome of this work was the publication of two articles, [1][2].

References

[1]   M. Zili and E. Zougar. "Exact variations for stochastic heat equations with piecewise constant coefficients and application to parameter estimation". In: *Theory of Probability and Mathematical Statistics* 100 (2020), pp. 77–106.

[2]   M. Zili and E. Zougar. "One-dimensional stochastic heat equation with discontinuous conductance". In: *Applicable Analysis* 98.12 (2019), pp. 2178–2191.

Mini-Courses

Multilevel Monte Carlo Methods

Anastasia Istratuca

University of Edinburgh, Heriot-Watt University, Scotland

Simulating computer models is of paramount importance in today's world. From climate modelling and weather forecasting to medical imaging and applications, mathematical models have revolutionised what can be achieved with computational budget at hand. Typically, these are subject to uncertainty arising from unknown model parameters which have to be estimated from (scarce) data, numerical errors arising from numerical approximations, or round-off errors and incomplete knowledge of the system. Tracing the propagation of the aforementioned uncertainty through the system is crucial, but it frequently increases the computational complexity of the deterministic algorithms associated with the original problem. Hence, in this mini-course we discuss an efficient method for tackling this issue, namely the multilevel Monte Carlo method [3, 4].

One example of interest in practice is simulating groundwater flow. Specifically, water resources, generally comprising of ground and surface water, must be preserved free of pollution. Thus, efficient methods for modelling and forecasting the movement of impurities through aquifers, which are used as supplies for potable water, are necessary. Such impurities can contaminate the groundwater flowing beneath earth's surface in various ways, such as carbon capture and underground storage, fracking, accidental spills, or spent nuclear fuel repositories. A mathematical model for simulating groundwater flow rests on Darcy's Law [1], where the main parameter is the hydraulic conductivity, that is, the ease with which a fluid can move through porous media or fractures under a given pressure gradient. In practice, this can only be measured at a finite, usually small, number of geographical points due to the difficulty involved in collecting physical measurements.
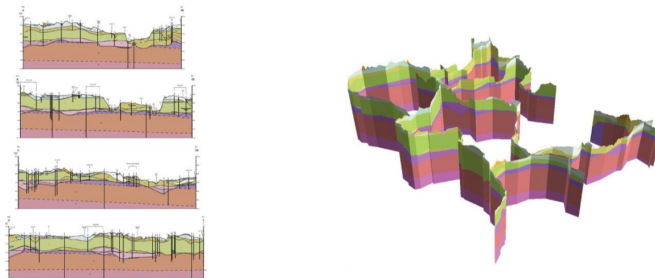
Figure 45.1: Cross-section of subsurface example using ArcScene. [2]

However, for numerical simulations, the value of this parameter is usually required at all the points in the computational domain, which constitutes the main source of uncertainty for this problem. This is illustrated in Figure 45.1.

Another example which arises in practice is climate modelling. These are usually complex models which are computationally expensive due to not only the spatial discretisation, but also the long simulation times involved in obtained accurate predictions. As such, one simplified model for atmospheric convection was developed by Lorenz in 1963 [5]. This is a three dimensional system of time dependent ordinary differential equations (ODEs) where x is proportional to the rate of convection, y to the temperature difference between ascending and descending currents, and z to the vertical temperature variation. Here, one important model parameter is the Rayleigh number which indicates whether the fluid flow is turbulent or laminar. Similar to the previous example, this parameter is not known exactly, and it is instead taken to be a random variable.

Returning to the problem of uncertainty quantification, we can classify the existing algorithms for tackling this issue in two main categories: intrusive and non-intrusive methods. In this mini-course, we focus on the latter and, more specifically, with sampling based approaches. One such method, which is still widely used in practice, is the Monte Carlo method [6]. For the problem at hand, this entails generating realisations from the distribution associated with the random parameter and subsequently solving the governing equation for many such samples to approximate a specific quantity of interest. In practice, this is straightforward to implement as it is heavily based on the deterministic solver for the model under consideration. In addition, the Monte Carlo computational complexity is independent of the dimension of the space associated with the random parameter. The disadvantage of this approach is that it has a very slow convergence rate, hence it quickly becomes computationally intractable, particularly for numerically discretised models.

A novel approach in addressing this problem consists in adopting Multilevel Monte Carlo (MLMC) algorithms [3, 4]. Such methods hinge on a multilevel variance reduction technique for the standard MC method. For the problem at hand, this is achieved by first expressing the quantity we wish to estimate on a relatively coarse grid. Thereafter, we successively add to it "correction" terms arising from adjusting the grid. Since most of the uncertainty can be captured on the coarse grid, fewer samples are thus needed on the finest grid to obtain truthful approximations. Due to the variance reduction, this contributes to a notable reduction in the computational cost associated with MLMC methods compared to standard MC approaches.

In this mini-course, we first investigate some examples which motivate the need for uncertainty quantification in practical applications, such as the ones gives above. We then revise appropriate methods for sampling from the random parameter of the model under consideration. Then, we review existing methods for tackling the uncertainty quantification problem, with a particular focus on Monte Carlo methods. We finally describe alternative approaches which outperform the standard Monte Carlo method, specifically the Multilevel Monte Carlo method. We conclude with an overview of different research directions which are still of interest in this community.

References

[1] G. De Marsily. *Quantitative hydrogeology*. London: Academic Press, 1986.

[2] M. DeMeritt. *Modeling the terrain below. Creating dynamic subsurface perspectives in ArcScene. Esri Writer*. 2012.

[3] M. B. Giles. "Multilevel Monte Carlo Path Simulation". en. In: *Operations Research* 56.3 (June 2008), pp. 607–617. ISSN: 0030-364X, 1526-5463. DOI: 10.1287/opre.1070.0496.

[4] S. Heinrich. "Multilevel monte carlo methods". In: *Large-Scale Scientific Computing: Third International Conference, LSSC 2001 Sozopol, Bulgaria, June 6–10, 2001 Revised Papers 3*. Springer, 2001, pp. 58–67.

[5] E. N. Lorenz. "Deterministic Nonperiodic Flow." In: *Journal of the Atmospheric Sciences* 20.2 (Mar. 1963), pp. 130–148. DOI: 10.1175/1520-0469(1963)020<0130:DNF>2.0.CO;2.

[6] A. B. Owen. *Monte Carlo theory, methods and examples*. https://artowen.su.domains/mc/, 2013.

Cubic and quadratic polynomial enrichments of the Crouzeix–Raviart finite element

Federico Nudo
University of Padua, Italy
email: federico.nudo@unipd.it

A finite element is defined as a triplet $(K_d, \mathbb{F}_{K_d}, \Sigma_{K_d})$, where:

- K_d is a polytope in $\mathbb{R}^d$,

- $\mathbb{F}_{K_d}$ is a vector space of dimension n composed of real-valued functions defined on K_d, also referred to as *trial functions*,

- $\Sigma_{K_d} = \{L_j : j = 1, \ldots, n\}$ is a set of linearly independent linear functionals from the vector space $\mathbb{F}_{K_d}$, also known as *degrees of freedom*, such that $\mathbb{F}_{K_d}$ is Σ_{K_d}-unisolvent. In simpler terms, if $f \in \mathbb{F}_{K_d}$ and

$$L_j(f) = 0, \qquad j = 1, \ldots, n,$$

then $f = 0$ [3].

The finite element method stands out as a highly favored approach for numerically solving partial differential equations, which are commonly encountered in engineering and mathematical modeling, over domains $D \subset \mathbb{R}^d$, where $d \geq 1$. Its widespread adoption can be attributed, in part, to its adaptability to different geometries. In this method, the domain $\bar{D}$ is partitioned into polytopes, and for each of them, a local approximation within $\mathbb{F}_{K_d}$ is computed to approximate the solution of the partial differential equation. The global approximation is then defined as a piecewise function composed of the local approximations.

The finite element can be classified as either conforming or nonconforming, depending on whether the global approximation exhibits discontinuities at the subdomain boundaries. Indeed, standard linear finite elements, which typically use polynomial functions within the F_{K_d} approximation space, might prove ineffective for solving problems involving singularities. To address this limitation, various strategies have been proposed. Among these, a notable approach involves augmenting the approximation space $\mathbb{F}_{K_d}$ with appropriate enrichment functions.

In particular, given the finite element $(K_d, \mathbb{F}_{K_d}, \Sigma_{K_d})$, the task at hand is to determine:

How to select suitable enrichment functions $e_1, \ldots, e_N$**, such that the triplet** $(K_d, \mathbb{F}_{K_d}^{\mathrm{enr}}, \Sigma_{K_d}^{\mathrm{enr}})$ **constitutes a new finite element?**

The Crouzeix–Raviart finite element is locally defined as $\left(T, \mathbb{P}_1(T), \Sigma_T^{\mathsf{CR}}\right)$, where

$$\mathbb{P}_1(T) := \mathsf{span}\left\{\lambda_1, \lambda_2, \lambda_3\right\}, \qquad \Sigma_T^{\mathsf{CR}} := \left\{\mathcal{I}_j^{\mathsf{CR}}\left(f\right) := \frac{1}{|\Gamma_j|}\int_{\Gamma_j} f\left(s\right)\,ds\,:\,j=1,2,3\right\},$$

with the convention that

$$\boldsymbol{v}_4 := \boldsymbol{v}_1, \quad \boldsymbol{v}_5 := \boldsymbol{v}_2, \quad \lambda_4 := \lambda_1, \quad \lambda_5 := \lambda_2.$$

Quadratic Polynomial Enrichments: By incorporating quadratic polynomial functions into the Crouzeix–Raviart element, we achieve a more accurate representation of the solution, particularly in regions with steep gradients or singularities. This enrichment is defined by adding functions from $\mathbb{P}_2(T)$, the space of quadratic polynomials, to the original space $\mathbb{P}_1(T)$. The resulting finite element is capable of capturing more complex behaviors of the solution, thus providing improved accuracy in numerical simulations [1,2].

Cubic Polynomial Enrichments: Further enhancement can be achieved by introducing cubic polynomial functions, resulting in a finite element space that includes functions from $\mathbb{P}_3(T)$. This cubic enrichment allows for even higher fidelity in approximating the solution, particularly for problems with higher regularity or more intricate solution structures. The addition of these higher-order polynomials leads to a richer approximation space, enabling more precise and reliable numerical results [3].

The mathematical formulation of these enriched elements involves defining new sets of degrees of freedom and constructing the corresponding shape functions. These enrichments maintain the desirable properties of the Crouzeix–Raviart element, such as its ability to handle nonconforming approximations while significantly improving the accuracy of the solution.

Numerical Experiments: Extensive numerical experiments have been conducted to validate the effectiveness of these enrichments. The results demonstrate that both quadratic and cubic enrichments lead to substantial improvements in the accuracy of the numerical solution, particularly for problems involving complex geometries or singularities. These experiments also highlight the practical benefits of using enriched finite elements in engineering and scientific applications, where high precision is crucial.

References

[1] F. Dell'Accio, A. Guessab, and F. Nudo. "A new quadratic and cubic polynomial enrichment of the Crouzeix-Raviart finite element". ARXIV: 2403.05844. 2024.

[2] F. Nudo. "A general quadratic enrichment of the Crouzeix–Raviart finite element". ARXIV: 2403.11915. 2024.

[3] F. Nudo. "Two one-parameter families of nonconforming enrichments of the Crouzeix–Raviart finite element". In: *Applied Numerical Mathematics* (2024).

PINA: A Python Software for Scientific Machine Learning

Giuseppe Alessio D'Inverno

SISSA, International School for Advanced Studies, Trieste

Physics Informed Neural network for Advanced modeling (PINA) [3, 4] is an open-source Python library[1] capable of solving differential equations using artificial intelligence models. It is built on top of `PyTorch` with `PyTorchLightning` [5] as backend and enables users to define their own problems and create models to easily compute differential equation solutions using Physics-based Neural Networks and Neural Operators (NOs). The modular structure of `PINA` allows it to be tailored to specific user needs, providing the freedom to choose the most suitable learning techniques for their specific problem domain. Additionally, by exploiting the capabilities of the `Lightning` package, `PINA` can adapt to various hardware setups, including GPUs and TPUs. This adaptability makes `PINA` an excellent choice for implementing these methodologies in production and industrial pipelines, where computational efficiency and scalability are crucial.

The pipeline to solve differential equations with `PINA` follows five main steps (also depicted in Figure 47.1):

Problem definition is formulated by constructing a class inheriting from one or more problem classes, depending on the nature of the problem treated. Currently, available implemented classes are `AbstractProblem`, `SpatialProblem`, `TimeDependentProblem`, `ParametricProblem`, and `InverseProblem`. Here geometries and conditions (*i.e.*, equations and constraints) are defined.

Data generation which could be observations obtained by numerical solver solutions for supervised learning (*e.g.* in NOs) or collocation points sampled inside the domain where the residual of the differential equation must be evaluated (*e.g.* in Physics Informed Neural Networks, or PINNs).

Model choice across many options such as standard multilayer perceptrons (MLPs), skip connection MLPs [11] (m-MLPs), hard constraint MLPs [7] (hard-MLPs), or Deep Operator Networks [6] (DeepONets) to cite a few.

Solver selection where solvers are Python objects which define the optimization strategy for the model. In `PINA`, the solver is constructed by inheriting from the abstract class `SolverInterface`, which wraps Lightning Modules. Available solvers include

---

[1] `https://github.com/mathLab/PINA`
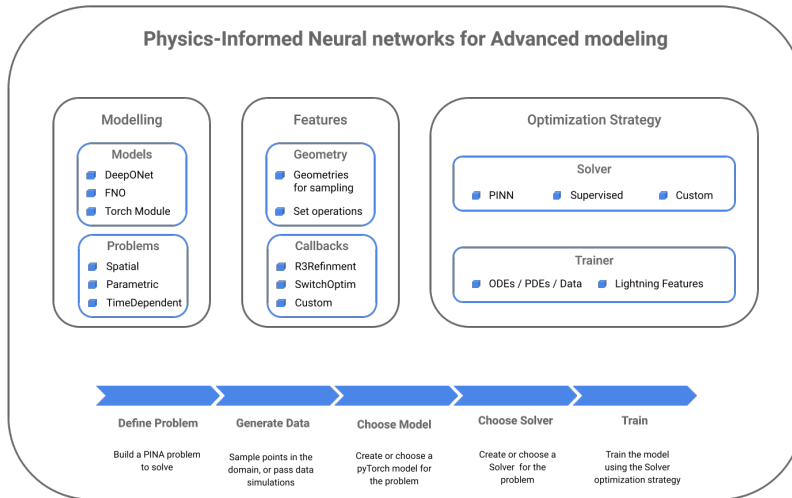
Figure 47.1: `PINA` package workflow. Starting from the problem definition, a specific model is passed to the solver, which defines, together with the trainer, the optimization strategy of the model.

physics-informed solvers (`PINN` [9], `SAPINN` [8], `CausalPINN` [10], `RBAPINN` [1]), supervised learning solvers (`SupervisedSolver`, `ReducedOrderModellingSolver`), particularly crafted for data-driven problems and NO approaches, and an adversarial solver (`GAROM` [2]).

Training is done using the `Trainer` class, which wraps the Lightning Trainer class. In the `Trainer` class, the user must pass a `SolverInterface` object in addition to all the available arguments of the Lightning Trainer. This strategy allows the user maximal training flexibility by exploiting fully `PytorchLightning` capabilities, *e.g.* low precision training, gradient accumulation, multiple GPU training, and different hardware training.

References

[1]   S. J. Anagnostopoulos, J. D. Toscano, N. Stergiopulos, and G. E. Karniadakis. "Residual-based attention in physics-informed neural networks". In: *Computer Methods in Applied Mechanics and Engineering* 421 (2024), p. 116805.

[2]   D. Coscia, N. Demo, and G. Rozza. "Generative adversarial reduced order modelling". In: *Scientific Reports* 14.1 (2024), p. 3826.
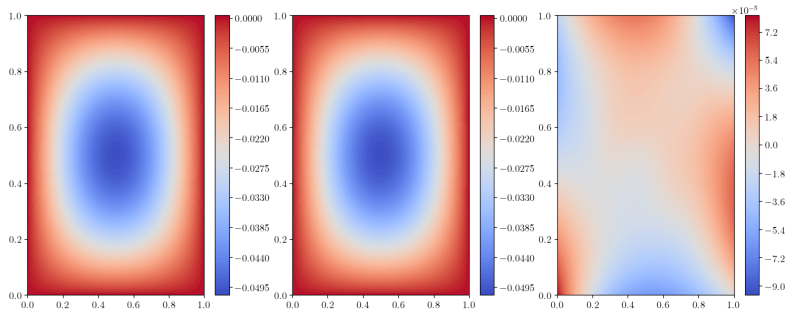
Figure 47.2: Example of visualization API for the Poisson problem in `PINA`. *Left*: `PINA` solution, *center*: real solution, *right*: absolute value difference of real and predicted solution.

[3] D. Coscia, N. Demo, and G. Rozza. "PINA: a PyTorch Framework for Solving Differential Equations by Deep Learning for Research and Production Environments". In: *ICLR 2024 Workshop on AI4DifferentialEquations In Science*.

[4] D. Coscia, A. Ivagnes, N. Demo, and G. Rozza. "Physics-informed neural networks for advanced modeling". In: *Journal of Open Source Software* 8.87 (2023), p. 5352.

[5] W. Falcon and The PyTorch Lightning team. *PyTorch Lightning*. Version 1.4. Mar. 2019. DOI: 10.5281/zenodo.3828935. URL: https://github.com/Lightning-AI/lightning.

[6] L. Lu, P. Jin, G. Pang, Z. Zhang, and G. E. Karniadakis. "Learning nonlinear operators via DeepONet based on the universal approximation theorem of operators". In: *Nature machine intelligence* 3.3 (2021), pp. 218–229.

[7] L. Lu, R. Pestourie, W. Yao, Z. Wang, F. Verdugo, and S. G. Johnson. "Physics-informed neural networks with hard constraints for inverse design". In: *SIAM Journal on Scientific Computing* 43.6 (2021), B1105–B1132.

[8] L. D. McClenny and U. M. Braga-Neto. "Self-adaptive physics-informed neural networks". In: *Journal of Computational Physics* 474 (2023), p. 111722.

[9] M. Raissi, P. Perdikaris, and G. Karniadakis. "Physics-informed neural networks: A deep learning framework for solving forward and inverse problems involving nonlinear partial differential equations". In: *Journal of Computational Physics* 378 (2019), pp. 686–707. ISSN: 0021-9991. DOI: 10.1016/j.jcp.2018.10.045.

[10] S. Wang, S. Sankaran, and P. Perdikaris. "Respecting causality for training physics-informed neural networks". In: *Computer Methods in Applied Mechanics and Engineering* 421 (2024), p. 116813.

[11] S. Wang, Y. Teng, and P. Perdikaris. "Understanding and mitigating gradient flow pathologies in physics-informed neural networks". In: *SIAM Journal on Scientific Computing* 43.5 (2021), A3055–A3081.

Mini-Symposium
Computational Techniques in Agriculture, Epidemiology, and Plant Pathology

Preface to the Symposium

Vincenzo Schiano di Cola[a], Fabio Vito Difonzo[b], and Giovanni Pagano[c], *Organizers*
[a] Istituto di Ricerca sulle Acque (IRSA), CNR, Bari, Italy
[b] Istituto per la Applicazioni del Calcolo "M. Picone" (IAC), CNR, Rome, Italy
[c] Università degli Studi di Salerno

This mini-symposium investigates the interaction of computational approaches, such as deep learning, artificial intelligence, parallel computing and quantum computing, with applications in agriculture, epidemiology, and plant pathology. The presentations will focus on research on: deep learning models for molecular diagnostics of plant pathogens; AI-driven interpretation of volatile organic molecules for plant communication; stable numerical methods for the efficient solution of models that give rise to Turing patterns; standard and non-standard numerical methods in epidemic modeling. The symposium will also discuss the use of quantum computers in agricultural research, as well as the employment of epidemiological models to forecast the spread of information on social media. Furthermore, theoretical aspects concerning algorithms used in the context of neural networks will be addressed. This event allows researchers to showcase their cutting-edge discoveries and discuss collaboration prospects to improve agricultural and epidemiological practices.

List of the Speakers

- Elisa Troiano, PhD student, Università degli Studi di Napoli Federico II

- Mariachiara Cangemi, PhD student, Università degli Studi di Napoli Federico II

- Raffaele Cecere, Post Doc ICAR–CNR, Napoli

- Claudia Panico, PhD student, Università degli Studi di Napoli Federico II

- Angela Monti, Post Doc, IAC–CNR, Bari

- Samira Iscaro, PhD student, Università degli Studi di Salerno

- Stefano Di Giovacchino, Post Doc, Università degli Studi dell'Aquila

- Fabio Cassini, Post Doc, Università degli studi di Verona

- Pasquale De Luca, PhD student, Università degli Studi di Napoli Parthenope

- Vincenzo Vocca, Postgraduate fellow, Università degli Studi di Napoli Federico II

A non-standard numerical method for an integral behavioural epidemic model

Claudia Panico

E-mail address: claudia.panico2@unina.it

Department of Mathematics and Applications, University of Naples Federico II, Naples, Italy

The spread of infectious diseases is commonly known to trigger changes in human behaviour, which can subsequently affect epidemic outcomes [3]. Our study introduces an integral epidemic model that links the contagiousness of a disease to the duration of infection, incorporating the impact of human behaviour on the progression of the disease [1, 2].

We examine the basic properties of the model solution, investigate the existence and stability of equilibria, and apply a non-standard discretization technique to numerically solve the model [4]. This technique, based on finite differences, preserves the key features of the original system, such as positivity, boundedness, and stability of equilibria. Through a comparative analysis with the continuous model, we highlight the efficacy of our numerical approach, particularly in long-time simulations. Our research underlines the crucial role of integrating behavioural dynamics into integral epidemic models, offering new insights into disease transmission and potential strategies for intervention. At the same time, it emphasizes the importance of having numerical methods that are efficient and qualitatively consistent with the model.

References

[1] B. Buonomo, E. Messina, C. Panico, and A. Vecchio. "An integral renewal equation approach to behavioural epidemic models with information index". ARXIV: 2402.08618. 2024.

[2] B. Buonomo, E. Messina, C. Panico, and A. Vecchio. "A stable Numerical method for integral epidemic models with behavioural changes in contact patterns". In: Submitted (2024).

[3] P. Manfredi and A. d'Onofrio, eds. *Modeling the interplay between human behavior and the spread of infectious diseases*. Springer, New York, 2013, pp. xix+329. ISBN: 978-1-4614-5473-1. DOI: 10.1007/978-1-4614-5474-8.

[4] E. Messina, M. Pezzella, and A. Vecchio. "A non-standard numerical scheme for an age-of-infection epidemic model". In: *Journal of Computational Dynamics* 9.2 (2022), pp. 239–252. ISSN: 2158-2491. DOI: 10.3934/jcd.2021029.

Deep Learning Models for Accurate Data Interpretation in Molecular Diagnostics of Plant Viruses

Elisa Troiano[a,b,c]
[a] Department of Biology, University of Naples Federico II, Napoli, Italy
[b] Institute for Sustainable Plant Protection (IPSP), CNR, Napoli, Italy
[c] Enbiotech s.r.l.
E-mail address: elisa.troiano@unina.it

Early detection of viral diseases is crucial for preventing the spread of pathogens that can have devastating impacts on agriculture and the environment. In particular, plant viruses (phytoviruses) represent a significant threat to plant health. Moreover, in mixed infection they can act synergically exacerbating the overall damage compared to those caused by single infections [7]. Factors such as climate change and global trade contribute to the spread and increase the incidence of phytoviruses in crop productions. Thus, there is the need to develop rapid and sensitive diagnostic methods as support for actions aimed at containing of their spread. The qPCR (quantitative Polymerase Chain Reaction) and the LAMP (Loop-mediated isothermal AMPlification) diagnostic methods are the most widely used molecular techniques for pathogen diagnosis because of their high sensitivity and specificity [6]. In the qPCR, detection of the specific target sequence of the pathogen in the sample (e.g. symptomatic leaves) takes place through the emission of fluorescence, using specific probes marked by a fluorophore or by DNA intercaling agents, which release fluorescence signals in real time during the detection [4]. Real time detection through fluorescence can also occur in the LAMP method, in addition to: measuring the samples turbidity, caused by the formation of aggregate during the reaction; observing samples color changes using chemical indicators; checking for amplification of target sequence by gel electrophoresis; adopting microfluidic chips or biosensors [2]. However, using these techniques for simultaneous multiplex detection of different pathogens in the same sample, involves several challenges, such as data interpretation from signals emitted by different fluorophores (each related to a specific pathogen) and the increased likelihood of obtaining false positives and false negatives. The COVID-19 pandemic has driven the widespread development and adoption of sensitive molecular techniques and stimulated the production of numerous scientific studies focused on improving these methods [3]. Several studies have explored the integration of deep learning models with molecular assays to enhance data interpretation and test accuracy. An example is the use of the qPCRdeepNet model, developed to analyze fluorescent readings obtained during the qPCR, showing promising results in detecting SARS-CoV-2 with commercial kits [1]. In this work we propose a similar approach for the molecular multiple detection of pathogens in the same plant sample using the artificial intelligence. In particular, the work aims to overcome the critical limitation of data interpretation by im-

plementing an advanced data analysis system based on Convolutional Neural Networks (CNNs). CNNs are inspired by the structure and function of the human visual system, particularly to the mechanism through which the human brain processes images [5]. For this reason, they are especially effective for processing grid-structured data, such as images resulting from qPCR and LAMP assays, that typically display amplification curves in which the fluorescence signal emitted during the reaction is correlated with the number of amplification cycles. The CNNs will be trained using a large number of images, in order to develop models able to interpret results in real time. This approach can improve the accuracy of pathogen detection and also simplifies data interpretation. The latter aspect is especially crucial in the case of LAMP, which was ideally conceived as a simple and accessible technique even for operators with a minimal level of training.

References

[1] D. J. Alouani, R. R. P. Rajapaksha, M. Jani, D. D. Rhoads, and N. Sadri. "Specificity of SARS-CoV-2 Real-Time PCR Improved by Deep Learning Analysis". In: *Journal of clinical microbiology* 59.6 (June 2021), pp. 1–4. ISSN: 0095-1137. DOI: 10.1128/JCM.0 2959–20.

[2] N. Garg, F. J. Ahmad, and S. Kar. "Recent advances in loop-mediated isothermal amplification (LAMP) for rapid and efficient detection of pathogens". In: *Current Research in Microbial Sciences* 3.100120 (Feb. 2022), pp. 1–7. ISSN: 2666-5174. DOI: 10.1016/j.crmicr.2022.100120.

[3] S. Hakimi. "Factors Associated with False Negative and False Positive RT-PCR Test Results for COVID-19 Detection". In: *Journal of Iranian Medical Council* 4.2 (Feb. 2021), pp. 102–110. ISSN: 2645-338X. DOI: 10.18502/jimc.v4i2.6465.

[4] P. Mara. "Duplex Real Time RT-PCR per la determinazione del Virus dell'Epatite A in campioni di molluschi eduli lamellibranchi con l'utilizzo del Calicivirus Felino come controllo di processo". PhD thesis. UNIVERSITÀ DEGLI STUDI DI ROMA TOR VERGATA, 2009.

[5] K. O'Shea and R. Nash. *An Introduction to Convolutional Neural Networks*. ARXIV: 1511.08458. 2015.

[6] G. Parrella, T. Elbeaino, and P. L. Guy. "Editorial: Emerging and reemerging plant viruses in a context of global change". In: *Frontiers in Plant Science* 13 (Dec. 2022), pp. 1–4. ISSN: 1664-462X. DOI: 10.3389/fpls.2022.1108211.

[7] P. Singhal, S. U. Nabi, M. K. Yadav, and A. Dubey. "Mixed infection of plant viruses: diagnostics, interactions and impact on host". In: *Journal of Plant Diseases and Protection* 128.2 (Sept. 2021), pp. 353–368. ISSN: 1861-3837. DOI: 10.1007/s41348–020 –00384–0.

Directional split exponential integrators, with applications to Turing patterns

Fabio Cassini

Department of Computer Science, University of Verona, Italy

Many significant physical phenomena can be effectively modeled by stiff systems of Advection–Diffusion–Reaction (ADR) equations. More in detail, we are interested in the numerical integration of two-component systems of ADR equations in the form

$$\begin{cases} \partial_t u(t, \boldsymbol{x}) = \mathcal{K}^u u(t, \boldsymbol{x}) + g^u(u(t, \boldsymbol{x}), v(t, \boldsymbol{x})), \\ \partial_t v(t, \boldsymbol{x}) = \mathcal{K}^v v(t, \boldsymbol{x}) + g^v(u(t, \boldsymbol{x}), v(t, \boldsymbol{x})) \end{cases} \tag{51.1}$$

that lead to the so-called Turing patterns [7]. Here $u, v \colon [0, T] \times \Omega \subset \mathbb{R} \times \mathbb{R}^d \to \mathbb{R}$ represent the unknowns, $\mathcal{K}^u, \mathcal{K}^v$ are linear advection–diffusion operators, while g^u, g^v are the nonlinear reaction terms. We assume that the spatial domain Ω is the Cartesian product of one-dimensional intervals, that is $\Omega = [a_1, b_1] \times \cdots \times [a_d, b_d]$. The system is finally completed with appropriate initial conditions and with homogeneous Neumann boundary conditions. We introduce a spatial grid of size $n_1 \times \cdots \times n_d$ and apply the method of lines to model (51.1) to get a system with *Kronecker sum* structure. Infact, assume we obtain a system of stiff ordinary differential equations such as

$$\begin{cases} \boldsymbol{u}'(t) = K^{\boldsymbol{u}} \boldsymbol{u}(t) + \boldsymbol{g}^{\boldsymbol{u}}(\boldsymbol{u}(t), \boldsymbol{v}(t)), \\ \boldsymbol{v}'(t) = K^{\boldsymbol{v}} \boldsymbol{v}(t) + \boldsymbol{g}^{\boldsymbol{v}}(\boldsymbol{u}(t), \boldsymbol{v}(t)), \end{cases} \tag{51.2}$$

where $K^{\boldsymbol{u}}$ and $K^{\boldsymbol{v}}$ are matrices of size $N \times N$, with $N = n_1 \cdots n_d$, that discretize the linear operators $\mathcal{K}^u$ and $\mathcal{K}^v$, respectively. The matrices $K^{\boldsymbol{u}}$ and $K^{\boldsymbol{v}}$ are Kronecker sums. By definition, a matrix $K \in \mathbb{C}^{N \times N}$ is a Kronecker sum if it can be decomposed as

$$K = A_d \oplus A_{d-1} \oplus \cdots \oplus A_1 = \sum_{\mu=1}^{d} A_{\otimes \mu}, \quad A_{\otimes \mu} = I_d \otimes \cdots \otimes I_{\mu+1} \otimes A_\mu \otimes I_{\mu-1} \otimes \cdots \otimes I_1.$$

In our context I_μ and A_μ, for $\mu = 1, \ldots, d$, are matrices of *small* size $n_\mu \times n_\mu$ and represent the identity and a one-dimensional linear differential operator along the direction μ, respectively. The symbol $\otimes$ denotes the standard Kronecker product between matrices.

Finding efficient numerical integrators for system (51.2) is of paramount importance to have fast and reliable simulations at disposal. In this context, time marching schemes of exponential type [5] have received much attention in recent years thanks to their excellent performance in the stiff regime [1, 2, 3, 4]. In contrast to implicit methods, these

schemes do not need the solution of (non)linear systems but rather the computation of the φ_ℓ functions, i.e., special entire functions linked to the exponential function and defined for a generic matrix X by $\varphi_\ell(X) = \sum_{k=0}^{\infty} \frac{X^k}{(k+\ell)!}$. Here, we present the so-called directional split exponential methods and show how to compute the relevant matrix φ_ℓ functions when the problem has a d-dimensional Kronecker sum structure. The technique is based on a suitable directional splitting, which allows for an efficient tensor-oriented evaluation through μ-mode products and Tucker operators (realized in practice by the high performance level 3 BLAS). In particular, we exploit the approximation

$$\varphi_\ell(\tau K)\boldsymbol{w} = \ell!^{d-1}\varphi_\ell(\tau A_{\otimes 1})\cdots\varphi_\ell(\tau A_{\otimes d})\boldsymbol{w} + \mathcal{O}(\tau^2), \quad \ell > 0, \qquad (51.3\text{a})$$

where τ is the time step size. This approximation can be efficiently computed in tensor form as

$$\ell!^{d-1}\varphi_\ell(\tau A_{\otimes 1})\cdots\varphi_\ell(\tau A_{\otimes d})\boldsymbol{w} = \ell!^{d-1}\mathsf{vec}\left(\boldsymbol{W}\underset{\mu=1}{\overset{d}{\bigtimes}}\varphi_\ell(\tau A_\mu)\right) \qquad (51.3\text{b})$$

thanks to the equivalence

$$(L_d \otimes L_{d-1} \otimes \cdots \otimes L_1)\boldsymbol{v} = \mathsf{vec}\left(\boldsymbol{V} \times_1 L_1 \times_2 \cdots \times_d L_d\right) = \mathsf{vec}\left(\boldsymbol{V}\underset{\mu=1}{\overset{d}{\bigtimes}}L_\mu\right).$$

Here, $\boldsymbol{V}$ is an order-d tensor of size $n_1 \times \cdots \times n_d$ such that $\boldsymbol{v} = \mathsf{vec}(\boldsymbol{V})$, where we denoted with vec the operator that stacks by columns the input tensor, and $L_\mu \in \mathbb{C}^{n_\mu \times n_\mu}$ is a generic matrix. Also, $\times_\mu$ denotes the μ-*mode product* [6], which multiplies the matrix L_μ onto the μ-fibers (i.e., the generalization to tensors of matrix columns and rows) of the tensor $\boldsymbol{V}$. Notice that formula (51.3) gives an approximation of the φ_ℓ functions compatible with second order integrators [1, 2], but extensions to higher order approximations can be constructed similarly. Also, the technique scales very favourably on modern computer hardware such as Graphic Processing Units (GPUs), since it is heavily based on level 3 BLAS [3].

The overall approach is shown to be numerically superior compared to state-of-the-art techniques for the time integration of semidiscretized systems of ADR equations. We show here in Figures 51.1 and 51.2 the results of ETD2RKds (one of the proposed directional split exponential integrators) on a 3D advective Schnakenberg model that leads to a spot-like pattern.

This is a work based on the published manuscripts [1, 2] and preprint [3].

References

[1]   M. Caliari and F. Cassini. "Direction splitting of φ-functions in exponential integrators for d-dimensional problems in Kronecker form". In: *J. Approx. Softw.* 1.1 (2023).

[2]   M. Caliari and F. Cassini. "A second order directional split exponential integrator for systems of advection–diffusion–reaction equations". In: *J. Comput. Phys.* 498 (2024), p. 112640. DOI: 10.1016/j.jcp.2023.112640.
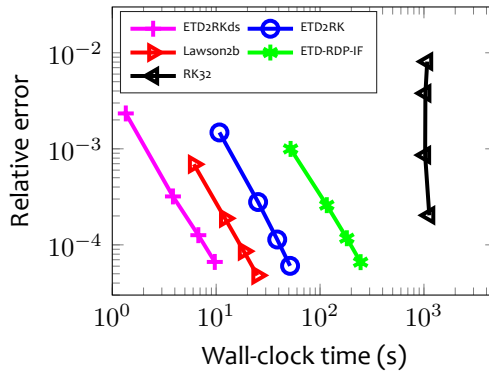
Figure 51.1: 3D advective Schnakenberg model with $N = 80^3$ discretization points.
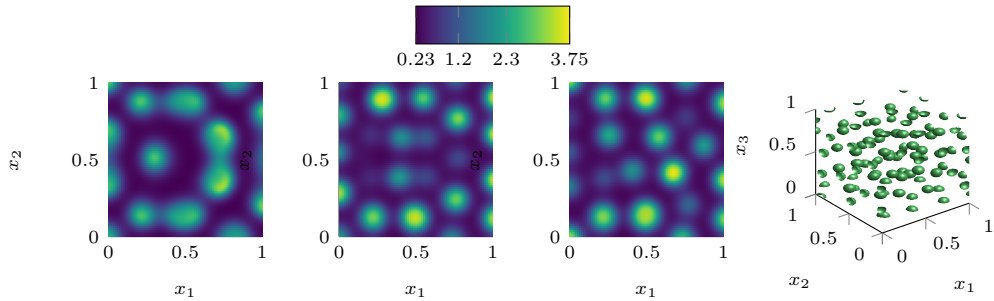
Figure 51.2: Spot-like pattern (u component) for 3D advective Schnakenberg model and ETD2RKds at final times $T = 0.8, 8$, and 80.

[3]   F. Cassini. "Efficient third order tensor-oriented directional splitting for exponential integrators". ARXIV: 2310.07551. 2024.

[4]   M. C. D'Autilia, I. Sgura, and V. Simoncini. "Matrix-oriented discretization methods for reaction–diffusion PDEs: Comparisons and applications". In: *Comput. Math. with Appl.* 79.7 (2020), pp. 2067–2085. DOI: 10.1016/j.camwa.2019.10.020.

[5]   M. Hochbruck and A. Ostermann. "Exponential integrators". In: *Acta Numer.* 19 (2010), pp. 209–286. DOI: 10.1017/S0962492910000048.

[6]   T. G. Kolda and B. W. Bader. "Tensor decompositions and applications". In: *SIAM Rev.* 51.3 (2009), pp. 455–500. DOI: 10.1137/07070111X.

[7]   H. Malchow, S. V. Petrovskii, and E. Venturino. *Spatiotemporal Patterns in Ecology and Epidemiology: Theory, Models, and Simulation*. first. CRC Mathematical Biology Series. Chapman & Hall, 2008.

Exploratory Data Analysis and Supervised Learning in Plant Phenotyping Studies

Mariachiara Cangemi[a,b]
[a] Department of Biology, University of Naples Federico II, Napoli, Italy
[b] Institute for Sustainable Plant Protection (IPSP), CNR, Napoli, Italy
E-mail address: mariachiara.cangemi@unina.it

Plant phenotyping, which studies plants' morpho-physiological traits to understand genotype-environment interactions, relies heavily on high-throughput image analysis. This analysis measures parameters such as biomass, leaf area, root growth, and stress response using techniques like visible light imaging, fluorescence imaging, and infrared thermal imaging. These images, processed with computer vision and machine learning, enhance accuracy and speed analyses, aiding breeding programs and environmental management [3]. In this presentation, I will investigate plant-plant communication via volatile organic compounds (VOCs), which affect genetic regulation, metabolism, and stress responses in plants through "priming" [2]. The aim is to identify phenotypic markers associated with VOC-sensing in plants. This presentation will explore the application of exploratory data analysis and supervised learning techniques in the study of plant phenotyping traits with a specific focus on i) genetic diversity (wild type vs mutant tomato plants); ii) plant-plant interactions (primed vs non-primed plants using volatiles emitted by other, stressed, plants); iii) plant stress response (using drought stress and comparing droughted plants with controls). The dataset comprises phenotypic characteristics of both wildtype and mutated tomato plants under water stress. The study underscores the value of advanced statistical and machine learning techniques in improving the precision and effectiveness of phenotypic analysis in plant sciences. It highlights the use of both unsupervised and supervised learning methods to analyze complex biological data: K-means clustering and PCA facilitate initial data exploration and dimensionality reduction, while the Naive-Bayes Classifier and Feature Permutation Importance [1] offer deeper insights into feature significance and model performance.

References

[1]   A. Altmann, L. Toloşi, O. Sander, and T. Lengauer. "Permutation importance: a corrected feature importance measure". In: *Bioinformatics* 26.10 (Apr. 2010), pp. 1340–1347. ISSN: 1367-4803. DOI: 10.1093/bioinformatics/btq134.

[2]   J. Midzi, D. W. Jeffery, U. Baumann, S. Rogiers, S. D. Tyerman, and V. Pagay. "Stress-Induced Volatile Emissions and Signalling in Inter-Plant Communication". en. In: *Plants* 11.19 (Jan. 2022), p. 2566. ISSN: 2223-7747. DOI: 10.3390/plants11192566.

[3] R. Pieruschka and U. Schurr. "Plant Phenotyping: Past, Present, and Future". In: *Plant Phenomics* 2019 (Mar. 2019), p. 7507131. DOI: 10.34133/2019/7507131.

Towards a Numerical Method for Angiogenesis Simulations

Pasquale De Luca
Parthenope University of Naples.
E-mail address: pasquale.deluca@studenti.uniparthenope.it.

Angiogenesis, the formation of new blood vessels from pre-existing vasculature, is a critical process in both physiological and pathological contexts, particularly in cancer development. Figure 53.1 shows an example of new blood vessel formation. The new vascular network increase the number of tumour cells from pre-existing one.
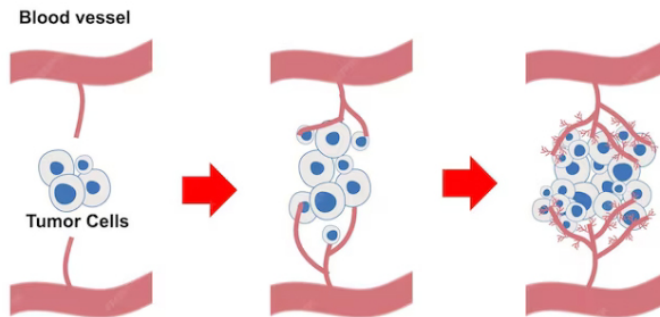
Figure 53.1: Dynamic of tumour angiogenesis evolution.

This work presents a comprehensive numerical approach for modelling tumour-induced angiogenesis, focusing on the complex interactions between endothelial cells, tumour angiogenic factors, matrix metalloproteinases, and angiogenic inhibitors. We introduce a system of partial differential equations (PDEs) that captures the spatio-temporal dynamics of angiogenesis. The model is based on the work of [3], but extends it by incorporating more detailed biological mechanisms and improved numerical methods. The starting point of our model is represented by the following system of PDEs:

$$\frac{\partial C}{\partial t} = d_C \frac{\partial^2 C}{\partial x^2} + \frac{\partial}{\partial x}\left(f_I \frac{\partial I}{\partial x}\right) - \frac{\partial}{\partial x}\left(f_F \frac{\partial F}{\partial x}\right) - \frac{\partial}{\partial x}\left(f_T \frac{\partial T}{\partial x}\right) + k_1 C(1 - C)$$

$$\frac{\partial P}{\partial t} = d_P \frac{\partial^2 P}{\partial x^2} - k_3 PI + k_4 TC + k_5 T - k_6 P$$

$$\frac{\partial I}{\partial t} = d_I \frac{\partial^2 I}{\partial x^2} - k_3 PI \tag{53.1}$$

$$\frac{\partial F}{\partial t} = -k_2 PF \qquad (x, t) \in [0, L_f] \times [0, T_f],$$

where C, P, I, and F represent the concentrations of endothelial cells, proteases, inhibitors, and extracellular matrix, respectively. The function related to tumor growing factor T is defined as: $\exp(\epsilon^{-1}(L_f - x)^2)$, where ϵ is a scaling factor. The terms f_I, f_F, and f_T model the chemotactic and haptotactic responses of endothelial cells. The system in (53.1) is subject to no-flux boundary conditions (Neumann). The proposed numerical approach involves a spatial discretization using the method of lines, transforming the PDE system into a semi-discrete problem. We then apply a Forward Euler method for time integration, resulting in the following discrete scheme:

$$U^{n+1} = U^n + \tau[AU^n + N(U^n)]$$

where $U = [C, P, I, F]^T$, A is a block matrix representing linear terms, $N(U)$ encapsulates the nonlinear interactions and τ is the time step.

To validate our method, we present a convergence analysis of our numerical scheme. Moreover, we present a stability study for validating the proposed numerical schema. A comprehensive analysis helps us to discuss on method's properties and issues. Future work will focus on extending the model to higher spatial dimensions, incorporating more advanced time integration schemes such as implicit-explicit (IMEX) methods [1], and including additional biological factors such as oxygen concentration and specific growth factors like VEGF [2].

References

[1] U. M. Ascher, S. J. Ruuth, and R. J. Spiteri. "Implicit-explicit Runge-Kutta methods for time-dependent partial differential equations". In: *Applied Numerical Mathematics* 25.2-3 (1997), pp. 151–167.

[2] P. Carmeliet and R. K. Jain. "Molecular mechanisms and clinical applications of angiogenesis". In: *Nature* 473.7347 (2011), pp. 298–307.

[3] P. G. Kevrekidis, N. Whitaker, and D. J. Good. "Towards a reduced model for angiogenesis: a hybrid approach". In: *Mathematical and computer modelling* 41.8-9 (2005), pp. 987–996.

Leveraging Quantum Technologies and Artificial Intelligence for Bee Behavior Studies

Raffaele Cecere

Institute for High Performance Computing and Networking of the National Research Council of Italy, Naples, Italy. E-mail address: raffaele.cecere@icar.cnr.it

World honey production stands at about 1.831 million tons, trending upward for the third consecutive year (+5,6% compared to 2021). China, India and Argentina are the top exporters in the world, Ukraine, Spain and Belgium are the top in Europe. As for italy, the number of beekeepers producing honey for marketing has grown by 8% between 2019 and 2023 [8].

As in other contexts, honey producers must incur costs. In particular, expenses incurred in the purchase of drugs and nutrition products are a major cost item [4]. In particular, climatic instability and desertification in some areas have forced many beekeepers to resort to rescue feeding, an extremely expensive operation that exacerbates production costs, and is more significant in terms of its weight on total costs as the economic size of the farm increases [4]. Informamiele's 2023 Honey Cost Report analyzes honey market trends in production costs, market prices, and economic factors. Beekeeping's economic viability, market demand, and environmental effects on honey production are covered in this detailed report. By highlighting the honey industry's challenges and opportunities, the findings benefit beekeepers, market analysts, and policymakers. This analysis is crucial for market understanding and strategic decision-making amid changing economic and environmental conditions [4].

Moreover, in order to survive in a competitive business environment, beekeeping producers must direct their resources towards innovative solutions, which can include honey quality assurance programmes and further product development, as well as creation of value-added honey products that is translated in good business performance [5]. In addition, the use of innovative techniques for predicting hive production performance is, therefore, a solution for predicting variations in honey production in hives. We used both random forest (RF) and extreme gradient boosting (XGB) algorithms. In particular, the study shows that rainfall, maximum and average temperature are the variables that most influence hive performance. [3].

Bee colonies are vital to agriculture and the environment. Beekeeping promotes rural development and plant reproduction through pollination. The European Commission prioritizes research programs, investments in tangible and intangible assets, and measures to combat hive invaders and diseases, prevent damage from adverse weather, promote adapted management practices, preserve and repopulate hives on EU territory, and support laboratories. The European Commission's honey sector overview outlines the reg-

ulatory and market landscape for honey production in the EU. It emphasizes the importance of quality control measures, such as stringent labeling requirements and origin tracing, to maintain product integrity. The resource also highlights the economic significance of honey and its role in pollination, which is vital for biodiversity. This information is crucial for researchers and industry stakeholders to understand the regulatory environment and economic factors impacting honey production in the EU [6].

The intersection of quantum technologies and artificial intelligence provides novel approaches to studying bee behavior, particularly through the application of quantum machine learning (QML) and artificial bee colony (ABC) algorithms. Quantum machine learning (QML) techniques employ quantum algorithms to solve complex problems more efficiently than traditional methods. These algorithms can analyze large datasets, potentially identifying patterns in bee behavior that traditional systems cannot detect [2]. The Artificial Bee Colony (ABC) algorithm emulates the foraging behavior of bees in order to optimize intricate problems. This method is effective in optimizing numerical test functions and its potential for analyzing bee behavior patterns in different scenarios. Incorporating quantum computing principles into ABC algorithms improves their performance, making them a valuable tool for studying and utilizing data in bee behavior research [9]. Machine learning algorithms can predict bee behavior in response to environmental changes, which helps forecast the impacts of climate change and pesticides on bee populations [7]. Enhancements such as chaotic maps are incorporated into the ABC algorithm to improve convergence rates and prevent local minima. These modifications use chaotic number generators to introduce randomness and diversity in the search process, thus improving the algorithm's performance in solving global optimization problems [1].

Quantum machine learning (QML) integrates advanced mathematical methods and computational power to improve bee behavior research. Possible research directions and challenges are related to Quantum neural networks, Quantum data mining algorithms, and hybrid approaches. Quantum neural networks, including variational quantum circuits, can use superposition and entanglement to efficiently process complex datasets to predict bee behavior. This method can reveal complex bee activity patterns influenced by environmental changes. To improve scalability and efficiency, the *Barren plateaus* problem—where gradients diminish and training is difficult—must be addressed. Quantum data mining algorithms efficiently search large, complex datasets, optimizing data analysis tasks. This is essential for detecting subtle bee behavior dataset trends that traditional algorithms may miss. Quantum optimization methods like Quantum Approximate Optimization Algorithm (QAOA) can improve beekeeping resource allocation, reducing costs and improving hive management. Combining quantum and classical machine learning techniques, known as hybrid approaches, can address limitations in quantum hardware and enable practical, scalable applications. Quantum algorithms select features and preprocess data, then classical algorithms train models. Hybrid models are useful when full quantum solutions are impractical. This research shows how quantum technologies and AI can help us understand bee behavior and ecology. Quantum computing and overcoming technical obstacles could revolutionize environmental monitoring and sustainable agriculture.

References

[1]   B. Alatas. "Chaotic bee colony algorithms for global numerical optimization". In: *Expert Systems with Applications* 37.8 (Aug. 2010), pp. 5682–5687. ISSN: 0957-4174. DOI: 10.1016/j.eswa.2010.02.042.

[2]   U. Alvarez-Rodriguez, L. Lamata, P. Escandell-Montero, J. D. Martín-Guerrero, and E. Solano. "Supervised Quantum Learning without Measurements". en. In: *Scientific Reports* 7.1 (Oct. 2017), p. 13645. ISSN: 2045-2322. DOI: 10.1038/s41598-017-13378-0.

[3]   A. Brini, E. Giovannini, and E. Smaniotto. *A Machine Learning Approach to Forecasting Honey Production with Tree-Based Methods*. ARXIV: 2304.01215. Mar. 2023.

[4]   C. Cardillo, M. Verrascina, and A. Giampaolo. *Indagine statistica Honey cost - Report 2023*. Nov. 2023. ISBN: 9788833853055. DOI: 10.5281/zenodo.10041207.

[5]   M. Čavlin, N. Prdić, S. Ignjatijević, J. Vapa Tankosić, N. Lekić, and S. Kostić. "Research on the Determination of the Factors Affecting Business Performance in Beekeeping Production". en. In: *Agriculture* 13.3 (Mar. 2023), p. 686. ISSN: 2077-0472. DOI: 10.3390/agriculture13030686.

[6]   E. Commission. *Honey - European Commission*. en. Jan. 2024. URL: https://agriculture.ec.europa.eu/farming/animal-products/honey_en.

[7]   V. Dunjko and H. J. Briegel. "Machine learning & artificial intelligence in the quantum domain: a review of recent progress". en. In: *Reports on Progress in Physics* 81.7 (June 2018), p. 074001. ISSN: 0034-4885. DOI: 10.1088/1361-6633/aab406.

[8]   I. M. www.ismeamercati.it. *Bilancio Amaro per il Miele Italiano*. it. URL: https://www.ismeamercati.it/flex/cm/pages/ServeBLOB.php/L/IT/IDPagina/13172 (visited on 07/30/2024).

[9]   X. Yuan, P. Wang, Y. Yuan, Y. Huang, and X. Zhang. "A new quantum inspired chaotic artificial bee colony algorithm for optimal power flow problem". In: *Energy Conversion and Management* 100 (Aug. 2015), pp. 1–9. ISSN: 0196-8904. DOI: 10.1016/j.enconman.2015.04.051.

Mathematical modeling for the description of information diffusion on social media

Dajana Conte, Samira Iscaro*, **and Beatrice Paternoster**
Department of Mathematics, University of Salerno.
E-mail address: siscaro@unisa.it.

Information diffusion on social media is a complex phenomenon to be described and analyzed. Social media, in fact, are free and easy to use so that anyone can easily spread any kind of information. If on one hand this characteristic gives the opportunity to any user to be informed about what is happening in the world at any moment, on the other hand also some problems linked to the diffusion of fake information have been observed. For example it was proved, as reported in [5], that even the outcome of social or political events such as the American Presidential Elections of 2016 or the Brexit, was deeply influenced by the spread out of fake information.

So, it's fundamental not only to find a proper way to describe the phenomenon, but also a strategy to try to predict its evolution and the moment of its peak. However, trying to predict the moment of the maximum diffusion of a news can be advantageous not only to deal with the spread out of a fake news, in order to block it, but also in the case of a real one. Indeed, knowing in advance the moment of the maximum interest towards a certain topic or product can be advantageous for companies in order to do proper advertising campaigns.

Actually, there are several mathematical models to describe information spreading: among these, there is the use of epidemiological models. These mathematical models are in general based on a system of ordinary or partial differential equations and are used to describe the spread out of epidemics. However, a news spread on a social media can be compared to a virus: as a virus spreads in a population of human beings, likewise information spreads in a population composed of virtual individuals [2, 3, 4]. Certainly, these models can be used to obtain a rough description of the evolution of a news spread through time, but if used alone they're not sufficient to make predictions.

Therefore, the main aim of this talk will be to show that, in order to obtain the desired predictions, even an adequate dataset of real data and a proper parameter estimation strategy (as showed in [1]) are required, as confirmed by numerical experiments.

References

[1] M. Castiello, D. Conte, and S. Iscaro. "Using Epidemiological Models to Predict the Spread of Information on Twitter". In: *Algorithms* 16, 391 (2023).

[2] R. D'Ambrosio, G. Giordano, S. Mottola, and B. Paternoster. "Stiffness analysis to predict the spread out of fake information". In: *Future Internet* 13(9), 222 (2021).

[3] M. Maleki, E. Mead, M. Arani, and N. Agarwal. "Using an epidemiological model to study the spread of misinformation during the Black Lives Matter Movement". In: *arXiv:2103.12191* (2021).

[4] M. Muhlmeyer and S. Agarwal. "Information spread in a social media age". In: *Modelling and Control, CRC Press. Taylor and Frencis Group: Boca Raton, London, New York.* (2021).

[5] The, Ji, Village, and News. "Mathematical modelling of fake-news". In: URL: `www.haidongji.com/2018/07/23/mathematical-modeling-of-fake-news/`.

Qualitative analysis of stochastic coordinate descent method. The backward error analysis perspective

Stefano Di Giovacchino

Department of Information Engineering, Computer Science and Mathematics,
University of L'Aquila, Via Vetotio 67100, Loc. Coppito, L'Aquila, Italy.
E-mail address: stefano.digiovacchino@univaq.it

Optimization algorithms, such as *gradient methods,* are powerful tools for numerically solving optimization problems [5]. However, when the dimension of the problem increases, a stochastic approach to the optimization problem has been introduced to reduce computational costs [3]. For example, when the problem admits a vector field that can be decomposed in N components, a standard method is given by the *stochastic gradient method*, i.e., the computation of the gradient of only a random subset of components of the full vector field under investigation.

In several real-world situations, the dimension of the problem, i.e., the dimension of the full state vector, is huge and, hence, computing full gradients may become computationally impracticable. For this reason, alternative methods have been introduced, such as *stochastic coordinate descent methods* [4], that computes the derivatives only along a random subset of directions of the state variable of the problem.

In this talk, we study the qualitative behaviour of such algorithms by exploiting the *weak backward error analysis* techniques [1, 6], i.e., by employing *modified equations.* More in particular, the starting point of this analysis is the derivation of the *weak modified equations* [6] associated with the stochastic optimization method. We then present a mean-square stability analysis for such stochastic differential equations, allowing us to gain more insights into the qualitative convergent character of the aforementioned algorithms towards the unique minimizer of the object function. The theoretical details of this study have been presented in [2].

References

[1] A. Abdulle, D. Cohen, G. Vilmart, and K. Zygalakis. "High weak order methods for stochastic differential equations based on modified equations". In: *SIAM J. Sci. Comput.* 34(3) (2012), A1800–A1823.

[2] S. D. Giovacchino, D. Higham, and K. Zygalakis. "Backward error analysis and the qualitative behaviour of stochastic optimization algorithms: application to stochastic coordinate descent". In: *J. Comput. Dyn.* (2024). DOI: 10.3934/jcd.2024008.

[3] J. Latz. "Analysis of stochastic gradient descent in continuous time". In: *Statistics and Computing* 31.4 (2021), p. 39.

[4] D. Leventhal and A. S. Lewis. "Randomized methods for linear constraints: convergence rates and conditioning". In: *Mathematics of Operations Research* 35.3 (2010), pp. 641–654.

[5] Y. Nesterov. "Efficiency of coordinate descent methods on huge-scale optimization problems". In: *SIAM J. Optim.* 22 (2012), pp. 341–362.

[6] K. Zygalakis. "On the existence and applications of modified equations for stochastic differential equations". In: *SIAM J. Sci. Comput.* 33 (2011), pp. 102–130.

Advancing Soil Health: Enhanced Microbial Growth Predictions with PINNs

Vincenzo Vocca

Research fellow, E-mail address: vincenzo.vocca@unina.it

Department of Mathematics and Applications "Renato Caccioppoli", University of Naples Federico II

The intricate network of microorganisms within the soil, known as the soil microbiota, is essential for maintaining healthy ecosystems. These microscopic organisms influence critical processes such as nutrient cycling, decomposition and plant growth. Understanding and predicting the growth patterns of this diverse community is crucial for sustainable agriculture and environmental conservation [2].

This study explores the use of physics-informed neural networks (PINNs) [1] for predictive modelling of soil microbiota growth [3]. PINNs integrate the physical laws governing the system into the neural network architecture, allowing the model to learn from both the data and the underlying physical principles. This integration increases the generalisability and robustness of the model, allowing accurate predictions even under unknown conditions.

Our results show that PINNs can accurately predict the growth of different soil microbial communities under different environmental conditions. The structure of PINNs allows generalisation through training with different combinations of coefficients and scenarios, unlike classical numerical methods which lack adaptability. This makes PINNs a valuable tool for soil scientists and agricultural researchers.

This work paves the way for the development of advanced models for soil ecosystem management. By using PINNs, we can gain deeper insights into the complex interactions between soil microbes and their environment, ultimately promoting sustainable agricultural practices.

References

[1] S. Cuomo, V. S. Di Cola, F. Giampaolo, G. Rozza, M. Raissi, and F. Piccialli. "Scientific machine learning through physics–informed neural networks: Where we are and what's next". In: *Journal of Scientific Computing* 92.3 (2022), p. 88.

[2] P. Gosling, A. Hodge, G. Goodlass, and G. Bending. "Arbuscular mycorrhizal fungi and organic farming". In: *Agriculture, ecosystems & environment* 113.1-4 (2006), pp. 17–35.

[3]   M. M. Martignoni, J. Garnier, M. M. Hart, and R. C. Tyson. "Investigating the impact of the mycorrhizal inoculum on the resident fungal community and on plant growth". In: *Ecological Modelling* 438 (2020), p. 109321.

The role of environmental variability for the onset of on-off intermittency in host-parasitoid models

Angela Monti

Istituto per la Applicazioni del Calcolo "M. Picone" (IAC), CNR, Rome, Italy
E-mail address: angela.monti@cnr.it

The interactions between insect parasitoids and their hosts [5] are of particular interest for the use of parasitoids as biological control agents. Moreover, host–parasitoid interactions allow to investigate the emergence of a variety of interesting nonlinear dynamical behaviours. In particular, we are interested in the so-called on-off intermittency [3, 6, 10], that is an aperiodic switching between static behaviour and chaotic bursts of oscillation.

Bursting behaviours, due to the environmental variability, can have a remarkable influence on ecosystems, potentially causing abrupt population breakouts in host-parasitoid systems [8, 11]. The environmental variability [4] has an important influence on ecological systems, since it is able to change community compositions and the coexistence of species, but it can also modify the degree of competition between individuals.

To explore the role of environmental variability on the host–parasitoid interaction, we consider independently the effect of grazing-dependent habitat variation on the host density and the effect of environmental fluctuations on the host growth rate. From the theoretical point of view, we can consider a dynamical system where the control parameter changes either due to stochastic [7, 11] or deterministic drivers [2].

We perform an investigation into the parameters that induce on-off intermittency in an extended version of the discrete Beddington-Free-Lawton [1] host-parasitoid model.

Firstly, we assume that these parameters have stochastic (random) temporal variations. Therefore, we introduce random forcing factors that impact independently the grazing intensity and the growth rate of the host population. These stochastic elements are essential in influencing the onset of on-off intermittency.

Starting from the existing literature, we introduce the concept of reactivity of a fixed point within the statistical framework, highlighting its importance as a key prerequisite for the emergence of on-off intermittency. The analysis provides numerical evidence that equilibrium reactivity is a necessary condition for on-off intermittency to occur. This approach reveals a critical aspect of the dynamics that has been overlooked in previous studies.

Then, we show that a more thorough mathematical analysis of the dynamics underlying the onset of on-off intermittency in host-parasitoid systems can be achieved by considering environmental variability as a deterministic aperiodic driving process. To this aim, we allow some of the model parameters to vary in time according to an evolution law that can exhibit deterministic chaos. Therefore, we choose the logistic map as a deterministic chaotic driver for the Beddington-Free-Lawton system. This yelds to a 3D discrete nonlinear dynamical system, that allows us to better understand the emergence of on–off in-

termittent behavior that is related to the occurrence of a blowout bifurcation [9]. On–off intermittency typically emerges only above the blowout bifurcation threshold. However, We show that this phenomenon can also occur below the threshold. To explain this, we introduce the novel concept of long-term reactivity. As for the stochastic framework, also in the deterministic framework the reactivity is found to be a necessary condition for the onset of on–off intermittency.

References

[1] J. Beddington, C. Free, and J. Lawton. "Concepts of stability and resilience in predator-prey models". In: *The Journal of Animal Ecology* (1976), pp. 791–816.

[2] F. Diele, D. Lacitignola, and A. Monti. "On–Off Intermittency and Long-Term Reactivity in a Host–Parasitoid Model with a Deterministic Driver". In: *International Journal of Bifurcation and Chaos* 34 (2), 2450041 (2024).

[3] H. Fujisaka and T. Yamada. "A New Intermittency in Coupled Dynamical Systems". In: *Progress of Theoretical Physics* 74 (4) (1985), pp. 918–921.

[4] R. M. Germain, M. M. Mayfield, and B. Gilbert. "The 'filtering' metaphor revisited: Competition and environment jointly structure invasibility and coexistence". In: *Biology Letters* 14, 20180460 (2018).

[5] M. Hassell. "Host–parasitoid population dynamics". In: *Journal of Animal Ecology* 69 (2000), pp. 543–566.

[6] J. Heagy, N. Platt, and S. Hammel. "Characterization of on-off intermittency". In: *Physical Review E* 49 (2), 1140 (1994).

[7] A. Monti, F. Diele, C. Marangi, and A. Provenzale. "On–off intermittency in population outbreaks: Reactive equilibria and propagation on networks". In: *Communications in Nonlinear Science and Numerical Simulation* 130, 107788 (2024).

[8] W. Moon. "On–off Intermittency in locally coupled maps". In: *Woods Hole Oceanographic Institution MA* (2010).

[9] Y. Nagai and Y. C. Lai. "Characterization of blowout bifurcation by unstable periodic orbits". In: *Physical Review E* 55 (1997), R1251–R1254.

[10] N. Platt, E. Spiegel, and C. Tresser. "On-off intermittency: A mechanism for bursting". In: *Physical Review Letters* 70 (3), 279 (1993), pp. 918–921.

[11] G. Vissio and A. Provenzale. "On–off intermittency and irruptions in host-parasitoid dynamics". In: *Journal of Theoretical Biology* 111174 (2022).

Mini-Symposium
Exploring efficient advanced numerical methods for Partial Differential Equations

Preface to the Symposium

Elisa Calzola[a] and Federica Ferrarese[b], *Organizers*
[a] University of Verona, Italy
[b] University of Ferrara, Italy

Evolutionary Partial Differential Equations (PDEs) are crucial for various scientific and engineering fields, serving as the basis for modeling a wide range of phenomena. However, due to the complexity of these equations, obtaining analytical solutions is often impractical, therefore developing efficient numerical techniques for approximating solutions is essential. This requires special attention to designing solvers capable of handling the challenges inherent in evolutionary PDEs, such as dimensionality, stiffness, non-linearities, and time-varying boundary conditions.

The mini-symposium aims to gather young researchers across different disciplines to share recent advancements in efficiently solving evolutionary PDEs. Diverse applications will be considered including uncertainty quantification, optimal control, multi-scale and multi-physics problems, and real-world applications in fields such as crowd dynamics, traffic flows and epidemiology.

List of the speakers

- Elisa Calzola, University of Verona, Italy

- Federica Ferrarese, University of Ferrara, Italy

- Fabio Cassini, University of Verona, Italy

- Elisa Iacomini, University of Ferrara, Italy

- Valeria Iorio, University of L'Aquila, Italy

- Chiara Segala, RWTH-Aachen University, Germany

- Anastasia Istratuca, University of Edinburgh, Scotland

- Alessandra Zappa, Università degli studi dell'Insubria, Italy

Numerical control and learning of magnetized plasma dynamics with uncertainties.

Federica Ferrarese
University of Ferrara, Italy

In recent years, there has been a significant focus on advancing numerical methods to address challenges in plasma physics [2, 4, 5]. Specifically, there is a growing interest in exploring magnetized plasma for its potential applications in fusion devices like Tokamaks and Stellarators [10, 12]. Plasma confinement devices rely on intricate magnetic fields to contain and stabilize the extremely hot and reactive plasma. Achieving and maintaining the desired plasma parameters, such as temperature, density, and confinement time, is essential for the success of fusion experiments. The complexity of plasma behavior, combined with the interplay of magnetic fields, introduces unique challenges that demand advanced mathematical modeling and computational techniques.

In this context, we consider a simplified scenario, restricting ourselves to a two dimensional setting in phase space. This situation mimics the evolution of a plasma inside a three dimensional axisymmetric toroidal device. To give a precise definition of our simplified setting, we first consider a two dimensional horizontal section of a three dimensional torus, which is obtained from the intersection of the $(x-y)$ plane with the solid. We then focus on a portion of this section, and we successively approximate it by a rectangle in a new reference frame to simplify the description of the computational domain, see [1] for further details. Additionally, we assume the model includes uncertainties. Uncertainty may be due to various reasons, like lack of knowledge on the microscopic interactions or incomplete informations at the boundaries. To model the evolution of the plasma density we rely on the Vlasov-Poisson equation which describes the evolution of charged particles in an electromagnetic self-consistent or externally applied field. For one single species of the plasma, these equations read as

$$
\frac{\partial f(t, \mathbf{x}, \mathbf{v}, \mathbf{z})}{\partial t} + \mathbf{v} \cdot \nabla_{\mathbf{x}} f(t, \mathbf{x}, \mathbf{v}, \mathbf{z}) + (\mathbf{E}(t, \mathbf{x}, \mathbf{z}) + \mathbf{v} \times \mathbf{B}(t, \mathbf{x})) \cdot \nabla_{\mathbf{v}} f(t, \mathbf{x}, \mathbf{v}, \mathbf{z}) = 0,
$$
$$
-\Delta_{\mathbf{x}} \phi(t, \mathbf{x}, \mathbf{z}) = \rho(t, \mathbf{x}, \mathbf{z}) - 1, \qquad \mathbf{E}(t, \mathbf{x}, \mathbf{z}) = -\nabla_{\mathbf{x}} \phi(t, \mathbf{x}, \mathbf{z}),
$$

(60.1)

with

$$
\rho(t, \mathbf{x}, \mathbf{z}) = \int_{\mathbb{R}^{d_v}} f(t, \mathbf{x}, \mathbf{v}, \mathbf{z}) d\mathbf{v}.
$$

In the above formulation, $\mathbf{E}(t, \mathbf{x}, \mathbf{z})$ represents the electric field, while $\mathbf{B}(t, \mathbf{x})$ is an external magnetic field, which does not depend on the uncertainty, and that here we assume to take the form

$$
\mathbf{B}(t, \mathbf{x}) = (0, 0, B(t, \mathbf{x})).
$$

We look for a control strategy based on $\mathbf{B}(t, \mathbf{x})$ obtained as a solution of an optimality principle, aiming at minimizing the mass which hits the boundaries and/or the thermal energy close to the walls, [9, 11]. To achieve this, we propose the following continuous-level control problem

$$\min_{\mathbf{B} \in \mathcal{B}_{adm}} \mathcal{J}(\mathbf{B}; f, f^0), \qquad \text{s.t. (60.1)}, \tag{60.2}$$

where

$$\mathcal{J}(\mathbf{B}; f, f^0) = \int_0^T \int_{\Omega_x} \left(\mathcal{P}\left[\mathcal{D}(f, \phi)(t, \mathbf{x}, \mathbf{z}) \right] + \frac{\gamma}{2} \|\mathbf{B}(t, \mathbf{x})\|^2 \right) d\mathbf{x} dt,$$

with $\Omega_x \in \mathbb{R}^{d_x}$ representing the spatial domain, and where $\gamma > 0$ is a penalization term, $\mathcal{P}[\cdot]$ is a suitable statistical operator taking into account the presence of the uncertainties, and $\mathcal{D}(\cdot)$ aims at enforcing a specific configuration in the distribution function. The control obtained by solving (60.2) depends on the position $\mathbf{x}$. However, a pointwise control is not realistic in this context, so we introduce a spatial discretization grid with N_c cells $C_k \subset \Omega_x$, where Ω_x is the space domain, such that $\bigcup_{k=1}^{N_c} C_k = \Omega_x$, $C_k \cap C_\ell = \emptyset$ for all $k \neq \ell$, and $k, \ell \in \{1, \ldots, N_c\}$. We define a piecewise constant control over these cells, with values interpolated at the cell centres $\mathbf{x}_c$. At the discretized level, we rely on a semi-implicit particle-in-cell methods. The Particle-In-Cell (PIC) method applied to the Vlasov equation involves discretizing the plasma into a large number of simulation particles, which represent the distribution function in phase space [7]. These particles move according to the characteristic curves of the Vlasov equation, interacting with the electromagnetic fields calculated on a grid. The method combines the particle representation of the distribution function with a grid-based solution of the fields, allowing for efficient and accurate simulation of plasma dynamics. The Particle-In-Cell method, while highly effective for solving the Vlasov equation, incurs significant computational costs due to the need to track a vast number of simulation particles, expecially in the presence of uncertainties, where a clasical Monte Carlo method has a convergerce error proportional to $\sigma M^{-1/2}$, being σ the variance of the solution and M the number of samples used. To mitigate the computational challenges posed by high-fidelity simulations, a multi-fidelity approach is adopted [6]. This approach leverages both high-fidelity and low-fidelity models to achieve accurate and efficient simulations. The high-fidelity model provides detailed and precise solutions but is computationally expensive. In contrast, the low-fidelity model offers approximate solutions with reduced computational cost. In this study, a feed-forward neural network is employed as the low-fidelity model [8]. The neural network is trained to predict the moments of the distribution function f. Additionally, other low-fidelity models, including the one suggested in [3], are considered to evaluate the effectiveness of this approach. Different numerical experiments validate our results, showing the controllability of the system in presence of uncertainties, and the capability of the multi scale control variate method to reduce the computational complexity of the classical Monte Carlo method.

References

[1] G. Albi, G. Dimarco, F. Ferrarese, and L. Pareschi. "Instantaneous control strategies for magnetically confined fusion plasma". ARXIV: 2403.16254. 2024.

[2] C.-Z. Cheng and G. Knorr. "The integration of the Vlasov equation in configuration space". In: *Journal of Computational Physics* 22.3 (1976), pp. 330–351.

[3] N. Crouseilles, G. Dimarco, and M.-H. Vignal. "Multiscale Schemes for the BGK–Vlasov–Poisson System in the Quasi-Neutral and Fluid Limits. Stability Analysis and First Order Schemes". In: *Multiscale Modeling & Simulation* 14.1 (2016), pp. 65–95.

[4] N. Crouseilles, M. Mehrenberger, and E. Sonnendrücker. "Conservative semi-Lagrangian schemes for Vlasov equations". In: *Journal of Computational Physics* 229.6 (2010), pp. 1927–1953.

[5] P. Degond and F. Deluzet. "Asymptotic-preserving methods and multiscale models for plasma physics". In: *Journal of Computational Physics* 336 (2017), pp. 429–457.

[6] G. Dimarco and L. Pareschi. "Multi-scale control variate methods for uncertainty quantification in kinetic equations". In: *Journal of Computational Physics* 388 (2019), pp. 63–89.

[7] F. Filbet and L. M. Rodrigues. "Asymptotically stable particle-in-cell methods for the Vlasov–Poisson system with a strong external magnetic field". In: *SIAM Journal on Numerical Analysis* 54.2 (2016), pp. 1120–1146.

[8] S. Jin, Z. Ma, and T.-a. Zhang. "Asymptotic-Preserving Neural Networks for Multiscale Vlasov–Poisson–Fokker–Planck System in the High-Field Regime". In: *Journal of Scientific Computing* 99.3 (2024), p. 61.

[9] P. Knopf and J. Weber. "Optimal control of a Vlasov–Poisson plasma by fixed magnetic field coils". In: *Applied Mathematics & Optimization* 81 (2020), pp. 961–988.

[10] E. Sonnendrücker, J. Roche, P. Bertrand, and A. Ghizzo. "The semi-Lagrangian method for the numerical resolution of the Vlasov equation". In: *Journal of computational physics* 149.2 (1999), pp. 201–220.

[11] J. Weber. "Optimal control of the two-dimensional Vlasov-Maxwell system". In: *ESAIM: Control, Optimisation and Calculus of Variations* 27 (2021), S19.

[12] C. Yang and F. Filbet. "Conservative and non-conservative methods based on Hermite weighted essentially non-oscillatory reconstruction for Vlasov equations". In: *Journal of Computational Physics* 279 (2014), pp. 18–36.

A data-driven kinetic model for opinion dynamics with social network contacts

Elisa Calzola

Department of Computer Science, University of Verona, Italy

In recent years, kinetic models, especially Boltzmann equations, have become powerful tools for describing and analyzing collective behaviors in systems of interacting agents [4, 11]. These models have been applied across various fields, contributing significantly to disciplines like economics, where they help predict market dynamics [14], bubbles and crashes [10], and analyze wealth distribution [5, 12]. In biology, kinetic models study population dynamics and disease spread, predicting the effectiveness of interventions like vaccination [6]. Boltzmann-type equations also examine cooperation and altruism in social systems, genetic mutations, and information diffusion in social sciences (see, *e.g.*, [3, 8]). They are used to understand traffic flow, crowd behavior, and optimize wireless network communications (as in, for example, [1, 7]). Within this broad application framework, opinion formation—how opinions evolve and spread—is critical for understanding societal phenomena like political polarization and consensus.

In this joint work with Giacomo Albi and Giacomo Dimarco [2] we introduce a new kinetic model starting from the microscopic description of the interaction between agents, then we scale the model to obtain the evolution of observable quantities, providing a framework for analyzing social events and designing interventions to promote constructive dialogue and reduce polarization. Our study highlights the role of influential individuals within social networks, particularly on platforms like Twitter (now X).

Each agent in our model has a number of followers $c > 0$ and an opinion on a certain topic, $v \in [-1, 1]$, where -1 indicates a strongly negative opinion and $+1$, on the contrary, a fully positive one (as modeled, *e.g.*, in [13]). We develop an evolutionary model for connections among individuals on social media, focusing on Twitter to match real data with our model's equilibrium distribution, and we get that the stationary distribution $h_\infty(c)$ of connections on the network, according to the model and the data, is given by

$$h_\infty(c) = \frac{1}{\sqrt{2\pi\nu c}} \exp\left\{ -\frac{(\ln c - \lambda)^2}{2\nu} \right\}, \tag{61.1}$$

for certain values of the parameters ν and λ. Opinions are continuous variables updated through social media interactions, which are influenced by the number of followers and opinion distance. We also incorporate randomness to model external factors like information access, and we get that the kinetic equation describing the evolution of the opin-

ion distribution in presence of social media interactions is given by

$$\frac{\partial f}{\partial t} = -\frac{\partial \left(\mathcal{E}[f](v,c,t)f\right)}{\partial v} + \frac{\partial (\Phi_0(c)f)}{\partial c} + \frac{1}{2}\sigma^2\frac{\partial^2 \left(D^2(v,c)f\right)}{\partial v^2} + \frac{1}{2}\nu^2\frac{\partial^2 (c^2 f)}{\partial c^2},$$

where $f(v,c,t)$ is the density of agents that at time t have opinion v and number of contacts c, the non-local operator $\mathcal{E}[f]$ models the interaction between agents, the function $D(v,c)$ weights the randomness, and the value function Φ_0 regulates the formation of the network and is such that its stationary state is given by (61.1). The model captures features like consensus and polarization, depending on the choice of interaction kernels.

We performed various simulations to validate our model, both with and without data incorporation. One of the simulations that includes data has been carried on as follows: we used the access to the Application Programming Interfaces (API) of Twitter to obtain the content of a number of tweets on the topic "Donald Trump" (and related hashtags) some days after the 20th November 2022 (re-admittance of Donald Trump on Twitter). We then employed VADER ([9]) to analyze the texts of the tweets and we obtained a rating between -1 and 1 for each text, which we considered to be the agents' opinion on the subject. To perform the model calibration we introduce a class of interacting functions, explicitly depending by a set of parameters (more details can be found in [2]), and we assume that the distribution of connections is at the stationary state (61.1). Then, we search the optimal value of the parameters that minimizes the ℓ_1 distance at the final time $t = 20$ of the marginal distribution of the simulated opinions $g(v,t)$ (obtained using a Monte Carlo algorithm) and the one reconstructed from the data $\hat{g}(v,t)$. Figure 61.1 shows the comparison between our results and the data: on the left, we have the marginal of the opinions at time $t = 20$ and the data, while on the right we have $f(v,c,t)$ (represented as $\log(f(v,c,t)+0.025)$) compared with the actual data extracted from the social network (represented by the orange dots).
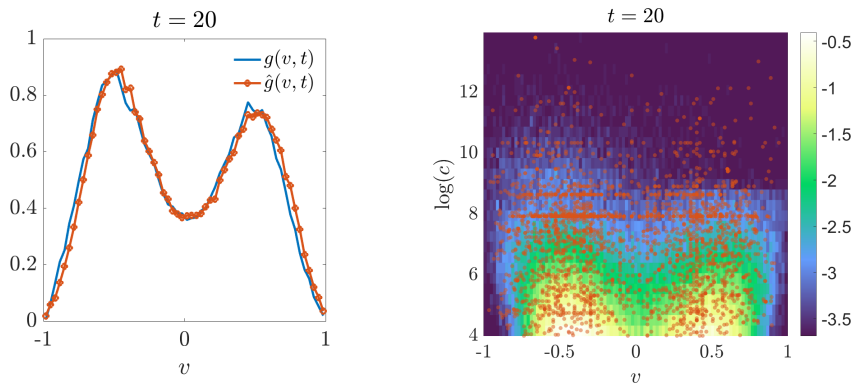

Figure 61.1: The marginal distribution of opinions at the final time (left) and the comparison between the reconstructed density of opinions and contacts and the real data set.

References

[1] G. Albi et al. "Vehicular traffic, crowds, and swarms: from kinetic theory and multi-scale methods to applications and research perspectives". In: *Math. Models Methods Appl. Sci.* 29.10 (2019), pp. 1901–2005.

[2] G. Albi, E. Calzola, and G. Dimarco. "A data-driven kinetic model for opinion dynamics with social network contacts". In: *European Journal of Applied Mathematics* (2024).

[3] G. Albi, P. Lorenzo, and M. Zanella. "Opinion dynamics over complex networks: kinetic modelling and numerical methods". In: *Kinet. Relat. Models* 10.1 (2017), pp. 1–32.

[4] N. Bellomo, F. Brezzi, and J. Soler. "Recent results and challenges in behavioral systems". In: *Math. Models Methods Appl. Sci.* 30.10 (2020), pp. 1857–1862.

[5] S. Cordier, L. Pareschi, and G. Toscani. "On a kinetic model for a simple market economy". In: *Journal of Statistical Physics* 120 (2005), pp. 253–277.

[6] G. Dimarco, G. Toscani, and M. Zanella. "Optimal control of epidemic spreading in the presence of social heterogeneity". In: *Philos. Trans. Roy. Soc. A* 380.2224 (2022), Paper No. 20210160, 16.

[7] A. Festa, A. Tosin, and M.-T. Wolfram. "Kinetic description of collision avoidance in pedestrian crowds by sidestepping". In: *Kinet. Relat. Models* 11.3 (2018), pp. 491–520.

[8] J. Franceschi and L. Pareschi. "Spreading of fake news, competence and learning: kinetic modelling and numerical approximation". In: *Philos. Trans. Roy. Soc. A* 380.2224 (2022), Paper No. 20210159, 18.

[9] C. Hutto and E. Gilbert. "VADER: A Parsimonious Rule-Based Model for Sentiment Analysis of Social Media Text". In: *Proceedings of the International AAAI Conference on Web and Social Media* 8.1 (2014), pp. 216–225.

[10] J.-C. Li, C. Tao, and H.-F. Li. "Dynamic forecasting performance and liquidity evaluation of financial market by Econophysics and Bayesian methods". In: *Physica A: Statistical Mechanics and its Applications* 588 (2022), p. 126546.

[11] L. Pareschi and G. Toscani. *Interacting multiagent systems: kinetic equations and Monte Carlo methods*. OUP Oxford, 2013.

[12] L. Pareschi and G. Toscani. "Wealth distribution and collective knowledge: a Boltzmann approach". In: *Philosophical Transactions of the Royal Society A: Mathematical, Physical and Engineering Sciences* 372.2028 (2014), p. 20130396.

[13] G. Toscani. "Kinetic models of opinion formation". In: *Communications in mathematical sciences* 4.3 (2006), pp. 481–496.

[14] G. Toscani. "A multi-agent approach to the impact of epidemic spreading on commercial activities". In: *Math. Models Methods Appl. Sci.* 32.10 (2022), pp. 1931–1948.

Exponential integrators for mean-field selective optimal control problems

Giacomo Albi, Marco Caliari, Elisa Calzola, and Fabio Cassini[*]
Department of Computer Science, University of Verona, Italy

Studying the collective motion of interacting agent systems is important for understanding the formation of coherent global behaviors with applications to economic, biological, and social phenomena. Modeling these systems poses a significant mathematical challenge. Nevertheless, the dynamics of the individuals have been successfully described by systems of ODEs from Newton's laws designing basic interaction rules (such as alignment, attraction, and repulsion) or by considering an evolutive game with dynamics driven by the simultaneous cost optimization of N players [6]. In this context, it is crucial to design centralized policies that can optimally enforce a desired state. When the number of agents is very large, directly performing simulations with the nonlinear system is computationally cumbersome (we face the so-called *curse of dimensionality*). For this reason, it is common practice to employ the corresponding *mean-field* optimal control problem instead [2, 3].

We consider in particular the mean-field optimal control problem defined by

$$\min_{u} \mathcal{J}(u; \rho_0) = \min_{u} \left\{ \frac{1}{2} \int_0^T \int_\Omega \left(e(t, x, \rho) + \gamma |u|^2 \rho \right) dx dt + \frac{1}{2} \int_\Omega c(T, x, \rho(T, x)) dx \right\} \quad \text{(62.1a)}$$

for a general running cost $e(t, x, \rho)$ and a terminal cost $c(T, x, \rho(T, x))$. Here, $\rho = \rho(t, x)$ is a probability density of agents satisfying

$$\begin{cases} \partial_t \rho + \nabla \cdot \left[(\mathcal{P}(\rho) + s(t, x, \rho) u) \rho \right] - \dfrac{\sigma^2}{2} \Delta \rho = 0, \\ \rho(0, x) = \rho_0(x), \\ \left((\mathcal{P}(\rho) + s(t, x, \rho) u) \rho - \dfrac{\sigma^2}{2} \nabla \rho \right) \cdot \vec{n} = \begin{cases} \beta \rho & \text{on } \Gamma_\mathsf{F}, \\ 0 & \text{on } \Gamma_\mathsf{Z}, \end{cases} \end{cases} \quad \text{(62.1b)}$$

and defined for each $(t, x) \in [0, T] \times \Omega$. The evolution of the density is driven by the non-local operator $\mathcal{P}(\rho)(t, x) = \int_\Omega p(x, y)(y - x)\rho(t, y)dy$ and by the control $u = u(t, x)$ weighted by the selective function $s(t, x, \rho)$. The boundary of Ω is partitioned in Γ_F (non-zero flux, $\beta \neq 0$) and Γ_Z (zero flux).

To determine a (sub)optimal solution to 62.1, we start by formally deriving the first order optimality conditions using a Lagrangian approach. This results in the gradient direction $\gamma u + s(t, x, \rho) \nabla \psi$ for the control variable (ψ is the adjoint function), in the forward

PDE for the density function 62.1b, and in the backward PDE for the adjoint

$$
\begin{cases}
-\partial_t \psi = \frac{\sigma^2}{2}\Delta\psi + (\mathcal{P}(\rho) + (s(t,x,\rho) + \rho D_\rho s(t,x,\rho))u)\cdot\nabla\psi + \mathcal{Q}(\rho,\psi) + \frac{1}{2}(D_\rho e(t,x,\rho) + \gamma|u|^2), \\
\psi(T,x) = \psi_T(x), \\
\frac{\sigma^2}{2}\nabla\psi\cdot\vec{n} = \begin{cases} -\beta\psi & \text{on } \Gamma_{\text{F}}, \\ 0 & \text{on } \Gamma_{\text{Z}}. \end{cases}
\end{cases}
$$

$$(62.2)$$

Here, $\mathcal{Q}(\rho,\psi)(t,x) = \int_\Omega p(y,x)(x-y)\cdot\nabla\psi(t,y)\rho(t,y)dy$ and the terminal condition is $\psi_T(x) = \frac{1}{2}D_\rho c(T,x,\rho(T,x))$. Then, we suitably combine the approximated solutions of the relevant equations in the context of a steepest descent approach [2].

For the numerical solution of 62.1b and 62.2 we use the method of lines by performing a semidiscretization in space using standard finite differences. The resulting *stiff* system of ODEs is integrated in time using suitable explicit *exponential integrators* [5], which are schemes tailored for these kinds of systems. In fact, these methods solve exactly linear homogeneous systems of ODEs with constant coefficients, they allow for time steps usually much larger than those required by classical explicit methods, and do not require the solution of (non)linear systems as implicit methods do. On the other hand, exponential integrators require the computation of the action of exponential-like matrix functions, for which efficient techniques have been developed in the recent years [4]. More in detail, for a *generic* selective function, the semidiscretized system of ODEs corresponding to the forward equation 62.1b is written as

$$\boldsymbol{\rho}'(t) = A_{\text{F}}\boldsymbol{\rho}(t) + \boldsymbol{g}_{\text{F}}(t,\boldsymbol{\rho}(t)), \quad \boldsymbol{\rho}(0) = \boldsymbol{\rho}_0,$$

with $A_{\text{F}} \approx \frac{\sigma^2}{2}\Delta\rho(t)$ and $\boldsymbol{g}_{\text{F}}(t,\boldsymbol{\rho}(t)) \approx -\nabla\cdot[(\mathcal{P}(\rho) + s(t,x,\rho)u)\,\rho]$. The boundary conditions are suitably discretized and directly embedded in A_{F} and $\boldsymbol{g}$. The exponential integrator that we employ for the time marching is

$$\boldsymbol{\rho}_{k+1} = \text{e}^{\tau A_{\text{F}}}\boldsymbol{\rho}_k + \tau\varphi_1(\tau A_{\text{F}})\boldsymbol{g}_{\text{F}}(t_k,\boldsymbol{\rho}_k),$$

where we used the notation $\boldsymbol{\rho}_j \approx \boldsymbol{\rho}(t_j)$, we set (for simplicity) a constant time step size $\tau = t_{k+1} - t_k$, and we introduced the exponential-like matrix function $\varphi_1(X) = \int_0^1 \text{e}^{(1-\theta)X}d\theta$. This scheme is known as *exponential Euler*. It is a fully explicit method of first (stiff) order and it is A-stable by construction. Similarly, we semidiscretize the backward equation 62.2 as

$$-\boldsymbol{\psi}'(t) = A_{\text{B}}(t)\boldsymbol{\psi}(t) + \boldsymbol{g}_{\text{B}}(t), \quad \boldsymbol{\psi}(T) = \boldsymbol{\psi}_T,$$

where we denoted $A_{\text{B}}(t) \approx \frac{\sigma^2}{2}\Delta\psi + (\mathcal{P}(\rho) + (s(t,x,\rho) + \rho D_\rho s(t,x,\rho))u)\cdot\nabla\psi + \mathcal{Q}(\rho,\psi)$ and $\boldsymbol{g}_{\text{B}}(t) \approx \frac{1}{2}(D_\rho e(t,x,\rho) + \gamma|u|^2)$. The time evolution is then performed as

$$\boldsymbol{\psi}_k = \text{e}^{\tau A_{\text{B}}(t_{k+1})}\boldsymbol{\psi}_{k+1} + \tau\varphi_1(\tau A_{\text{B}}(t_{k+1}))\boldsymbol{g}_{\text{B}}(t_{k+1}).$$

We call this first order explicit method *exponential Euler–Magnus* scheme.

We perform extensive numerical experiments that assess the efficiency of the proposed approach[1]. In particular, we consider different control problems for collective motion in the context of opinion formation and pedestrian dynamics. For compactness of presentation, we show in Figure 62.1 just the results on a popular opinion model, i.e., the Sznajd one [2], and on a pedestrian dynamics model for the fast exit of two groups [3].

A preprint version of the complete manuscript is available [1].
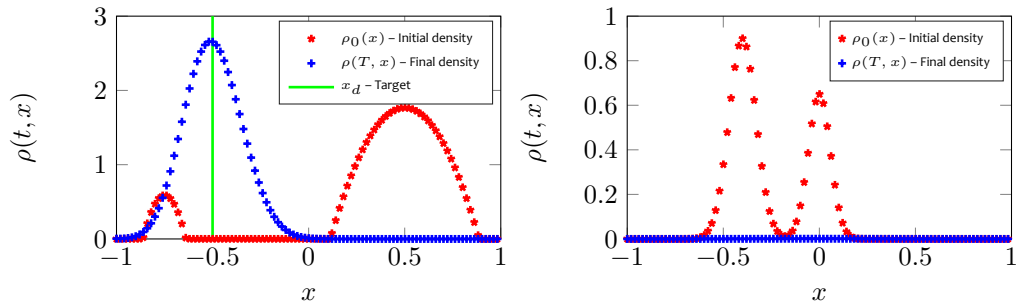
Figure 62.1: Density at initial and final times for the opinion formation model (left) and for the pedestrian dynamics model (right).

References

[1] G. Albi, M. Caliari, E. Calzola, and F. Cassini. "Exponential integrators for mean-field selective optimal control problems". ARXIV: 2302.00127. 2023.

[2] G. Albi, Y.-P. Choi, M. Fornasier, and D. Kalise. "Mean Field Control Hierarchy". In: *Appl. Math. Optim.* 76 (2017), pp. 93–135. DOI: 10.1007/s00245-017-9429-x.

[3] M. Burger, M. Di Francesco, P. A. Markowich, and M.-T. Wolfram. "On a mean field game optimal control approach modeling fast exit scenarios in human crowds". In: *52nd IEEE Conference on Decision and Control*. 2013. DOI: 10.1109/CDC.2013.6760 360.

[4] S. Gaudreault, G. Rainwater, and M. Tokman. "KIOPS: A fast adaptive Krylov subspace solver for exponential integrators". In: *J. Comput. Phys.* 372 (2018), pp. 236–255. DOI: 10.1016/j.jcp.2018.06.026.

[5] M. Hochbruck and A. Ostermann. "Exponential integrators". In: *Acta Numer.* 19 (2010), pp. 209–286. DOI: 10.1017/S0962492910000048.

[6] J. M. Lasry and P. L. Lions. "Mean field games". In: *Japanese J. Math.* 2 (2007), pp. 229–260. DOI: 10.1007/s11537-007-0657-8.

---

[1]The codes are publicly available at `https://github.com/cassinif/expint_mfsoc`.

Uncertainty quantification in traffic flow models

Elisa Iacomini

Department of Mathematics and Computer Science, University of Ferrara

Traffic flow modeling is a crucial component in the design, management, and optimization of transportation systems. One of the most powerful mathematical tools used in this field is partial differential equations (PDEs). PDEs offer a robust framework for describing the dynamics of traffic flow, capturing essential features such as density, speed, and flux over time and space. These equations enable researchers to predict and analyze complex traffic patterns, facilitating the development of effective traffic management strategies and infrastructure improvements.

However, real-world traffic is inherently uncertain due to various factors such as fluctuating demand, unforeseen incidents, and varied driver behaviors. This uncertainty can significantly impact the accuracy and reliability of traffic flow models [5]. Therefore, integrating uncertainty into traffic models is essential for developing more realistic and trustful solutions.

Investigating the propagation of uncertainties in traffic flow models is indeed the core of this talk.

Several approaches to quantify uncertainty are presented in the literature and can be classified in non-intrusive and intrusive methods. The main idea underlying the former approach is to solve the model for fixed number of samples using deterministic numerical algorithms. Typical examples are Monte-Carlo and stochastic collocation methods [1].

On the other side, intrusive approaches are based on the fact that the governing equations have to be modified to incorporate the probabilistic character of the model parameters. The stochastic Galerkin method is one of the most famous in this framework.

In this talk we will present both of the methodologies, highlighting advantages and limitations of each approach, in order to have a more comprehensive analysis.

The first part will be devoted to the intrusive approach, in particular the stochastic Galerkin approach, which has been applied to study the impact of the uncertainty at different scales of observation [6]. The uncertainty is introduced in the initial data at a microscopic, mesoscopic and macroscopic scale, and the resulting stochastic models have been analyzed. In this context, stochastic processes are represented using piecewise orthogonal functions, known as generalized polynomial chaos expansion (gPC), which are then substituted into the governing equations. A Galerkin projection is applied to obtain deterministic evolution equations for the coefficients of the series expansions [7].

Many challenges arise here, since some desired properties of the original system are not necessarily transferred to the intrusive formulation, in particular at the macroscopic

level we face the loss of hyperbolicity of the system [3]. In order to ensure this property, the basis functions have to fulfill additional assumptions and a consistent gPC expansion has to be provided for the Galerkin product. Moreover exploiting the link with the kinetic model [4], we are able to study the probability of having high risk traffic zones, i.e. area in which instabilities may occur.

However, in many practical scenarios the uncertainty distribution is either unknown or irregular, posing challenges for the stochastic Galerkin method, which relies on regularity. Consequently, non-intrusive methods are more appropriate for these situations. Despite their suitability, the Monte Carlo method, the common prototype for non-intrusive approach, suffers from slow convergence. To address this limitation, various strategies have been developed. In this presentation, we will focus on the multi fidelity control variate method, described in [2].

This approach exploits the multiscale nature of the problem to reduce variance within the Monte Carlo simulations. Specifically, we exploit the hierarchical relationship between scales, where high-fidelity models, such as kinetic models, are computationally expensive but provide high accuracy, and low-fidelity models, like macroscopic models, are computationally efficient but less precise.

The key point is that the low fidelity model must be an approximation of the high fidelity model. By conducting a limited number of high-fidelity evaluations and numerous low-fidelity evaluations, we can achieve improved accuracy without increasing computational costs.

At the end of this talk we will see an application of this methodology to a kinetic traffic flow model. Through numerical tests, we will illustrate the significant improvement in the convergence rate achieved by this approach.

References

[1]   G. Bertaglia, L. Liu, L. Pareschi, and X. Zhu. "Bi-fidelity stochastic collocation methods for epidemic transport models with uncertainties". In: *Networks and Heterogeneous Media* 17.3 (2022), pp. 401–425.

[2]   G. Dimarco and L. Pareschi. "Multi-scale control variate methods for uncertainty quantification in kinetic equations". In: *Journal of Computational Physics* 388 (2019), pp. 63–89.

[3]   S. Gerster, M. Herty, and E. Iacomini. "Stability analysis of a hyperbolic stochastic Galerkin formulation for the Aw-Rascle-Zhang model with relaxation". In: *Mathematical Biosciences and Engineering* 18.4 (2021), pp. 4372–4389.

[4]   M. Herty and E. Iacomini. "Uncertainty quantification in hierarchical vehicular flow models." In: *Kinetic & Related Models* 15.2 (2022), pp. 239–256.

[5]   M. Herty, A. Tosin, G. Visconti, and M. Zanella. "Reconstruction of traffic speed distributions from kinetic models with uncertainties". In: *Mathematical Descriptions of Traffic Flow: Micro, Macro and Kinetic Models*. Springer. 2021, pp. 1–16.

[6] E. Iacomini. "Overview on Uncertainty Quantification in Traffic Models via Intrusive Method Check for updates". In: *Advances in Numerical Methods for Hyperbolic Balance Laws and Related Problems* 32 (2023), p. 121.

[7] P. Pettersson, G. Iaccarino, and J. Nordström. "A stochastic Galerkin method for the Euler equations with Roe variable transformation". In: *Journal of Computational Physics* 257 (2014), pp. 481–500.

Controllability of continuous networks and a kernel-based learning approximation

Chiara Segala

RWTH Aachen University

In recent years, there has been an increasing interest in machine learning and data science [6, 13] with applications such as human speech recognition, competition in strategic game systems, intelligent routing in content delivery networks, and autonomous vehicles operations. The intersection of mathematics and artificial intelligence allows the use of machine learning tools to tackle difficulties arising in numerical methodologies, such as high-dimensional parameter optimization, in the modelling of physics-based operators through experimental data or uncertainty quantification, see e.g. [7].

Here, we are interested in a particular class of learning-based methods, the deep residual neural networks (ResNets). Given a set of input data x_i^0, $i = 1, \ldots, M$, the ResNet propagates those through the layers $\kappa = 0, \ldots, L + 1$, to provide a state prediction $x_i(L + 1)$. This state is compared with given reference data y_i. The dynamics depend on a large set of parameters, called weights $w(\kappa)$ and biases $b(\kappa)$. Their values are obtained as a solution to an optimization problem and the typically iterative process is called training. The objective or cost is given by a distance ℓ between predictions $x_i(L + 1)$ and the reference y_i. ResNets have also been formulated for infinitely many layers, leading to the definition of neural differential equations [1] and to mean-field neural equations [5]. The continuous formulations are subject to theoretical investigations and may reduce the computational cost of the training, especially in the case when M is large, see e.g. [3, 8].

In this work, we take a different point of view and model the training process as a controllability problem. In very particular cases, the Hilbert Uniqueness Method (HUM) yields the existence of optimal weights. The HUM is a mathematical technique used in the study of partial differential equations that has been applied in control theory of partial differential equations, see e.g. [2]. Here, we also show the applicability of suitably formulated training problems for ResNet.

The problem of controllability of continuous neural networks has been discussed for example in [4, 8, 10]. In [10] the controllability of continuous-time recurrent neural networks has been established provided that the activation function is the hyperbolic tangent. This work assumes infinitely many layers $L \to \infty$ but still a finite size samples $M < \infty$.

More recently [4], the controllability is discussed for L and M tending to infinity, leading to the mean-field equation. Therein, its controllability using weights that are piecewise constant (in time) has been established. For further results, we refer to the recent review [8]. While the controllability can be established here in the case of linear activation functions, we are also interested in their numerical for general training tasks. To this

end, we propose an approach based on kernel learning methods. In particular, we approximate the ResNets loss function using kernel based estimation. Those methods are commonly used as powerful machine learning tools, see e.g. [9, 12], and they are supported by a well-defined theory [11].

Summarizing, this work explores deep residual neural networks (ResNets) and their connection to time-continuous and mean-field equations. It presents controllability results for linear ResNets, examining both microscopic and mean-field perspectives. Additionally, the paper proposes a numerical approach based on kernel learning methods and demonstrates this approach through numerical experiments for both microscopic and mean-field neural networks.

References

[1] T. Q. Chen, Y. Rubanova, J. Bettencourt, and D. K. Duvenaud. "Neural ordinary differential equations". In: *Advances in neural information processing systems*. 2018, pp. 6571–6583.

[2] J. M. Coron. *Control and nonlinearity*. American Mathematical Society, 2007.

[3] J. Crevat. "Mean-field limit of a spatially-extended Fitzhugh-Nagumo neural network". In: *Kinet. Relat. Models* 12.6 (2019), pp. 1329–1358. ISSN: 1937-5093. DOI: 10 .3934/krm.2019052.

[4] K. Elamvazhuthi, B. Gharesifard, A. L. Bertozzi, and S. Osher. "Neural ODE Control for Trajectory Approximation of Continuity Equation". In: *IEEE Control Systems Letters* 6 (2022), pp. 3152–3157.

[5] M. Herty, T. Trimborn, and G. Visconti. "Mean-field and kinetic descriptions of neural differential equations". In: *Foundations of Data Science* 4.2 (2022), pp. 271–298.

[6] S. Lalmuanawma, J. Hussain, and L. Chhakchhuak. "Applications of machine learning and artificial intelligence for Covid-19 (SARS-CoV-2) pandemic: a review". In: *Chaos Solitons Fractals* 139 (2020), pp. 110059, 6. ISSN: 0960-0779. DOI: 10 . 1016 /j.chaos.2020.110059.

[7] S. Mishra. "A machine learning framework for data driven acceleration of computations of differential equations". In: *Math. Eng.* 1.1 (2019), pp. 118–146. DOI: 10.39 34/Mine.2018.1.118.

[8] D. Ruiz-Balet and E. Zuazua. "Neural ODE Control for Classification, Approximation and Transport". In: *SIAM Review* 65 (3 2023), pp. 735–773.

[9] B. Scholkopf and A. J. Smola. *Learning with kernels: support vector machines, regularization, optimization, and beyond*. MIT press, 2002.

[10] E. Sontag and H. Sussmann. "Complete controllability of continuous-time recurrent neural networks". In: *Systems & Control Letters* 30.4 (1997), pp. 177–183.

[11] I. Steinwart and A. Christmann. *Support vector machines*. Springer Science & Business Media, 2008.

[12] C. K. Williams and C. E. Rasmussen. *Gaussian processes for machine learning*. Vol. 2. 3. MIT press Cambridge, MA, 2006.

[13] M. Wooldridge. "Artificial Intelligence requires more than deep learning - but what, exactly?" In: *Artificial Intelligence* 289 (2020), p. 103386. ISSN: 0004-3702. DOI: `10.1016/j.artint.2020.103386`.

A convergent finite volume method for a kinetic model for interacting species

Valeria Iorio
University of L'Aquila

In this talk, we study an upwind finite volume method to construct approximate numerical solutions to a system of two kinetic equations in one dimension that are coupled through non-local interaction terms. The system we deal with is

$$\begin{cases} \partial_t f + v\partial_x f = (K'_{11} * \rho + K'_{12} * \eta)\partial_v f, \\ \partial_t g + v\partial_x g = (K'_{22} * \eta + K'_{21} * \rho)\partial_v g, \end{cases} \tag{65.1}$$

where (f, g) is a pair of phase-space densities describing the distribution of the two species on the domain $[0, T] \times \mathbb{R} \times \mathbb{R}$. The potentials K'_{11} and K'_{22} are *self-interaction potentials* and model the behaviour between agents of the same species, whereas K'_{12} and K'_{21} are *cross-interaction potentials* and describe the interplay between individuals of opposite species. Moreover, ρ and η denote the associated macroscopic population densities, i.e.,

$$\rho(t,x) = \int_{\mathbb{R}} f(t,x,v)\,dv, \qquad \text{and} \qquad \eta(t,x) = \int_{\mathbb{R}} g(t,x,v)\,dv.$$

We equip system (65.1) with a non-negative initial datum $(f_0, g_0) \in L^1(\mathbb{R} \times \mathbb{R})^2$.

Models for collective behaviour have gained popularity in describing emergent phenomena in numerous fields such as social sciences [8], pedestrian flows [1], traffic flow, [2], and biology, see [3, 5, 7], and references therein. In particular, biological applications are often devoted to understanding the formation of patterns and self-organisation observed in nature, for instance, in swarms, schools of fish, and flocks of birds, see [6].

The existence theory for system (65.1) is studied in arbitrary dimension in [4].

Derivation of the numerical method

Consider the domain $Q_T := (0, T) \times (-L, L) \times \mathbb{R}$. In order to discretize it, we introduce the following strictly increasing sequences: $(t^n)_{n \in \{0,\dots,N_T\}} \subset [0, T]$ to discretize the time variable; $(x_{i-1/2})_{i \in \{0,\dots,N_x\}} \subset (-L, L)$ such that $x_{-1/2} = -L$ and $x_{N_x-1/2} = L$ to discretize the space variable; and $(v_{j+1/2})_{j \in \mathbb{Z}} \subset \mathbb{R}$ such that $v_{j+1/2} \to \pm\infty$ as $j \to \pm\infty$ to discretize the velocity variable. We then set $\Delta t := T/N_T, \Delta x_i = x_{i+1/2} - x_{i-1/2}$, and $\Delta v_j = v_{j+1/2} - v_{j-1/2}$, and we introduce the cells $C_{i,j} = (x_{i-1/2}, x_{i+1/2}) \times (v_{j-1/2}, v_{j+1/2})$, for $i \in \{0, \dots, N_x - 1\}$ and $j \in \mathbb{Z}$. We define $h := \max\{\Delta x_i, \Delta v_j\} > 0$, and we say the mesh is *admissible* if there is an $\alpha \in (0, 1)$ such that $\alpha h \leq \Delta x_i, \Delta v_j \leq h$.

To implement our scheme, we truncate the velocity domain choosing $v_h > 0$, such that $v_h \to \infty$ as $h \to 0$ and restrict $v \in (-v_h, v_h)$.

By integrating the differential equation over the cell $(t^n, t^{n+1}) \times C_{i,j}$, and using an upwind scheme to approximate the terms with the derivatives w.r.t. x and v and an explicit Euler approximation on the terms involving the time derivative, we end up with the scheme

$$p_{i,j}^{n+1} = \left(1 - \Delta t\left[\frac{|v_j|}{\Delta x_i} + \frac{|(\Upsilon_p)_i^n|}{\Delta v_j}\right]\right)p_{i,j}^n + \Delta t\frac{[v_j]^-}{\Delta x_i}p_{i+1,j}^n + \Delta t\frac{[v_j]^+}{\Delta x_i}p_{i-1,j}^n$$
$$+ \Delta t\frac{[(\Upsilon_p)_i^n]^+}{\Delta v_j}p_{i,j+1}^n + \Delta t\frac{[(\Upsilon_p)_i^n]^-}{\Delta v_j}p_{i,j-1}^n,$$

for $p \in \{f, g\}$, with $\Upsilon_f = K_{11}' * \rho + K_{12}' * \eta$ and $\Upsilon_g = K_{22}' * \eta + K_{21}' * \rho$.

Properties of the numerical method

We assume the CFL condition:

$$\frac{\Delta t}{|C_{i,j}|} \le \frac{(1-\xi)\alpha}{v_h + \mathcal{C}_W},$$

where $\mathcal{C}_W := \max_{i=1,2}\sum_{j=1}^2\|K_{ij}'\|_\infty$, with $\xi \in (0,1)$. The scheme preserves positivity and conservation of the mass. Moreover, the solutions to the scheme are bounded in L^p uniformly in time $t \in (0,T)$. Finally we provide an estimate on the tails of (f_h, g_h), proving that if $0 \le f_0 \le R$ and $0 \le g_0 \le R$, where $R(x,v) := \frac{C}{1+|v_j|^{\lambda_1}+|x_i|^{\lambda_2}}$, for $(x,v) \in C_{i,j}$, with $\lambda_1 > 1$, $\lambda_2 \ge 1$ and $\lambda_2 \le \lambda_1$, and $C > 0$, then f_h and g_h remain bounded.

Convergence of the numerical method and error estimate

The main result concerns the convergence of the numerical scheme. In particular, if $0 \le f_0 \le R$ and $0 \le g_0 \le R$, the CFL is satisfied, $K_{ij} \in W^{2,\infty}(-L, L)$, and $v_h h^{1/2} \to 0$ as $h \to 0$. Furthermore, we get

$$f_h(t,x,v) \rightharpoonup f(t,x,v), \qquad g_h(t,x,v) \rightharpoonup g(t,x,v),$$

weakly-$*$ in $L^\infty(Q_T)$ as $\Delta t, h \to 0$, where (f,g) is a solution to system (65.1), in the weak sense.

We now state our result concerning the error estimate. Let $f_0, g_0 \in C^2$ be non-negative such that $\text{supp}(p_0(x, \cdot)) \subset (-v_h, v_h)$, for $p_0 \in \{f_0, g_0\}$. Assume the CFL condition is satisfied and $K_{ij} \in W^{2,\infty}$. Then, we can establish the following convergence result:

$$\|f - f_h\|_{L^2}^2 + \|g - g_h\|_{L^2}^2$$
$$\le C\big[\Delta t + h^{1/2} + \|f_0 - f_h(0)\|_{L^2} + \|g_0 - g_h(0)\|_{L^2}\big],$$

for some $C > 0$ depending on T, L, v_h, $\mathcal{C}_W$, α, λ_1, λ_2, $\|f\|_{L^\infty}$, and $\|g\|_{L^\infty}$.

Finally, we provide some numerical results.

References

[1]   C. Appert-Rolland, P. Degond, and S. Motsch. "Two-way multi-lane traffic model for pedestrians in corridors". In: *Networks and Heterogeneous Media* 6 (2011), pp. 351–381.

[2]   R. Borsche, A. Klar, and M. Zanella. "Kinetic-controlled hydrodynamics for multilane traffic models". In: *Physica A: Statistical Mechanics and its Applications* 587 (2022), p. 126486. DOI: 10.1016/j.physa.2021.126486.

[3]   J. A. Cañizo, J. A. Carrillo, and J. Rosado. "A well-posedness theory in measures for some kinetic models of collective motion". In: *Math. Models Methods Appl. Sci.* 21 (July 2009). DOI: 10.1142/S0218202511005131.

[4]   Y.-P. Choi, S. Fagioli, and V. Iorio. *Small inertia limit for coupled kinetic swarming models*. 2024. arXiv: 2402.02854 [math.AP].

[5]   A. Mogilner and L. Edelstein-Keshet. "A non-local model for a swarm". In: *Journal of Mathematical Biology* 38.6 (June 1999), pp. 534–570. ISSN: 1432-1416. DOI: 10.1007/s002850050158.

[6]   C. M. Topaz and A. Bertozzi. "Swarming patterns in a two-dimensional kinematic model for biological groups". In: *SIAM Journal on Applied Mathematics* 65.1 (2004), pp. 152–174.

[7]   C. M. Topaz, A. Bertozzi, and M. A. Lewis. "A nonlocal continuum model for biological aggregation". In: *Bulletin of Mathematical Biology* 68 (2005), pp. 1601–1623.

[8]   G. Toscani. "Kinetic models of opinion formation". In: *Commun. Math. Sci.* 4 (Sept. 2006), pp. 481–496. DOI: 10.4310/CMS.2006.v4.n3.a1.

Entropy Residual Indicator for Finite Volume ADER schemes

Matteo Semplice and Alessandra Zappa*

Dipartimento di Scienza e Alta Tecnologia, Università dell'Insubria (Como, Italy)

Whenever we deal with conservation laws, the study of numerical entropy plays an important role for several reasons. Firstly, solutions for a system of conservation laws may lose their regularity in a finite time even if the initial data are smooth, giving rise to discontinuities. In this case, the existence of strong solution and the uniqueness of weak solutions are lost. To recover uniqueness, we consider as admissible only the weak solutions that satisfy an entropy inequality. For exact solutions, the inequality holds as equality unless a shock wave is present in the solution. This inequality derives from physical observations. In fact, in applications the entropy represents for convention the opposite of the physical entropy and the inequality means that for non-regular solutions the entropy must decrease (and the physical entropy increases).

We can define the numerical entropy production S_j^n in the $j - th$ cell at time t^n as the residual of the entropy inequality computed on the numerical solutions of the conservation law. In [2], it is been proved that for a first-order Runge-Kutta scheme, if the numerical entropy flux is consistent with the entropy flux, then S_j^n converges to zero with the same rate of the local truncation error in a region of smoothness and it is bounded by terms of order $O\left(\dfrac{1}{\Delta t}\right)$ if there is a region with a shock wave. Moreover, S_j^n is essentially negative definite for scalar conservation laws. For this reason, S_j^n can be considered as a posteriori error indicator for the finite volume scheme: indeed we obtain information about the size of the local truncation error and the presence of singularities in the solution. Therefore, an important application of the study of the numerical entropy is in developing stable high-order adaptive schemes which exploit the numerical entropy production to change the grid refinement or the order of the scheme to obtain more accurate predictions in a wide range of fields, such as fluid dynamics, gas dynamics, acoustics, electromagnetism, and traffic flow (see for example [3, 4]).

This work aims to extend this idea to ADER (Arbitrary Accuracy DERivative Riemann problem) time-stepping techniques, which are fully discrete schemes that solve the high-order Riemann problem approximately without semi-discretization nor Runge-Kutta methods (see [1]), in order to compare the results with the entropy production by the standard semidiscrete finite volume schemes. We will show that the numerical entropy production can be defined also in this context and it provides a scalar quantity computable for each space-time volume which, under grid refinement, decays to zero with the same rate of convergence of the scheme for smooth solutions, it is bounded on contact discontinuities

and divergent on shock waves. We will also present numerical evidence showing that it is essentially negative definite.

References

[1] M. Dumbser, D. S. Balsara, E. F. Toro, and C. D. Munz. "A Unified Framework for the Construction of One-Step Finite Volume and Discontinuous Galerkin Schemes on Unstructured Meshes". In: *J. Computat. Phys.* 227 (2008), pp. 8209–8253.

[2] G. Puppo and M. Semplice. "Numerical Entropy and Adaptivity for Finite Volume Schemes". In: *Commun. Computat. Phys.* 10.5 (2011), pp. 1132–1160.

[3] M. Semplice, A. Coco, and G. Russo. "Adaptive Mesh Refinement for Hyperbolic Systems based on Third-Order Compact WENO Reconstruction". In: *J. Sci. Comput.* 66 (2016), pp. 692–724. DOI: 10.1007/s10915-015-0038-z.

[4] M. Semplice and R. Loubere. "Adaptive-Mesh-Refinement for hyperbolic systems of conservation laws based on a posteriori stabilized high order polynomial reconstructions". In: *J. Computat. Phys.* 354 (2018), pp. 86–110. DOI: 10.1016/j.jcp.2017.10.031.

Multilevel Monte Carlo Methods with Smoothing

Anastasia Istratuca

University of Edinburgh, Heriot-Watt University

Uncertainty quantification (UQ) is a contemporary research area that deals with identifying, assessing and reducing uncertainties related to physical models, numerical algorithms, experiments and their predicted outcomes, and quantities of interest. Methodical computations of uncertainties and errors in simulations, and careful exploration of how they propagate through a model and impact its expected outcome, are vital in many applications for principled risk assessments and decision making.

One of the most common approaches to modelling physical phenomena consists of partial differential equations (PDEs), which allow for computer simulations through the use of modern numerical solvers. Such models can be found, for instance, in electrodynamics [13], fluid dynamics [6], and quantum mechanics [5]. In the latter case, the uncertainty arises from unknown parameters whose estimation from physical or experimental data is impractical.

The specific UQ path we follow in this work is based on modelling the unknown PDE coefficients as random parameters, so that their uncertainty can be defined in terms of statistical quantities such as probability density functions or covariance functions. Furthermore, this uncertainty can be traced through the model to the output by resolving the statistical estimates of various functionals related to the solution of the PDE model. These estimates are called quantities of interests and they can take, for example, the form of expected values or variances.

An effective approach to tackle these problems is the Monte Carlo (MC) method, which consists of generating several realisations of parameter values and subsequently solving the governing equation for many of these samples to approximate a specific quantity of interest. The advantages of MC are the ease of implementation, as well as the fact that the associated computational complexity does not grow with dimension [8]. Of course, these benefits are severely weakened if one considers that one or more PDEs must be solved for each MC sample, the cost of which is naturally dimension-dependent. In addition, MC suffers from an extremely slow convergence rate, making this approach intractable.

An alternative which aims to alleviate these issues is the Multilevel Monte Carlo (MLMC) method [2, 4]. It involves defining multiple levels of approximation that differ in computational cost. In the context of solving PDEs with random coefficients, MLMC levels can be defined by different grid resolutions to solve the governing equation. Thereafter, we cluster much of the computational effort into cheap estimates on a coarse mesh with low

accuracy. To increase the quality of the approximation, we compute "correction terms" on finer levels with progressively higher precision. Since most of the uncertainty can be captured on the coarsest grid, comparatively fewer samples are required on the subsequent finer levels to obtain a sufficiently good estimate of the quantity of interest. This architecture of levels, which divides the work required to achieve a certain accuracy, leads to a significant reduction in the overall computational complexity of MLMC compared to standard MC.

A technique widely used for sampling from a random field is the Karhunen-Loève (KL) expansion [7]. This technique has been extensively studied both theoretically and numerically for PDEs with log-normal random input with MLMC , e.g. [1], as well as with Quasi-Monte Carlo methods (QMC) and Multilevel Quasi-Monte Carlo methods (MLQMC), see, for example, the survey [9] and the references therein. Further alterations of this algorithm to accommodate the difficulties arising from random field models with short correlation lengths have been proposed in [12].

In this work, we focus on the circulant embedding technique for sampling from the random parameter. This technique offers a discrete representation of a random field on a given mesh, but it is both exact at these grid points and computationally efficient. This is in comparison with the KL-expansion, which, once truncated, offers a continuous approximation whose rate of convergence is intrinsically linked to the decay of the eigenvalues of the covariance kernel, which has a direct impact on the computational cost. The circulant embedding method has been integrated with MLMC and MLMQMC in [3, 10].

The main novelty of this work is the adaptation of the circulant embedding method to produce smooth approximations on coarse meshes of samples from extremely oscillatory random fields, i.e. with small correlation length, high variance and low regularity. This problem usually arises when considering large computational domains, in which the correlation length is considerably smaller than the size of the domain. This is of particular interest in MLMC for PDEs with random coefficients since the computational gains prompted by MLMC rest on using coarse meshes, which is usually not feasible for the problem at hand. A similar algorithm has been proposed in [11], albeit for random fields with large-scale fluctuations which still require a fine grid representation. In particular, Sawko et al. focus on deriving low-rank approximations of the covariance matrix of the random field without providing a theoretical analysis of the corresponding error.

Hence, we consider the computational efficiency of MC and MLMC methods applied to partial differential equations with random coefficients. In particular, we apply them to groundwater flow modeling, where a commonly used model for the unknown parameter is a random field. We use the circulant embedding procedure for sampling from the aforementioned coefficient. To improve the computational complexity of the MLMC estimator in the case of highly oscillatory random fields, we devise and implement a smoothing technique integrated into the circulant embedding method. This allows us to choose the coarsest mesh at the first level of MLMC regardless of the correlation length of the covariance function of the random field, leading to considerable savings in computational cost. We illustrate our results with numerical experiments, where we observe a saving of up to factor 5-10 in computational cost for accuracies of practical interest.

References

[1] K. A. Cliffe, M. B. Giles, R. Scheichl, and A. L. Teckentrup. "Multilevel Monte Carlo methods and applications to elliptic PDEs with random coefficients". en. In: *Comput. Visual Sci.* 14 (2011), pp. 3–15.

[2] M. B. Giles. "Multilevel Monte Carlo Path Simulation". en. In: *Operations Research* 56.3 (June 2008), pp. 607–617. ISSN: 0030-364X, 1526-5463. DOI: 10.1287/opre.1070.0496.

[3] I. G. Graham, F. Y. Kuo, D. Nuyens, R. Scheichl, and I. H. Sloan. "Quasi-Monte Carlo methods for elliptic PDEs with random coefficients and applications". en. In: *J. Comput. Phys.* 230 (2011), pp. 3668–3694.

[4] S. Heinrich. "Multilevel monte carlo methods". In: *Large-Scale Scientific Computing: Third International Conference, LSSC 2001 Sozopol, Bulgaria, June 6–10, 2001 Revised Papers 3.* Springer, 2001, pp. 58–67.

[5] I. H. Herron and M. R. Foster. *Partial Differential Equations in Fluid Dynamics*. Cambridge: Cambridge University Press, 2008.

[6] R. Howe. "Quantum mechanics and partial differential equations". In: *J. Funct. Anal.* 38 (1980), pp. 188–254.

[7] D. D. Kosambi. "Statistics in function space". In: *J. Indian Math. Soc. (N.S.)* 7 (1943), pp. 76–88.

[8] F. Y. Kuo and I. H. Sloan. "Lifting the curse of dimensionality". In: *Notices of the AMS* 52 (2005), pp. 1320–1328.

[9] F. Y. Kuo and D. Nuyens. "Application of Quasi-Monte Carlo Methods to PDEs with Random Coefficients – An Overview and Tutorial". In: *Monte Carlo and Quasi-Monte Carlo Methods*. Ed. by A. B. Owen and P. W. Glynn. Cham: Springer International Publishing, 2018, pp. 53–71.

[10] F. Y. Kuo, R. Scheichl, C. Schwab, I. H. Sloan, and E. Ullmann. "Multilevel Quasi-Monte Carlo methods for lognormal diffusion problems". en. In: *Math. Comp* 86 (2017), pp. 2827–2860.

[11] R. Sawko and M. J. Zimoń. "Effective Generation of Compressed Stationary Gaussian Fields". en. In: *SIAM/ASA J. Uncertain. Quantif.* 10 (2022), pp. 439–452.

[12] A. L. Teckentrup, R. Scheichl, M. B. Giles, and E. Ullmann. "Further analysis of multilevel Monte Carlo methods for elliptic PDEs with random coefficients". en. In: *Numer. Math.* 125 (2013), pp. 569–600.

[13] N. E. Tovmasyan, G. Zakaryan, and G. L.Z. *Boundary value problems for partial differential equations and applications in electrodynamics*. Singapore: World Scientific Publishing, 1994.

Mini-Symposium
Hierarchical Forecasting

Preface to the Symposium

Lorenzo Zambon, *Organizer*
IDSIA USI-SUPSI, Lugano

Hierarchical time series are collections of time series formed via aggregation. For example, the aggregation of the time series of the regional levels of tourism yields the time series of the national level of tourism. Forecasts for hierarchical time series should be *coherent*: the sum of the forecasts of the regional tourism levels should match the forecast for the national tourism level. The most popular technique to enforce coherence is called *reconciliation*, which adjusts the base forecasts computed for each time series to satisfy the summing constraints implied by the hierarchy. Forecast coherence is often required for aligned decision making; moreover, reconciliation has been shown to improve the quality of the forecasts. Hierarchical forecasting is a very active and rapidly growing research topic, with several significant applications in different areas, such as energy, retail, and macroeconomics. This mini-symposium will cover recent advancements in different aspects of the field.

List of the speakers

- Chiara Carrara, Università di Pavia

- Daniele Girolimetto, Università di Padova

- Raffaele Mattera, Università di Roma "La Sapienza"

- Lorenzo Zambon, IDSIA USI-SUPSI, Lugano

Enhanced Covariance Estimation for Hierarchical Time Series

Chiara Carrara[a,*]**, Dario Azzimonti**[b]**, Lorenzo Zambon**[b]**, and Giorgio Corani**[b]
[a] Department of Mathematics, Università degli studi di Pavia, Italy
[b] Idsia (Dalle Molle Institute for Artificial Intelligence), USI-SUPSI, Lugano, Switzerland.

Hierarchical time series (HTS) are a structured set of time series that are organized into multiple levels, reflecting different levels of aggregation. For example, in a business setting, sales data might be collected at various levels, such as individual stores, regions, and total national sales. These levels form a hierarchy where lower-level series (like individual store sales) sum up to higher-level series (like regional or national sales).

Accurate modelling of dependencies among these series is crucial in many fields, including the reconciliation of hierarchical forecasts. In this process, the h-step ahead base forecasts $\hat{y}_h$ are generated independently for each time series at all levels of the hierarchy. Forecast reconciliation then adjusts these forecasts to satisfy the linear constraints imposed by the hierarchical structure, ensuring consistency across all levels. The reconciled point forecasts $\tilde{y}_h$ are:

$$\tilde{y}_h = SG\hat{y}_h$$

where G is a suitable matrix and S represents the hierarchical constraints (Hyndman et al. [1]). A crucial problem in forecast reconciliation is to optimally determine matrix G.

Wickramasuriya et al.[3] formulated the problem as minimizing the trace (MinT) of the covariance matrix of the reconciled forecasts error $\text{Var}[y_{t+h} - \tilde{y}_h]$.

The resulting optimal matrix G is $G = (S'WS)^{-1}S'W^{-1}$, where W is the covariance matrix of the errors of the base forecasts. Thus, the accuracy of the reconciled forecasts substantially depends on the estimation of W.

Estimating the covariance matrix W is challenging. While the sample covariance matrix of residuals is a common choice, it can be unreliable or singular, especially when $n > T$. The most effective approach so far is to adopt the shrinkage estimator of the covariance matrix (Schäfer & Strimmer[2]), which computes a weighted average between the entries of the sample covariance matrix and those of the sample diagonal matrix.

In the experiments by Wickramasuriya et al.[3], the shrinkage estimator consistently yields better-reconciled forecasts than the sample covariance matrix. However, by shrinking towards a diagonal matrix, this approach assumes no prior information about the dependency structure among the variables. Yet, in reconciliation problems, the hierarchical structure suggest the presence of some conditional independencies.

To exploit this prior information we introduce a shrinkage method that shrinks the sample covariance matrix towards both the sample diagonal matrix and a third covariance matrix which encodes the conditional independences suggested on the hierarchical

structure.

This method could improve the accuracy of covariance estimation, particularly when the number of time series n is large or where the assumptions of conditional dependencies are well-supported by the data. In cases where these assumptions do not hold, the method should effectively reduce to the Schäfer & Strimmer[2] estimation.

To construct the third matrix, we analyze realistic dependency patterns within hierarchical time series. Our experimental results indicate that the most likely dependencies in the hierarchy occur among sibling variables when conditioned on their parent, a relationship naturally suggested by the hierarchical structure itself. It is reasonable to assume that variables aggregating to the same parent share substantial information, resulting in strong intercorrelations. Consequently, we integrate this hierarchical dependency structure in the construction of the third matrix used in the shrinkage process. Additionally, we derive a closed-form solution for the shrinkage coefficients by applying the strategy in Schäfer & Strimmer[2]. In this way, we aim to provide an efficient algorithm for computing the shrunk matrix that minimize the mean square error relative to the true covariance matrix.

References

[1]   R. J. Hyndman, R. A. Ahmed, G. Athanasopoulos, and H. L. Shang. "Optimal combination forecasts for hierarchical time series". In: *Computational Statistics & Data Analysis* 55.9 (2011), pp. 2579–2589.

[2]   J. Schäfer and K. Strimmer. "A shrinkage approach to large-scale covariance matrix estimation and implications for functional genomics". In: *Stat Appl Genet Mol Biol.* (2005).

[3]   S. L. Wickramasuriya, G. Athanasopoulos, and R. J. Hyndman. "Optimal Forecast Reconciliation for Hierarchical and Grouped Time Series Through Trace Minimization". In: *Journal of the American Statistical Association* 114.526 (2019), pp. 804–819.

Forecast reconciliation with fuzzy clustering

Raffaele Mattera

Sapienza University of Rome, Italy

Forecast reconciliation is a statistical technique dealing with multivariate time series following a hierarchical structure, or that more generally adhere to linear constraints [1, 4].

Let $\boldsymbol{b}_t$ be the vector of all N time series of interest observed at time t, and let $\boldsymbol{a}_t$ be a corresponding vector of n_a aggregated time series, that is,

$$\boldsymbol{a}_t = \boldsymbol{A}\boldsymbol{b}_t,$$

with $\boldsymbol{A}$ the aggregation matrix, defining how the bottom time series $\boldsymbol{b}_t$ aggregate according to the linear constraints. The full vector of time series at time t is given by

$$\boldsymbol{y}_t = \begin{bmatrix} \boldsymbol{a}_t \\ \boldsymbol{b}_t \end{bmatrix} = \boldsymbol{S}\boldsymbol{b}_t, \tag{70.1}$$

where $\boldsymbol{S} = \begin{bmatrix} \boldsymbol{A} \\ \boldsymbol{I}_N \end{bmatrix}$ denotes the "summation" matrix of dimension $n \times N$, where $n = n_a + N$ and $\boldsymbol{I}_N$ is the N-dimensional identity matrix.

Let $\hat{\boldsymbol{y}}_h$ be the vector of h-step-ahead base forecasts obtained with a generic forecasting model applied to each n time series separately. The motivation behind forecast reconciliation is that, while time series $\boldsymbol{y}_t$ naturally aggregate according to a hierarchical structure given by $\boldsymbol{A}$, the forecasts $\hat{\boldsymbol{y}}_h$ do not. Optimal forecast reconciliation techniques, such as the Minimuim Trace (MinT) [5], provide an ex-post adjustment to the forecasts $\hat{\boldsymbol{y}}_h$ and make them coherent with the aggregation structure. More precisely, we define coherent forecasts as

$$\tilde{\boldsymbol{y}}_h = \boldsymbol{M}\hat{\boldsymbol{y}}_h,$$

where $\boldsymbol{M}$ is a $n \times n$ mapping matrix, whose role is to make the base forecasts $\hat{\boldsymbol{y}}_h$ coherent with the aggregation (70.1).

Following a recent literature, we note that the aggregation matrix $\boldsymbol{A}$ is not always known in practice. This is the case of cause of death in mortality forecasting [2] or of stock prices in the case of financial forecasting [3]. Nevertheless, also when suitable known hierarchies can be found, it is always possible to define additional hierarchies using unsupervised learning approaches [6]. Following [3], we define the aggregation matrix under unknown hierarchy assumption as

$$\boldsymbol{A} = \begin{bmatrix} \boldsymbol{1}' \\ \boldsymbol{U}' \end{bmatrix}, \tag{70.2}$$

with U being a membership matrix of dimension $n_a \times G$ with G the number of clusters or groups. Each element of U, called $u_{i,g}$ takes value of $u_{i,g} = 1$ if the ith bottom time series belongs to the gth cluster and $u_{i,g} = 0$ otherwise.

In this paper, we consider the case of fuzzy hierarchies in (70.2). With fuzziness, the elements of the U matrix are no longer binary, and can take values between 0 and 1, indicating the likelihood of each unit being clustered in the gth cluster. The membership matrix can be found using fuzzy clustering algorithms. The fuzzy G-means algorithm can be used to estimate the matrix U. The fuzzy G-means is the iterative solution of the following minimization problem

$$\min_{u_{i,g}, \boldsymbol{b}_g} J(\boldsymbol{U}, \boldsymbol{B}) = \sum_{i=1}^{N} \sum_{g=1}^{G} u_{i,g}^m d^2(\boldsymbol{b}_i, \boldsymbol{b}_g),$$

under the constraint $\sum_{g=1}^{G} u_{i,g} = 1$, where U is the membership degree matrix with generic element $0 \leq u_{i,g} \leq 1$ defining the membership degree of the ith unit to the gth cluster, $\boldsymbol{B}$ the set of cluster prototypes, $d^2(\boldsymbol{b}_i, \boldsymbol{b}_g)$ is the distance between the ith bottom time series and the g-th cluster prototype and $m > 1$ is the fuzzifier parameter. We discuss the properties of fuzzy hierarchical forecasting and some of possible applications.

References

[1] D. Girolimetto and T. Di Fonzo. "Point and probabilistic forecast reconciliation for general linearly constrained multiple time series". In: *Statistical Methods & Applications* 33.2 (2024), pp. 581–607.

[2] H. Li, H. Li, Y. Lu, and A. Panagiotelis. "A forecast reconciliation approach to cause-of-death mortality modeling". In: *Insurance: Mathematics and Economics* 86 (2019), pp. 122–133.

[3] R. Mattera, G. Athanasopoulos, and R. J. Hyndman. *Improving out-of-sample forecasts of stock price indexes with forecast reconciliation and clustering.* Monash University, Department of Econometrics and Business Statistics, 2023.

[4] A. Panagiotelis, G. Athanasopoulos, P. Gamakumara, and R. J. Hyndman. "Forecast reconciliation: A geometric view with new insights on bias correction". In: *International Journal of Forecasting* 37.1 (2021), pp. 343–359.

[5] S. L. Wickramasuriya, G. Athanasopoulos, and R. J. Hyndman. "Optimal forecast reconciliation for hierarchical and grouped time series through trace minimization". In: *Journal of the American Statistical Association* 114.526 (2019), pp. 804–819.

[6] B. Zhang, A. Panagiotelis, and H. Li. *Constructing hierarchical time series through clustering: Is there an optimal way for forecasting?* ARXIV: 2404.06064. 2024.

Forecast reconciliation: Not only hierarchies

Daniele Girolimetto
Department of Statistical Sciences, University of Padova
Via Cesare Battisti 241, 35121 Padova, Italy

Time series can often be naturally disaggregated by various nested and/or crossed attributes of interest [3]. As an example, sales data can be disaggregated by product categories, and then by product subcategories, down to the Stock Keeping Unit level. Alternatively, sales data can be disaggregated by geographic divisions. Following [5], a hierarchical (grouped) time series is a linearly constrained multiple time series consisting of a collection of time series that follows one (or more) hierarchical aggregation structures (*i.e.* Figure 71.1). Forecast reconciliation is the post-forecasting process intended to revise a set of incoherent forecasts (also known as base) into coherent forecasts (also known as reconciled) which satisfy a given set of linear constraints.

Most of the forecast reconciliation results move from the classic reconciliation formula valid for the *structural representation* [1] of a hierarchical time series:

$$\widetilde{\boldsymbol{y}} = \boldsymbol{S} \left(\boldsymbol{S}' \boldsymbol{W}^{-1} \boldsymbol{S} \right)^{-1} \boldsymbol{S}' \boldsymbol{W}^{-1} \widehat{\boldsymbol{y}} \tag{71.1}$$

where $\widehat{\boldsymbol{y}}$ is the $(n \times 1)$ vector of base forecasts, $\boldsymbol{W}$ is an $(n \times n)$ positive definite matrix [6] and $\boldsymbol{S}$ is the $(n \times n_b)$ summing matrix with elements in $\{0, 1\}$, indicating simple summation relationships between variables. The formula (71.1) essentially maps the base forecasts into a lower-dimensional space defined by the (n_b) bottom-level series of the hierarchy, reconciles them in this space, and then aggregates the reconciled bottom-level forecasts back to the higher levels using a structural matrix. Unlike the structural approach, the projection approach [6] doesn't depend on classifying variables as belonging to a specific level within a hierarchy. Instead, it utilizes a *zero-constrained representation* that expresses the constraints within the data as a system of linear equations. The projection approach determines reconciled forecasts by finding the closest point in the "coherent subspace" [5], defined by the constraints, to the initial set of base forecasts.
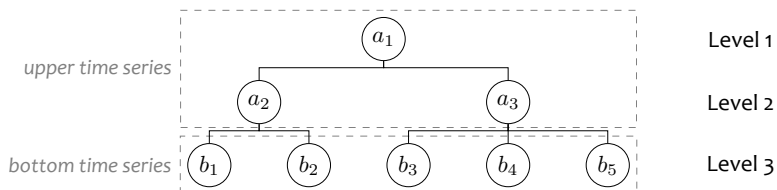

Figure 71.1: A hierarchical structure for a linearly constrained multiple time series.
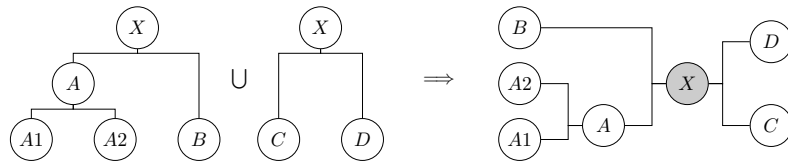
Figure 71.2: A general linearly constrained structure: two hierarchies sharing only the same top-level variable X, with different bottom variables, $\{A1, \ A2, \ B\}$ and $\{C, \ D\}$.

The interchangeability between *structural* and *zero-constrained* representations, easily recovered for a grouped time series, is not always straightforward when a general linearly constrained multiple time series (*i.e.* Figure 71.2) is considered. In this case, to derive a *structural-like* reconciliation formula, we need to represent the constraints as a system of linear equations, moving away from the summing matrix S to a matrix that captures these relationships [2]. Using linear algebra techniques like Reduced Row Echelon Form or QR decomposition [4], the system is simplified to identify free and constrained variables. These variables play a role analogous to the bottom and upper variables, respectively, in a grouped setting. A new representation is thus created that resembles traditional hierarchical reconciliation approaches. The transformation results in a linear combination matrix that adjusts the base forecasts to ensure they satisfy all the constraints, producing coherent forecasts that maintain the integrity of the underlying linear relationships. This method extends the applicability of forecast reconciliation to a broader range of scenarios, ensuring consistency across forecasts in complex, real-world structures.

References

[1]   G. Athanasopoulos, R. A. Ahmed, and R. J. Hyndman. "Hierarchical forecasts for Australian Domestic Tourism". In: *International Journal of Forecasting* 25.1 (2009), pp. 146–166.

[2]   D. Girolimetto and T. Di Fonzo. "Point and probabilistic forecast reconciliation for general linearly constrained multiple time series". In: *Statistical Methods & Applications* 33 (2024), pp. 581–607.

[3]   R. J. Hyndman and G. Athanasopoulos. *Forecasting: Principles and Practice*. 3rd. Melbourne: OTexts. https://otexts.com/fpp3/, 2021.

[4]   T. Lyche. *Numerical Linear Algebra and Matrix Factorizations*. New York: Springer, 2020. ISBN: 978-3-030-36468-7.

[5]   A. Panagiotelis, G. Athanasopoulos, P. Gamakumara, and R. J. Hyndman. "Forecast reconciliation: A geometric view with new insights on bias correction". In: *International Journal of Forecasting* 37.1 (2021), pp. 343–359.

[6]   S. L. Wickramasuriya, G. Athanasopoulos, and R. J. Hyndman. "Optimal forecast reconciliation for hierarchical and grouped time series through trace minimization". In: *Journal of the American Statistical Association* 114.526 (2019), pp. 804–819.

Probabilistic forecast reconciliation via conditioning
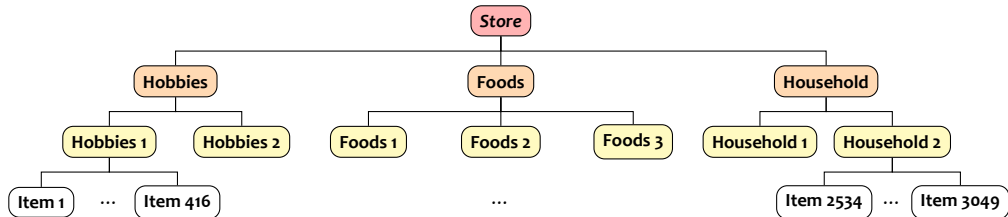
Lorenzo Zambon

IDSIA USI-SUPSI, Lugano

Figure 72.1: Example of hierarchical time series, taken from the *M5* competition [6].

Hierarchical time series are collections of time series that are formed via aggregation, and therefore satisfy some summing constraints. For example, the total daily sales of a store is given by the sum of the daily sales of each individual item; there may also be other aggregated levels, such as product category or store department (Fig. 72.1). The hierarchy can be expressed as

$$\mathbf{u}_t = \mathbf{A}\mathbf{b}_t,$$

where $\mathbf{u}_t$ is the vector of all the aggregated, or *upper*, time series, and $\mathbf{b}_t$ is the vector of all the disaggregated, or *bottom*, time series. The aggregation matrix $\mathbf{A}$, which is made of 0 and 1, describes how the bottom series aggregate to the upper series. Hierarchical forecasts should be *coherent*: i.e., they should satisfy the hierarchy constraints. This means that the sum of the forecasts for each individual item should match the forecast for the store, and analogously for the other aggregation levels.

Hierarchical forecasts are usually generated in two steps. First, incoherent forecasts are generated independently for each time series (*base forecasts*). Then, they are adjusted to become coherent (*reconciliation*). Reconciled forecasts, besides being coherent, are generally more accurate than the base forecasts. Most methods [5, 7] only reconcile the point forecasts. Only probabilistic forecasts [4], however, allow the quantification of uncertainty of the predictions, which is of crucial importance for decision making. We thus focus on the probabilistic case, where the base forecast of each time series is in the form of a predictive distribution, rather than a single point.

We denote by $\hat{\pi}$ the joint base forecast distribution for all the n time series of the hierarchy, computed at some time t for time $t + h$ (the time index is dropped for simplicity).
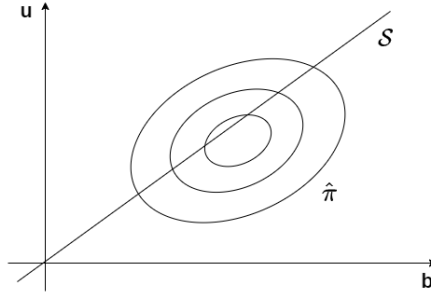
Figure 72.2: 2-dimensional representation of the joint base forecast distribution $\hat{\pi}$ and the coherent subspace $\mathcal{S}$

Moreover, we define the coherent subspace $\mathcal{S}$ as the set of points of $\mathbb{R}^n$ that satisfy the hierarchy constraints, i.e.

$$\mathcal{S} := \left\{ \begin{bmatrix} \mathbf{u} \\ \mathbf{b} \end{bmatrix} s.t.\ \mathbf{u} = \mathbf{Ab} \right\}.$$

In Figure (72.2), we show a two-dimensional representation of $\hat{\pi}$, which has support over $\mathbb{R}^n$. The base forecast distribution $\hat{\pi}$ in incoherent, since it gives positive probability to regions of points that do not satisfy the constraints; in other words, its support is not contained in $\mathcal{S}$. Probabilistic reconciliation yields a coherent joint predictive distribution for the entire hierarchy, i.e., a distribution supported on $\mathcal{S}$.

Our approach to probabilistic reconciliation is based on conditioning [2, 8, 9, 10]: the reconciled distribution $\tilde{\pi}$ is obtained by conditioning the base forecast distribution $\hat{\pi}$ on the hierarchy constraints. From a geometric perspective, reconciliation via conditioning is equivalent to slicing $\hat{\pi}$ over the coherent subspace $\mathcal{S}$. The reconciled distribution $\tilde{\pi}$ can be expressed, up to a normalizing constant, as

$$\tilde{\pi}(\mathbf{u}, \mathbf{b}) \propto \hat{\pi}(\mathbf{Ab}, \mathbf{b}) \mathbf{1}_{\mathbf{u}=\mathbf{Ab}}. \tag{72.1}$$

Here, $\hat{\pi}$ and $\tilde{\pi}$ denote either the density or the probability mass function, depending whether the distributions are continuous or discrete, but the same formula (72.1) holds in both cases [9]. Moreover, eq. (72.1) has been recently proved to hold also in the *mixed* case, where the bottom base forecasts are discrete and the upper are continuous [10].

If the base forecast distribution is a multivariate Gaussian, the reconciled distribution is Gaussian and can be analytically computed [2, 8]. Interestingly, the reconciled mean coincides with the optimal reconciled point forecast (minT [7]). In general, however, the reconciled distribution is not available in parametric form: we thus need to resort to sampling approaches [3, 9, 10].

Reconciliation via conditioning works with any type of base forecasts: continuous, discrete, or even mixed. Several experiments show substantial improvements in the quality of the reconciled forecasts over the base forecasts. Finally, all of the algorithms are very

efficient, and require few seconds even for large hierarchies; they are implemented in the R package *bayesRecon* [1].

References

[1]   D. Azzimonti, N. Rubattu, L. Zambon, and G. Corani. *bayesRecon: Probabilistic Reconciliation via Conditioning*. R package version 0.2.0. 2023. URL: `https://CRAN.R-project.org/package=bayesRecon`.

[2]   G. Corani, D. Azzimonti, J. P. Augusto, and M. Zaffalon. "Probabilistic Reconciliation of Hierarchical Forecast via Bayes' Rule." In: *Proc. European Conf. On Machine Learning and Knowledge Discovery in Database ECML/PKDD*. Vol. 3. 2020, pp. 211–226.

[3]   G. Corani, D. Azzimonti, and N. Rubattu. "Probabilistic reconciliation of count time series". In: *International Journal of Forecasting* 40.2 (2024), pp. 457–469.

[4]   T. Gneiting and M. Katzfuss. "Probabilistic forecasting". In: *Annual Review of Statistics and Its Application* 1.1 (2014), pp. 125–151.

[5]   R. J. Hyndman, R. A. Ahmed, G. Athanasopoulos, and H. L. Shang. "Optimal combination forecasts for hierarchical time series". In: *Computational Statistics & Data Analysis* 55.9 (2011), pp. 2579–2589.

[6]   S. Makridakis, E. Spiliotis, and V. Assimakopoulos. "The M5 competition: Background, organization, and implementation". In: *International Journal of Forecasting* 38.4 (2022), pp. 1325–1336.

[7]   S. L. Wickramasuriya, G. Athanasopoulos, and R. J. Hyndman. "Optimal forecast reconciliation for hierarchical and grouped time series through trace minimization". In: *Journal of the American Statistical Association* 114.526 (2019), pp. 804–819.

[8]   L. Zambon, A. Agosto, P. Giudici, and G. Corani. "Properties of the reconciled distributions for Gaussian and count forecasts". In: *International Journal of Forecasting* In press (2024).

[9]   L. Zambon, D. Azzimonti, and G. Corani. "Efficient probabilistic reconciliation of forecasts for real-valued and count time series". In: *Statistics and Computing* 34.1 (2024), p. 21.

[10]   L. Zambon, D. Azzimonti, N. Rubattu, and G. Corani. "Probabilistic reconciliation of mixed-type hierarchical time series". In: *The 40th Conference on Uncertainty in Artificial Intelligence*. 2024.

Mini-Symposium Mathematical Frameworks and Numerical Methods for Complex Physical Systems

Preface to the Symposium

Nella Rotundo, *Organizer*
Department of Mathematics "Ulisse Dini", University of Florence, Italy

This mini-symposium will bring together young applied mathematicians to discuss recent advancements in mathematical modeling and numerical analysis of complex physical systems. The focus will be on Hybrid Boltzmann–BGK Models and Hydrodynamic Limits, which use kinetic theory and fluid dynamics to describe the behavior of gas mixtures and derive macroscopic equations from microscopic interactions. Discussions will also cover Numerical Methods for Kinetic Equations, emphasizing the development and analysis of computational algorithms that ensure high accuracy, stability, conservation, and positivity. Additionally, the Schrödinger-Poisson System will be examined, focusing on quantum mechanical modeling and numerical techniques for solving the Schrödinger equation in quantum devices. Lastly, the symposium will address Classical and Quantum Transport Models, studying transport phenomena using equations like the Wigner equation and exploring optimal control problems in both classical and quantum contexts.

List of the speakers

- Giulia Aliffi, University of Catania giulialiffi16@icloud.com

- Bernardo Collufio, Gran Sasso Science Institute bernardocollufio00@gmail.com

- Giorgio Martalò, University of Parma giorgio.martalo@unipr.it

- Sara Nicoletti, University of Florence sara.nicoletti@unifi.it

Semi-lagrangian schemes in Kinetic Theory of Gases and Plasmas

Bernardo Collufio
GSSI Institute

Kinetic equations are well known for their applications in several fields such as gas dynamics [5], plasma physics [12], traffic flow [11], swarming dynamics [4], and socioeconomic modelling [13]. For this reason, several numerical methods for solving this type of equations have been introduced and studied in the last decades. Among these, there are the Eulerian methods, which consist of a direct discretization of the involved equation on an Eulerian grid. Although this approach provides an highly accurate approximation of the solution with good preservation of underlying fundamental properties of the system, such as the positivity of the solution [10], it suffers from classic CFL condition on the time step, which may compromise the efficiency of the schemes. Particle methods are another class of approaches that recently gained popularity. This class of methods includes the Direct Simulation Monte Carlo (DSMC) [1], which approximates the Boltzmann equation of rarefied gas dynamics by simulating pairwise collisions stochastically, and the *particle-in-cell* methods [2] widely adopted in plasma physics, where the unknown PDF is approximated by Delta functions centred on a finite number of macroparticles trajectories determined by Newton's laws. Stochastic methods are advantageous because they are able to better handle the convection term and avoid memory waste, expansive computations of integral terms and CFL restrictions, and automatically preserves macroscopic moments. Despite these benefits, Stochastic methods are strongly affected by noise, and thus require a prohibitive amount of computations to produce an accurate solutions, especially when the solution is close to thermodynamical equilibrium.

Recently, semi-Lagrangian schemes have shown promising results in terms of accuracy and stability across a wide range of problems including Boltzmann equations [3], BGK equations [6, 9], and Vlasov-type equations [8]. These methods rely on a Cartesian mesh, but they handle the convective part by considering the Lagrangian formulation of the given equation and applying a time scheme over characteristics. After that, the PDF is reconstructed on internal values of the mesh through a suitable interpolation technique. The main advantage of semi-Lagrangian methods is that the CFL conditions are much less restricted if compared to Eulerian-based methods, resulting in a higher efficiency and avoiding accumulation of interpolation errors. Regardless, significant conservation errors may appear even with high order time schemes and spatial reconstructions when non-linear interpolation techniques are involved.

The talk is divided in two parts. In the first part, we review conservative semi-Lagrangian schemes for kinetic equations, which allow conservation of density, mean velocity and temperature by using a conservative reconstruction introduced in [7] together with suitable techniques for ensuring conservation in presence of Boltzmann or BGK operators. In the second part of the talk, we present our original contribution on the preservation of some fundamental properties of the equations, in particular we discuss the positivity preservation of the solution, which is often not guaranteed for semi-Lagrangian schemes.

References

[1]   G. Bird. *Molecular Gas Dynamics and the Direct Simulation of Gas Flows*. Molecular Gas Dynamics and the Direct Simulation of Gas Flows v. 1. Clarendon Press, 1994.

[2]   C. K. Birdsall and A. B. Langdon. *Plasma physics via computer simulation*. Taylor and Francis, 2005.

[3]   S. Boscarino, S. Y. Cho, and G. Russo. "A conservative semi-Lagrangian method for inhomogeneous Boltzmann equation". In: *Journal of Computational Physics* 498 (2024).

[4]   J. A. Carrillo, M. Fornasier, G. Toscani, and F. Vecil. "Particle, kinetic, and hydrodynamic models of swarming". In: *Mathematical Modeling of Collective Behavior in Socio-Economic and Life Sciences*. Birkhäuser Boston, 2010, pp. 297–336.

[5]   C. Cercignani. *The Boltzmann equation and its applications*. Vol. 67. Applied Mathematical Sciences. Springer, 1988.

[6]   S. Y. Cho, S. Boscarino, M. Groppi, and G. Russo. *Conservative semi-Lagrangian schemes for a general consistent BGK model for inert gas mixtures*. 2020.

[7]   S. Y. Cho, S. Boscarino, G. Russo, and S.-B. Yun. "Conservative semi-Lagrangian schemes for kinetic equations Part I: Reconstruction". In: *Journal of Computational Physics* 432 (2021).

[8]   S. Y. Cho, S. Boscarino, G. Russo, and S.-B. Yun. "Conservative semi-Lagrangian schemes for kinetic equations Part II: Applications". In: *Journal of Computational Physics* 436 (2021).

[9]   M. Groppi, G. Russo, and G. Stracquadanio. "Semi-Lagrangian Approximation of BGK Models for Inert and Reactive Gas Mixtures". In: *From Particle Systems to Partial Differential Equations*. Springer International Publishing, 2018, pp. 53–80.

[10] J. Hu, R. Shu, and X. Zhang. *Asymptotic-preserving and positivity-preserving implicit-explicit schemes for the stiff BGK equation*. ARXIV: 1708.06279. 2018.

[11] A. Klar and R. Wegener. "Kinetic Traffic Flow Models". In: *Modeling in Applied Sciences: A Kinetic Theory Approach*. Birkhäuser Boston, 2000, pp. 263–316.

[12] D. Nicholson. *Introduction to Plasma Theory*. Plasma Physics Series. Wiley, 1983.

[13] L. Pareschi and G. Toscani. *Interacting Multiagent Systems: Kinetic equations and Monte Carlo methods*. OUP Catalogue. Oxford University Press, 2013.

New Strategy for Solving the Schrödinger-Poisson System

Giulia Elena Aliffi*, **Giovanni Nastasi**, and **Vittorio Romano**

Dipartimento di Matematica e Informatica, Università degli Studi di Catania, Italy

A Resonant Tunnelling Diode (RTD) is a semiconductor device that thanks to its properties (low power, high-speed, compatibility with MOSFETs…) has gained increasing relevance in the electronic field. The typical structure of a resonant tunnelling diode is a Double Barrier Quantum Well Structure.

The aim of this talk is to introduce a new strategy to get stationary solutions of a RTD in a ballistic regime. Following the approach of [4, 6], we treat the device as an open-quantum system of one dimension, composed of an active region and two large reservoirs which are in thermal equilibrium and constant potential. The active region, which is the region where electrons are injected and the relevant physical effects take place, consists of a quantum well surrounded by barriers [4, 6]. The length of the device is supposed to be L so that the computational domain to consider is $[0, L]$. The active area, is also divided in three regions: two of them equipped with high doping density n_D^1 and one with low density n_D^2 [4, 6]:

$$n_D(x) = \begin{cases} n_D^1 & \text{if } x \in [0, a_1] \cup [a_6, L] \\ n_D^2 & \text{else} \end{cases}$$

where $a_i, i = 1, \ldots, 6$ are points of the domain such that $a_1 < a_2 < \ldots < a_6$. In addition, we apply to the active region an electrostatic potential V_e whose expression can be found [4]. The waves ψ of the electrons injected at $x = 0$ or $x = L$ satisfy the stationary Schrödinger equation and according to the sign of the momentum p, a suitable set of boundary conditions. In particular, we get that in the active region, the equation to solve is [4, 6]:

$$-\frac{\hbar^2}{2m^*}\Psi'' - qV(x)\Psi = E\Psi \tag{75.1}$$

under the conditions:

- if $p > 0$:

$$\begin{aligned} \Psi'(L) &= i\frac{p_+(p)}{\hbar}\Psi(L) \\ 2i\frac{p}{\hbar} &= i\frac{p}{\hbar}\Psi(0) + \Psi'(0) \end{aligned} \tag{75.2}$$

with $E = \frac{p^2}{2m^*} - qV_0$ and

$$p_+(p) = \begin{cases} \sqrt{p^2 + 2m^*q(V_L - V_0)} & \text{if } p^2 + 2m^*q(V_L - V_0) > 0 \\ i\sqrt{-p^2 - 2m^*q(V_L - V_0)} & \text{otherwise} \end{cases}$$

- if p<0:

$$\begin{aligned} \Psi'(0) &= -i\frac{p_-(p)}{\hbar}\Psi(0) \\ 2i\frac{p}{\hbar} &= i\frac{p}{\hbar}\Psi(L) + \Psi'(L) \end{aligned} \tag{75.3}$$

with $E = \frac{p^2}{2m^*} - qV_L$ and

$$p_-(p) = \begin{cases} \sqrt{p^2 - 2m^*q(V_L - V_0)} & \text{if } p^2 - 2m^*q(V_L - V_0) > 0 \\ i\sqrt{2m^*q(V_L - V_0) - p^2} & \text{otherwise} \end{cases}$$

In literature there are several numerical methods to solve these equations [1, 4, 6]. Our approach to the problem consists in writing the wave function ψ in terms of the phase function $S(x)$ and the density function $n(x)$, leading to $\psi(x) = \sqrt{n(x)}\exp\frac{iS(x)}{\hbar}$. Then, by substituting $\psi(x) = \sqrt{n(x)}\exp\frac{iS(x)}{\hbar}$ in the equations (75.1), (75.2), (75.3), we then obtain the following quantum hydrodynamic model [5]:

$$\begin{cases} div\left(\frac{n}{m^*}\nabla S\right) = 0 \\ \frac{|\nabla S|^2}{2m^*} - \frac{\hbar^2}{2m^*}\frac{1}{\sqrt{n}}\Delta\sqrt{n} - qV = E \end{cases}$$

under the conditions[1]:

- if $p > 0$ and $p^2 + 2m^*q(V_L - V_0) > 0$:

$$\cos\left(\frac{S(0)}{\hbar}\right)\frac{n'(0)}{2\sqrt{n(0)}} - \frac{p}{\hbar}\sqrt{n(0)}\sin\left(\frac{S(0)}{\hbar}\right) - \sin\left(\frac{S(0)}{\hbar}\right)\frac{S'(0)}{\hbar}\sqrt{n(0)} = 0$$

$$\frac{2p}{\hbar} = \cos\left(\frac{S(0)}{\hbar}\right)\frac{p}{\hbar}\sqrt{n(0)} + \cos\left(\frac{S(0)}{\hbar}\right)\frac{S'(0)}{\hbar}\sqrt{n(0)} + \sin\left(\frac{S(0)}{\hbar}\right)\frac{n'(0)}{2\sqrt{n(0)}}$$

$$n'(L) = 0 \qquad\qquad S'(L) = p_+(p)$$

- if $p > 0$ and $p^2 + 2m^*q(V_L - V_0) < 0$:

$$\cos\left(\frac{S(0)}{\hbar}\right)\frac{n'(0)}{2\sqrt{n(0)}} - \frac{p}{\hbar}\sqrt{n(0)}\sin\left(\frac{S(0)}{\hbar}\right) - \sin\left(\frac{S(0)}{\hbar}\right)\frac{S'(0)}{\hbar}\sqrt{n(0)} = 0$$

$$\frac{2p}{\hbar} = \cos\left(\frac{S(0)}{\hbar}\right)\frac{p}{\hbar}\sqrt{n(0)} + \cos\left(\frac{S(0)}{\hbar}\right)\frac{S'(0)}{\hbar}\sqrt{n(0)} + \sin\left(\frac{S(0)}{\hbar}\right)\frac{n'(0)}{2\sqrt{n(0)}}$$

$$\frac{n'(L)}{2\sqrt{n(L)}} + \frac{\sqrt{n(L)}}{\hbar}\sqrt{-p^2 - 2m^*q(V_L - V_0)} = 0 \qquad\qquad \frac{\sqrt{n(L)}}{\hbar}S'(L) = 0$$

[1] the value of E depends on the sign of p

- if $p < 0$ and $p^2 - 2m^* q(V_L - V_0) > 0$:

$$n'(0) = 0 \qquad\qquad S'(0) = -p_-(p)$$

$$\cos\left(\frac{S(L)}{\hbar}\right)\frac{n'(L)}{2\sqrt{n(L)}} - \frac{p}{\hbar}\sqrt{n(L)}\sin\left(\frac{S(L)}{\hbar}\right) - \sin\left(\frac{S(L)}{\hbar}\right)\frac{S'(L)}{\hbar}\sqrt{n(L)} = 0$$

$$\frac{2p}{\hbar} = \cos\left(\frac{S(L)}{\hbar}\right)\frac{p}{\hbar}\sqrt{n(L)} + \cos\left(\frac{S(L)}{\hbar}\right)\frac{S'(L)}{\hbar}\sqrt{n(L)} + \sin\left(\frac{S(L)}{\hbar}\right)\frac{n'(L)}{2\sqrt{n(L)}}$$

- if $p < 0$ and $p^2 - 2m^* q(V_L - V_0) < 0$:

$$\cos\left(\frac{S(L)}{\hbar}\right)\frac{n'(L)}{2\sqrt{n(L)}} - \frac{p}{\hbar}\sqrt{n(L)}\sin\left(\frac{S(L)}{\hbar}\right) - \sin\left(\frac{S(L)}{\hbar}\right)\frac{S'(L)}{\hbar}\sqrt{n(L)} = 0$$

$$\frac{2p}{\hbar} = \cos\left(\frac{S(L)}{\hbar}\right)\frac{p}{\hbar}\sqrt{n(L)} + \cos\left(\frac{S(L)}{\hbar}\right)\frac{S'(L)}{\hbar}\sqrt{n(L)} + \sin\left(\frac{S(L)}{\hbar}\right)\frac{n'(L)}{2\sqrt{n(L)}}$$

$$\frac{n'(0)}{2\sqrt{n(0)}} - \frac{\sqrt{n(0)}}{\hbar}\sqrt{-p^2 + 2m^* q(V_L - V_0)} = 0 \qquad\qquad \sqrt{n(0)}S'(0) = 0$$

The goal of my talk is to show how to handle these equations, discuss the advantages of this procedure, and present some numerical results.

References

[1] A. Arnold. "Mathematical Concepts of Open Quantum Boundary Conditions". In: *Transport Theo. Stat.* 30.4-6 (2001), pp. 561–584. DOI: 10.1081/TT-100105939.

[2] R. Bhukya, G. Hampika, and M. Guduri. "Resonant Tunneling Diodes: Working and Applications". In: *Energy Systems, Drives and Automations*. Springer Singapore, 2020, pp. 187–192. ISBN: 9789811550898. DOI: 10.1007/978-981-15-5089-8_17.

[3] D. Dragoman and M. Dragoman. "Tunneling Devices". In: *Encyclopedia of Condensed Matter Physics*. Elsevier, 2005, pp. 269–277. ISBN: 9780123694010. DOI: 10.1016/b0-12-369401-9/01143-8.

[4] X. He and K. Wang. "Efficient approximation algorithm for the Schrödinger-Poisson system". In: *Numerical Methods for Partial Differential Equations* 37.1 (2021), pp. 422–443. DOI: 10.1002/num.22534.

[5] A. Jüngel. *Quasi-hydrodynamic Semiconductor Equations*. Birkhäuser Basel, 2001. ISBN: 9783034883344. DOI: 10.1007/978-3-0348-8334-4.

[6] J.-F. Mennemann, A. Jüngel, and H. Kosina. "Transient Schrödinger-Poisson simulations of a high-frequency resonant tunneling diode oscillator". In: *J. Comp. Phys.* 239 (2013), pp. 187–205. ISSN: 0021-9991. DOI: 10.1016/j.jcp.2012.12.009.

Some results on a class of hybrid Boltzmann-BGK models

Marzia Bisi, Maria Groppi, Enrico Lucchin, Anna Macaluso, and Giorgio Martalò[*]
University of Parma, Italy

We present a class of hybrid kinetic descriptions modelling the dynamics of an inert mixture of monatomic gases [1]. These mixed models combine the positive features of known Boltzmann and BGK formulations; in particular, the collision phenomenon dominating the gas evolution is modelled by Boltzmann terms, which describe in detail the microscopic interactions; the remaining processes are modelled by BGK operators, resulting in more manageable from an analytical and numerical point of view. The relaxation terms are inspired by a recent relaxation model [3], miming the structure of the Boltzmann collision operator as the sum of binary contributions, one for each type of interaction.

The evolution of the mixture is governed by a set of integro-differential equations

$$\frac{\partial f_i}{\partial t} + \mathbf{v} \cdot \nabla_{\mathbf{x}} f_i = \mathcal{Q}_i = \sum_{j=1}^{N} \left[\chi_{ij} \hat{\mathcal{Q}}_{ij} + (1 - \chi_{ij}) \tilde{\mathcal{Q}}_{ij} \right], \quad i = 1, \ldots, N,$$

where f_i is the distribution function of the $i-$th component. The term $\hat{\mathcal{Q}}_{ij}$ is the bi-species Boltzmann operator while the operator $\tilde{\mathcal{Q}}_{ij}$ is of BGK type. The coefficients $\chi_{ij} \in \{0, 1\}$, such that $\chi_{ij} = \chi_{ji}$, allow us to fix which binary interactions are described by Boltzmann integrals or by BGK relaxation operators. The classical Boltzmann model for inert mixtures is recovered by the option $\chi_{ij} = 1$, for any $i, j = 1, \ldots, N$, while the BGK model proposed in [3] is obtained by the option $\chi_{ij} = 0$, for any $i, j = 1, \ldots, N$.

The model is proved to be consistent; more precisely, one can show

- the positivity of species temperatures;

- the usual conservation of global momentum and total energy;

- the Maxwellian equilibrium solutions as functions of the global mean velocity and temperature;

- the existence of an entropy functional guaranteeing the relaxation to the equilibrium.

Starting from the kinetic description, we can deduce proper evolution equations for the main macroscopic fields (densities, mean velocities and temperatures) in different hydrodynamic regimes (when the Knudsen number goes to 0), by the standard Chapman-Enskog procedure based on the expansion of the distribution functions.

In this talk, we analyze the regime dominated by the entire collision process, leading to classical Euler and Navier-Stokes equations for mixtures, and the regime dominated by intra-species interactions; these latter results are better suited to describe gas mixtures whose components have very disparate masses [4] (e.g. ions and electrons [5]), and leads to multi-velocity and multi-temperature Euler and Navier-Stokes equations [2].

References

[1]   M. Bisi, M. Groppi, E. Lucchin, and G. Martalò. "A mixed Boltzmann-BGK model for inert gas mixtures". In: *Kinetic and Related Models* (2023). early access.

[2]   M. Bisi, M. Groppi, and G. Martalò. "Macroscopic equations for inert gas mixtures in different hydrodynamic regimes". In: *Journal of Physics A: Mathematical and Theoretical* 54.8 (2021), p. 085201. DOI: 10.1088/1751−8121/abda08.

[3]   A. V. Bobylev, M. Bisi, M. Groppi, G. Spiga, and I. F. Potapenko. "A general consistent BGK model for gas mixtures". In: *Kinetic Related Models* 11.6 (2018), pp. 1377–1393. DOI: 10.3934/krm.2018052.

[4]   V. Galkin and N. Makashev. "Kinetic derivation of the gas-dynamic equation for multicomponent mixtures of light and heavy particles". In: *Fluid Dynamics* 29.1 (1994), pp. 140–155. DOI: 10.1007/BF02044896.

[5]   M. Pirner. *Kinetic modelling of gas mixtures*. Würzburg University Press, 2018. ISBN: 978-3-95826-093-1.

Optimal Transport of Neutral Atoms in Optical Tweezers

Sara Nicoletti

Dipartimento di Matematica e Informatica "Ulisse Dini", Università degli Studi di Firenze

Engineering a quantum system that evolves into a target state has relevance in quantum information science [13]. In particular, the realization of a controllable quantum system is an interesting topic in modern physical science [10]. In recent years a new promising platform emerges in the area of quantum simulation and quantum computing based on the so-called optical tweezers [4, 7, 9, 17], highly focused laser beams able to trap and move individual neutral atoms. In this setting, it is possible to manipulate and move the tweezers and the atoms trapped within them in such a way as to create an array of individual atoms with arbitrary geometry [2, 3, 18, 19]. Arrays of atoms represent a useful resource for quantum information because atoms in optical tweezers can be used as elementary quantum information carriers.

An optical tweezer is an optical dipole trap that is tightly focused on a length scale of around $1 \mu m$. Thanks to light-assisted collisions it is possible to trap one single atom in optical tweezers making this tool able to control and address single atoms. The idea of trapping individual atoms can be extended to many optical tweezers that can be assembled to form an array of traps. The assembly of several optical tweezers can be experimentally achieved by making use of devices, like the acousto-optical-deflectors (AODs) and light modulators (SLMs) [8]. The position and the intensity of these tightly focused dipole traps can be individually controlled. This technique takes an initially randomly loaded trap array and rearranges the atoms into an arbitrary configuration, most usually into an array with no defects or empty traps between atoms [6, 14, 16]. Typically, in the experiments, the quantum platform is based on Rydberg atoms of rubidium or strontium, and the motivation for using this platform is well known in literature [1, 5, 11, 15, 20].

In this context, we aim to formulate an optimal control problem on the transport of atoms in optical tweezers. The problem is formulated as an ensemble optimal control problem based on the Wigner equation. The optimality system consists of the forward Wigner problem, the adjoint problem, and the optimality condition [12]. We describe any noise or perturbation of the ideal case in terms of a Fokker-Plank term included in the Wigner equation.

In particular, we consider the following simple scenario. We consider two static optical traps at a distance d of the order of $10 \mu m$. We assume that one static trap is initially occupied by a single Sr atom and the second trap (target trap) is void. We derive an optimal control procedure aimed at steering the atom from the first to the target position under the guidance of optical tweezers. The time-dependent optical tweezers field al-

lows to move the atoms from an initial to a target position. The main parameters are designed in order to achieve some optimality conditions by maximizing the success rate of the protocol and at the same time minimizing the energetic cost of the control. For the sake of simplicity, we assume that the system is confined to a 1D region. The optical field of the tweezers and the static traps are modelled by the Gaussian field where the controlled parameters are the mean position and the strength of the Gaussian distribution. The control parameters are obtained by minimizing the distance of the particle distribution function with a target region of the phase space and at the same time maintaining the energy cost for the control as small as possible.

We describe the optimal control of the trajectories of flying atoms driven by the optical tweezers field at various degrees of precision. At first, we assume that the particle dynamics is completely deterministic. We assume that each atom is well described by a single classical trajectory with the known initial position that evolves without any source of external noise. This idealized description of the atom dynamics allows us to calculate the optimal trajectory efficiently. In a second step, we introduce in our model the main sources of uncertainties found in the experimental protocol to manipulate flying neutral atoms. The initial condition of the atom is known only approximately and various sources of external perturbations are typically present. For this reason, we describe the atom system as a classical ensemble of particles described by a statistical distribution in the phase space. Dissipation effects and external noises are modelled by a Liouville-Fokker-Plank equation for the particle density. As an alternative, we include the source of noise in the terms describing a stochastic signal over the control parameters. We remark that at this stage the atom dynamics is purely classical. Finally, we describe the atom dynamics in a fully quantum context. In order to highlight the correction to the previous classical results we adopt a kinetic description of the quantum motion provided by the Wigner formalism of pseudo-distribution function. Due to the non-linearity of the optimality systems associated with the optimal control, each step of our modelization of the controlled dynamics is used as a convenient initial guess to initialize the optimization procedure.

References

[1] D. Barredo et al. "Demonstration of a Strong Rydberg Blockade in Three-Atom Systems with Anisotropic Interactions". In: *Phys. Rev. Lett.* 112 (18 May 2014), p. 183002. DOI: 10.1103/PhysRevLett.112.183002.

[2] D. Barredo, V. Lienhard, S. de Leseleuc, T. Lahaye, and A. Browaeys. "Synthetic three-dimensional atomic structures assembled atom by atom". In: *Nature* 561 (Sept. 2018). DOI: 10.1038/s41586-018-0450-2.

[3] J. Beugnon et al. "Two-dimensional transport and transfer of a single atomic qubit in optical tweezers". In: *Nature Physics* (May 2007).

[4] D. Bluvstein et al. "Logical quantum processor based on reconfigurable atom arrays". In: *Nature* 626 (Dec. 2023). DOI: 10.1038/s41586-023-06927-3.

[5]   A. Browaeys, D. Barredo, and T. Lahaye. "Experimental investigations of dipole–dipole interactions between a few Rydberg atoms". In: *J. Phys. B* 49.15 (June 2016), p. 152001. DOI: 10.1088/0953-4075/49/15/152001.

[6]   M. Endres et al. "Atom-by-atom assembly of defect-free one-dimensional cold atom arrays". In: *Science* 354 (2016), pp. 1024–1027. DOI: 10.1126/science.aah3752.

[7]   J. Gieseler et al. "Optical tweezers — from calibration to applications: a tutorial". In: *Adv. Opt. Photon.* 13.1 (Mar. 2021), pp. 74–241. DOI: 10.1364/AOP.394888.

[8]   A. Glicenstein et al. "Preparation of one-dimensional chains and dense cold atomic clouds with a high numerical aperture four-lens system". In: *Phys. Rev. A* 103 (4 Apr. 2021), p. 043301. DOI: 10.1103/PhysRevA.103.043301.

[9]   L. Henriet. "Quantum computing with neutral atoms". In: *Quantum* 4 (Sept. 2020), p. 327. DOI: 10.22331/q-2020-09-21-327.

[10] C. Koch et al. "Quantum optimal control in quantum technologies. Strategic report on current status, visions and goals for research in Europe". In: *EPJ Quantum Technology* 9 (Dec. 2022). DOI: 10.1140/epjqt/s40507-022-00138-x.

[11] I. S. Madjarov. "PhD thesis: Entangling, Controlling, and Detecting Individual Strontium Atoms in Optical Tweezer Arrays". In: (2021).

[12] O. Morandi, N. Rotundo, A. Borzì, and L. Barletti. "An Optimal Control Problem for the Wigner Equation". In: *SIAM J. Appl. Math.* 84.2 (2024), pp. 387–411. DOI: 10.1137/22M1515033.

[13] M. A. Nielsen and I. L. Chuang. *Quantum Computation and Quantum Information: 10th Anniversary Edition*. Cambridge University Press, 2010.

[14] F. Nogrette et al. "Single-Atom Trapping in Holographic 2D Arrays of Microtraps with Arbitrary Geometries". In: *Phys. Rev. X* 4 (2 May 2014), p. 021034. DOI: 10.1103/PhysRevX.4.021034.

[15] M. A. Norcia, A. W. Young, and A. M. Kaufman. "Microscopic Control and Detection of Ultracold Strontium in Optical-Tweezer Arrays". In: *Phys. Rev. X* 8 (4 Dec. 2018), p. 041054. DOI: 10.1103/PhysRevX.8.041054.

[16] D. Ohl de Mello et al. "Defect-Free Assembly of 2D Clusters of More Than 100 Single-Atom Quantum Systems". In: *Phys. Rev. Lett.* 122 (20 May 2019), p. 203601. DOI: 10.1103/PhysRevLett.122.203601.

[17] M. Saffman. "Quantum computing with neutral atoms". In: *National Science Review* 6 (Jan. 2019), pp. 24–25. DOI: 10.1093/nsr/nwy088.

[18] K.-N. Schymik et al. "Enhanced atom-by-atom assembly of arbitrary tweezer arrays". In: *Phys. Rev. A* 102 (Dec. 2020). DOI: 10.1103/PhysRevA.102.063107.

[19] K.-N. Schymik et al. "In situ equalization of single-atom loading in large-scale optical tweezer arrays". In: *Phys. Rev. A* 106 (2022). DOI: 10.1103/PhysRevA.106.022611.

[20] J. T. Wilson et al. "Trapping Alkaline Earth Rydberg Atoms Optical Tweezer Arrays". In: *Phys. Rev. Lett.* 128 (Jan. 2022). DOI: 10.1103/PhysRevLett.128.033201.

Mini-Symposium
Recent advances in enriched finite element and isogeometric analysis

Preface to the Symposium

Federico Nudo[a] and Salah Eddargani[b], *Organizers*
[a] University of Padua, Italy
[b] University of Roma Tor Vergata

The finite element method (FEM) is a highly versatile technique widely employed for the numerical solution of partial differential equations. In addressing complex scenarios, strategies such as enriched finite element methods (EFEM) and isogeometric analysis (IGA) come to the fore. EFEM involves augmenting the approximation space with suitable enrichment functions, enhancing its capacity to address challenging phenomena like singularities and discontinuities. Conversely, IGA takes advantage of spline-based geometric representations to enhance the integration of geometric design and analysis. These approaches represent significant advancements in computational mechanics and numerica analysis.

This mini-symposium focuses on presenting recent applications and tools that advance both EFEM formulations and robust IGA techniques. It brings together young researchers working in these fields. Specific topics of interest include, but are not limited to:

- Finite element methods

- Enriched finite element methods

- Efficient weighted quadrature rules for isogeometric analysis

- B-spline based adaptive isogeometric analysis

List of the speakers

- Federico Nudo, University of Padua

- Salah Eddargani, University of Roma Tor Vergata

- Krunal Raval, University of Roma Tor Vergata

Enrichment strategy for the standard triangular and simplicial linear finite element

Federico Nudo

University of Padua, Italy

email: federico.nudo@unipd.it

A finite element is defined as a triplet $(K_d, \mathbb{F}_{K_d}, \Sigma_{K_d})$, where:

- K_d is a polytope in $\mathbb{R}^d$,

- $\mathbb{F}_{K_d}$ is a vector space of dimension n composed of real-valued functions defined on K_d, also referred to as *trial functions*,

- $\Sigma_{K_d} = \{L_j \ : \ j = 1, \ldots, n\}$ is a set of linearly independent linear functionals from the vector space $\mathbb{F}_{K_d}$, also known as *degrees of freedom*, such that $\mathbb{F}_{K_d}$ is Σ_{K_d}-unisolvent. In simpler terms, if $f \in \mathbb{F}_{K_d}$ and

$$L_j(f) = 0, \qquad j = 1, \ldots, n,$$

then $f = 0$ [7].

The finite element method stands out as a highly favored approach for numerically solving partial differential equations, which are commonly encountered in engineering and mathematical modeling, over domains $D \subset \mathbb{R}^d$, where $d \geq 1$. Its widespread adoption can be attributed, in part, to its adaptability to different geometries. In this method, the domain $\bar{D}$ is partitioned into polytopes, and for each of them, a local approximation within $\mathbb{F}_{K_d}$ is computed to approximate the solution of the partial differential equation. The global approximation is then defined as a piecewise function composed of the local approximations.

The finite element can be classified as either conforming or nonconforming, depending on whether the global approximation exhibits discontinuities at the subdomain boundaries. Indeed, standard linear finite elements, which typically use polynomial functions within the F_{K_d} approximation space, might prove ineffective for solving problems involving singularities. To address this limitation, various strategies have been proposed. Among these, a notable approach involves augmenting the approximation space $\mathbb{F}_{K_d}$ with appropriate enrichment functions.

In particular, given the finite element $(K_d, \mathbb{F}_{K_d}, \Sigma_{K_d})$, the task at hand is to determine:

How to select suitable enrichment functions $e_1, \ldots, e_N$**, such that the triplet** $(K_d, \mathbb{F}_{K_d}^{\text{enr}}, \Sigma_{K_d}^{\text{enr}})$ **constitutes a new finite element?**

One of the fundamental finite elements is the standard triangular linear finite element, specifically defined within two-dimensional Euclidean space. This element is

$$\mathcal{P}_1(S_2) = (S_2, \mathbb{P}_1(S_2), \Sigma_{S_2}^{\text{lin}}),$$

where S_2 is a non-degenerate triangle with vertices $\boldsymbol{v}_0$, $\boldsymbol{v}_1$, $\boldsymbol{v}_2$, $\mathbb{P}_1(S_2)$ is the space of all bivariate linear polynomials and $\Sigma_{S_2}^{\text{lin}}$ is the set of point evaluation functionals at the vertices of S_2. Despite its widespread application, the standard triangular linear finite element sometimes fails to deliver satisfactory outcomes due to the low-order approximation inherent in the associated trial functions. To improve the approximation accuracy, we explore the concept of enriching $\mathcal{P}_1(S_2)$ with suitable enrichment functions. More precisely, in this work we focus on the development of a unified and general framework for the enrichment of standard triangular linear finite elements in $\mathbb{R}^2$ and standard simplicial linear finite elements in $\mathbb{R}^d$. As we have already mentioned, a crucial point in this approach is to determine the conditions on the enrichment functions so that they generate a finite element. In [3], we proposed a polynomial enrichment technique for the standard triangular linear finite element, leveraging it to enhance the triangular Shepard operator. Subsequently, in [2], we introduced a novel class of nonconforming finite elements by enriching the standard triangular linear finite element with linearly independent continuous enrichment functions (not necessarily polynomials) $\{e_i \ : \ i = 0, 1, 2\}$ such that

$$e_i(\boldsymbol{v}_j) = 0, \qquad i, j = 0, 1, 2.$$

Additionally, we established necessary and sufficient conditions on the enrichment functions to guarantee the validity of the enriched triplet as a finite element. We demonstrated that the approximation error can be decomposed into two components: one associated with the standard triangular linear finite element and the other dependent on the enrichment functions. This decomposition facilitated the derivation of error bounds in both L^∞-norm and L^1-norm.

Building upon these findings, in [4], we extended our investigations to enrich the standard simplicial linear finite element defined as

$$\mathcal{P}_1(S_d) = (S_d, \mathbb{P}_1(S_d), \Sigma_{S_d}^{\text{lin}}),$$

where S_d represents a non-degenerate simplex in $\mathbb{R}^d$ with vertices $\boldsymbol{v}_0, \dots, \boldsymbol{v}_d$, $\mathbb{P}_1(S_d)$ denotes the space of all linear polynomials in $\mathbb{R}^d$, and $\Sigma_{S_d}^{\text{lin}}$ is the set of point evaluation functionals at the vertices of S_d. We enriched the standard simplicial linear finite element $\mathcal{P}_1(S_d)$ with $d + 1$ linearly independent continuous functions $\{e_i \ : \ i = 0, \dots, d\}$, such that $e_i(\boldsymbol{v}_j) = 0, i, j = 0, \dots, d$.

In our subsequent work [5], we proposed a general approach to enrich the standard simplicial linear finite element $\mathcal{P}_1(S_d)$ without imposing restrictive conditions on the enrichment functions, such as their vanishing at the vertices of S_d.

Another commonly used finite element in practical applications is the simplicial vector linear finite element, defined as

$$\boldsymbol{\mathcal{P}}_1(S_d) = (S_d, \boldsymbol{P}_1(S_d), \boldsymbol{\Sigma}_{S_d}^{\text{lin}}),$$

where $\mathbb{P}_1(S_d)$ represents the direct product, d times, of the vector space $\mathbb{P}_1(S_d)$ with itself, and

$$\mathbf{\Sigma}_{S_d}^{\mathsf{lin}} = \{\boldsymbol{L}_j \; : \; j = 0, \dots, d\},$$

with $\boldsymbol{L}_j$ defined as

$$\boldsymbol{L}_j(\boldsymbol{f}) = \boldsymbol{f}(\boldsymbol{v}_j) = [f_1(\boldsymbol{v}_j), \dots, f_d(\boldsymbol{v}_j)]^T, \quad \boldsymbol{f} = [f_1, \dots, f_d]^T, \quad j = 0, \dots, d.$$

Although widely used for solving the stationary Stokes equations, the simplicial vector linear finite element exhibits limitations when applied to complex scenarios. In [1], Bernardi and Raugel proposed a polynomial enrichment of the standard simplicial vector linear finite element, finding application across a broad spectrum of engineering computation fields. However, the use of polynomial enrichment functions often results in issues related to linear dependence. In alignment with previous research, we present a comprehensive strategy for enriching the simplicial vector linear finite element with nonpolynomial enrichment functions [6]. This enriched finite element, adaptable to any simplex, represents an extension of Bernardi Raugel finite element, offering improved versatility and applicability.

References

[1] C. Bernardi and G. Raugel. "Analysis of some finite elements for the Stokes problem". In: *Mathematics of Computation* 44.169 (1985), pp. 71–79.

[2] F. Dell'Accio, F. Di Tommaso, A. Guessab, and F. Nudo. "A unified enrichment approach of the standard three-node triangular element". In: *Applied Numerical Mathematics* 187 (2023), pp. 1–23.

[3] F. Dell'Accio, F. Di Tommaso, A. Guessab, and F. Nudo. "On the improvement of the triangular Shepard method by non conformal polynomial elements". In: *Applied Numerical Mathematics* 184 (2023), pp. 446–460.

[4] F. Dell'Accio, F. Di Tommaso, A. Guessab, and F. Nudo. "A general class of enriched methods for the simplicial linear finite elements". In: *Applied Mathematics and Computation* 456 (2023), p. 128149.

[5] F. Dell'Accio, F. Di Tommaso, A. Guessab, and F. Nudo. "Enrichment strategies for the simplicial linear finite elements". In: *Applied Mathematics and Computation* 451 (2023), p. 128023.

[6] F. Dell'Accio, A. Guessab, and F. Nudo. "Improved methods for the enrichment and analysis of the simplicial vector-valued linear finite elements". In: *Mathematics and Computers in Simulation* (2024).

[7] A. Guessab. *Sharp Approximations Base on Delaunay Triangulations and Voronoi Diagrams*. 2022.